



## Durham E-Theses

---

### *Crustal and upper mantle structures in oceanic regions*

Haigh, B. I. R.

#### How to cite:

---

Haigh, B. I. R. (1973) *Crustal and upper mantle structures in oceanic regions*, Durham theses, Durham University. Available at Durham E-Theses Online: <http://etheses.dur.ac.uk/8797/>

#### Use policy

---

The full-text may be used and/or reproduced, and given to third parties in any format or medium, without prior permission or charge, for personal research or study, educational, or not-for-profit purposes provided that:

- a full bibliographic reference is made to the original source
- a [link](#) is made to the metadata record in Durham E-Theses
- the full-text is not changed in any way

The full-text must not be sold in any format or medium without the formal permission of the copyright holders.

Please consult the [full Durham E-Theses policy](#) for further details.

CRUSTAL AND UPPER MANTLE STRUCTURES IN OCEANIC REGIONS

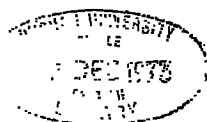
by B. I. R. Haigh.

A thesis presented for the degree of Doctor of Philosophy  
in the University of Durham.

Graduate Society

August 1973.

1



## ABSTRACT

Bathymetric data from the North Atlantic and other oceans reveal that, in addition to the well-documented variations of structure which occur at right angles to the ocean ridge crests, variations of structure also exist parallel to the strikes of the ridges. A thermal model of sea-floor spreading, together with data concerning possible mineralogical phase changes, is used to generate synthetic ocean ridge topography. Comparison of this with observed bathymetric data indicates that a peridotitic composition including water is favoured for at least the top half of the lithosphere, and allows a picture of the variations of structure in the upper mantle to be built up. It is found that lateral inhomogeneities in mantle temperatures are able to explain both the variation of ocean ridge dimensions and the uplift of different parts of the ocean basins relative to sea level which are evidenced by observed data. An empirical relationship between the calculated thicknesses of the lithosphere and the depths of the ocean basins is suggested.

A major area of raised temperatures may underly the North Atlantic, stretching from the Azores to a focus at Iceland. There is evidence for the existence of other regional anomalies in mantle temperatures, but none of the magnitude of that suggested to lie beneath the northern North Atlantic. The time taken for thicker lithospheres to cool <sup>to</sup> equilibrium following their formation at the ocean ridges imposes a fundamental limitation on the capabilities of the model, and makes undisturbed bathymetric profiles essential if reliable measurements are to be made in areas of lower mantle temperatures.

The results support suggestions that large scale mantle convection, not necessarily related geographically to the ridge crests, may occur, and indicate that active replenishment of the thermal anomalies may be required to sustain them over geologically significant periods of time.

## ACKNOWLEDGEMENTS

I am indebted to many members of the Geology department at Durham for advice and useful discussions during the course of this work. In particular to Professor M. H. P. Bott for his encouragement and supervision over the last three years, to Professor G. M. Brown and Dr. C. H. Emeleus for help in the fields of mineralogical phase changes and Skye. Also to Jennifer Marr and Jennifer Haigh for helping me to mould the manuscript into some semblance of shape. My thanks are due to Brian Lander, Bob Sheehan and other members of the Durham computer unit for invaluable assistance with calculations and data storage, and to the other institutions, both in Britain and abroad, from whom I obtained data, as referenced in the text.

The work was financed by a grant from the Natural Environment Research Council.

CONTENTS.

Abstract.....	i
Acknowledgements.....	ii
Contents.....	iii
List of Figures.....	ix
Chapter 1 - Observations and presentation of data.....	1
1.1 - Introduction.....	1
1.2 - The North Atlantic.....	3
1.2.1 - Bathymetry	
1.2.2 - Sedimentary thickness	
1.2.3 - Gravity	
1.2.4 - Spreading rates	
1.2.5 - Discussion of North Atlantic data	
1.2.6 - Summary	
1.3 - The South Atlantic.....	10
1.3.1 - Bathymetry.	
1.3.2 - Sedimentary thickness	
1.3.3 - Gravity	
1.3.4 - Spreading rates	
1.4 - The Norwegian - Greenland sea.....	11
1.4.1 - Bathymetry	
1.4.2 - Sedimentary thickness and gravity	
1.4.3 - Spreading rates	
1.4.4 - Discussion	

cont.....

1.5 - The Indian Ocean.....	13
1.5.1 - Bathymetry	
1.5.2 - Sedimentary thickness and gravity	
1.5.3 - Spreading rates	
1.5.4 - Discussion	
1.6 - The Australia - Antarctic Sea.....	14
1.6.1 - Bathymetry	
1.6.2 - Sedimentary thickness and gravity	
1.6.3 - Spreading rates	
1.6.4 - Discussion	
1.7 - The Pacific Ocean.....	16
1.7.1 - Bathymetry	
1.7.2 - Sedimentary thickness and gravity	
1.7.3 - Spreading rates	
1.7.4 - Discussion	
Introduction to chapters 2, 3 and 4 with a review of previous work..	19
Chapter 2 - Calculation of the temperature distribution in a spreading lithospheric slab.....	21
2.1 - The physical model.....	21
2.2 - The numerical model.....	23
2.3 - The equations of heat flow.....	23
2.4 - Values of physical constants and stability of the calculations.....	25
2.5 - Calibration of the temperature distribution calculations...	27
Chapter 3 - Composition and mineral assemblages of the lithosphere.....	29
3.1 - Bulk composition of the lithosphere.....	29

3.2 - Relevant minerals and phase changes.....	30
3.2.1 - Relevant minerals	
3.2.2 - Phase changes	
3.3 - Mineral assemblages and rock densities.....	33
3.3.1 - General	
3.3.2 - Mineral proportions in the low pressure assemblage	
3.3.3 - Mineral proportions in the intermediate pressure assemblage	
3.3.4 - Mineral proportions in the high pressure assemblage	
3.3.5 - Mineral proportions in assemblages including water	
3.3.6 - Calculation of mineral and rock densities at R.T.P.	
3.3.7 - Bulk density variations and mineral assemblages	
3.3.8 - The effect of water on rock densities	
3.3.9 - Bulk density variations at temperatures above the solidus	
Chapter 4 - Calculation of ocean ridge topography and general results and conclusions from the model.....	44
4.1 - Method.....	44
4.2 - The effect of the crust.....	46
4.3 - A computer program to calculate topography.....	47
4.4 - Introduction to general results.....	49
4.5 - Composition, lithospheric thickness, conductivity.....	49
4.5.1 - Lithospheric thickness	
4.5.2 - Lithospheric composition	
4.5.3 - Thermal conductivity variation	
4.5.4 - The preferred lithospheric model	

cont.....

4.6 - Discussion.....	52
4.7 - The effect of spreading rates.....	54
4.8 - Calculation of topographic profiles from age-elevation data.....	55
4.9 - Density and mineral phase distributions.....	56
4.10- Gravity anomalies over ocean ridges.....	57
4.11- Heat flow data.....	58
4.12- Seismic velocity in the modelled lithosphere.....	59
Chapter 5 - Application of the model to observed data.....	61
Introduction	
5.1 - A preliminary study of the northern North Atlantic.....	62
5.1.1 - The purpose of the study	
5.1.2 - The data	
5.1.3 - Analysis of the northward diminution of ridge dimensions	
5.1.4 - Analysis of the general northwards decrease of sea depths	
5.1.5 - Results of the preliminary study	
5.2 - Detailed study of the North Atlantic between 15 and 61°N.....	67
5.2.1 - Introduction	
5.2.2 - The data	
5.2.2.1 - Bathymetric profiles	
5.2.2.2 - Sedimentary cover	
5.2.3 - The analysis	
5.2.4 - Implication of the results	
5.2.5 - Limitations of the model	

cont.....



5.3 - Study of data from oceans other than the North Atlantic...	75
5.3.1 - Introduction	
5.3.2 - The data	
5.3.3 - Analysis and results	
Chapter 6 - Interpretation of results and conclusions.....	79
6.1 - The North Atlantic.....	79
6.2 - Iceland, the flanking aseismic ridges and the Norwegian - Greenland sea.....	80
6.2.1 - Iceland	
6.2.2 - The Iceland-Faeroes Rise	
6.2.3 - The Norwegian - Greenland sea	
6.3 - The South Atlantic.....	82
6.4 - The Indian, Southern and Pacific oceans.....	83
6.5 - Lateral variations in the mantle.....	83
6.5.1 - Introduction	
6.5.2 - Mantle temperatures and spreading rates	
6.5.3 - Mantle convection	
6.5.4 - Mantle hotspots	
6.5.5 - Stability of lateral inhomogeneities in the upper mantle	
6.6 - Summary of results.....	89
6.7 - Conclusion.....	91
The appendices.....	92
General notes on the computer programs.....	92
Appendix 1. Theoretical geotherms in lithospheres containing heat productive materials.....	93

Appendix 2. Calculation of basin uplift.....	94
Appendix 3. Stability of lateral variations in the mantle.....	97
Appendix 4. Listing of age - elevation - thickness table.....	99
Appendix 5. The program HEAT.....	100
Appendix 6. The program TEMDEN.....	107
Appendix 7. The program HOTMAP.....	113
Appendix 8. The program SYN.....	115
Appendix 9. The program LIGRAV.....	119
Appendix 10. The subroutine GRAPH.....	121
Appendix 11. The subroutine DISAZ.....	122
Bibliography.....	123

## LIST OF FIGURES

- 1.1 Location of bathymetric profiles (world).
- 1.2 Location of bathymetric profiles (N. Atlantic).
- 1.3 Bathymetric profiles (N. Atlantic).
- 1.4 " " "
- 1.5 " " "
- 1.6 " " "
- 1.7 Sediment isopach map (Atlantic).
- 1.8 Magnetic anomalies (N. Atlantic).
- 1.9 Various dimensions of North Atlantic topography.
- 1.10 Bathymetric profiles (S. Atlantic).
- 1.11 Location of bathymetric profiles (S. Atlantic).
- 1.12 Magnetic anomalies (S. Atlantic).
- 1.13 Location of bathymetric profiles (Norwegian - Greenland Sea).
- 1.14 Bathymetric profiles (Norwegian - Greenland Sea).
- 1.15 Location of bathymetric profiles (Indian Ocean).
- 1.16 Bathymetric profiles (Indian Ocean).
- 1.17 Sediment isopach map (Indian Ocean).
- 1.18 Magnetic anomalies (Indian Ocean).
- 1.19 Bathymetric profiles (Australia - Antarctic Sea).
- 1.20 Location of bathymetric profiles (Australia - Antarctic Sea).
- 1.21 Location of bathymetric profiles (Pacific).
- 1.22 Bathymetric profiles (Pacific).
- 1.23 Magnetic anomalies (Pacific).
- 1.24 Magnetic anomalies (Pacific).
- 2.1 Arrangement of the lithospheric model.
- 2.2 Comparison of temperature distribution with previous work.
- 2.3 Geotherms in modelled lithospheres.
- 3.1 Phase diagram for peridotite.

- 3.2 Pyroxene densities.
- 3.3 Mineral proportions in peridotites.
- 4.0 Density of olivine as a function of temp. and pres.
- 4.1 Digital phase diagram for peridotite.
- 4.2 Various calculated ocean ridge profiles.
- 4.3 Age - elevation curves for several spreading rates.
- 4.4 Age - elevation curves for several lithospheric thicknesses.
- 4.5 Calculated density, mineral phase and temperature distributions in a modelled lithosphere.
- 4.6 Calculated density and mineral phase distributions.
- 4.7 Free air anomaly over an ocean ridge.
- 4.8 Observed and calculated gravity anomalies over a modelled lithospheric slab.
- 4.9 Observed and calculated heat flow anomalies.
- 4.10 Heat flow as a function of lithospheric thickness.
- 4.11 Calculated velocity depth profiles.
- 5.1 Variances of bathymetric fits (N. Atlantic).
- 5.2 Observed and calculated bathymetric profiles (N. Atlantic).
- 5.3 Geotherms down to 400 km.
- 5.3a Partial melting of peridotite.
- 5.4 Uplift of ocean basins relative to sea level.
- 5.5 North Atlantic basin depths, before and after removal of sediment.
- 5.6 Observed and calculated bathymetric profiles (N. Atlantic).
- 5.7 " " " " " "
- 5.8 Variances of bathymetric fits (N. Atlantic).
- 5.9 " " " "
- 5.10 Lithospheric thickness against latitude.(N. Atlantic).
- 5.11 Lithospheric thickness against basin depth (N. Atlantic).
- 5.12 Temperature profiles in lithospheric slabs 80 My old.
- 5.13 Variances of bathymetric fits (S. Atlantic).

- 5.14 Variances of bathymetric fits (Indian, Southern and Pacific Oceans).
- 5.15 Variances of bathymetric fits (Norwegian - Greenland Sea).
- 5.16 Lithospheric thickness against latitude (S. Atlantic).
- 5.17 Lithospheric thickness against distance (Indian, Southern and Pacific Oceans).
- 5.18 Lithospheric thickness against basin depth (all oceans).
- A1 Illustration of effects of boundary conditions on the output of the programs.
- A2 Illustration of mantle stability calculations.



## CHAPTER 1

Observations and presentation of data1.1 Introduction

According to the theory of sea floor spreading, oceanic lithosphere forms by the upwelling, cooling and accretion of hot mantle material in the region between two separating plate margins. The topographic shape of ocean ridges may be explained by gradual cooling and contraction of the newly formed lithosphere as it moves away from the spreading centre. If this process took place above a laterally uniform asthenosphere, then the spreading rate would be the only variable factor affecting ridge shape and dimensions. Several authors have produced thermal models to predict the structure of the lithosphere across ocean ridges (McKenzie, 1967; Sleep, 1969; Sclater and Francheteau, 1970; Forsyth and Press 1971), and all conclude that the effect of the spreading rate is contained almost entirely in the horizontal scale of the topographic profile, an increase in spreading rate producing a lengthened section and vice versa. Virtually no variation of vertical dimensions is produced by spreading rate differences.

Cursory examination of a bathymetric map of the Atlantic suggests that, in the North Atlantic at least there may be variations of ridge and basin structure with latitude which are not attributable to differences in spreading rate. If the current models of sea floor spreading are in any way adequate, such variations would be evidence that the spreading of the sea floor occurs above a laterally non-uniform upper mantle, and detailed study of the oceanic topography might provide a means of investigating any inhomogeneities present.

The work of the authors mentioned above concentrated on examining the variations of structure which occur across the ocean ridges in directions at

right angles to the ridge axes. The structures beneath the spreading centres were compared with those existing beneath the ocean basins on either side. In contrast to this, the purpose of the present work is to investigate any variations of structure which may occur along the ocean ridges and basins in directions parallel to the strike of the ridges, with a view to determining the distribution of possible lateral variations in the upper mantle as mentioned above. The study was carried out by comparing observed bathymetric data, in the form of profiles perpendicular to the ridge axes, with profiles calculated using the thermal model described in later chapters. By repeated application of this transverse model to data from different parts of the ocean ridge system, a picture of the longitudinal variations was built up, and the results are presented in chapters 4, 5 and 6.

The thermal model described in chapters 2, 3 and 4 is based on the cooling and contraction of a lithospheric slab which is assumed to rest isostatically on the asthenosphere. Subsequent loading of the slab by sediments is not considered in the model and consequently the observed bathymetric data must be corrected for sediment thicknesses where necessary (see section 1. 2. 5). In order to compare observed and calculated bathymetry with any effectiveness the following data are thus required for each profile across the ocean ridge:-

- (1) bathymetry
- (2) sedimentary thickness
- (3) gravity (as a test of isostasy)
- (4) spreading rates applicable at all times during the ocean's formation.

The major area of interest in this work is the North Atlantic, which displays the largest variations of bathymetry parallel to the ocean ridge. Data from the North Atlantic were studied first, and the empirical relationship between basin depth and ridge dimensions which was then able to be suggested was tested

by investigating whether or not data from other parts of the world were in agreement with it.

While data from the North Atlantic were readily available, delays in publication of technical reports at the Lamont-Doherty Geological Observatory prevented the receipt of any other data until February 1973. It was therefore necessary to use bathymetric profiles taken directly from the literature for some parts of the oceans. Fortunately, it was possible with the aid of the D-mac digitizing table, to achieve a reasonable accuracy for the purposes of this work. Figure 1.1 shows the locations of the bathymetric profiles studied.

## 1.2 The North Atlantic

### 1.2.1 Bathymetry

The sources of bathymetric data in the North Atlantic are the British and Dutch Naval NAVADO cruises of 1964/5. The 16 traverses of the Atlantic ocean used in this work were collected along east-west lines at  $3^{\circ}$  latitude spacings from  $16^{\circ}\text{N}$  to  $61^{\circ}\text{N}$  (Figure 1.2), and have been published in the form of continuous profiles by the respective hydrographic offices. These profiles were digitised on a D-mac table and converted into bathymetry - distance relationships by interpolating across the spheroid between the navigational fixes of the ship, making use of the subroutine DISAZ (appendix 11) which is a Fortran version of that written by Hutton (1970). The profiles are shown in figures 1.3 to 1.6.

### 1.2.2 Sedimentary thickness

The general trend of sedimentary thicknesses in the oceans is well known. Sediments are thinnest or absent on the ocean ridges and gradually increase in thickness with distance from the spreading axis (Ewing, Ewing and Talwani, 1964;



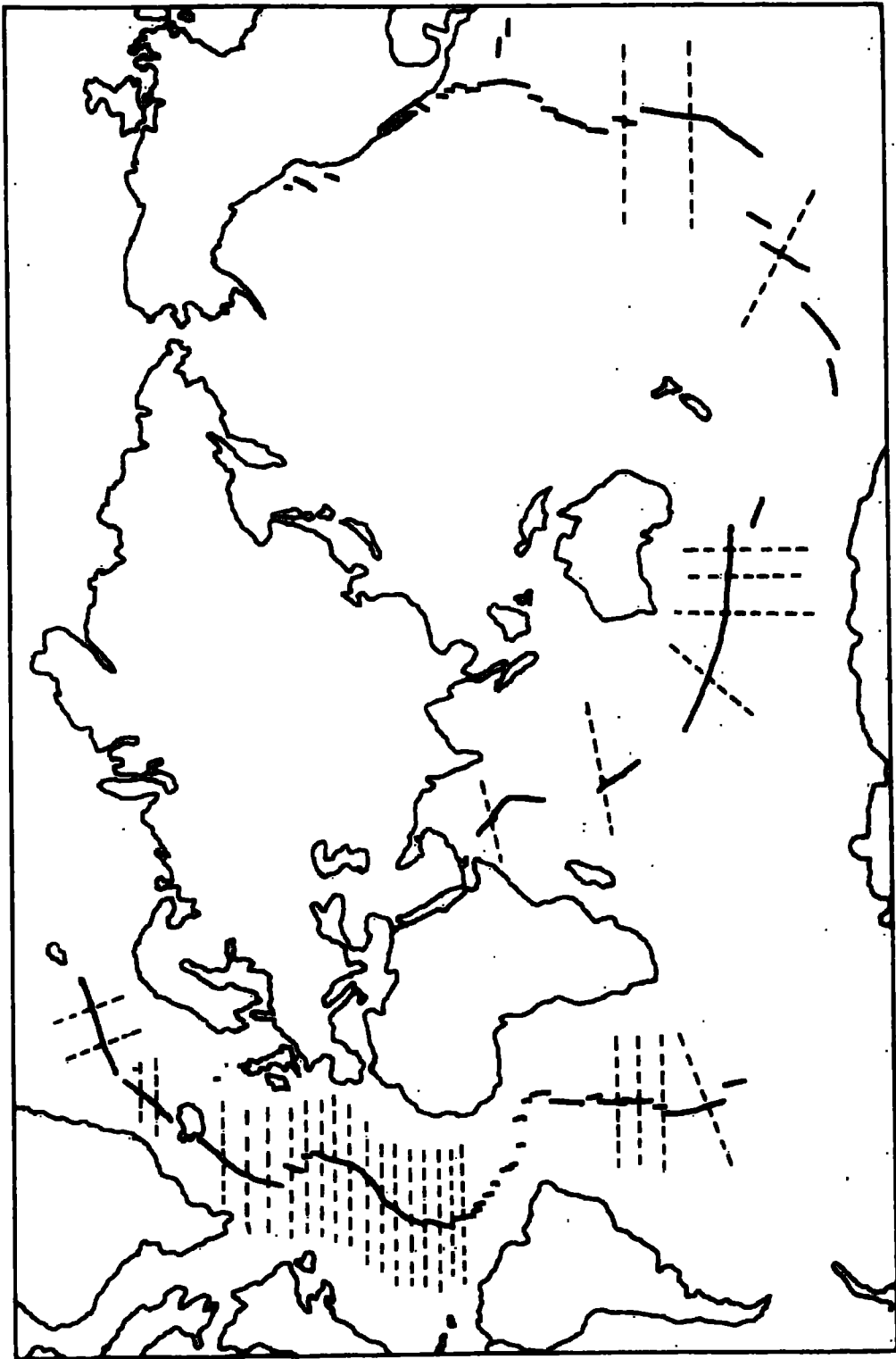


Figure 1.1. Map showing the locations of the bathymetric profiles studied in this work. The profiles are shown as dashed lines, the mid ocean ridge axis as a heavy line.

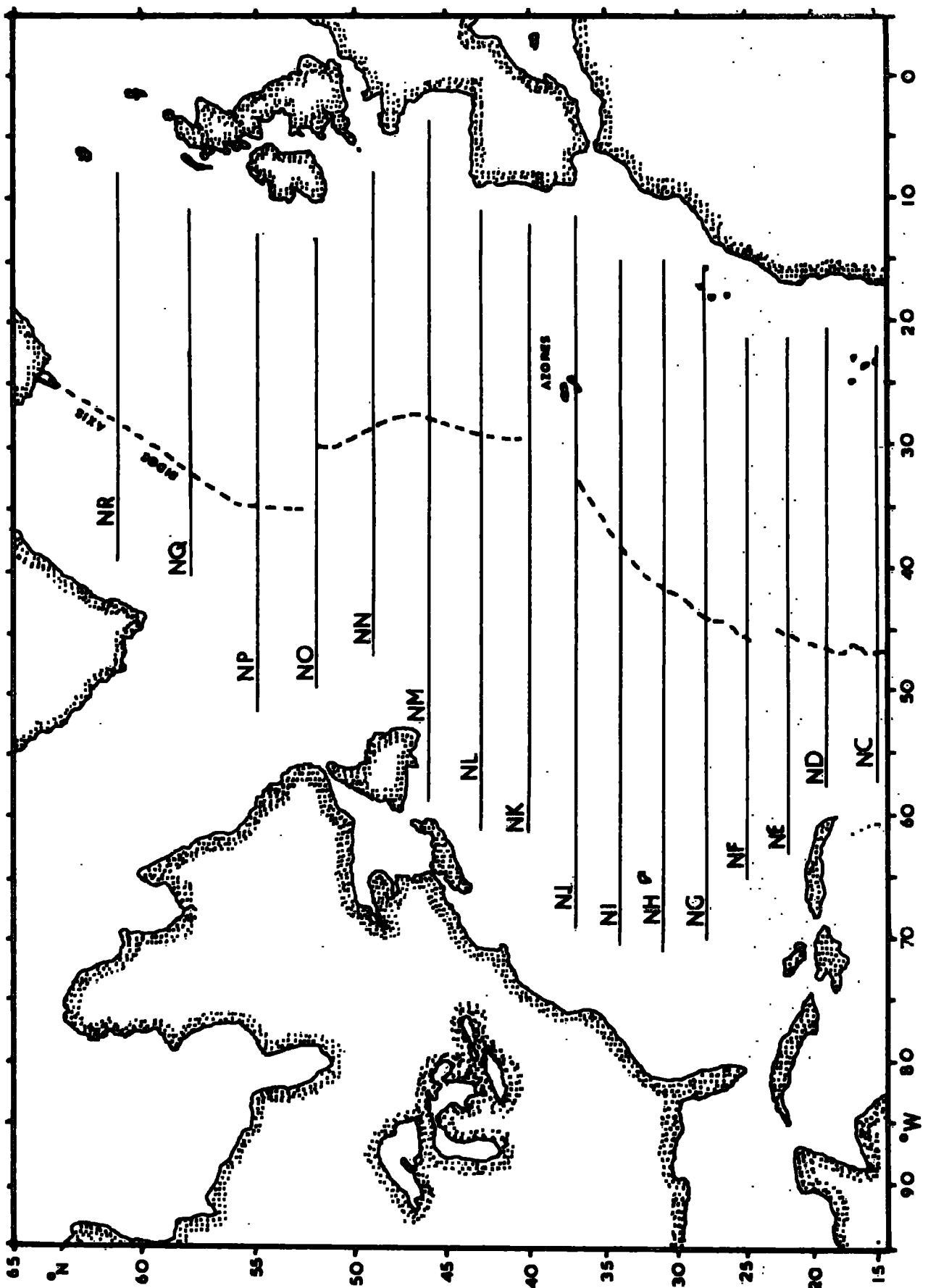


Figure 1.2. Map showing the location of the bathymetric profiles in the North Atlantic which are used in this work. The ocean ridge crest is shown as a dashed line.

Figure 1.3. Bathymetric profiles from the North Atlantic. Refer to figure 1.2 for locations.

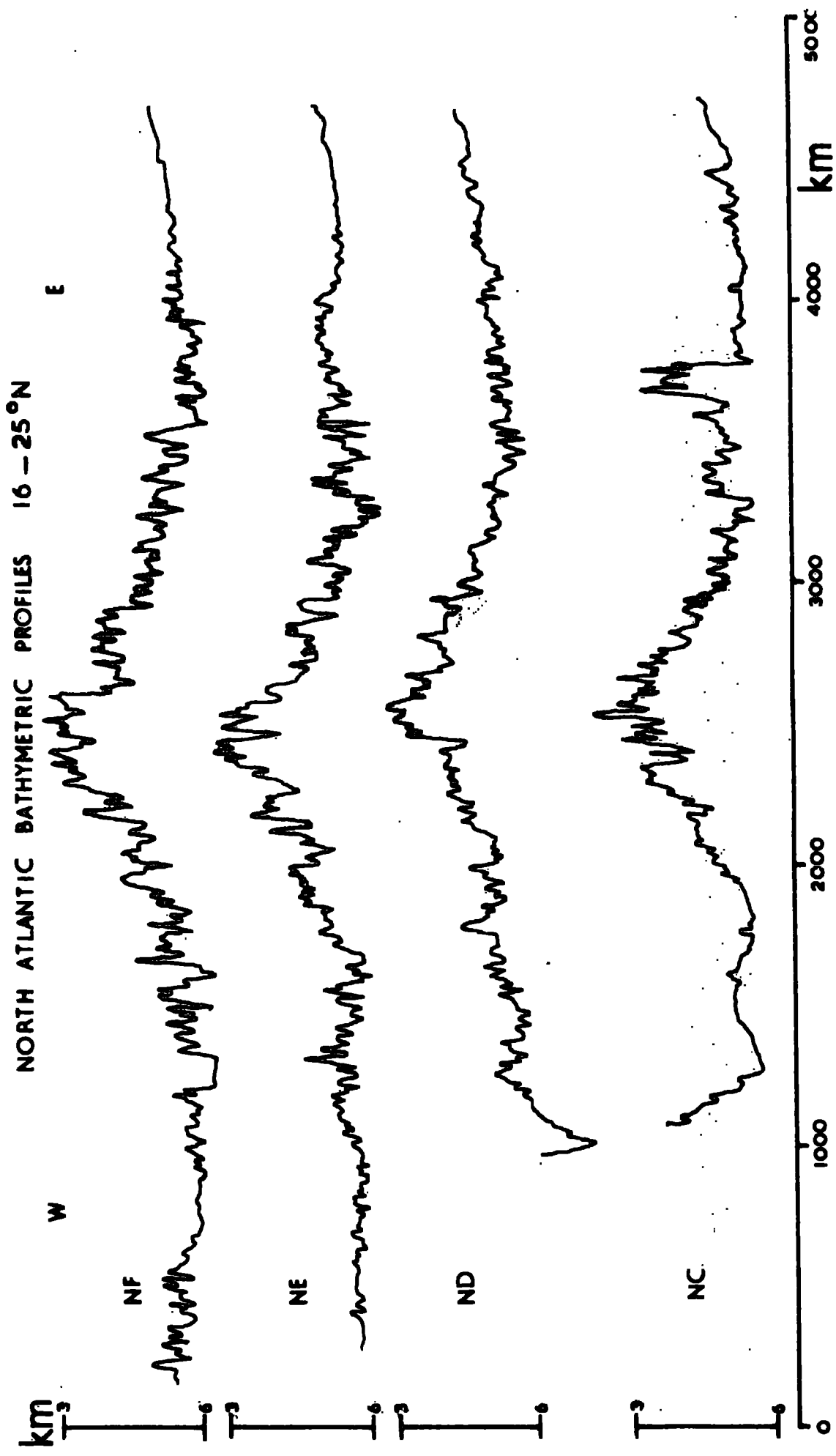


Figure 1.3.

Figure 1.4. Bathymetric profiles from  
the North Atlantic. Refer to figure 1.2 for locations.

NORTH ATLANTIC BATHYMETRIC PROFILES 28-37°N

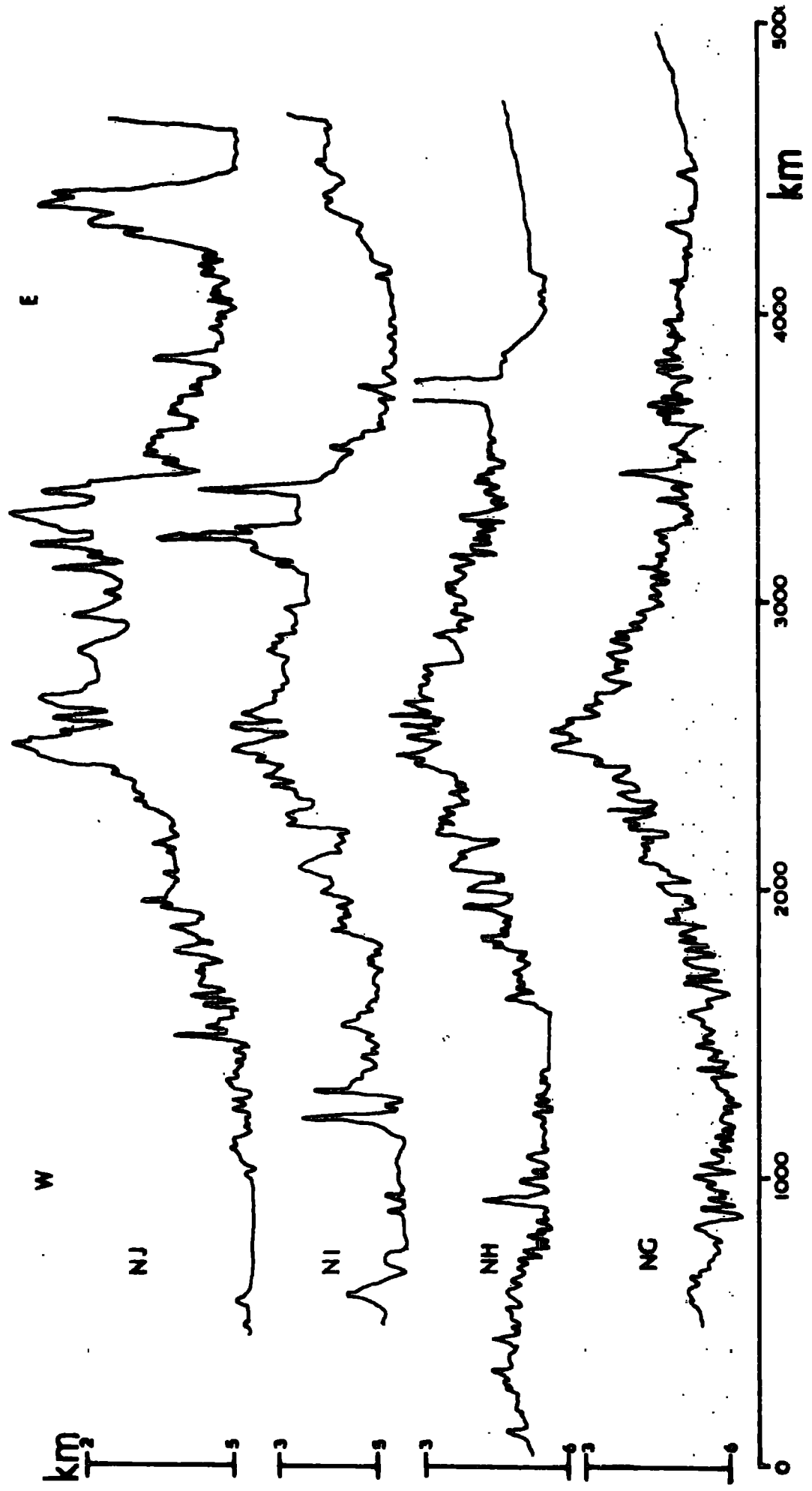


Figure 1.4.

Figure 1.5. Bathymetric profiles from the North Atlantic. Refer to figure 1.2 for locations.

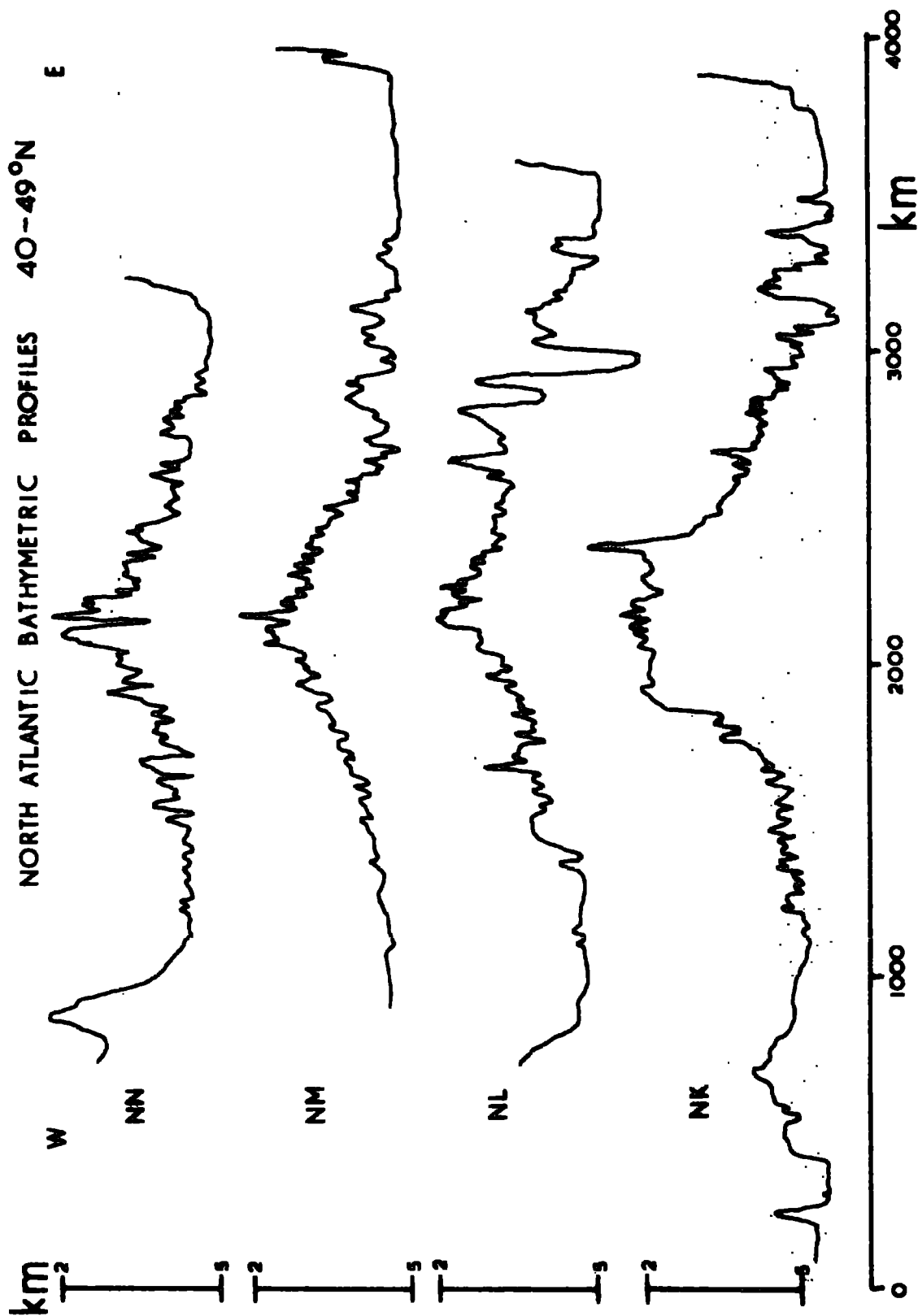


Figure 1.5.



Figure 1.6. Bathymetric profiles from the North Atlantic. Refer to figure 1.2 for locations.

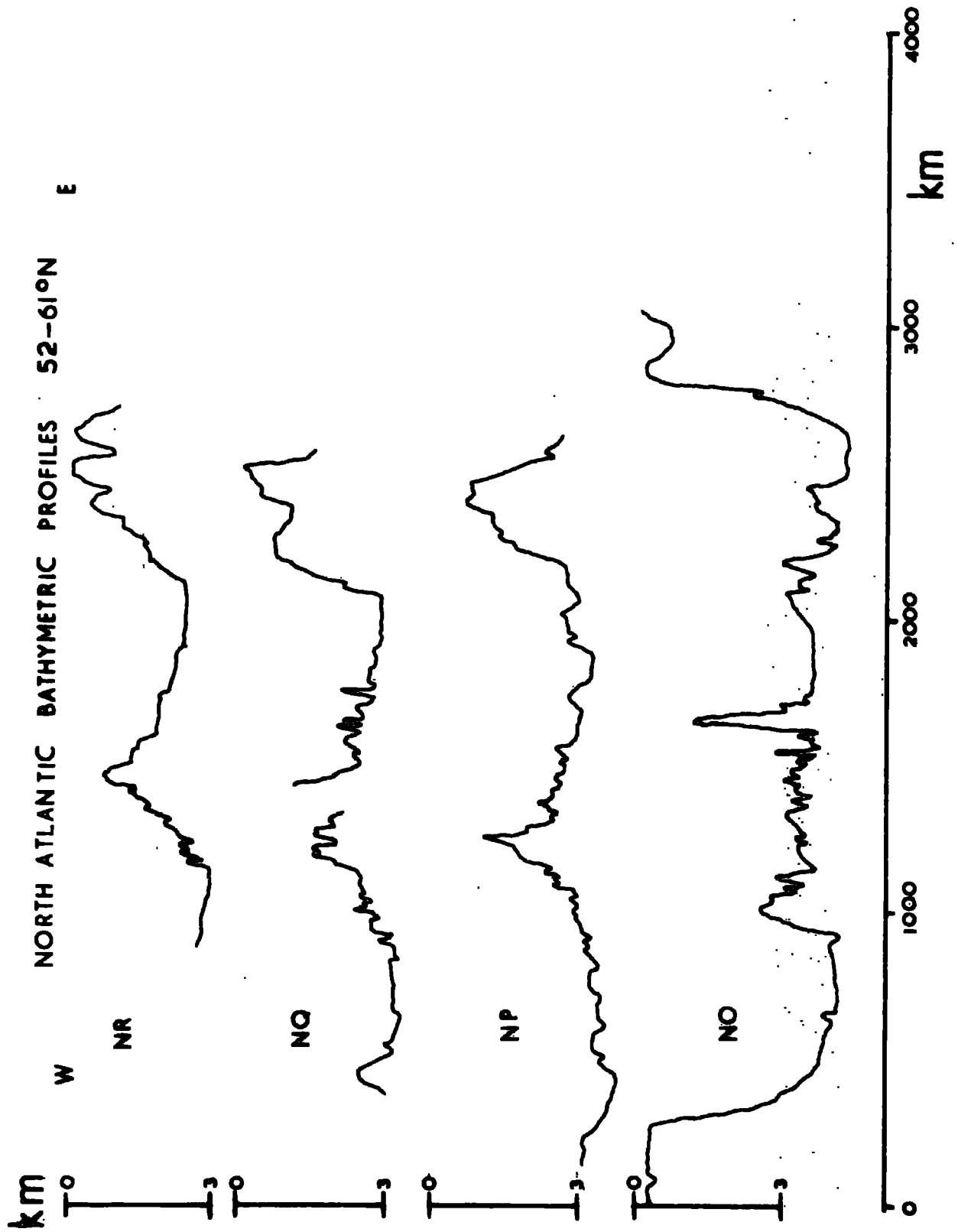


Figure 1.6.

Ewing, Le Pichon and Ewing, 1966). However, discontinuities of spreading (Jones et al, 1970), major deep currents (Jones et al, 1970) and proximity to large rivers (Bullard et al, 1965) may effect the sediment distribution. Since the NAVADO bathymetric data are not accompanied by simultaneously collected seismic reflection profiles, it was necessary to infer the sedimentary thicknesses present from any other nearby data which was available.

Accordingly the results of a large number of seismic refraction experiments were plotted in an attempt to estimate relevant thicknesses, the data used being from the following sources; Tolstoy, Edwards and Ewing (1953); Houtz and Ewing (1963); Ewing, Sutton and Officer (1954); Katz and Ewing (1956); Gaskell, Hill and Swallow (1958); Ewing and Ewing (1959); Le Pichon, Houtz, Drake and Nafe (1965); and Bott, Browitt and Stacey (1971). While this data shows general agreement with the expected trends, the scatter is too large to make it possible to estimate with any reliability the thickness of sediment present at one latitude by extrapolating from that present at another. However Ewing, Carpenter, Windisch and Ewing (1973) have recently published a sediment isopach map for the North and South Atlantic oceans based on many thousands of kilometres of seismic reflection profiling. Assuming an average velocity in the sediments, this map may be used to estimate the thickness of the sedimentary layers anywhere in the ocean. The map is reproduced in figure 1.7, and a sedimentary velocity of 2 Km/s was assumed, as suggested by the authors.

### 1.2.3 Gravity

The gravity data were taken from the same source as the bathymetry - the Navado cruises (see section 1.2.1) and a similar process of digitisation was followed in order to obtain free air gravity - distance profiles. The data were required in the present work only as a confirmation of isostasy, although some profiles (at 22, 46 and 61°N) were compared with gravity anomalies produced by the modelled lithospheric slab in order to check the modelling

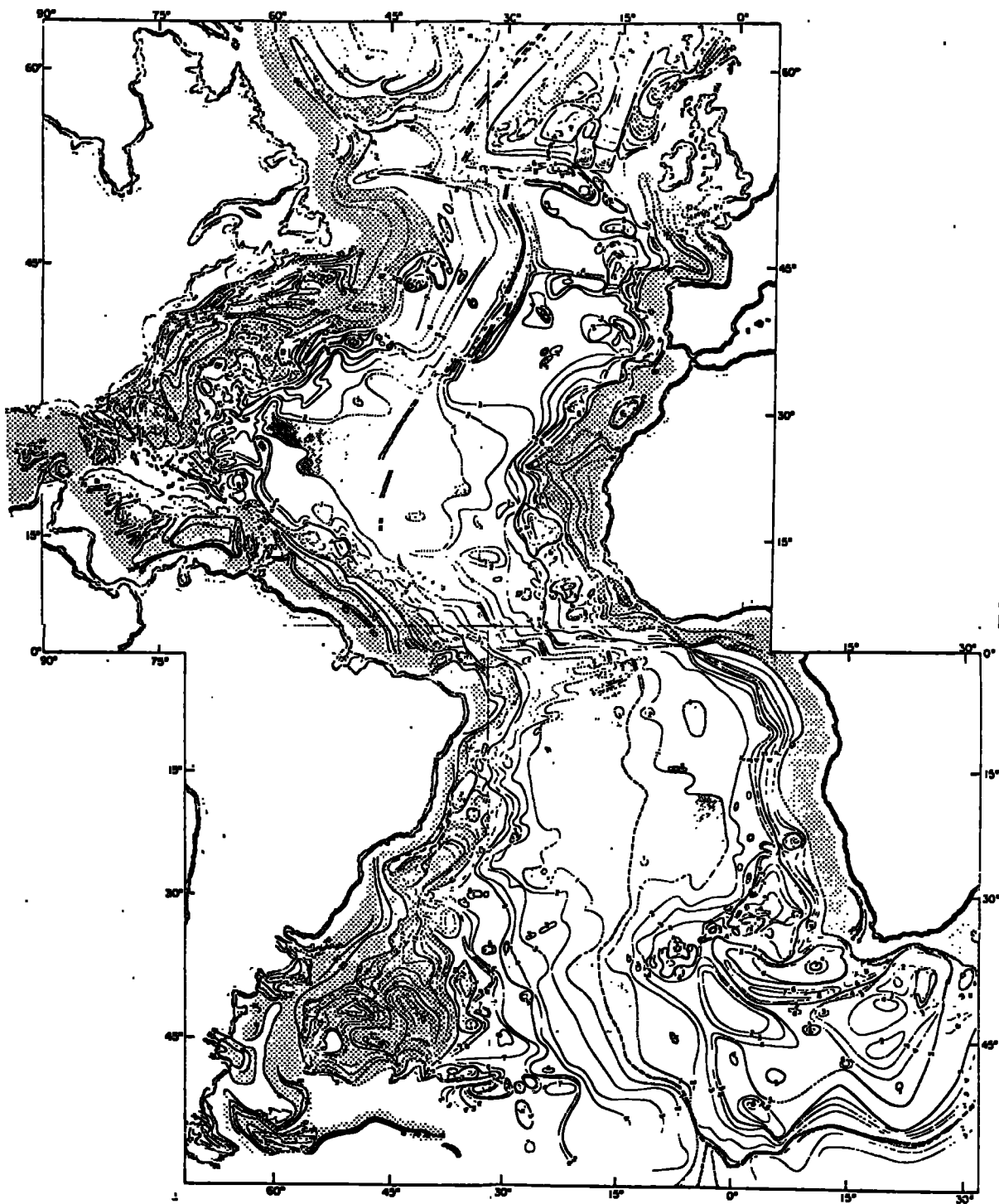


Figure 1.7. Sediment isopach map for the Atlantic ocean. Reproduced from Ewing, Carpenter, Windisch and Ewing (1973). Contours in tenths of seconds two way travel time.

procedure (see section 4.9).

#### 1.2.4 Spreading Rates

In order to make meaningful comparisons of bathymetric data from several locations along an ocean ridge, the effects of differing spreading rates on the horizontal dimensions of the profiles must be removed. For this purpose spreading rates were calculated from the interpretation of oceanic magnetic anomalies made by Pitman and Talwani (1972), and the anomalies used in the calculations are shown in figure 1.8, which is reproduced from the above paper. The relationship between magnetic anomalies and time used throughout this work is that of Heirtzler, Dickson, Herron, Pitman and Le Pichon (1968). Examination of figure 1.8 along the line  $43^{\circ}$  gives the following spreading rates:-

Time B.P. (My)	Spreading Rate cm/y
0 - 9	1.40
9 - 38	0.93
38 - 53	0.96
53 - 63	1.80
63 - 81	2.35

To a close approximation, the spreading rates at other latitudes may be found by dividing those given above for  $43^{\circ}$ N by two factors, one to account for the difference in distance between lines of longitude at different latitudes, and the other to account for the fact that the magnetic anomalies occur at different longitudes at each latitude. These two factors are combined in table 1.1.

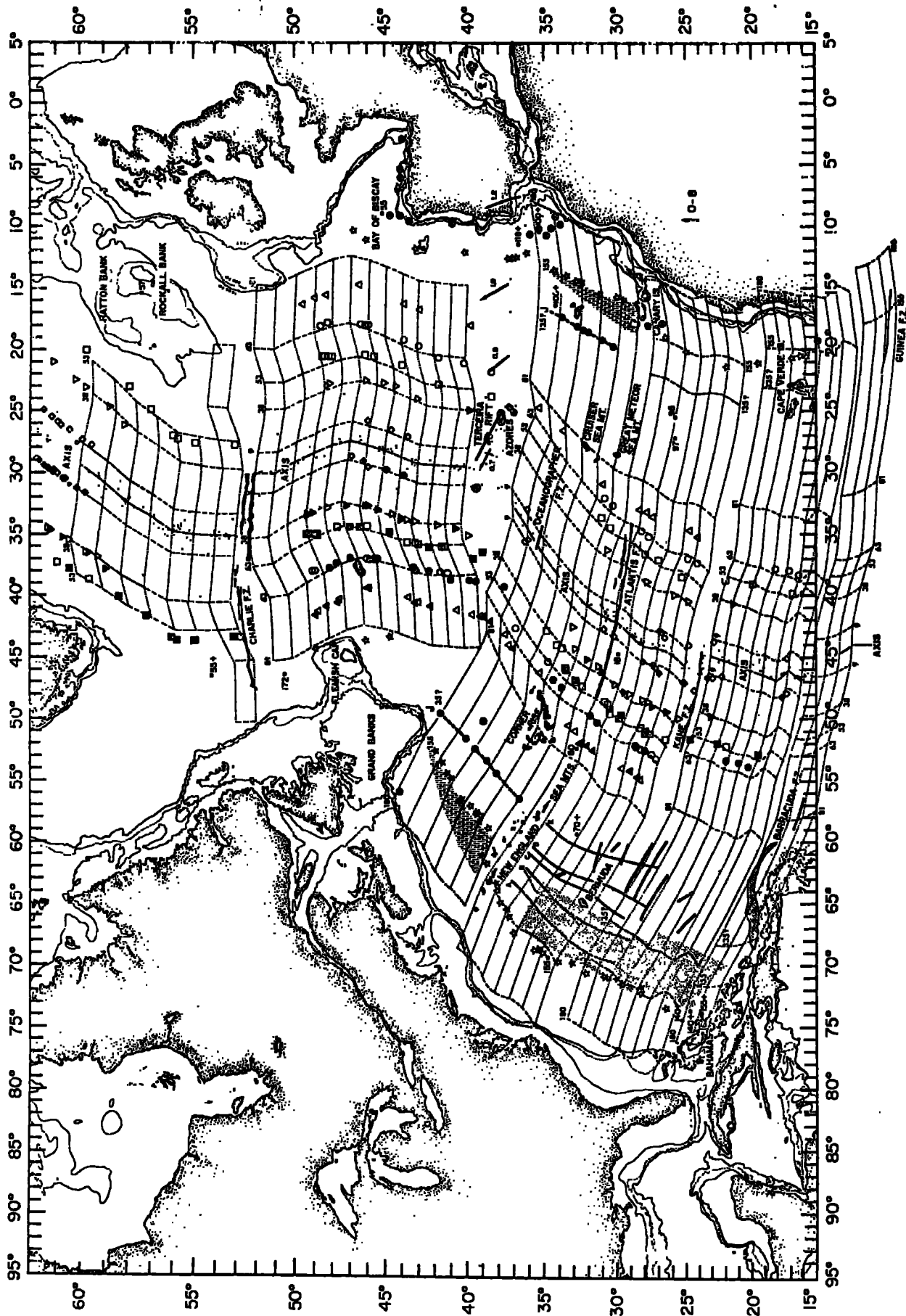


Figure 1.8. Magnetic Anomalies in the North Atlantic. Reproduced from Pitman and Talwani (1972). The anomalies are numbered in millions of years, other symbols are not relevant.

Table 1.1. Spreading Rates in the North Atlantic

Factors to give rates at any latitude from those at 43°N

LATITUDE	DISTANCE BETWEEN ANOMS. 21	COS. LAT	FACTOR	FACTOR
°Lat.	°Long.		$\frac{13.5}{\text{Distance}} \times \frac{0.730}{\text{Cos. Lat}}$	
16	14.5	0.960	$\frac{13.5}{14.5} \times \frac{0.730}{0.960}$	0.708
19	14.5	0.945	$\frac{13.5}{14.5} \times \frac{0.730}{0.945}$	0.719
22	14.5	0.925	$\frac{13.5}{14.5} \times \frac{0.730}{0.925}$	0.734
25	15.0	0.905	$\frac{13.5}{15.0} \times \frac{0.730}{0.905}$	0.725
28	15.0	0.882	$\frac{13.5}{15.0} \times \frac{0.730}{0.882}$	0.744
31	14.0	0.856	$\frac{13.5}{14.0} \times \frac{0.730}{0.856}$	0.719
34	16.0	0.828	$\frac{13.5}{16.0} \times \frac{0.730}{0.828}$	0.743
37	16.0	0.798	$\frac{13.5}{16.0} \times \frac{0.730}{0.798}$	0.771
40	13.0	0.765	$\frac{13.5}{13.0} \times \frac{0.730}{0.765}$	0.991
43	13.5	0.730	$\frac{13.5}{13.5} \times \frac{0.730}{0.730}$	1.000
46	14.0	0.694	$\frac{13.5}{14.0} \times \frac{0.730}{0.694}$	1.015
49	14.0	0.655	$\frac{13.5}{14.0} \times \frac{0.730}{0.655}$	1.075
52	15.0	0.615	$\frac{13.5}{15.0} \times \frac{0.730}{0.615}$	1.068
55	16.0	0.573	$\frac{13.5}{16.0} \times \frac{0.730}{0.573}$	1.072
58	17.5	0.529	$\frac{13.5}{17.5} \times \frac{0.730}{0.529}$	1.065
61	17.5	0.484	$\frac{13.5}{17.5} \times \frac{0.730}{0.484}$	1.165

### 1.2.5 Discussion of North Atlantic data

Various parameters of ocean ridge shape and size are shown in figure 1.9, the data being uncorrected for sedimentary thicknesses. The depths at which the topographic profiles become horizontal in the ocean basins are plotted against latitude in figure 1.9 (a) and show a decrease northwards from 5.5 Km at  $30^{\circ}\text{N}$  to 2.9 Km at  $61^{\circ}\text{N}$ . It must be emphasised that these measurements are taken from parts of the profiles which correspond to lithospheric ages of about 60 my or more. Empirical relationships between age and elevation (Sclater, Anderson and Bell, 1971) and the results of the present work (section 4.7) indicate that beyond this age topographic profiles are so nearly horizontal that additional time produces negligible changes in elevation. Consequently, the variation of basin depth with latitude shown in figure 1.9 (a) cannot be attributed to differences in lithospheric ages.

The cross-sectional area of the ocean ridge measured above the basin levels of figure 1.9 (a) is plotted against latitude in figure 1.9 (b), after being multiplied by the factors given in table 1.1 in order to remove the effects of spreading rate differences on the horizontal dimensions of the profiles. This scaling results in an increase in the cross-section north of  $43^{\circ}\text{N}$  and a decrease south, but nevertheless, there is a marked diminution of the cross-sectional area of the Mid Atlantic ridge northwards from the Azores. A slight accompanying decrease in the amplitude of the basin to ridge elevation is also apparent (figure 1.9 (c)). Both these parameters are disturbed by the Azores fracture zone between  $37$  and  $40^{\circ}\text{N}$  and the Gibbs fracture zone at  $53^{\circ}\text{N}$ .

To the south of the Azores, the basin depths plotted in figure 1.9 (a) are sensibly constant, but trends in the cross-section and elevation (figure 1.9 (b and c)) may exist, although they are less well defined than to the north. Comments on this observation are given in section 5.2.3.



- Figure 1.9. Various dimensions of North Atlantic topography plotted against latitude:-
- a) Depth of the western ocean basin.
  - b) Cross-sectional area of the ocean ridge measured above the basin levels shown in (a) after scaling horizontally to adjust spreading rates to those of  $43^{\circ}$  N (see section 1.2.5). Note that this scaling lessens the diminution of the cross section towards the north.
  - c) Bathymetric amplitude of the ocean ridge measured from the basin levels to the crest.

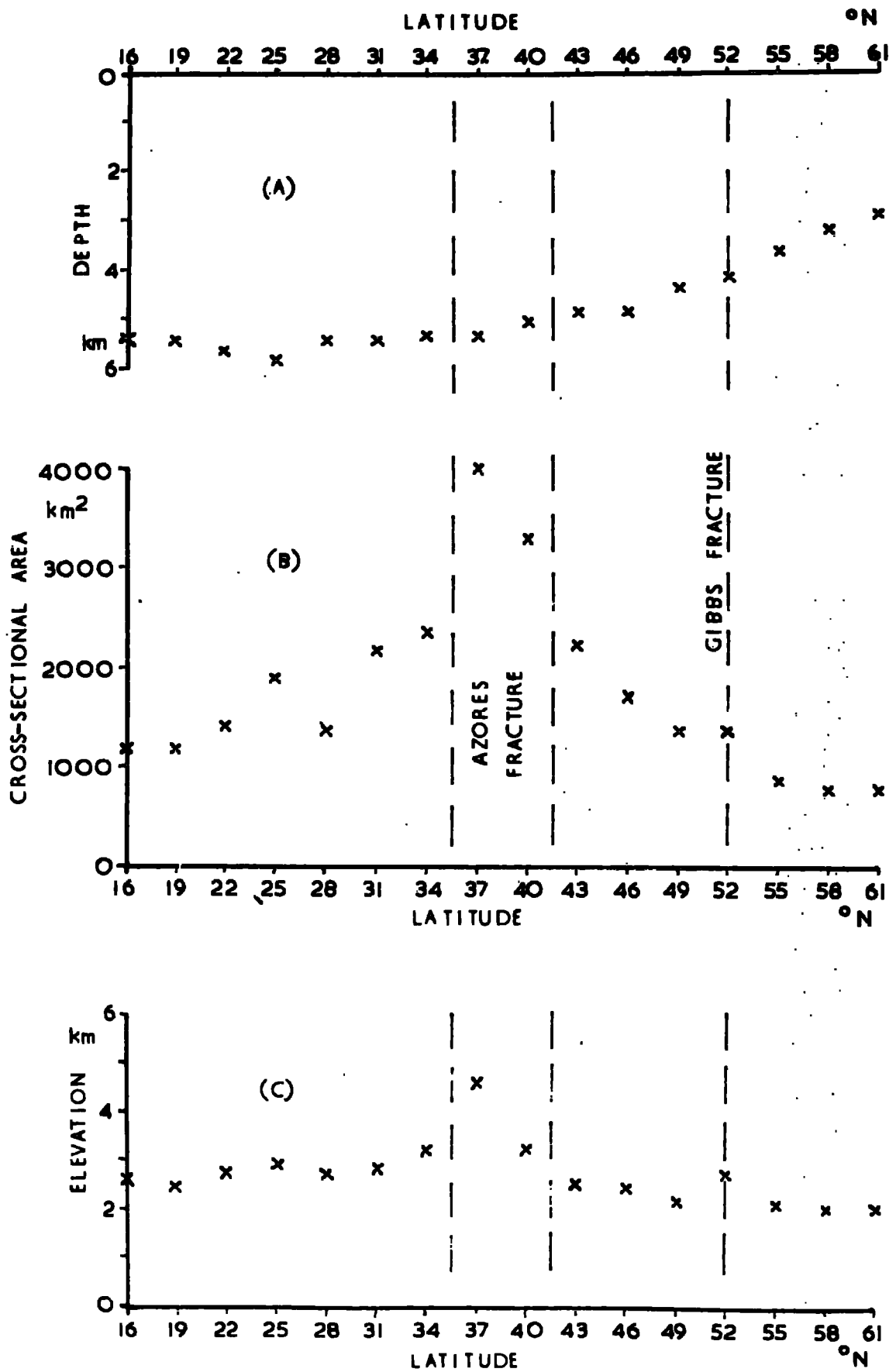


Figure 1.9.

### The effect of sediments

As mentioned previously, the data plotted in figure 1.9 take no account of sedimentary thicknesses. Variations of sedimentary cover with latitude would affect the above observations, but until the publication of the isopach map of Ewing, Carpenter, Windisch and Ewing (1973) lack of more than isolated information precluded any accurate corrections being made. However, because of the exceptionally large thicknesses of sediment known to exist east of the Reykjanes ridge (Jones, personal communication), data for the western basin are plotted in the figure. Assuming the sediments to have an average density of  $2 \text{ g/cm}^3$ , isostatic adjustment of the lithosphere reduces their effect on long-wavelength topography by about half. A pile of sediments  $x$  Km thick depresses the crystalline basement by  $x/2$  Km so that the water depth is only decreased by  $x/2$  Km and not the full  $x$  Km. With this in mind, it is clear that the variations of sedimentary thickness with latitude known from the sources quoted in section 1.2.2, and also from Ewing, Ewing and Talwani, 1964; Jones, Ewing, Ewing and Eittreim, 1970 and Talwani, Windisch and Langseth, 1971, are sufficient to modify the results in terms of magnitude but not to remove the trends noted above. This conclusion is supported by the new information contained in the isopach map of Ewing et al (1973) (figure 1.7), and calculations including the effects of sedimentary layers are given in section 5.2.

### The effects of gravity variations

While the gravity field over the Atlantic indicates that the conditions for isostasy are generally satisfied, long wavelength anomalies do exist (Talwani and Le Pichon, 1969) and these, if sufficiently large, could affect the analysis. In fact the observed variation of free air gravity is an order of magnitude less than the 250 mgals which would be produced were the differences of basin depth shown in figure 1.9 (a) the result of isostatically uncompensated

structural differences. Discussion of the correlation between the free air anomaly and the depth to the ocean ridge crest reported recently by Anderson, McKenzie and Sclater (1973) is given in chapter 6. At this stage it is sufficient to note that free air gravity variations are too small to have an appreciable effect on the model.

#### The effect of variations of crustal thickness

Assuming a density contrast between crust and mantle of  $0.4 \text{ g/cm}^3$ , the uplift of the sea floor by  $2\frac{1}{2}$  Km which occurs in the northern North Atlantic between the Azores and Iceland (figure 1.9 (a)) could be explained by crustal variations alone if the crust at  $61^\circ\text{N}$  was about 12 Km thicker than that at  $43^\circ\text{N}$ . The seismic refraction data quoted in section 1.2.2 were examined for variations in crustal thickness with latitude but no indications of noticeable thickening were found except on the Iceland - Faeroes rise around  $64^\circ\text{N}$ . Consequently variations of crustal thickness cannot account for the bathymetric trends noted previously.

#### 1.2.6 Summary

The above observations on North Atlantic bathymetry may be summarised as follows:-

- (1) Between the Azores and Iceland, the Mid Atlantic ridge is characterised by a northwards decrease in cross-section and height and this is accompanied by an increase in the elevation of the whole ridge-basin system relative to sea level.
- (2) South of the Azores, a diminution of ridge dimensions towards the equator may be present, but this is less marked than that to the north and the data are more scattered. Basin depths are sensibly constant with no regional trend being apparent.
- (3) Variations of free air gravity and crustal thickness are at least one order of magnitude too small to explain the features noted in (1), above. Variations of sedimentary cover will affect the magnitude of

of these features but are insufficient to remove the trends to an appreciable degree.

- (4) Two highly anomalous areas exist - Iceland and the Azores. The lack of disturbance of the oceanic topography to the west suggests that the uplift of the Azores may be a result of the intersection of the Mid Atlantic ridge and the Azores - Gibraltar fracture zone. In contrast some other explanation is required for the uplift of Iceland since no similar intersection occurs beneath it.

### 1.3 The South Atlantic

#### 1.3.1 Bathymetry

Four profiles in the South Atlantic were considered. Three were collected by the Lamont-Doherty Geological Observatory on R.V. Vema (profiles AV18, AV20, and AV22, figure 1.10) and one by the Argentine Hydrographic Office on A.R.A. Zapiola (Profile SAZ2, figure 1.10). The data were taken, in the form of profiles projected onto lines perpendicular to the ridge axis, from the following papers:-

AV18, AV20, AV22-Dickson, Pitman and Heirtzler, (1968)

SAZ2-Ewing, Le Pichon and Ewing, (1966).

A map showing the location of the tracks followed by the ships is presented in figure 1.11. The two way travel times of profile SAZ2 given by Ewing et al. (1966) were converted into depths by assuming a water velocity of 1.5 Km/s.

#### 1.3.2 Sedimentary Thickness

The isopach map of Ewing, Carpenter, Windisch and Ewing (1973) (figure 1.7) was used to estimate the sedimentary thicknesses in the South Atlantic. The velocity assumed for this purpose was that suggested by the authors, which is 2 Km/s.

Figure 1.10. Bathymetric profiles from the South Atlantic. Refer to figure 1.11 for locations.

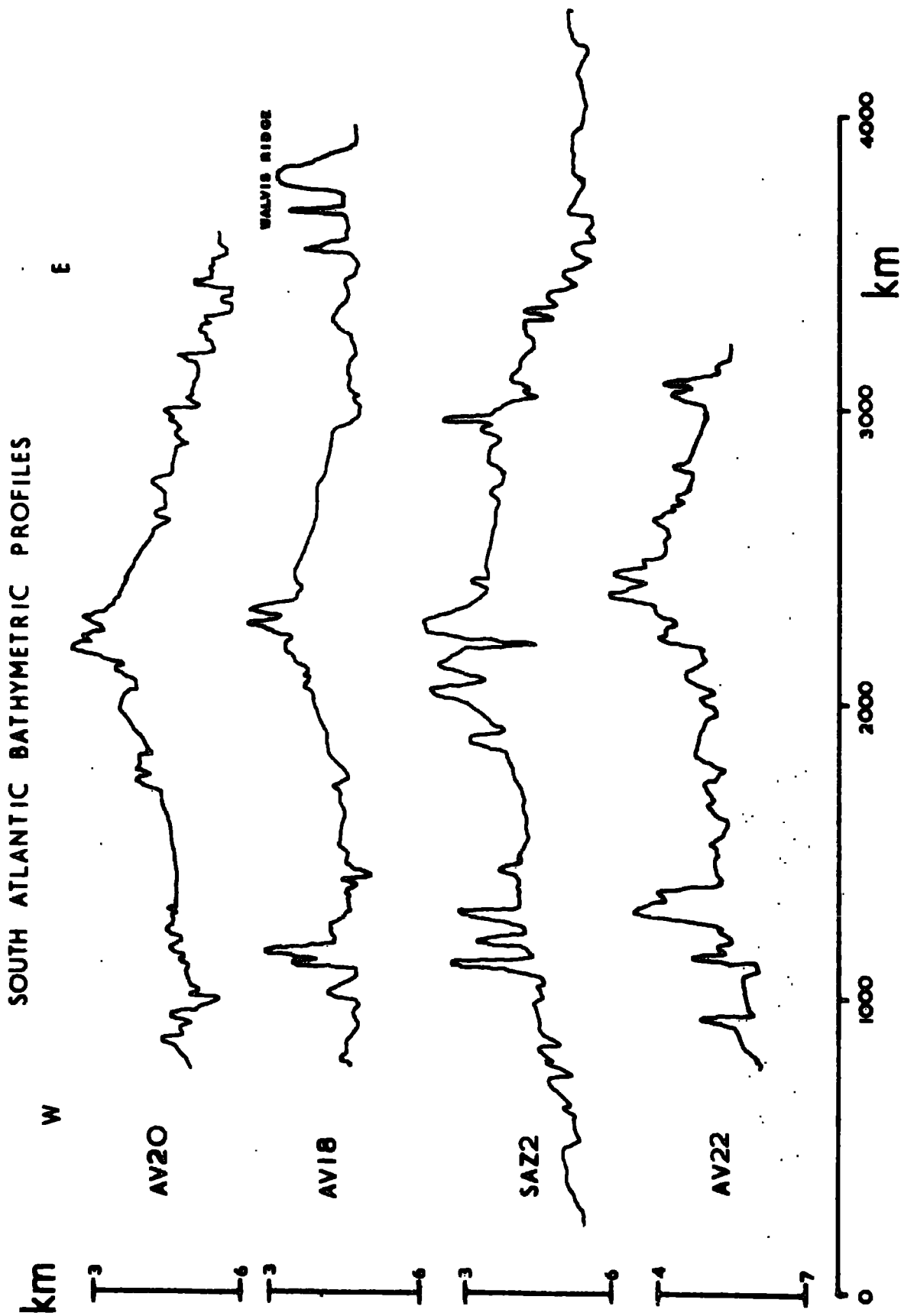


Figure 1.10.

Figure 1.11. Map showing the location of the bathymetric profiles in the South Atlantic which are used in this work. The ocean ridge crest is shown as a dashed line, the 2000fm contour as a dotted line. Redrawn from Dickson, Pitman and Heirtzler (1968).



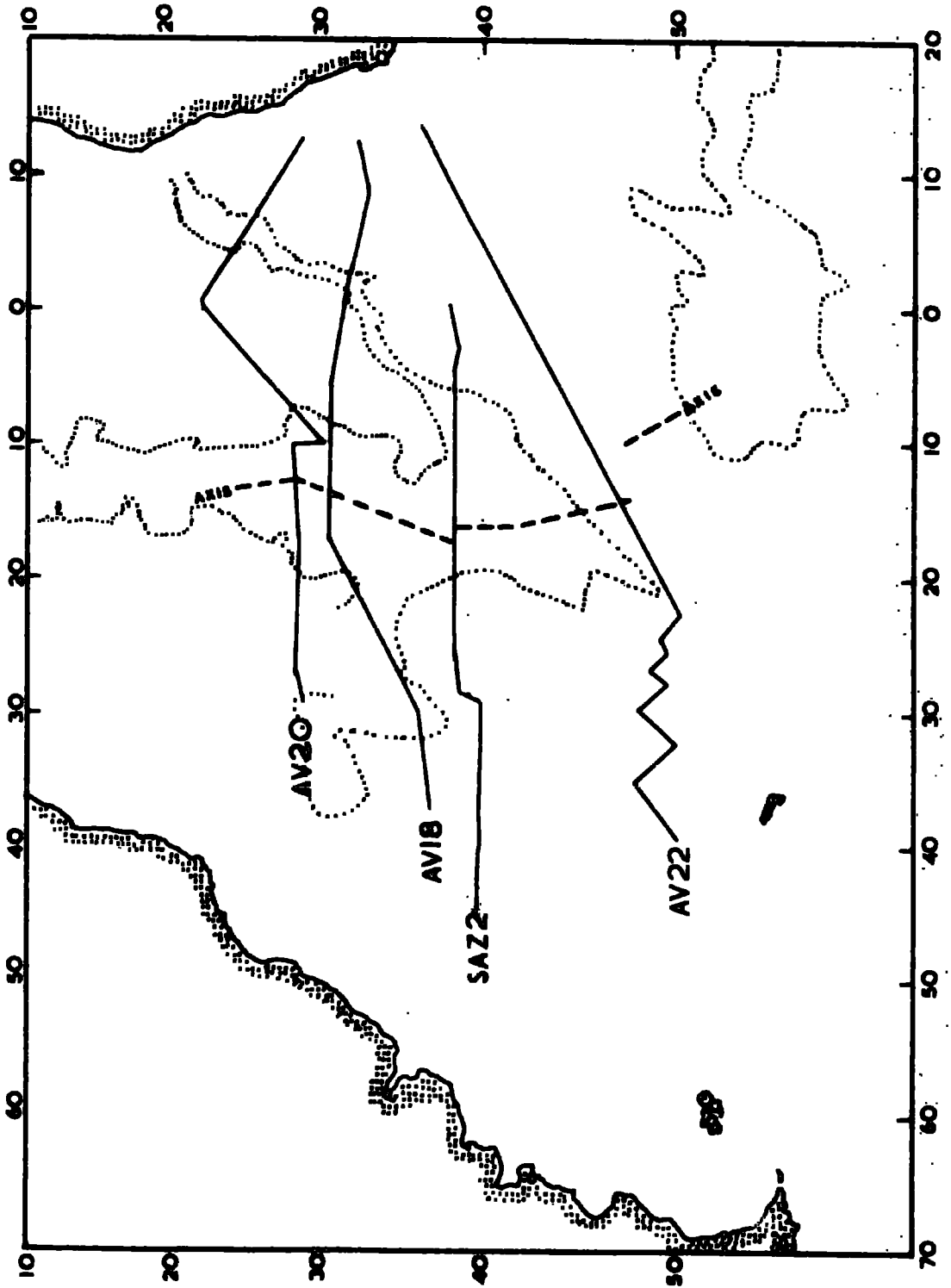


Figure 1.11.

### 1.3.3. Gravity

No simultaneously collected gravity data were available, but published global free air maps (e.g. Anderson, McKenzie and Sclater, 1973) confirm that the conditions of isostasy necessary for the model are met.

### 1.3.4. Spreading Rates

An interpretation of the relevant magnetic data is included in the above mentioned paper of Dickson, Pitman and Heirtzler (1968) where it is shown that the spreading in the South Atlantic has always occurred about the same pole of rotation. Plotting the magnetic anomalies back to 80 My B.P against distance from the ridge crest reveals that one spreading rate may be used for each profile throughout this period (figure 1.12). The following values for the spreading rates were used, being those derived by Dickson et al:-

Profile	Time B.P. (My)	Spreading Rate (cm/y)
AV20	0 - 80	2.0
AV18	0 - 80	2.0
SAZ2	0 - 80	2.1
AV22	0 - 80	1.7

## 1.4 The Norwegian - Greenland Sea

### 1.4.1 Bathymetry

No satisfactory data in the form of continuous profiles being available, it was necessary to derive such profiles from published contoured and uncontoured maps and charts. Four lines were studied and their positions are shown on figure 1.13. Profiles IJMN and IJMS were taken from bathymetric charts compiled by the German Hydrographic Institute in Hamburg at a scale of 1:1,000,000. Profiles MRAB and MRCB were taken from the bathymetric map of

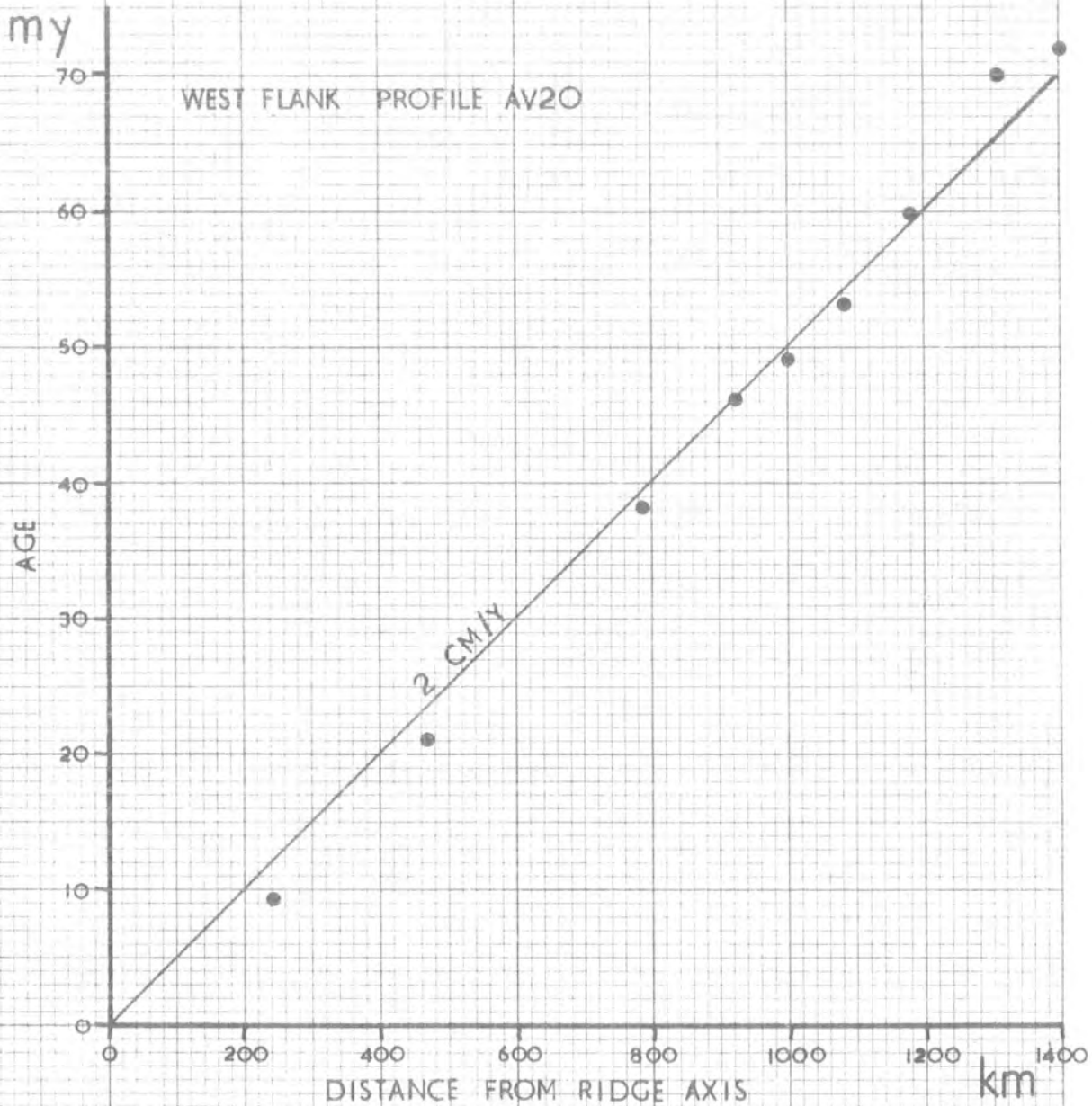


Figure 1.12 Magnetic anomalies in the South Atlantic plotted against distance from the mid ocean ridge axis. The data are from Dickson, Pitman and Heirtzler (1968), and indicate a uniform spreading rate over the last 75 my.

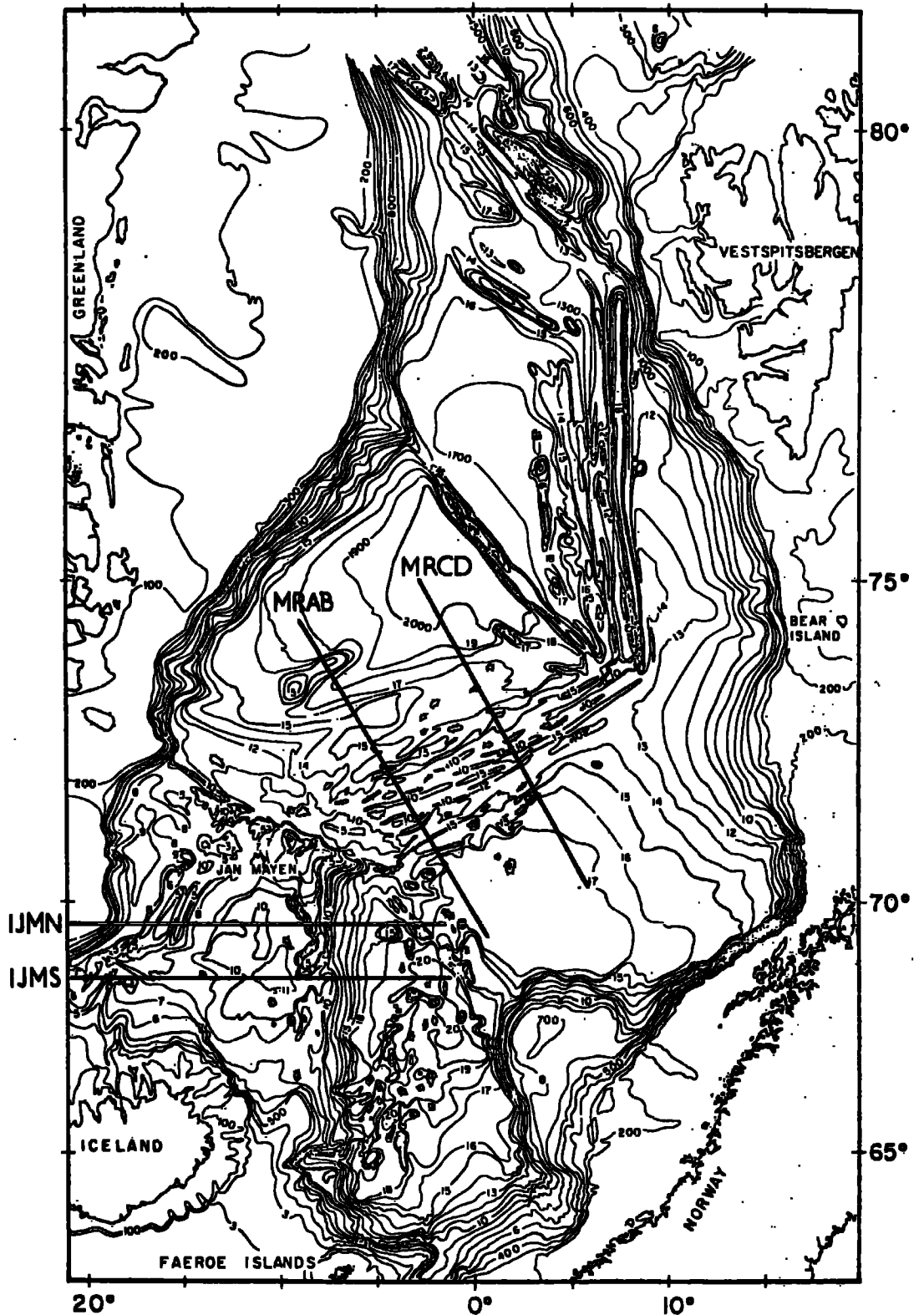


Figure 1.13. Bathymetric map of the Norwegian-Greenland sea showing the locations of the profiles used in this work. Reproduced from Johnson and Heezen (1967). Contours in units of milliseconds travel time.

Johnson and Heezen (1967), assuming a water velocity of 1.5 Km/s. The profiles are shown in figure 1.14.

#### 1.4.2 Sedimentary thickness and gravity

Insufficient information on sediment distribution was available to enable any accurate account of variations of thickness in this area to be taken. No gravity data other than the global free air maps were available, but these confirm the existence of isostasy.

#### 1.4.3. Spreading rates

The magnetic field in the Norwegian - Greenland sea has been investigated by Vogt, Ostenso and Johnson (1970), who suggested that sea floor spreading may have occurred at an average rate of 1 cm/y from both the Iceland - Jan Mayen ridge and the Mohns ridge. Evidence from the Reykjanes ridge (Vogt et al, 1970; Bott, 1973) indicated that the initial rates may have been higher than this figure, but the spreading north of Iceland is not well defined and the average rate of 1 cm/y was used in the present work.

#### 1.4.4 Discussion

The tectonic structure of the Norwegian - Greenland Sea is complex. According to Vogt, Ostenso and Johnson (1970) sea floor spreading may have begun at a now extinct axis midway between Norway and the Jan Mayen sedimentary ridge. Subsequently, the spreading axis shifted to its present location along the Iceland - Jan Mayen ridge, about which there is evidence that asymmetric spreading has occurred. The Jan Mayen sedimentary ridge has been interpreted as an isolated continental fragment detached from Greenland by the shift of the spreading centre. Although to north of the Jan Mayen fracture zone the spreading history is probably more simple, the complexity of the whole area, together with the proximity of the continental shelves to the ocean ridge and consequent masking of the topography by sediments (Johnson and Heezen, 1967),

BATHYMETRIC PROFILES IN THE NORWEGIAN-GREENLAND SEA

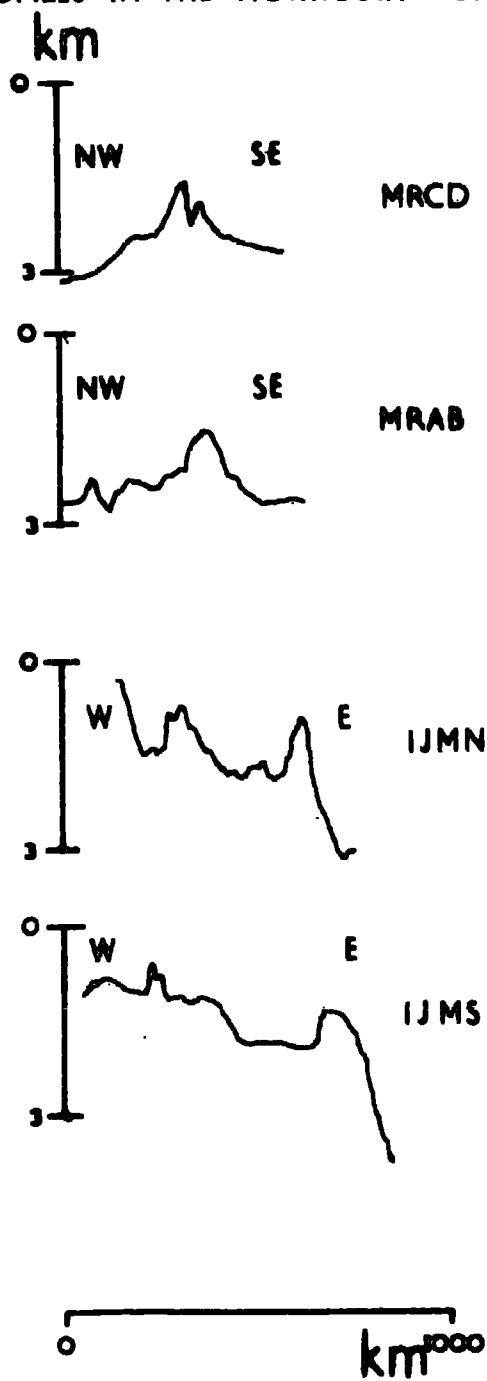


Figure 1.14. Bathymetric profiles in the Norwegian-Greenland sea. Refer to figure 1.13 for locations.

makes the data from this area unsatisfactory for the present purpose.

Further discussion is given in section 5.3.

## 1.5 The Indian ocean

### 1.5.1 Bathymetry

Three profiles from the Indian ocean were studied, and the tracks of the R.V. Vema and R.V. Conrad which collected the data are shown in figure 1.15. Le Pichon and Heirtzler (1968) have published the information in the form of profiles projected onto lines perpendicular to the ridge axis and these are shown in figure 1.16.

### 1.5.2 Sedimentary thickness and gravity

Sedimentary thicknesses in the Indian ocean were estimated from the isopach map of Ewing, Eittreim, Truchan and Ewing (1969), assuming a sedimentary velocity of 2 Km/s. This map is reproduced as figure 1.17. Only global gravity data, which again confirm isostasy, were available.

### 1.5.3 Spreading rates

Le Pichon and Heirtzler (1968) have plotted the distance from the ridge crest to several magnetic anomalies along the lines of the profiles considered in this work against the corresponding distance to the same anomalies in the South Atlantic, where the spreading rate is 2 cm/y. The graphs, which are reproduced in figure 1.18, allow the following spreading rates to be determined for different parts of the Indian ocean:-

North Indian ocean, Carlsberg ridge, profile IOAB

Time B.P. (My)	Spreading rate (cm/y)
0 - 9	1.50
9 - 27	0.22
27 - 55	2.45

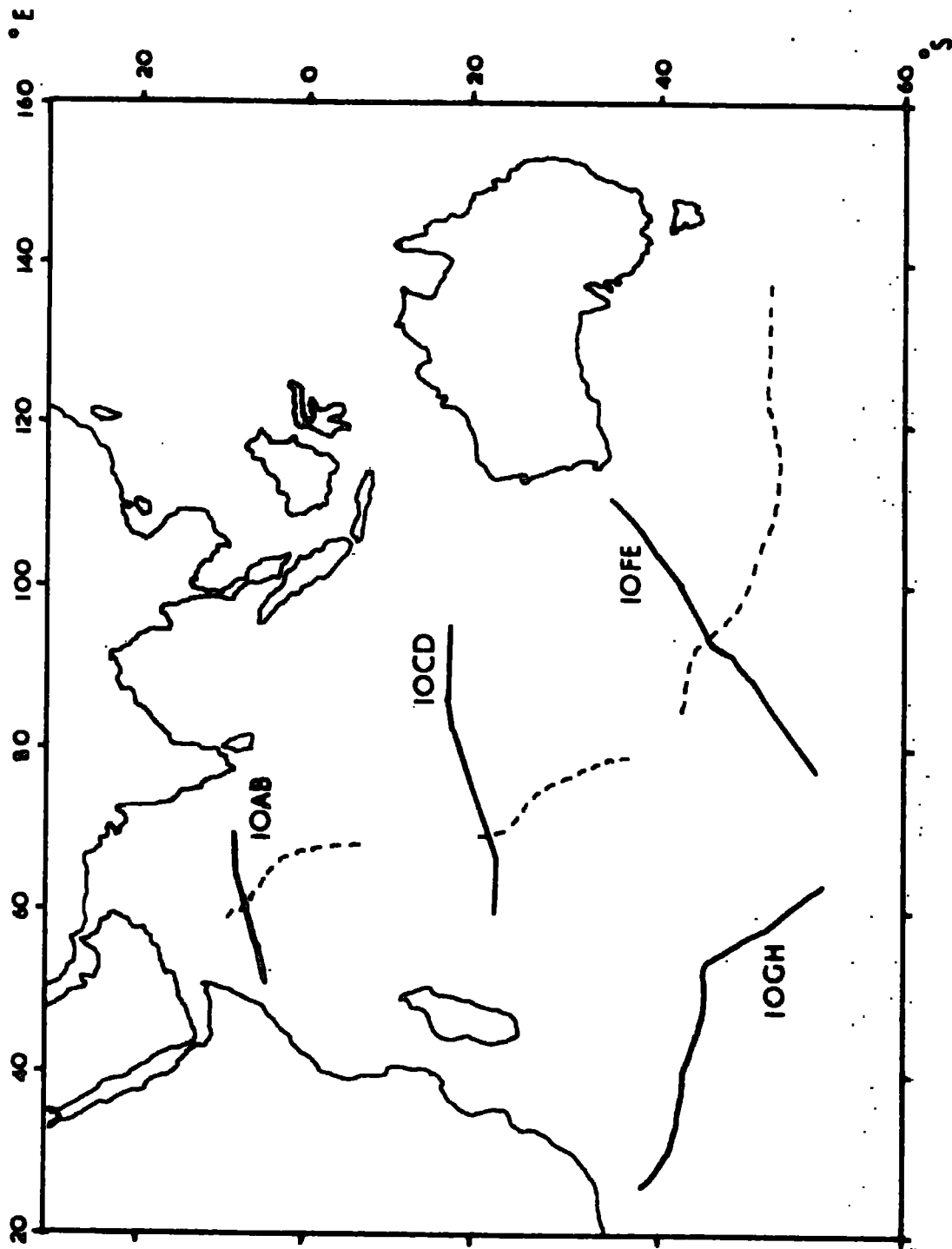


Figure 1.15. Map showing the location of bathymetric profiles in the Indian ocean which are used in this work. The ocean ridge crest is shown as a dashed line.



# INDIAN OCEAN BATHYMETRIC PROFILES

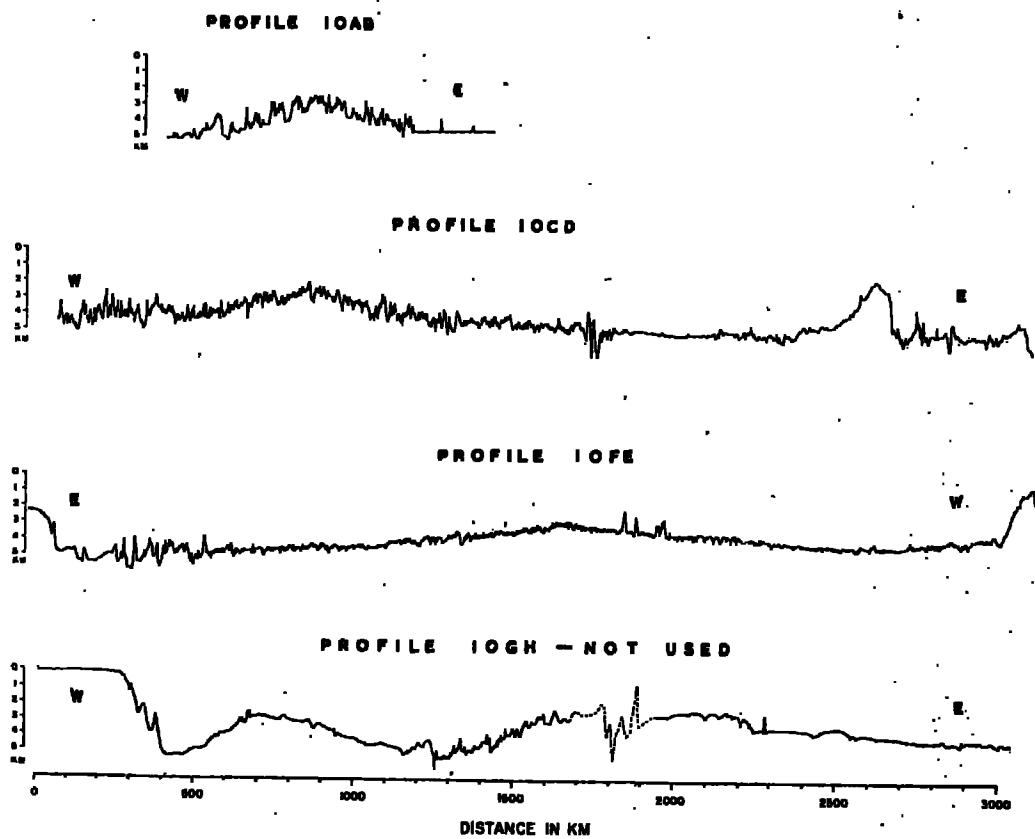


Figure 1.16. Bathymetric profiles from the Indian ocean. Refer to figure 1.15 for locations.



Figure 1.17. Sediment isopach map for the Indian ocean. Reproduced from Ewing, Eittrheim, Truchan and Ewing (1969). Contours in tenths of seconds two way travel time.

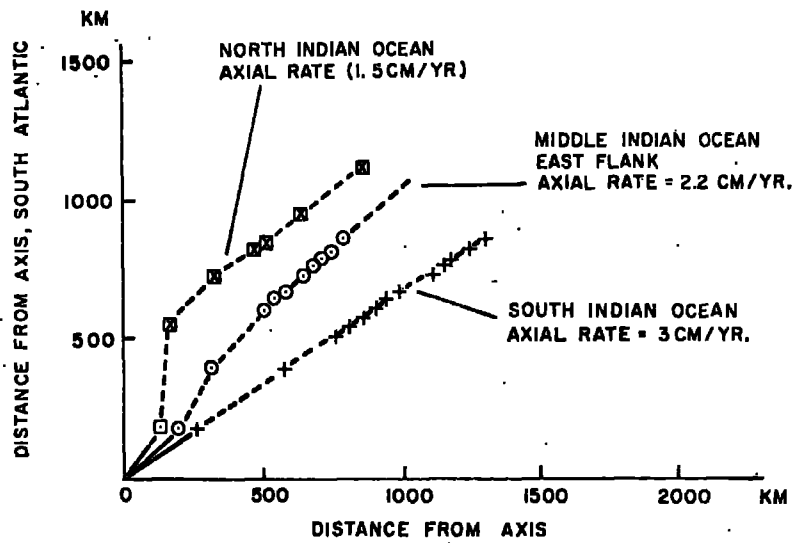


Figure 1.18. Distances to several magnetic anomalies in the Indian ocean compared with the distances to the corresponding anomalies in the South Atlantic. Reproduced from Le Pichon and Heirtzler (1968).

## Middle Indian Ocean, East flank, profile IOCD

Time B.P. (My)	Spreading rate (cm/y)
0 - 9	2.20
9 - 23	1.00
23 - 43	2.14

## South Indian Ocean, Eastern limb, profile IOFE

Time B.P. (My)	Spreading rate (cm/y)
0 - 43	3.00

## 1.5.4 Discussion

One available profile across the ocean ridge in the south west Indian ocean (Le Pichon and Heirtzler, 1968) was not used since the complexity of the structure in this region, which contains raised submarine plateaux and a major fracture zone, is outside the scope of the present model. Further discussion is given in section 5.3.

1.6 The Australia - Antarctic sea

## 1.6.1 Bathymetry

Data from three crossings of the Australia - Antarctic sea by the U.S.N.S. Eltanin were used in this work. The data have been published by Weissel and Hayes (1971) and are shown in figure 1.19. Figure 1.20 shows the locations of the profiles.

## 1.6.2. Sedimentary thickness and gravity

The profile EL45 (figure 1.19) falls within the area covered by the sediment isopach map of Ewing, Eittreim, Truchan and Ewing (1969) (figure 1.17). This map indicates that almost no sediment has been deposited to the north of the mid ocean ridge but that a substantial sedimentary cover may exist to the south.

BATHYMETRIC PROFILES IN THE AUSTRALIA-ANTARCTIC SEA

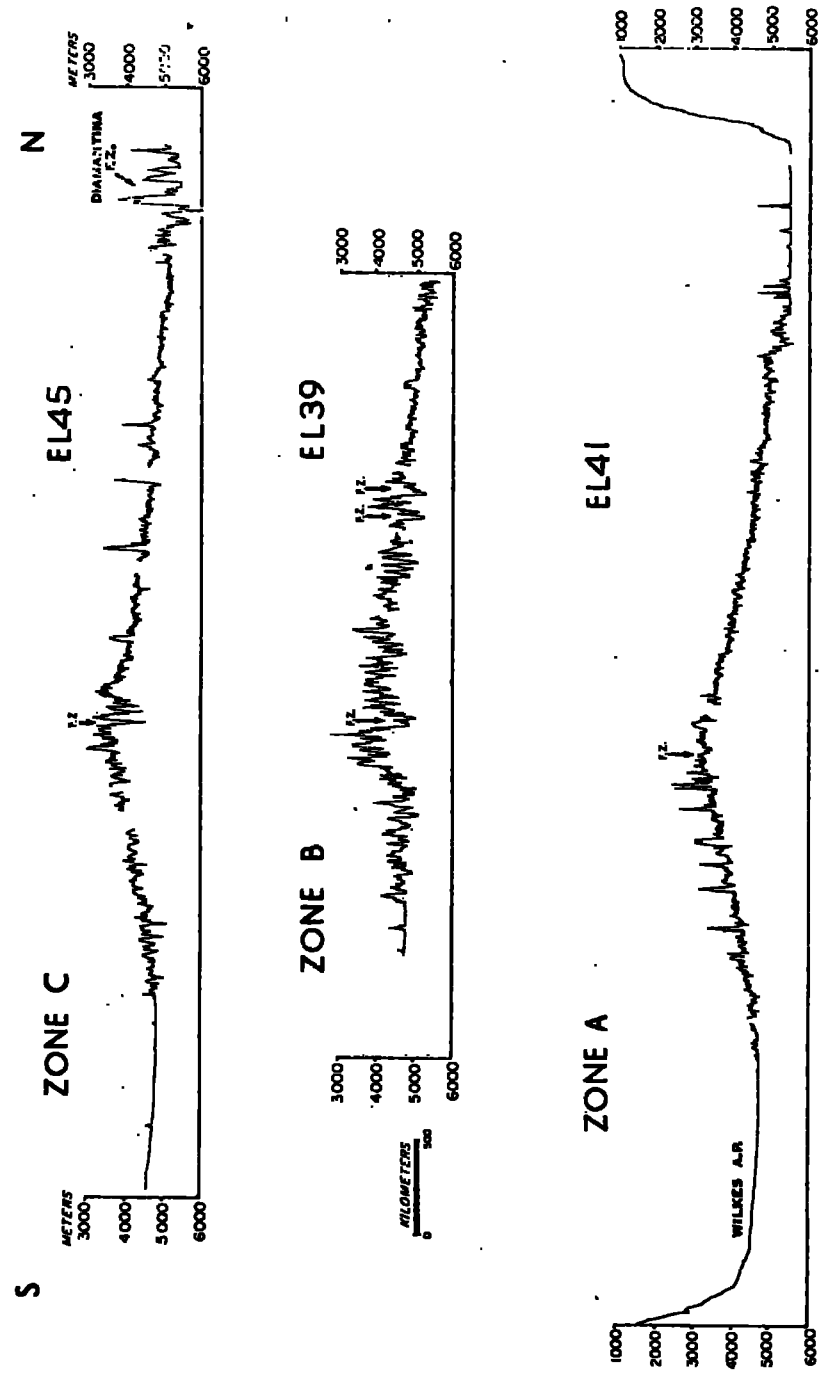


Figure 1.19. Bathymetric profiles in the Australia-Antarctic sea. Refer to figure 1.20 for locations. Reproduced from Weissel and Hayes (1971).

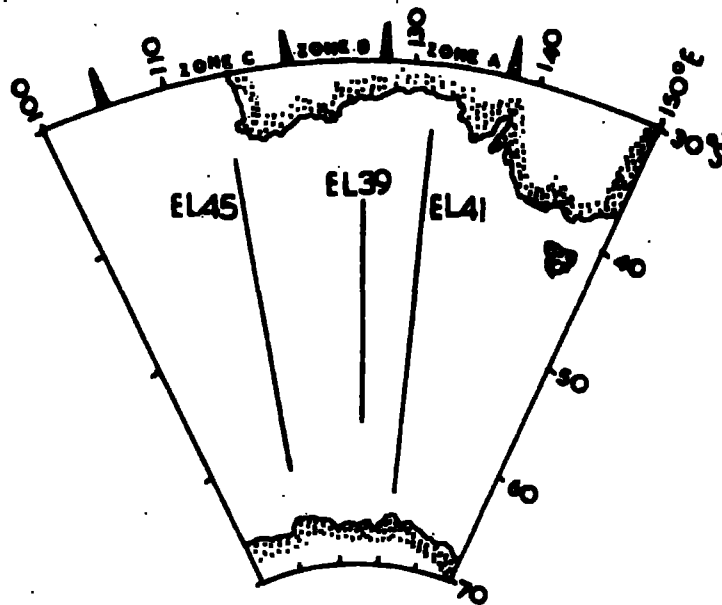


Figure 1.20. Map of the Australia-Antarctic sea showing the location of the bathymetric profiles which are used in this work, and also the zones into which Weissel and Hayes (1971) divided the area on the basis of seismicity (see section 1.6.4).

Further examination of the map suggests that this situation may extend eastwards across all three profiles. Accordingly, since no further sedimentary data was available, the study of these profiles was confined to their northern flanks, where errors due to the rather scanty supply of data are likely to be small. Once again only global free air gravity data was available.

### 1.6.3 Spreading rates

The magnetic anomalies in the Australia-Antarctic sea have been interpreted by Weissel and Hayes (1971) and indicate that sea floor spreading in this area may have occurred asymmetrically. The following values for spreading rates are taken from Weissel and Hayes and apply to the northern flank of the ridge.

Profile	Time B.P. (My)	Spreading Rate (cm/y)
EL41	0 - 10	3.60
	10 - 20	2.85
	20 - 38	3.11
	38 - -	2.35
EL39	0 - 10	4.54
	10 - 20	2.35
	20 - 38	2.63
	38 - -	2.36 - assumed
EL45	0 - 10	3.71
	10 - 20	2.69
	20 - 38	2.82
	38 - -	2.38

#### 1.6.4 Discussion

By studying earthquake distributions Weissel and Hayes (1971) identified three different zones within the Australia - Antarctic sea (figure 1.20), and the three profiles used in this work are each taken from a different zone. Profiles EL39 and EL45 (zones B and C) are from areas where seismic activity, greater in zone B than in zone C, indicates that offsets of the ridge axis occur, while EL41 is from the seismically quiet zone A. The classical shape of an ocean ridge, such as is displayed by EL41, is disturbed to such an extent in zone B that the above authors were only able to determine the position of the ridge crest on EL39 from the distribution of the earthquake epicentres. Possible effects of these considerations on the results are discussed in section 5.3.

### 1.7. The Pacific ocean

#### 1.7.1 Bathymetry

Three profiles in the south Pacific ocean were taken from published data obtained during cruises of the R.V. Vema and the U.S.N.S. Eltanin. Profile PV16 has been published by Pitman, Herron and Heirtzler (1968), while profiles EL28 and EL29 are contained in the Technical Report No. CU-1-72 which covers Eltanin cruises 28-32 and is published by the Lamont-Doherty Geological Observatory. The tracks of the ships are shown in figure 1.21 and the profiles themselves in figure 1.22.

#### 1.7.2. Sedimentary thickness and gravity

Seismic reflection data recorded simultaneously with the bathymetric profiles EL28 and EL29 are included in the Technical Report referred to above. According to this data, sediment is only present along these profiles in thicknesses of the order of 0.1 Km, which is insufficient to have an



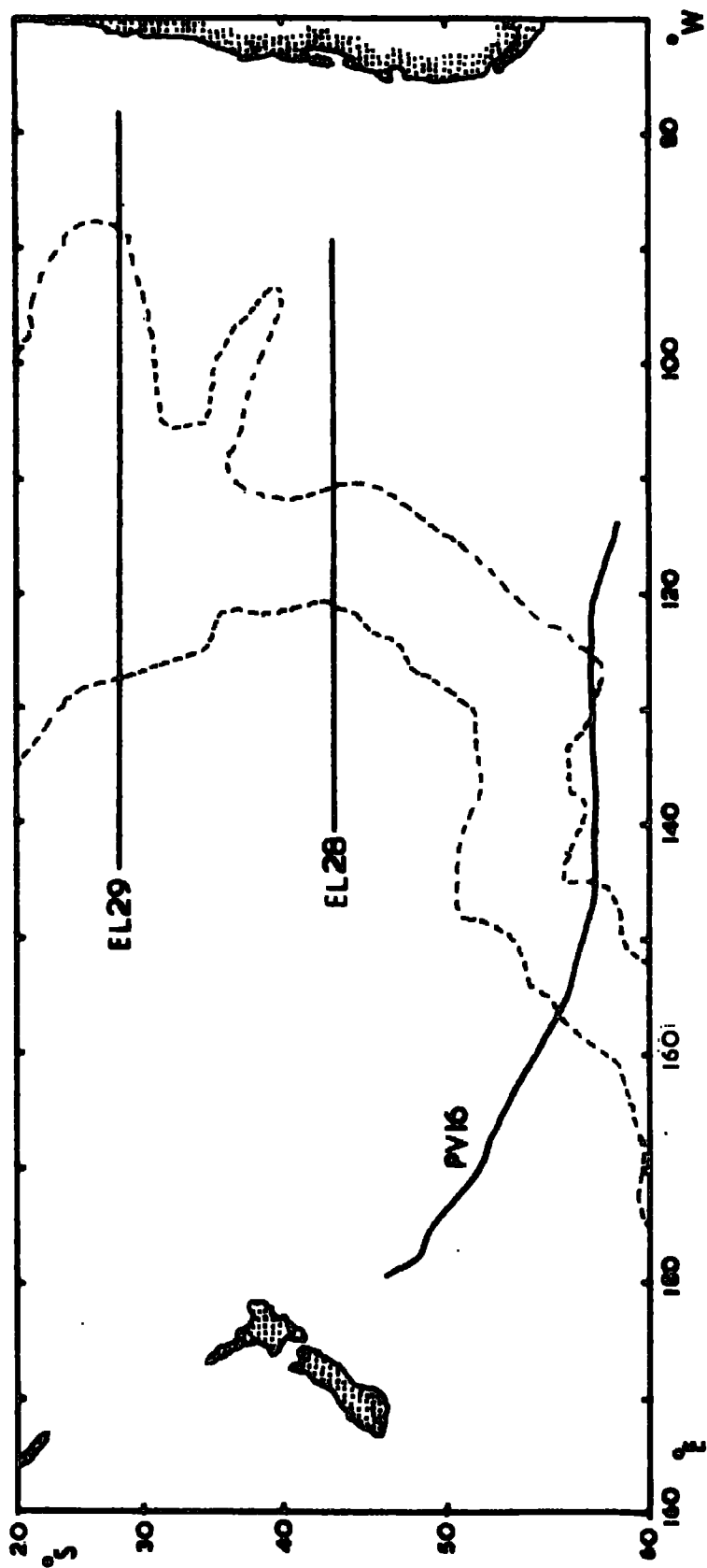


Figure 1.21. Map showing the location of the bathymetric profiles in the Pacific ocean which are used in this work. The 2000fm contour is shown by a dashed line.

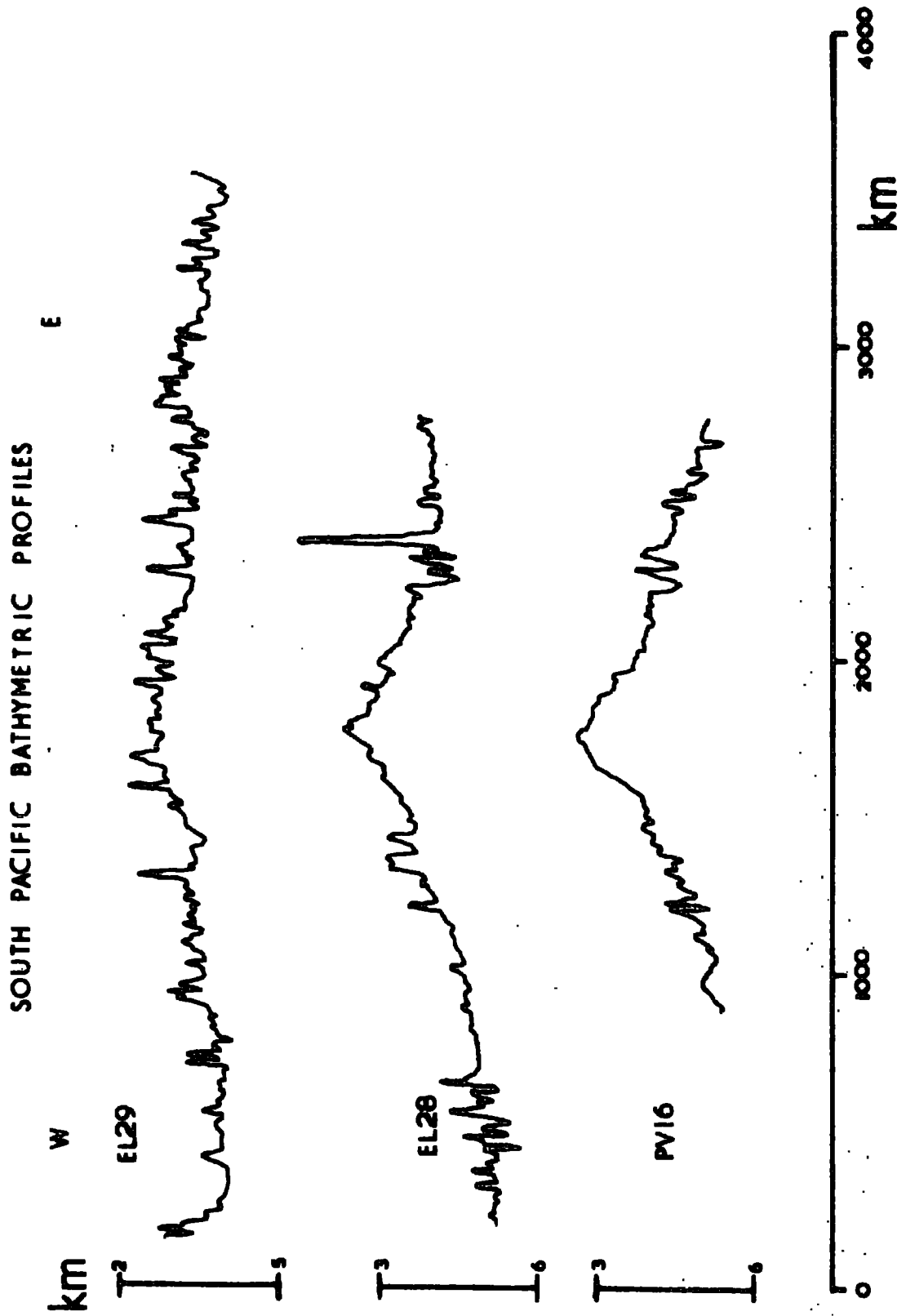


Figure 1.22. Bathymetric profiles from the Pacific ocean. Refer to figure 1.21 for locations.

appreciable effect on the results. A similar indication is given by the isopach map of Ewing, Houtz and Ewing (1969) which also covers profile PV16. Profiles EL28 and EL29 are also accompanied by gravity data, which, together with the global free air maps, once more confirm the presence of isostasy.

### 1.7.3. Spreading rates

Spreading rates for the profile PV16 were derived by plotting the relevant data from figure 8 of Pitman, Herron and Heirtzler (1968). Three episodes of spreading may be distinguished (figure 1.23) which correspond to the following rates:-

Profile	Time B.P. (My)	Spreading Rate (cm/y)
PV16	0 - 9	3.89
	9 - 62	1.63
	62 - -	4.29

Spreading rates for the profiles EL28 and EL29 were derived from the interpretation of magnetic anomalies given by Herron (1972). Figure 1.24 shows the anomalies identified by Herron plotted, in terms of age, against longitude. The following spreading rates are indicated by this data:-

Profile	Time B.P. (My)	Spreading Rate (cm/y)
EL28	0 - 9	3.61
	9 - 28	2.58
	28 - 53	4.24
	53 - 81	2.30
EL29	0 - 21	5.60
	21 - 27	12.30
	27 - 43	5.50
	43 - 81	2.58

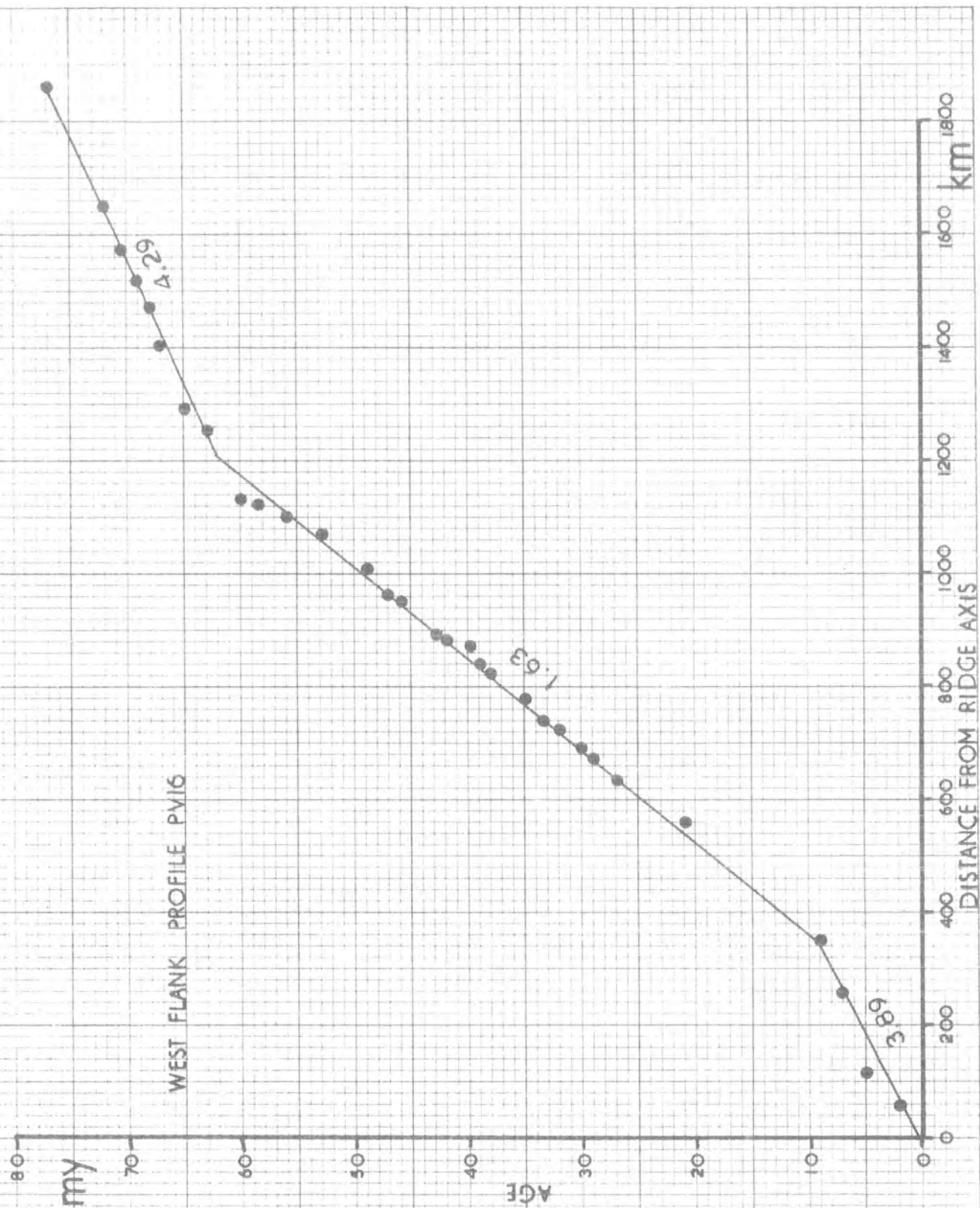


Figure 1.23. Magnetic anomalies along profile PVL6 plotted (in terms of age) against distance from the ridge crest. Data from Pitman, Herron and Heirtzler (1968). Spreading rates estimated from this data marked on the graph (cm/y).

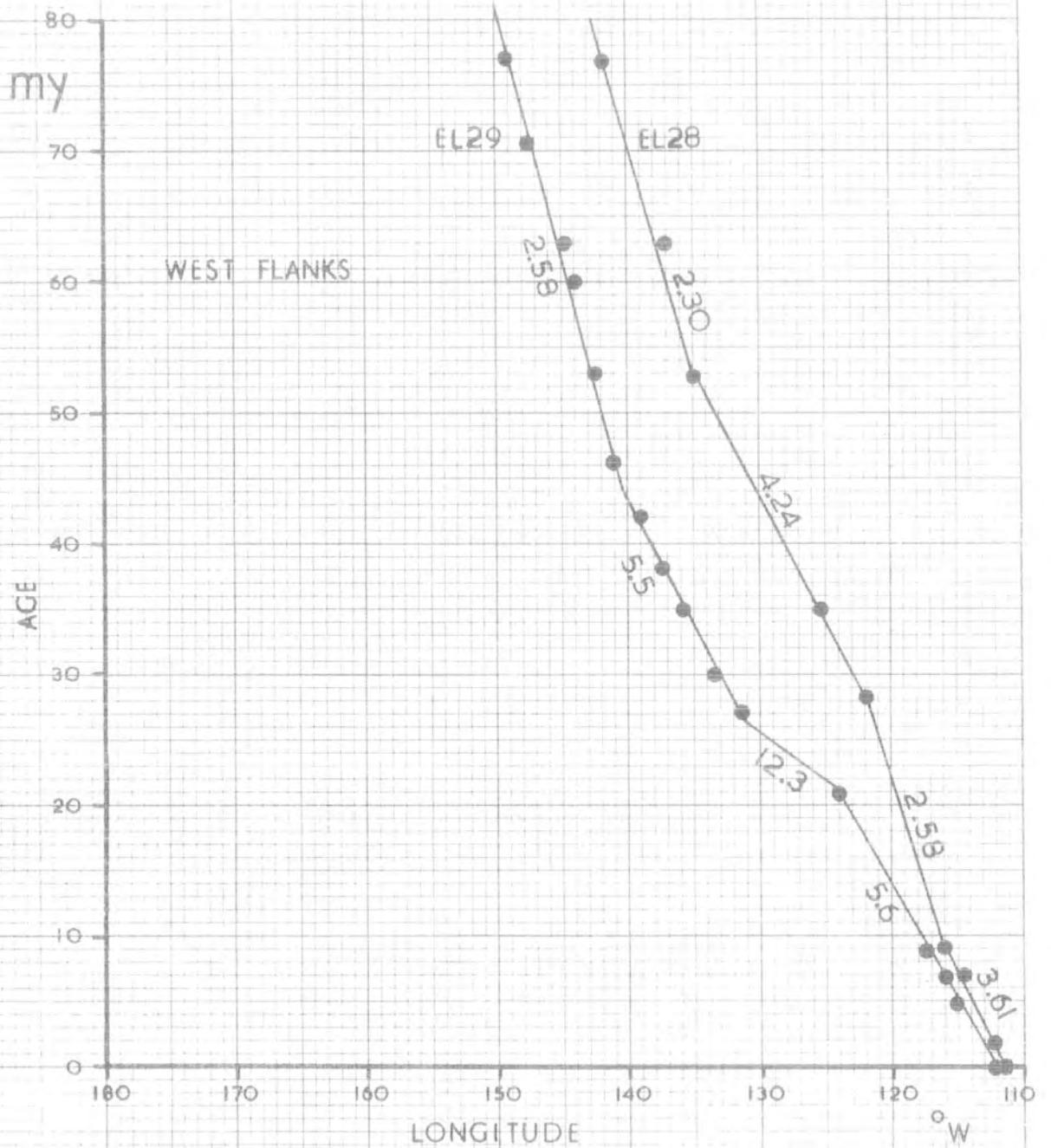


Figure 1.24. Magnetic anomalies along profiles EL28 and EL29 plotted (in terms of age) against distance from the ridge crest. Data from Herron (1972). Spreading rates estimated from this data marked on the graphs (cm/y).

#### 1.7.4. Discussion

The high spreading rates quoted above, particularly for profile EL29 require some explanation. Both EL28 and EL29 were collected along lines of constant latitude. Since the spreading direction is not parallel to this direction, these spreading rates are the effective values along the lines of the profiles and not the true rates of production of new lithosphere. Furthermore, the values quoted contain the effects of offsets of magnetic anomalies caused by transform faults and changes in the spreading regime (Herron, 1972). The figure of 12.3 cm/y between 21 and 27 My B.P. on EL29 is particularly prominent for these reasons.

Introduction to chapters 2, 3 and 4, with a review of previous work

In the following chapters, a model of sea-floor spreading, designed primarily to reproduce the dimensions of topographic profiles across ocean ridges, is described. The method is not new (see below), although the application of the model to the study of variations of structure parallel to the strikes of the ocean ridges is, to the best of my knowledge, a new departure.

The temperature distribution in a spreading lithospheric slab has been calculated by McKenzie (1967). He used analytically solved equations for a simple case requiring constant physical parameters and spreading rate, and no heat production within the lithospheric material. Sleep (1969) extended this work by calculating the topographic profile which would result from thermal contraction of the newly formed lithosphere, but he also dealt only with simple analytically soluble cases and included no allowance for possible mineralogical phase changes. Sclater and Francheteau (1970) added a further dimension by including internally generated heat in the calculations. In 1971, Forsyth and Press published the results of models based on numerical solution of the heat flow equations which incorporated all the above-mentioned features - variable physical parameters, internal heat production and consideration of mineral phase changes. The present models are similar to those of Forsyth and Press and also allow simulation of varying spreading rates. There is, however, a marked difference between the present work and that of previous authors as regards the consideration of lithospheric thickness. The practice of the authors mentioned above was to fix the lithospheric thickness and thus, according to the chosen criterion - usually the solidus of the proposed mantle material, the temperature at its base. The value of thermal conductivity was then adjusted to produce the correct heat flow at the sea floor. In contrast, in the present work the value of the thermal conductivity is taken from experimental data and the heat flow at the sea floor calculated as a by-product of the modelling procedure. The results show a remarkable constancy of heat flow for a

variety of lithospheric thicknesses (section 4.11), thereby indicating that surface heat flow is insensitive as a boundary condition. Furthermore, the lithospheric thickness is found to be one of the most important variables involved in fitting modelled topography to observed data, a point which is virtually unmentioned by previous authors.

In the present model, a numerical procedure based on the method of finite differences is employed to calculate the temperature distribution in a spreading lithospheric slab. This temperature distribution is then used to estimate the distribution of density within the slab, whence the topographic profile may be calculated. Since the procedures deal with digital data throughout, graphs and other data sets produced by the calculations contain minor steps and discontinuities which may be disregarded when interpreting the results.



## CHAPTER 2

Calculation of the temperature distribution in a spreading lithospheric slab2.1 The physical model

In common with the models of the authors mentioned above, the lithosphere is represented as a slab of uniform thickness resting isostatically on the asthenosphere. The bottom surface of the slab is assumed to be at the same temperature beneath the spreading centre, the ridge flanks and the ocean basin. New material at this temperature is added progressively to one end of the slab, gradually increasing its length. A given point in the slab thus moves away from the hot edge, effectively modelling sea floor spreading, the spreading rate being controlled by the rate of addition of material. The arrangement of the model is shown in figure 2.1.

Temperatures at the boundaries of the slab are specified as follows:-

1. Top surface of the slab

Since this surface represents the sea bed, the temperatures at all points on it are set to  $0^{\circ}\text{C}$ . (at the spreading centre dykes and lava flows may cause transient raised temperatures, but their effect is negligible in both spatial extent and time in a model of this type).

2. The base of the slab

This represents the surface on which decoupling of the asthenosphere and lithosphere occurs. Both the need for a mechanism for decoupling and the existence of the low velocity zone in the asthenosphere suggest that the mantle may be partially molten at this depth. Consequently the base temperature is defined to lie on the solidus of the mantle material and will therefore vary with the thickness of the lithosphere and the mantle composition postulated.

Figure 2.1. Diagram to illustrate the physical arrangement of the lithospheric model. Two stages of sea floor spreading are shown in the top sections. The shaded blocks are held at constant temperature to form the boundary conditions (marked in deg. C.). Dots show the positions at which temperatures are calculated. Typical isotherms calculated by the model are shown in the bottom section. Note the relative magnitude of the vertical and horizontal temperature gradients as indicated by this data.

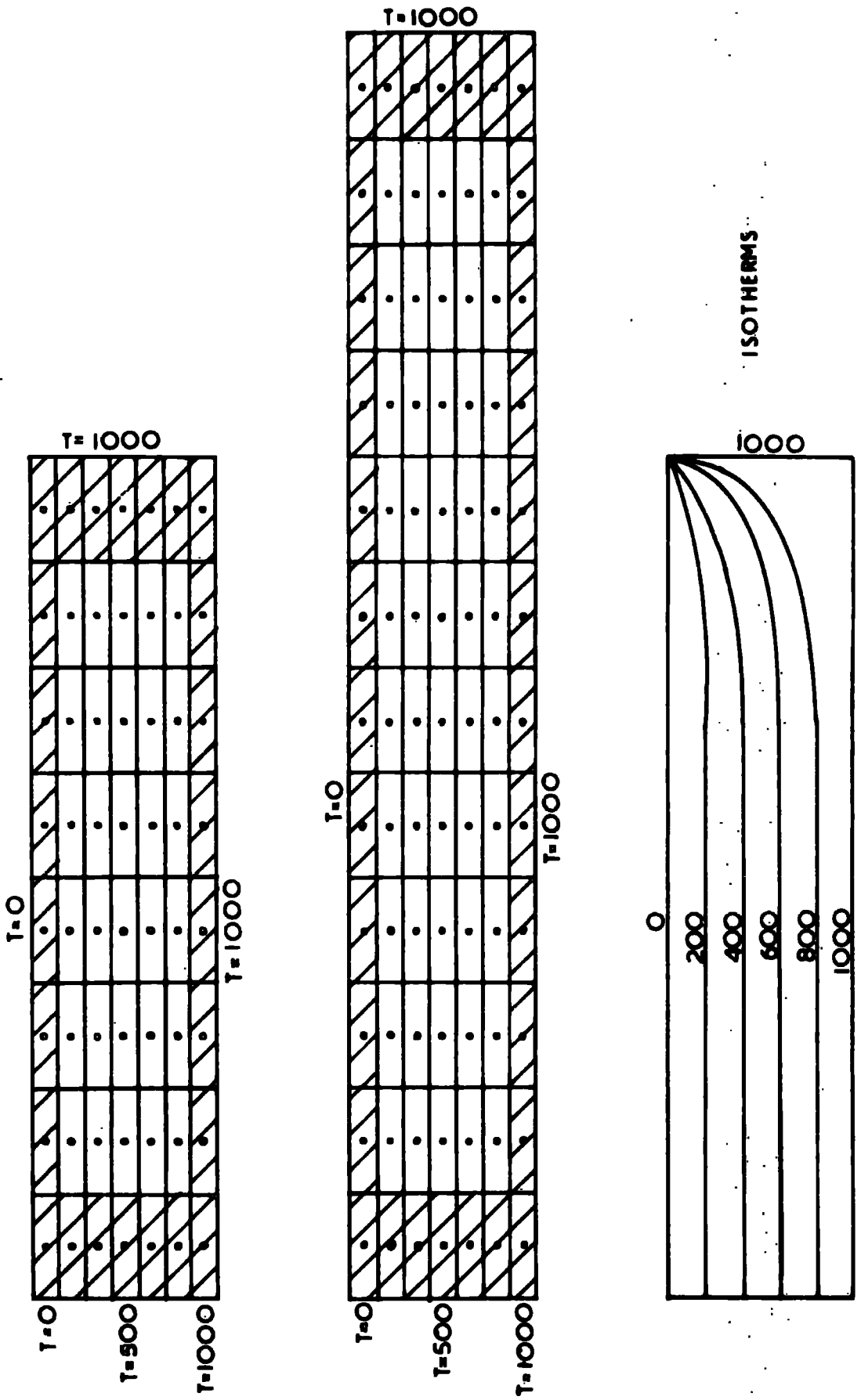


Figure 2.1.

It is to be expected that material rising from lower in the mantle to fill the space between the two separating plates will raise the asthenospheric temperatures under the spreading centre relative to those existing at the same depth under the ocean basins. The amount by which the temperatures are raised will depend on the spreading rate and the vertical dimensions of the convective movements associated with the upward flow of mantle material. Andrews (1972) has shown that, for a spreading rate of 1 cm/y, a convective cell penetrating to the mantle transition zone (350km) only causes the temperature under the ocean ridge at 100 km depth to exceed that at the same depth under the basins by about  $70^{\circ}\text{C}$  in 1300. The effect of this local variation is not taken into account in the above specification but the error incurred by defining the base temperature to lie on the solidus at all points along the slab is small. Discussion of the effect of greater degrees of local asthenospheric heating (such as would be expected over mantle hot spots) is given in section 6.2.1.

### 3. The ends of the slab

#### (a) the cool edge

The temperatures at the end of the slab remote from the spreading centre are set to lie on a linear geotherm between the adopted base temperature and  $0^{\circ}\text{C}$ .

#### (b) the hot edge

Temperatures at the hot edge of the slab are set equal to the adopted base temperature in order to model the rising of asthenospheric material. Adiabatic cooling of this material as it rises is estimated to be only  $30^{\circ}\text{C}$  over 100km (Sclater & Francheteau 1970) and is ignored.

Comments on the effects of these boundary conditions on the interpretation of the calculated topography will be found in appendix 6.

## 2.2 The Numerical Model

A two dimensional cross section of the slab is subdivided into rectangular blocks of uniform size, the centres of the blocks forming a grid of points at which temperatures (and subsequently densities etc.) may be calculated (figure 2.1.). The boundary conditions specified in section 2.1, above, are applied by holding constant the temperatures of the outer ring of blocks while allowing those of the inner blocks to vary. The method of finite differences is used to solve the differential equations involved in determining the temperature distribution in the slab, this being expressed in terms of the temperatures at the centres of the individual blocks. Spreading is achieved by adding new columns of blocks to the hot edge at time intervals calculated to reproduce the desired spreading rates. Variation of these time intervals allows simulation of changing spreading rates. As each new column is added it serves to provide the boundary condition at the hot edge of the slab and the temperatures of the preceding column are released to fall in accordance with the equations of heat flow set out below.

## 2.3 The Equations of Heat Flow

The general heat flow equation for a moving slab may be expressed as follows:-

(McKenzie 1967, p6264.)

$$\rho \sigma \left[ \frac{\partial T}{\partial t} + \mathbf{v} \cdot \nabla T \right] = K \nabla^2 T + \phi \quad (1)$$

where  $\rho$  = density,  $\sigma$  = specific heat,  $T$  = temperature,  $t$  = time,  $\mathbf{v}$  = velocity,  $K$  = thermal conductivity and  $\phi$  = heat production/unit vol. (due, in this case, to radioactivity in the lithosphere).

For a two-dimensional model  $\partial/\partial y = 0$ , and for sea floor spreading  $v_y = v_z = 0$  and  $v_x = v$  = spreading rate, where  $x$  is the horizontal distance perpendicular

to the ridge axis and  $z$  is the depth below the sea bed.

Equation (1) then becomes

$$\rho \sigma \left[ \frac{\partial T}{\partial t} + v \frac{\partial T}{\partial x} \right] = K \left[ \frac{\partial^2 T}{\partial x^2} + \frac{\partial^2 T}{\partial z^2} \right] + \phi \quad (2)$$

In the model under consideration spreading is achieved by extending the lithosphere at predetermined intervals between which it is considered to be stationary, the temperature distribution calculated at each step being used as the starting point for the next. The calculation is thus a succession of solutions for all of which  $v = 0$ .

If  $v = 0$  equation (2) becomes

$$\frac{\partial T}{\partial t} = \frac{K}{\rho \sigma} \left[ \frac{\partial^2 T}{\partial x^2} + \frac{\partial^2 T}{\partial z^2} \right] + \phi / \rho \sigma \quad (3)$$

In the block representation of this model the functions  $\partial^2 T / \partial x^2$  and  $\partial^2 T / \partial z^2$  may be expressed as

$$(T_L + T_R - 2T_C) / l^2 \quad \text{and} \quad (T_A + T_B - 2T_C) / h^2 \quad (4)$$

where  $T_C$ ,  $T_L$ ,  $T_R$ ,  $T_A$ , and  $T_B$  are the temperatures at the centres of a particular block (C) and those Left, Right, Above and Below it. Also  $l$  = length of the blocks and  $h$  = height of the blocks. More accurate expressions for estimating second derivatives of functions known only numerically have been derived for use in gravity interpretation (e.g. Elkins 1951). These involve the use of more than three points for each calculation and if employed in this model would lead to additional programming to counteract difficulties near the boundaries of the slab and slightly increased computer time. Since the model is designed to produce temperature distributions, and only requires the second derivatives for calculation purposes (in contrast to the gravity interpretation requirements), the simpler expressions (4) are used. The final temperature distribution is the product of

several hundreds of successive solutions of the equations and subject to the stability of the method (q.v. below) errors introduced at any stage to the temperature of a particular block by using inaccurate values for the second derivatives will be removed by subsequent stages.

Substituting (4) in (3) gives

$$\frac{dT_c}{dt} = \frac{k}{\rho\sigma} \left[ \frac{(T_L + T_R - 2T_c)}{l^2} + \frac{(T_A + T_B - 2T_c)}{h^2} \right] + \phi/\rho\sigma \quad (5)$$

Each block thus produces one first order differential equation. A computer program HEAT was written (appendix 5.) to solve the set of simultaneous equations resulting from the assembly of many blocks to form a lithospheric slab. Using the Runge-Kutta procedure, the equations are solved repeatedly for values of  $t$  which increase by finite increments.

#### 2.4 Values of physical constants and stability of the calculations

To account for variations due to the cooling of each block, in a rigorous manner, a continual adjustment of the model parameters, in particular the densities, should be made as part of an iterative procedure. Such a procedure would require large amounts of computer time and, in view of the relatively small adjustments involved, would not produce results differing significantly from those obtained by calculating the temperature distribution with fixed parameter values and subsequently estimating the densities and ridge elevation once only as the final step. Accordingly, the following values were used throughout the slab during the temperature distribution calculations:-

density  $3.35 \text{ g/cm}^3$

specific heat  $0.26 \text{ cal/g.}^\circ\text{C}$

(c.f. 0.25 of McKenzie (1967) and Sclater & Francheteau (1970),  
and 0.275 of Sleep 1969)

thermal conductivity  $0.006 \text{ cal/cm} \cdot \text{s} \cdot ^\circ\text{C}$

(Clark and Ringwood, 1964)

Some calculations were made with a thermal conductivity increasing above  $800^\circ\text{C}$  to  $0.016$  at  $1100^\circ\text{C}$  to test the effect of the temperature dependent conductivity suggested by these authors.

heat production  $30$  or  $60 \text{ cal} \times 10^{-8} / \text{g} \cdot \text{y}$  (dependent on composition). These figures are derived from the data for present day basalts given by MacDonald (1965), assuming the mantle to contain a basalt fraction.

latent heat of solid-solid and solid-liquid phase transitions was ignored.

#### Block dimensions and stability

A sufficient (though not necessary) condition for stability of the finite difference method applied to the equation

$$\frac{\partial^2 v}{\partial x^2} - \frac{1}{Q} \frac{\partial v}{\partial t} = 0$$

is that

$$Q\tau / \epsilon^2 \leq \frac{1}{2}$$

(Carslaw & Jaeger 1959)

where  $\tau$  is the time increment between successive solutions, and  $\epsilon$  is the increment of distance between successive values of the function  $v$ . For equation (5) (section 2.3 above), ignoring the heat production term

$$Q = K/\rho\sigma, \text{ and } \epsilon = h \text{ or } l$$

(block height or length)



In this model  $l/h$  is usually of the order of 5. Consequently the stability condition becomes

$$\frac{K\tau}{\rho\sigma} / h^2 \leq \frac{1}{2}.$$

(6)

The values chosen for the block height and the increment of time between successive solutions of the heat flow equations must therefore be such as to ensure that temperature calculations remain stable. A model in which the lithosphere is represented by an assembly of many blocks of finite width and height will, owing to the digitised nature of the calculations, produce stepped elevation profiles. In order to smooth these steps the block size should be as small as possible. However, the computer time required is directly related to the total number of blocks used to model the lithospheric slab, a greater number of smaller blocks requiring more time. Furthermore, the computer time is inversely proportional to the time increment  $\tau$  between successive solutions of the equations, and reference to equation (6) shows that  $\tau$  must be decreased as the block size is decreased if stability is to be maintained. Consequently a compromise must be reached between the desire for smooth elevation profiles and the need to avoid excessive computer time. In the present work the blocks are typically 3 to 5 km high and 15 to 25 km long, with time increments of 0.25 to 0.5 My.

### 2.5 Calibration of the temperature distribution calculations

Several test runs of the program HEAT were carried out in order to check the working of the method of deriving lithospheric temperature distributions described above, by adjusting each variable separately to observe its effect. In addition, the results were compared with the temperature distribution calculated for a simple case by McKenzie (1967) and gave good agreement (figure 2.2).

Figure 2.2. Lithospheric temperature distributions: comparison of the results of the present model with those of McKenzie (1967). Isotherms in identical lithospheres are shown, and good agreement is indicated.

— MCKENZIE (1967)

○ ○ ○ ○ ○ ○ THIS WORK

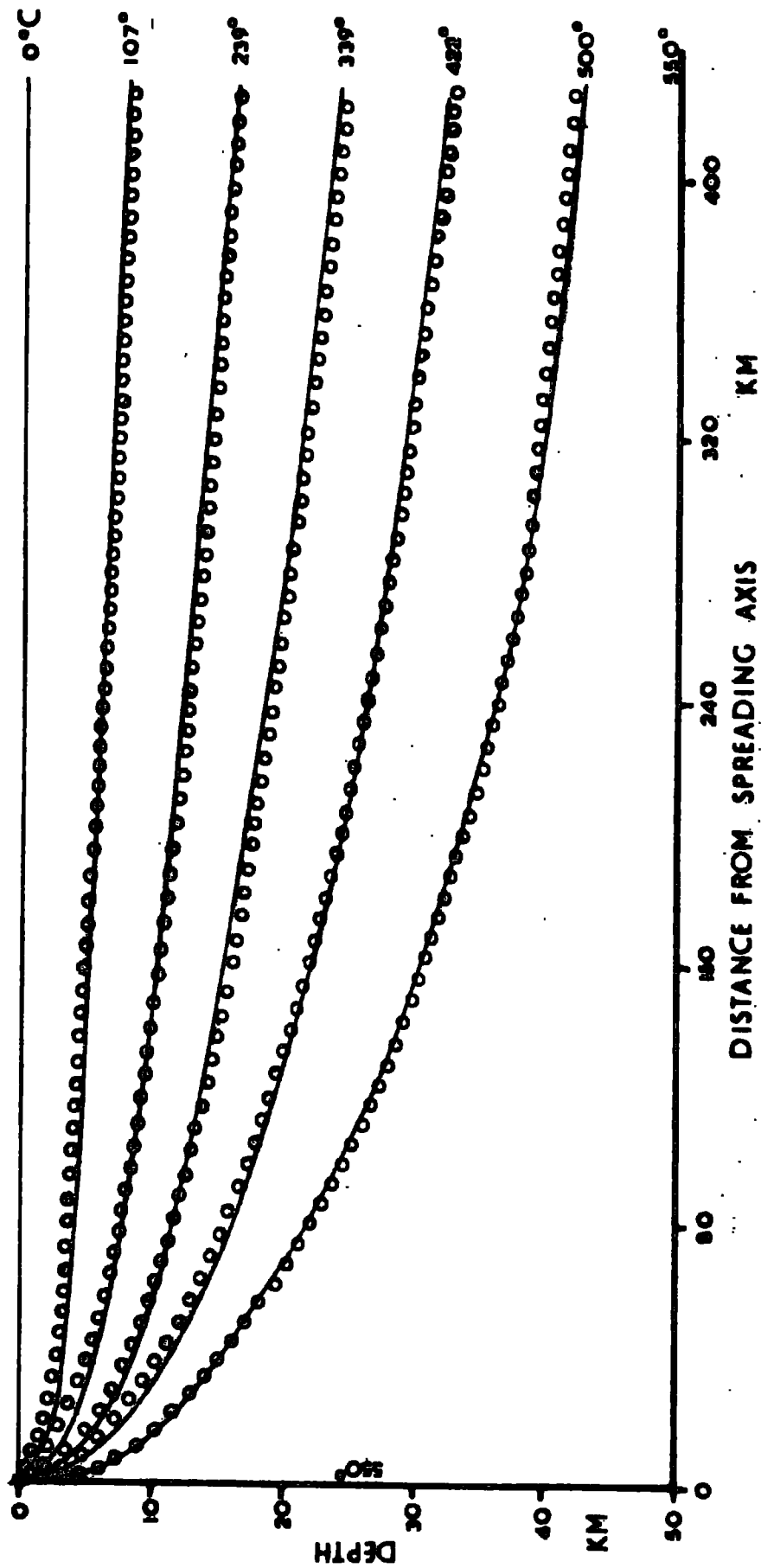


Figure 2.2.

The model was also used to calculate the geotherms which would exist in various thermally-undisturbed lithospheric slabs, including some composed of heat productive materials and others in which the conductivity varied with temperature. The results are shown, plotted with a theoretically derived geotherm, in figure 2.3, and good agreement with theory is again indicated. The derivation of the theoretical geotherm is given in appendix 1.

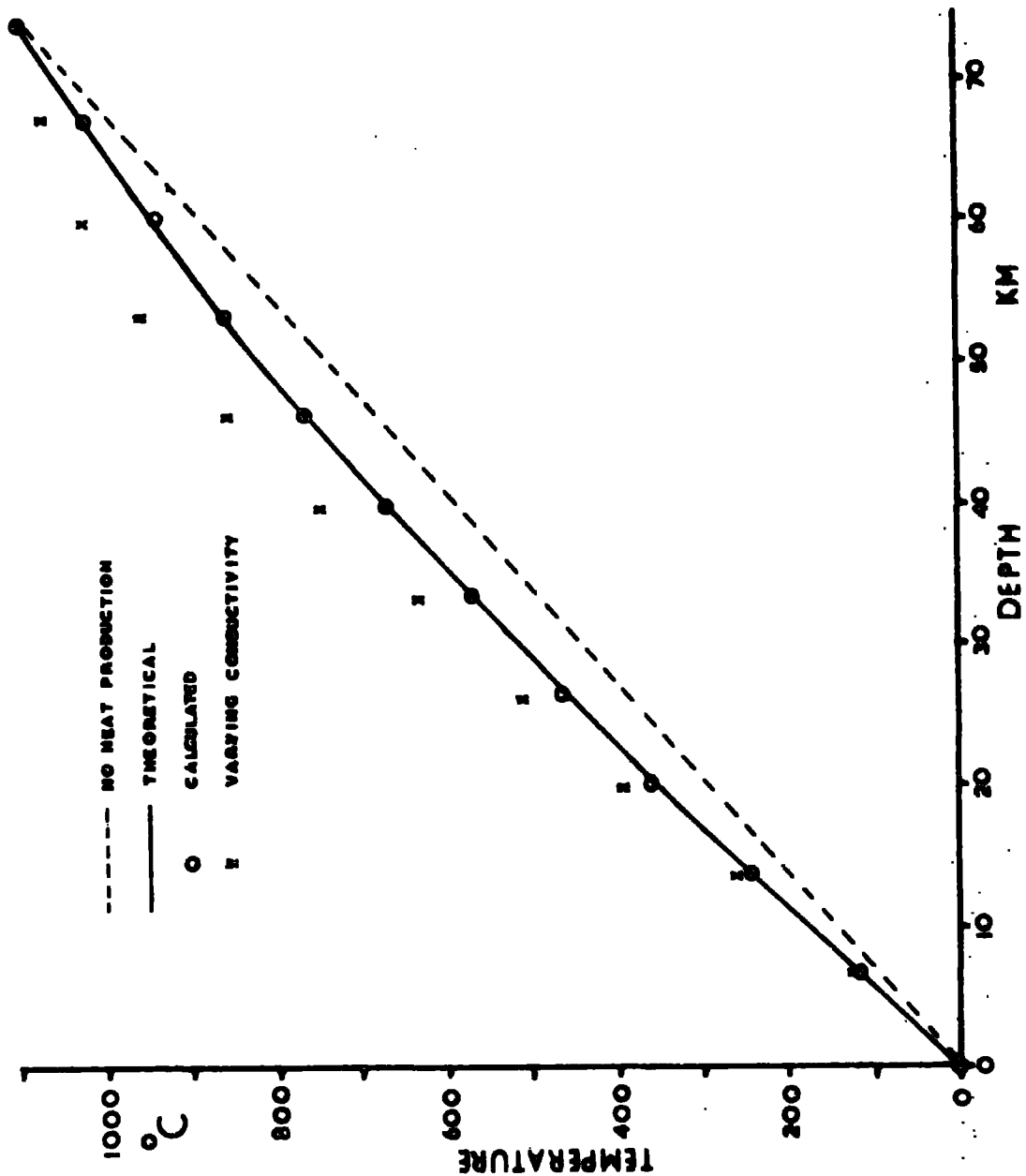


Figure 2.3. Equilibrium temperature gradients in theoretical and modelled lithospheres. The temperature gradient calculated by the present model to exist in a lithosphere with heat production  $60 \text{ cal} \cdot \text{cm}^{-3} \cdot \text{y}^{-1}$  is plotted with open circles. The continuous line is the theoretical geotherm calculated for an identical lithosphere according to the method set out in appendix 1. Good agreement is indicated. Also shown is the geotherm for a lithosphere in which the thermal conductivity increases above  $800^\circ\text{C}$  to  $0.016$  at  $1100^\circ\text{C}$  (plotted with crosses).

## CHAPTER 3

Composition and Mineral Assemblages of the Lithosphere3.1 Bulk Composition of the lithosphere

In order to derive an elevation profile from the temperature distribution in a model lithosphere it is necessary to know the density of the lithospheric material for an appropriate range of pressures, temperatures and mineral assemblages. The composition of the lithosphere is at present the subject of debate, a review of which will be presented in chapter 4 along with relevant conclusions from the model. At this stage it is sufficient to note that the compositions suggested range from peridotite to eclogite and that, in terms of bulk composition at least, these may be thought of as members of a continuous series of materials between dunite and eclogite, differing proportions of basaltic constituents relative to olivine being responsible for the variations of properties and nomenclature (summary in Ringwood, 1969). Furthermore, geochemical and petrological arguments (Ringwood, 1962a) and previous studies of ocean ridge topography (Forsyth & Press, 1971) limit the possible ranges of upper mantle compositions to mixtures between 1 part basalt + 3 dunite and 1 part basalt + 1 dunite. In addition, the mantle may contain small amounts of water (Ringwood, 1969; Green, 1970). In this chapter, the densities of the different mineral assemblages are investigated for a variety of compositions, these densities being calculated by considering the mantle material to be made up of a mixture of end members of the solid solutions of the minerals present. For example, plagioclase feldspars are considered as a mixture of albite,  $\text{NaAlSi}_3\text{O}_8$  and anorthite  $\text{CaAl}_2\text{Si}_2\text{O}_8$  even though in reality they might exist at many compositions between these extremes. The procedure is thus simplified without affecting the overall densities calculated for each mineral assemblage. An exception is that iron and magnesium are considered in terms of a single combined oxide since all the minerals relevant to

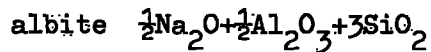
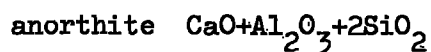
this work in which they occur are members of similar solid solutions. It is emphasized that this use of end members in no way implies that the upper mantle is actually composed of them but simply provides a straightforward way of calculating overall densities.

### 3.2 Relevant Minerals and Phase Changes

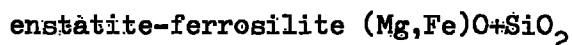
#### 3.2.1 Relevant Minerals

According to Green and Ringwood (1967) the following major minerals, expressed in terms of end members, may occur in the upper mantle in proportions depending on pressure, temperature and overall composition:-

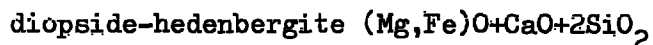
plagioclase (low pressures only)



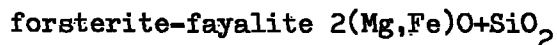
orthopyroxene.



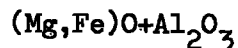
clinopyroxene



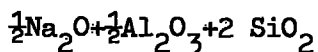
olivine



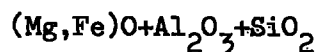
aluminous spinel (intermediate pressures only)



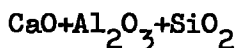
sodic aluminous pyroxene (intermediate and high pressure only)



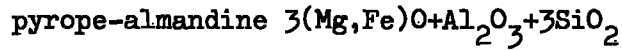
aluminous orthopyroxene (intermediate and high pressures only)



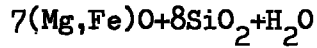
calcic aluminous clinopyroxene (intermediate and high pressures only)



garnet (high pressures only)



amphibole (in presence of water only)



The following table shows the molecular proportions of the different oxides present in each of the above minerals relative to  $24\text{SiO}_2$ , together with the molecular weights of the oxides.

Table 3.1 Mineral Compositions (Ratios of Oxides)

Minerals	Molecular Proportions					
	$\text{SiO}_2$	$(\text{Mg,Fe})\text{O}$	$\text{CaO}$	$\text{Al}_2\text{O}_3$	$\text{Na}_2\text{O}$	$\text{H}_2\text{O}$
olivine	24	48				
orthopyroxene	24	24				
clinopyroxene	24	12	12			
garnet	24	24		8		
calcic plag.	24		12	12		
sodic plag.	24			4	4	
sodic pyroxene	24			6	6	
alum. orthopx.	24	24		24		
alum. clinopx.	24		24	24		
alum. spinel		24		24		
amphibole	24	21				3
molecular wts.	60	(40,72)	56	102	62	18

### 3.2.2 Phase Changes

Several authors have investigated the phase transitions undergone by rocks containing the above minerals in the varying pressure/temperature conditions of the upper mantle (in particular, Green and Ringwood, 1967). The phase diagram



derived experimentally by Green and Ringwood forms the basis of figure 3.1, and indicates that, in the absence of water, three subsolidus mineral assemblages may occur:-

1. Low Pressurés  
olivine, pyroxenes, plagioclase.
2. Intermediate Pressures  
olivine, pyroxenes, aluminous pyroxenes, aluminous spinel.
3. High Pressures  
olivine, pyroxenes, aluminous pyroxenes, garnet.

The amount of garnet present in the high pressure region is dependent on temperature since the solubility of alumina in the pyroxenes increases with increasing temperature at a given pressure thus enabling aluminous pyroxenes to develop at the expense of garnet. Lines of constant alumina solubility ( and therefore of constant garnet content) from Green and Ringwood (1967) are marked on the garnet region of figure 3.1.

In the presence of water, amphibole forms from pyroxene throughout the pressure range. However, above about 1000°C amphibole is unstable, and the fluid released by its decomposition causes partial melting of the mantle material to occur at lower temperatures than are required for a non-hydrous composition (Wyllie, 1970; Green, 1970). The wet solidus and the 4% partial melting lines in figure 3.1 are from Green (1970). According to Ringwood (1969) the presence of water also inhibits large scale partial melting at temperatures immediately above the solidus, and this is indicated by the relative positions of the liquidus, wet solidus and 4% partial melting lines on figure 3.1. Consequently the formation of large and unstable magma bodies by small changes of temperature is prevented. Below the solidus the positions of the phase boundaries are unaffected by the inclusion of small amounts of water in the mantle material (Green, 1970). Ito and Kennedy (1971) have derived a phase diagram for the basalt-eclogite transformation, and this shows

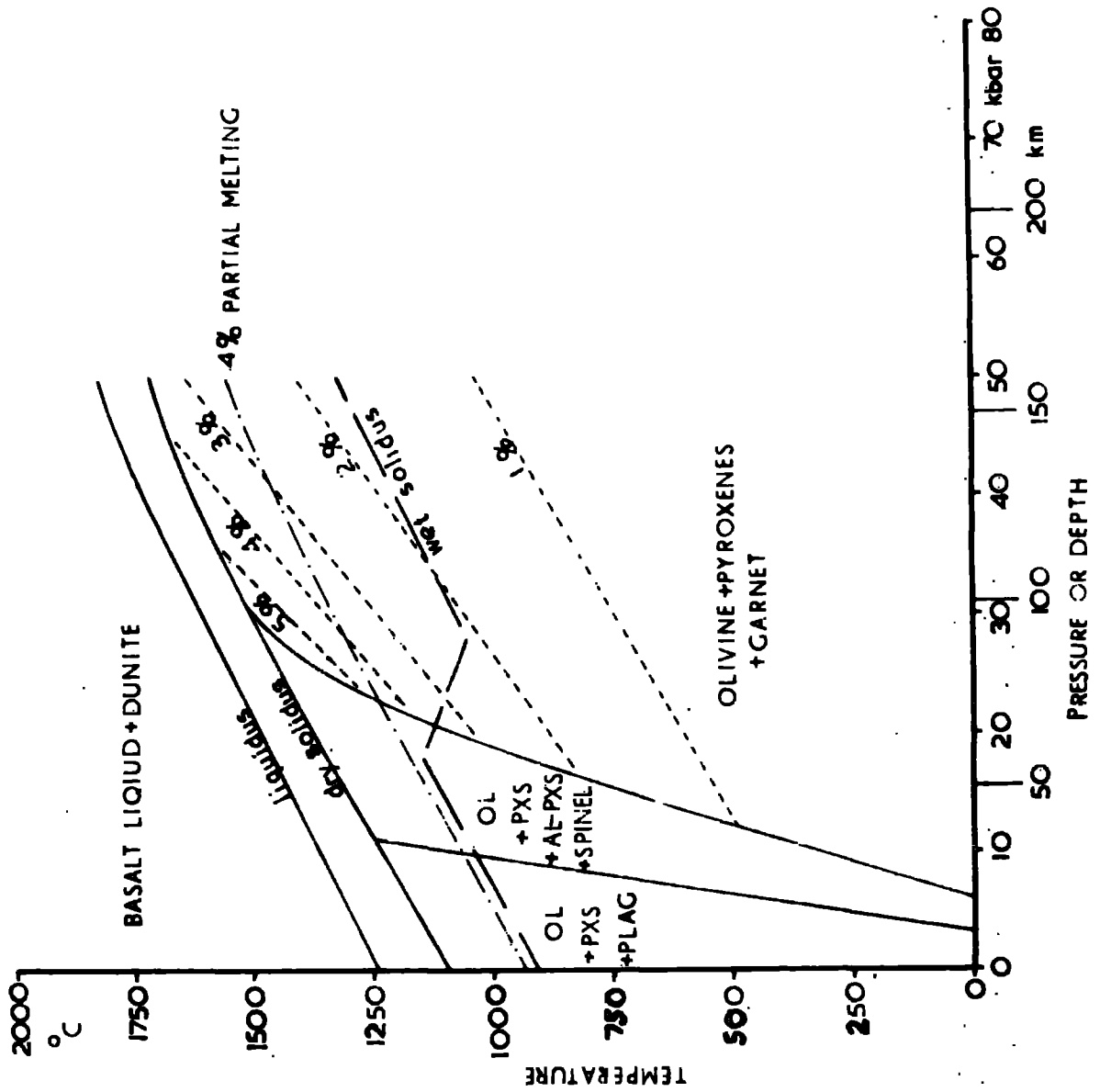


Figure 3.1. The phase diagram for a peridotitic upper mantle, based on Green and Ringwood (1967) and Green (1970). Lines of constant solubility of alumina in pyroxenes are shown dashed, and these are also lines of constant garnet content. The percentages refer to the alumina solubilities. OL=olivine, PXS=pyroxenes

many of the features which occur in the peridotite phase diagram of Green and Ringwood (1967) (figure 3.1) - e.g. the disappearance of plagioclase and the development of garnet with increasing pressure. The intermediate region containing aluminous pyroxenes and spinel which exists for peridotite has no counterpart in Ito and Kennedy's work. It is interesting to note that this region escaped Ringwood's attention initially (Ringwood, 1962a) and its importance was not realized until later (Ringwood, 1962b). However, apart from this factor only nomenclature distinguishes the two phase diagrams from each other.

The ratio of basalt to dunite in peridotites for which the phase diagram of figure 3.1 applies is not critical (Ringwood, 1969), whereas Ito and Kennedy's diagram applies to rocks in which the olivine proportion is small. Consequently, the diagram of Green and Ringwood (1967) was adopted for this work.

### 3.3 Mineral assemblages and Rock densities

#### 3.3.1 General

In this section, the relative proportions of each of the minerals present in the various assemblages are calculated from simple chemical equations based on the molecular proportions of the various oxides in the minerals. The densities of the assemblages are then calculated from the known densities and quantities of the individual minerals present.

Two bulk compositions are considered and these are equivalent to mixtures of:-

1. 1 part basalt to 3 dunite
2. 1 part basalt to 1 dunite

The relevant oxide percentages (by weight) are shown in table 3.2, the figures for basalt being from Ringwood and Green (1966).

Table 3.2 Rock Compositions

	SiO <sub>2</sub>	MgO	FeO	CaO	Al <sub>2</sub> O <sub>3</sub>	Na <sub>2</sub> O	Fe <sub>2</sub> O <sub>3</sub>	K <sub>2</sub> O	TiO <sub>2</sub>	total
Dunite (Fo <sub>90</sub> )	41.00	49.17	9.80							99.97
Basalt	48.71	9.37	9.91	10.76	14.93	2.09	1.84	0.30	1.52	99.43
1 b: 3 d	42.93	39.22	9.83	2.69	3.73	0.52	0.46	0.07	0.38	99.84
1 b: 1 d	44.86	29.29	9.86	5.38	7.47	1.05	0.92	0.15	0.76	99.70

(b = basalt, d = dunite)

When required, the effective molecular weight of a mixture of x gms MgO and y gms FeO is calculated as follows, using the molecular ratio:-

$$\text{Mol Wt (Mg,Fe)O} = (x+y)/(x/40+y/72)$$

40 and 72 being the molecular weights of the individual oxides.

### 3.3.2 Mineral proportions in the low pressure assemblage

The major minerals present are olivine, orthopyroxene, clinopyroxene and plagioclase (section 3.2.2). Some of the constituent oxides are present only in one mineral in this assemblage (e.g. TiO<sub>2</sub>, Na<sub>2</sub>O etc.). Consequently it is possible to calculate immediately the weights of the minerals containing these oxides which are present in a given weight of mantle material. The appropriate oxides are combined in the ratios given in table 3.1 and subtracted from the overall compositions given in table 3.2. This results in another oxide having only one further mineral to enter and thus allows the process to be repeated (e.g. Al<sub>2</sub>O<sub>3</sub> then CaO below). The

calculation eventually requires the solution of simultaneous equations to determine the relative quantities of different minerals containing the same oxides (e.g. olivine and orthopyroxene both containing  $(\text{Mg,Fe})\text{O}$  and  $\text{SiO}_2$ ). For the low pressure assemblage the steps are as follows:-

1. Minor Elements

Oxide	Mineral	Containing
$\text{TiO}_2$ -----	Rutile	Ti
$\text{Fe}_2\text{O}_3$ -----	Magnetite	$\text{Fe}^{++}$ , $\text{Fe}^{+++}$
$\text{K}_2\text{O}$ -----	Orthoclase	K, Al, Si

2. Sodium

$\text{Na}_2\text{O}$ -----	Albite	Na, Al, Si
-----------------------------	--------	------------

3. Remaining Aluminium

$\text{Al}_2\text{O}_3$ -----	Anorthite	Ca, Al, Si
-------------------------------	-----------	------------

At this stage the remaining weights of  $\text{MgO}$  and  $\text{FeO}$  are combined and the effective molecular weight of the mixture calculated as described in section 3.3.1. The calculation then proceeds:-

4. Remaining Calcium

$\text{CaO}$ -----	Clinopyroxene	Ca, $(\text{Mg, Fe}^{++})$ , Si
--------------------	---------------	---------------------------------

5. Two simultaneous equations are then formed to determine the relative amounts of

1. Orthopyroxene  $(\text{Mg, Fe}^{++})$ , Si and
2. Olivine  $(\text{Mg, Fe}^{++})$ , Si

The results are presented in section 3.3.7

### 3.3.3 Mineral proportions in the intermediate pressure assemblage

The major minerals present are olivine, orthopyroxene, clinopyroxene, sodic pyroxene, aluminous pyroxenes and spinel. A similar procedure is followed:-

## 1. Minor Elements

$\text{TiO}_2$ -----	Rutile	Ti
$\text{Fe}_2\text{O}_3$ -----	Magnetite	$\text{Fe}^{++}$ , $\text{Fe}^{+++}$
$\text{K}_2\text{O}$ -----	Sanidine	K, Al, Si

## 2. Sodium

$\text{Na}_2\text{O}$ -----	Sodic pyroxene	Na, Al, Si
-----------------------------	----------------	------------

At this stage four oxides--Si, (Mg,  $\text{Fe}^{++}$ ), Ca and Al, and six mineral phases remain. In order to form simultaneous equations to solve for further minerals it is necessary to reduce the number of independent variables, i.e. the number of independent mineral phases, present. According to experimental work by Green and Ringwood (1967) (in which sodic pyroxenes were considered separately), the solubilities of alumina in ortho- and clino- pyroxenes are similar. In addition, the proportion by weight of alumina in the pyroxenes commonly reaches a maximum of 6 $\frac{1}{2}$ % in the region of the phase diagram containing no plagioclase and no garnet. Making use of these results, it is assumed here that the proportions of aluminous to non-aluminous pyroxenes are such as to result in overall compositions in which alumina forms 6 $\frac{1}{2}$ % of the total pyroxene phases by weight (excluding sodic pyroxene). Four simultaneous equations may then be formed to solve for the remaining minerals. The results are given in section 3.3.7.

## 3.3.4 Mineral proportions in the high pressure assemblage

The major minerals present (section 3.2.2) are olivine, orthopyroxene, clinopyroxene, aluminous pyroxenes and garnet. The balance between garnet and aluminous pyroxenes is dependent on temperature (section 3.2.2) and gives rise to a range of assemblages between two extremes:-

- a) No garnet - equivalent to the intermediate pressure assemblage at the phase boundary.
- b) No aluminous pyroxenes, maximum garnet.

The calculation for (a) is that of the previous section. Consequently only the calculation for (b) remains to be described. The method is as follows:-

1. Minor Elements

$TiO_2$ -----	Rutile	Ti
$Fe_2O_3$ -----	Magnetite	$Fe^{++}$ , $Fe^{+++}$
$K_2O$ -----	Sanidine	K, Al, Si

2. Sodium

$Na_2O$ -----	Sodic pyroxene	Na, Al, Si
---------------	----------------	------------

3. Remaining Aluminium

$Al_2O_3$ -----	Garnet	(Mg, $Fe^{++}$ ), Al, Si
-----------------	--------	--------------------------

4. Remaining Calcium

$CaO$ -----	Clinopyroxene	Ca, (Mg, $Fe^{++}$ ), Si
-------------	---------------	--------------------------

5. Two simultaneous equations are then formed to determine the amounts of orthopyroxene and olivine present (both containing (Mg,  $Fe^{++}$ ), Si). The results are presented in section 3.3.7.

### 3.3.5 Mineral proportions in assemblages including water

The effect of water on the subsolidus mineral assemblages is dependent on the quantity postulated to be present. Estimates based on the relative degassing of nitrogen and water from the mantle (Ringwood, 1969; Green, 1970) suggest that water might be present in amounts of the order of 0.1%. This water would be held mainly as amphibole formed in place of pyroxenes, with small amounts of phlogopite perhaps being present.

Amphibole derived from orthopyroxene has a composition equivalent to  $7(Mg, Fe)O + 8SiO_2 + H_2O$ . Calculated according to this formula, 0.1%  $H_2O$  would give rise to 5% amphibole. Calculations for the inclusion of water in clinopyroxenes give a similar result. The effect of this amount of amphibole on upper mantle densities is small and is discussed in section 3.3.8.

### 3.3.6 Calculation of mineral and rock densities at R.T.P.

The results of the four previous sections provide the percentage by weight of individual minerals in each assemblage. Knowing the densities of the minerals, the volume of each in a given weight of material may be calculated. The sum of these volumes for all the minerals, together with the weight of material in question, then provide the overall density of the assemblage.

The densities of individual mineral phases (at room temperature and pressure) are taken from Deer, Howie and Zussman (1966) and are shown in table 3.3.

Table 3.3 Mineral Densities (Source - Deer, Howie and Zussman (1966))

Mineral	Experimental Densities g/cm <sup>3</sup>	Ferro-magnesian minerals: densities for mixtures of basalt and dunite in ratios:	
		1:3	1:1
olivine	3.22-4.39	3.33	3.39
orthopyroxene	3.21-3.96	3.30	3.33
clinopyroxene	3.22-3.56	3.26	3.28
garnet	3.58-4.32	3.67	3.70
anorthite	2.76		
albite	2.63		
sodic pyroxene	3.40		
alum. orthopx.	2.97-3.52	3.04	3.06
alum. clinopx.	2.97-3.52	3.05	3.08
alum. spinel	3.55-4.40	3.66	3.68
amphibole	3.02-3.45	3.11	3.13
orthoclase	2.59		
rutile	4.23		
magnetite	5.20		
sanidine	2.60		





# PYROXENE DENSITIES $g/cm^3$

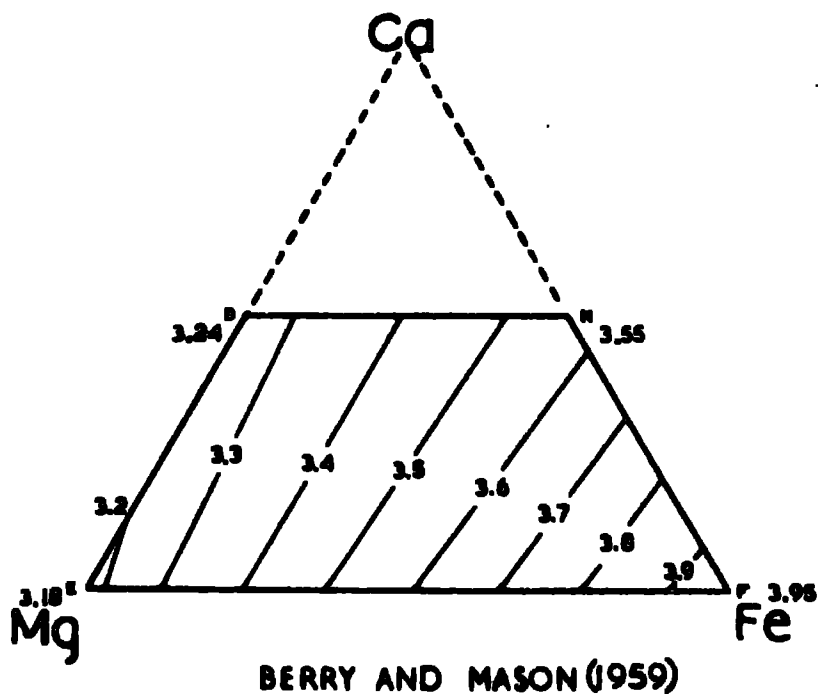
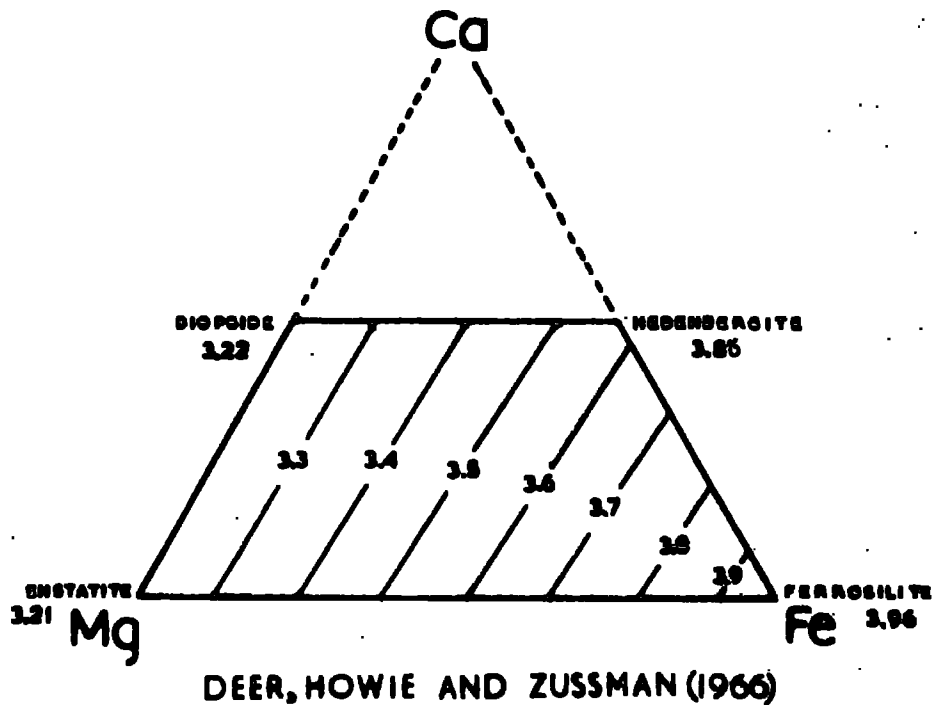


Figure 3.2. Diagrams to show the effect of iron content on mineral densities, in this case pyroxenes. The data of Deer, Howie and Zussman are more recent.

The densities of the different mineral assemblages for each of the bulk compositions considered were calculated as described in this section and the results are shown in table 3.4.

Table 3.4 Rock Densities (at room temperature and pressure)

Composition	Low Pressures	Intermediate Pressures	High Pressures
Basalt:Dunite	g/cm <sup>3</sup>	g/cm <sup>3</sup>	g/cm <sup>3</sup>
1:1	3.19	3.35	3.45
1:3	3.24	3.32	3.36

### 3.3.7 Bulk density variations and mineral assemblage

The relative abundance of the various mineral phases calculated by the procedures described in the previous sections for each of the assemblages are presented diagrammatically in figure 3.3. This figure includes the calculated bulk densities of the different mineral assemblages. The following division of minerals in terms of density and abundance may be made, the two densities quoted for the ferromagnesian minerals corresponding to the two bulk compositions considered:-

Density g/cm <sup>3</sup>	Major Constituents	Minor Constituents
High	Garnet 3.67 or 3.70	Aluminous spinel 3.66 or 3.68
Intermed.	Olivine 3.33 or 3.39	
	Orthopyroxene 3.30 or 3.33	
	Clinopyroxene 3.26 or 3.28	
	Sodic pyroxene 3.40	
Low	Calcic plagioclase 2.76	Aluminous clinopx. 3.04 or 3.06
	Sodic plagioclase 2.63	Aluminous orthopx. 3.04 or 3.05
		Amphibole 3.11 or 3.13

Figure 3.3. Mineral proportions in peridotites of the overall compositions indicated, subject to various conditions of temperature and pressure (refer to figure 3.1). The corresponding overall densities are plotted above the diagrams. Shaded areas represent aluminous minerals. OL=olivine, HY=hypersthene, DI=diopside, CP=anorthite, SP=albite, AH= aluminous orthopyroxene, AD=aluminous clinopyroxene, S=spinel, J=sodic pyroxene, GT=garnet, X=others.

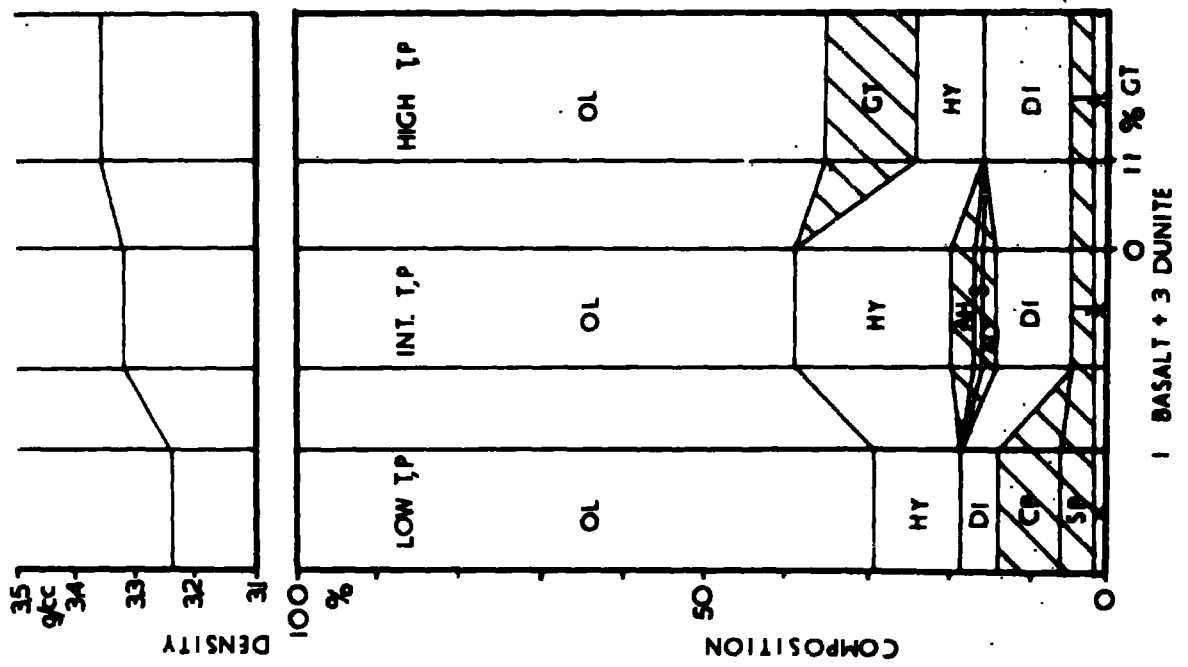
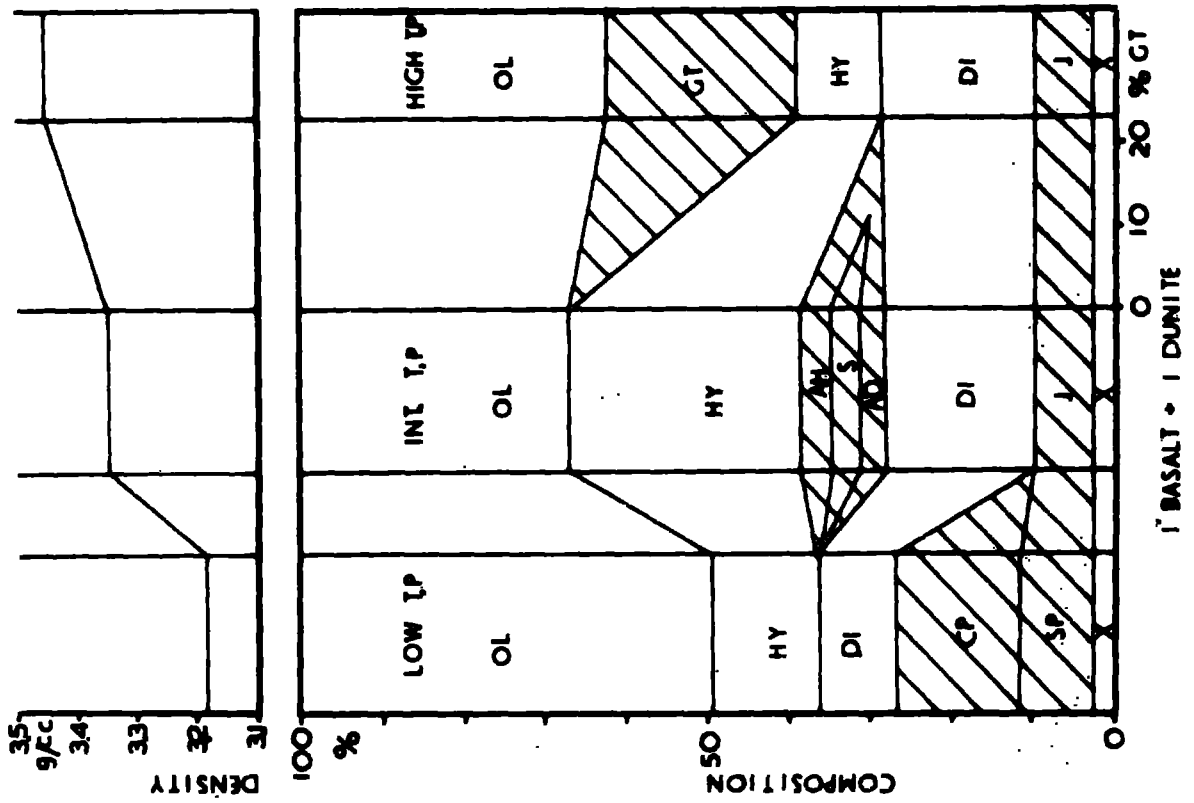


Figure 3.3.

In all the assemblages, olivine and pyroxenes together account for at least 70% of the total composition. In the intermediate pressure range, the effect on overall densities of small and similar quantities of spinel (high density) and aluminous pyroxenes (low density) effectively cancel out, so that the densities of the relevant assemblages are equal to those of olivine and pyroxenes in appropriate proportions. Consequently it is convenient to regard the differences of density between the assemblages which exist at different pressures in terms of deviations from the densities given in table 3.4 for the intermediate pressure region:-  
 $3.32 \text{ g/cm}^3$  for a 1:3 basalt:dunite composition and  $3.35 \text{ g/cm}^3$  for a 1:1 mix.

In the low pressure region, the existence of plagioclase (low density) causes the bulk density of the assemblage to fall to  $3.24$  or  $3.19 \text{ g/cm}^3$  according to the composition; in the high pressure region, the existence of garnet (high density) raises the assemblage density to  $3.36$  or  $3.45 \text{ g/cm}^3$ .

A feature of these high and low density minerals is that they contain aluminium. Areas representing aluminous minerals in figure 3.3 have been shaded, and it is clear that it is the changes of mineralogy associated with the alumina content of the mantle rock which are responsible for the density variations that occur under the varying conditions of temperature and pressure encountered in the lithosphere. Basalt contains alumina while pure dunite does not (table 3.2). Consequently the density variations in a given lithospheric slab, and thus the bathymetric amplitude of the associated mid-ocean ridge (see chapter 4), are directly related to the proportion of basalt present in the lithospheric material, in increase in the basalt fraction producing an increased topographic elevation and vice versa. This conclusion is in agreement with the results of Forsyth & Press (1971) and demonstrates that the peridotitic and eclogitic models for the upper mantle differ, in this respect at least, only in degree.

### 3.3.8 The effect of water on rock densities

In section 3.3.5 it was stated that the quantities of water suggested to exist in the upper mantle (0.1% H<sub>2</sub>O) would result in approximately 5% amphibole being present in the lithosphere. Reference to table 3.3 shows that the density difference between amphibole and the pyroxenes which it replaces is of the order of 0.2 g/cm<sup>3</sup>. 5% amphibole would therefore result in a lowering of overall densities only by about 0.01 g/cm<sup>3</sup>.

Above approximately 1000°C amphibole decomposes, the fluid thus released precipitating some partial melting (Green, 1970; Wyllie, 1970). As the lithosphere cools the amount of partial melt present in a given column of the lithosphere decreases and a corresponding increase in the amount of amphibole present takes place. However, since the presence of both amphibole and small amounts of partial melting cause slight lessening of overall densities, the formation of one at the expense of the other produces a negligible change in the topographic elevation.

The important effect of the inclusion of water in the mantle is the lowering of the temperature at which partial melting begins (figure 3.1). This allows the decoupling of the asthenosphere and lithosphere to take place at lower temperatures than are required for a dry mantle and, together with the stabilisation of partial melting noted in section 3.2.2, results in a lessening of the calculated amplitude of ocean ridge elevation profiles.

### 3.3.9 Bulk density variations at temperatures above the solidus

Experimental work by Dane (1941) indicates that basalt undergoes a reduction of density of 9% on melting. It is assumed in this work that the total melting of the basalt fraction of a particular basalt/dunite mix results in a proportionate density

reduction (i.e. 4.5% for a 1:1 mix, 2.25% for a 1:3 mix) and the density of the olivine+basaltic liquid phase is calculated according to these figures. Densities corresponding to the region between the solidus and liquidus of the basalt fraction are calculated by interpolating between the relevant values for material above and below this region of the phase diagram.



## CHAPTER 4

Calculation of Ocean Ridge topography, and general results and conclusions  
from the model

The previous two chapters have described the procedure used to calculate a) the temperature distribution in a model lithosphere, and b) the densities (at room temperature and pressure) of appropriate mineral assemblages of the adopted mantle material. In this chapter the method of determining oceanic topography from these two sets of data is described and some preliminary results are noted.

4.1 Method

The following procedure is repeated for each block of the lithospheric model:-

1. The pressure at the centre of the block is calculated from the block height used in the temperature calculations and the position of the block in the model, using 150 km depth = 47 kbar (This relationship is that used by Green and Ringwood (1967) to produce the phase diagram of figure 3.1).
2. The mineral assemblage present at the temperature and pressure of the block is then referenced using the phase diagram, and its density at room temperature and pressure is determined from the results of chapter 3.
3. The above density is then adjusted to account for compression and thermal expansion relative to room conditions. For this calculation, the material is assumed to behave as olivine - an approximation which is considered good by Birch (1969), since pyroxenes in particular have similar elastic constants to olivine. Relevant data from Birch (1969, table 8) are plotted in figure 4.0 and show linearity at depths less than 150 km. Appropriate coefficients may therefore be derived from this data and correspond to a bulk modulus of 1.16 mbar, and a volume coefficient of thermal expansion of  $4 \times 10^{-5}/^{\circ}\text{C}$ .

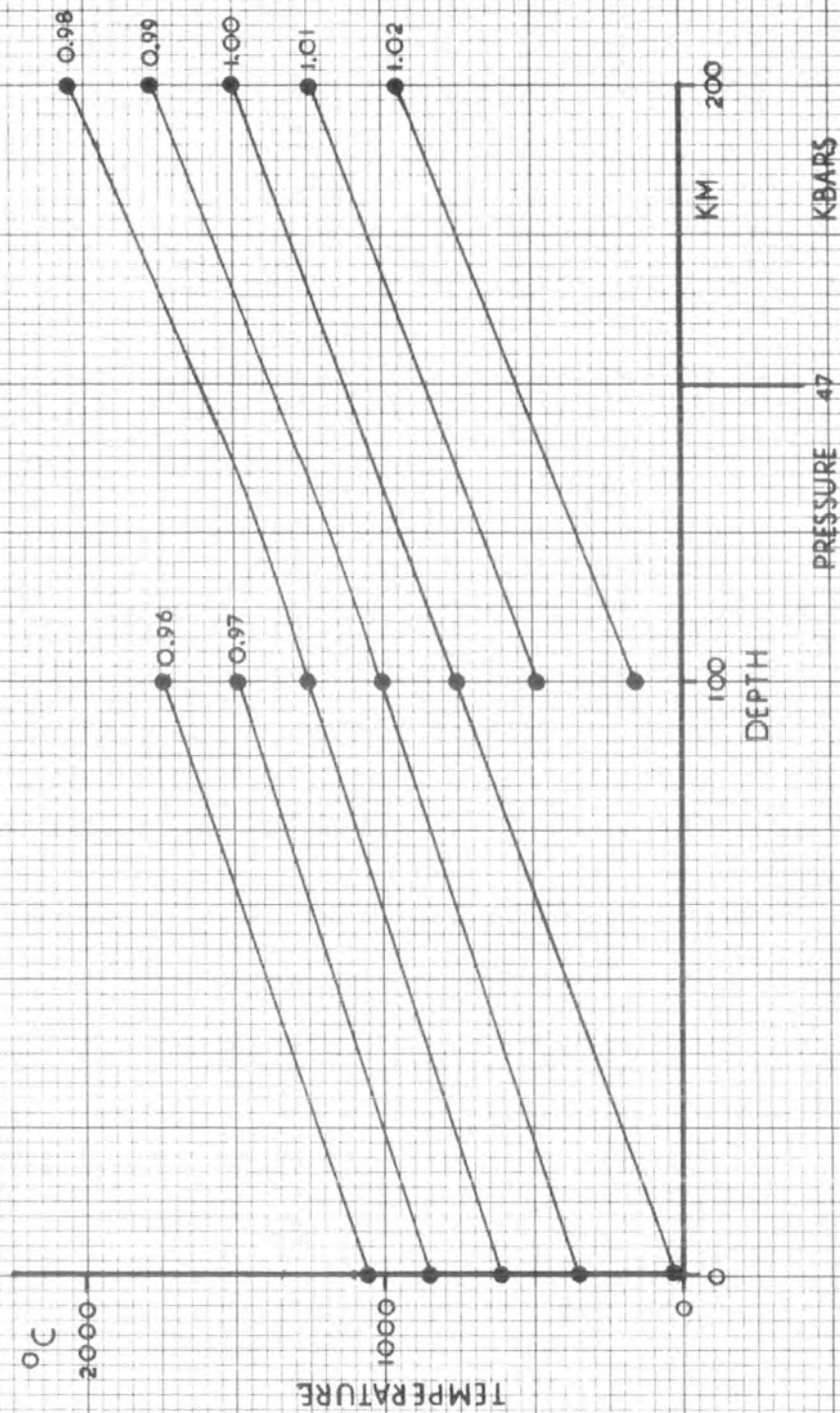


Figure 4.0. The density of olivine as a function of temperature and pressure. Lines along which the value of the ratio  $\rho_{T,p} / \rho_{25,0}$  is constant are shown, with the values of the ratio marked. Data from Birch (1969).

Having thus determined the density distribution in the model lithosphere, the topographic elevation may be calculated by comparing the densities of each column of blocks with those of the column at the end of the slab remote from the spreading centre. In order for the slab to be in isostatic equilibrium, the total mass in each column of blocks must be equal. Consequently, for each column:-

$$\sum_{i=1}^n \rho_i h_i = \sum_{i=1}^n \rho'_i h'_i$$

where  $n$  is the number of layers of blocks in the model,  $\rho_i, h_i$  are the densities and heights of each block in the given column and  $\rho'_i, h'_i$  are the densities and heights of each block in the end (reference) column.

The contribution to the total elevation from a given block in a given column ( $\delta h_i$ ) is the difference in height between the given block and the corresponding block in the reference column. Since all the blocks are of the same mass then:

$$\rho_i h_i = \rho'_i h'_i$$

where  $\rho_i, h_i$  refer to a block in the given column and  $\rho'_i, h'_i$  refer to the corresponding block in the reference column.

If  $\rho'_i = \rho_i + \delta \rho_i$  and  $h_i = h'_i + \delta h_i$  then  $\delta h_i = h'_i \delta \rho_i / \rho_i$ .  $h'_i$  is known, being the block height used in the lithospheric temperature calculations. Consequently the total elevation of a given column is calculated as

$$E = \sum_{i=1}^n h'_i \delta \rho_i / \rho_i$$

- by summing the

contributions from each block in the column.

Since the contraction of the lithosphere takes place under water and is subject to isostatic adjustment to preserve equilibrium, it is necessary to adjust the calculated elevation accordingly. Consideration of the isostatic balance shows

that the elevation  $E$  (above) must be multiplied by a factor

$$\left( 1 + \rho_w / (\rho_m - \rho_w) \right)$$

where  $\rho_w$  = density of water

and  $\rho_m$  = density of the rocks at the base of the lithosphere.

In the above calculations it is assumed that all contraction takes place vertically with horizontal stresses relieved by creep, and the topographic profile may be obtained by estimating  $E$  for each of the columns of the lithospheric model.

#### 4.2 The effect of the crust

In the model no distinction is made between crust and mantle, the whole lithosphere being considered as material of the same composition. Since the object of the calculations is to produce topographic profiles, only a variation of crustal thickness from ocean ridge to basin would be of relevance, a layer of constant thickness causing no topographic effect. However, since the crust is assumed to form by differentiation of basalt from the lithospheric material, it follows that the subcrustal lithosphere must be depleted in basaltic materials by amounts proportional to the thickness of the crust. Consequently, the overall composition averaged over the top few kilometres of the lithosphere must remain constant from ridge to basin. The slight thickening of the crust with distance from the spreading centre (Talwani, Le Pichon & Ewing, 1965) will therefore have no effect on the topographic elevation and may be considered simply as a redistribution of minerals, resulting in an increase in the thickness of the low density crustal layer (containing large amounts of plagioclase) and a complementary increase in density of the underlying topmost mantle by reduction of the plagioclase content. It is emphasised that this argument applies only to small scale mineral redistributions in which no phase changes take place (c.f. the Icelandic region- section 6.2.2).

### 4.3 A computer program to calculate topography

A computer program TEMDEN was written to perform the calculations outlined in this chapter and is described in appendix 6. In addition to producing the elevation profiles in both numeric and graphical form, the program maps the density and mineral assemblage distributions. A separate program HOTMAP was written earlier to map the temperature distributions (appendix 7). The phase diagram was divided into zones  $25^{\circ}\text{C}$  by 1 kbar in order to describe it to the computer (figure 4.1). Table 4.1 lists the densities supplied for each zone, for both the compositions studied.

Figure 4.1. The phase diagram of figure 3.1 in digitised form. The values of temperature and pressure at the corners of the diagram are shown, and an explanation of the mineral assemblages represented by the letter and number codes is given in table 4.1.



Table 4.1 Densities associated with zones of the digitised phase diagram

The phase diagram in its digitised form is shown in figure 4.1

Zone	Mineral Assemblage	Density 1:3 mix	Density 1:1 mix
L	Basalt liquid + olivine	3.17	3.05
P	Olivine + pyroxenes + plagioclase	3.24	3.19
O	Olivine + pyroxenes + spinel	3.32	3.35
1	Olivine + pyroxenes + garnet with % $Al_2O_3$ in pyroxenes indicated by the value of the zone key.	3.36	3.44
2		3.35	3.42
3		3.34	3.40
4		3.33	3.38
5		3.33	3.37
A	Partial melting in 17% steps between zones P and L	3.23	3.18
B		3.22	3.15
C		3.21	3.13
D		3.20	3.10
E		3.19	3.08
F		3.18	3.06
G	Partial melting in 25% steps between zones 5 and L	3.32	3.33
H		3.28	3.25
I		3.24	3.17
J	Partial melting in 25% steps between zones 4 and L	3.20	3.09
K		3.31	3.35
M		3.27	3.26
N		3.23	3.17
V	Partial melting in 20% steps between zones P and L	3.20	3.09
Q		3.23	3.17
R		3.22	3.15
S		3.21	3.12
T		3.20	3.09
U	Partial melting in 25% steps between zones O and L	3.19	3.06
W		3.29	3.31
X		3.26	3.24
Y	O and L	3.23	3.16
Z		3.20	3.09



#### 4.4 Introduction to general results

While fitting the sea floor spreading model described in the previous chapters to observed topographic data it became clear that the acceptable range of lithospheric thicknesses and compositions is limited because many models produce too great a ridge elevation. Topographic profiles across ocean ridges in all parts of the world require similar restrictions to be placed on the model parameters, and consequently a single, preferred, lithospheric composition may be derived and used to model the local variations of topography within each ocean. In the following sections the results leading to the preferred composition are presented together with other general conclusions applicable to all oceans.

#### 4.5 Composition, lithospheric thickness, conductivity

Topographic profiles were calculated to examine the effect of variations of the following model parameters:-

- 1) lithospheric thickness
- 2) lithospheric composition
- 3) thermal conductivity

By varying each of these separately its effect on the topography may be isolated. Figure 4.2 shows several ridge profiles calculated for spreading rates equivalent to those of the Mid-Atlantic ridge at  $22^{\circ}\text{N}$ , together with the observed topography at that latitude, which is typical for most ocean ridges.

##### 4.5.1 Lithospheric thickness

Examination of the profiles in the lower half of figure 4.2 shows that the cross-sectional area and bathymetric amplitude of an ocean ridge increase with increasing lithospheric thickness. Since the base of the lithosphere is assumed to be at the solidus of the mantle material, a thinned lithosphere will exist in the presence of raised mantle temperatures which result in an upward migration of phase boundaries

Figure 4.2 Calculated ocean ridge profiles.

(above) Lithosphere 70km thick with the following parameters:-

- Ref. 1. comp. 1 basalt : 3 dunite, base temp- wet solidus.
- Ref. 2. comp. 1 basalt : 3 dunite, base temp- dry solidus.
- Ref. 3. comp. 1 basalt : 3 dunite, base temp- dry solidus, conductivity doubling between 800 and 1100°C.
- Ref. 4. comp. 1 basalt : 1 dunite, base temp- dry solidus.
- Ref. 5. comp. 1 basalt : 3 dunite, base temp- dry solidus, conductivity set to higher value than others- 0.0075 cf. 0.006.

(below) Lithospheric thickness varying from 50 to 80km, comp. 1 basalt : 3 dunite, base temp- dry solidus.

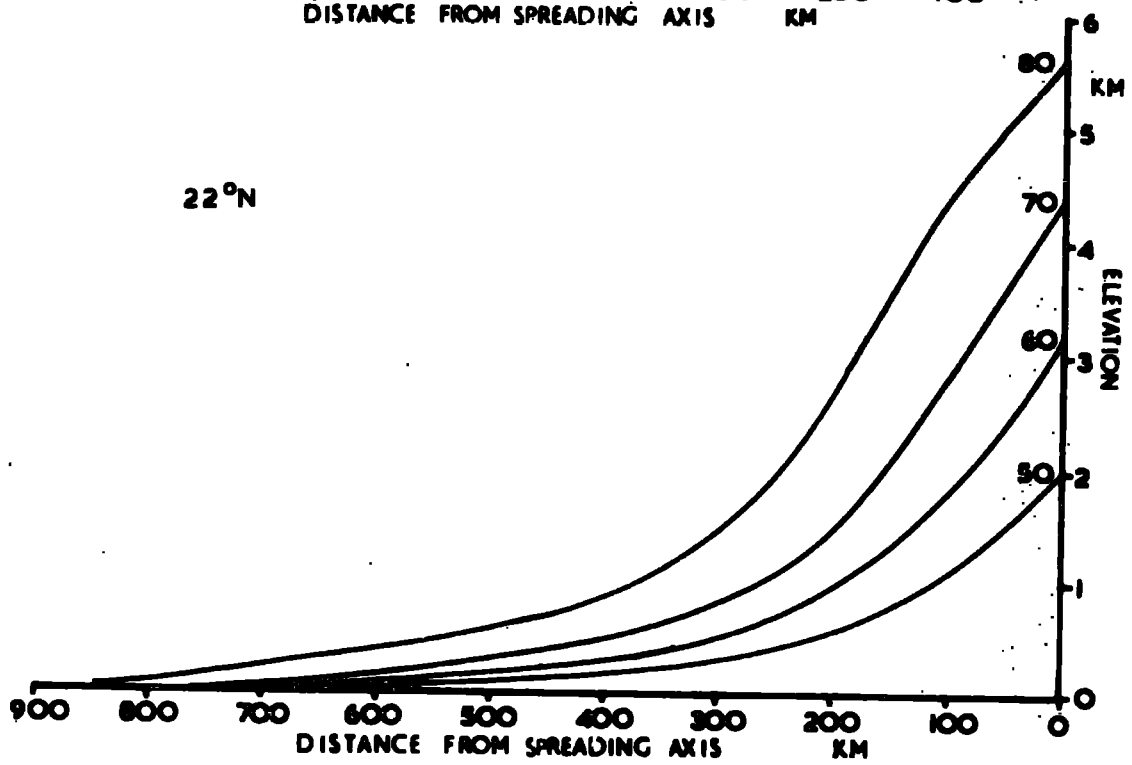
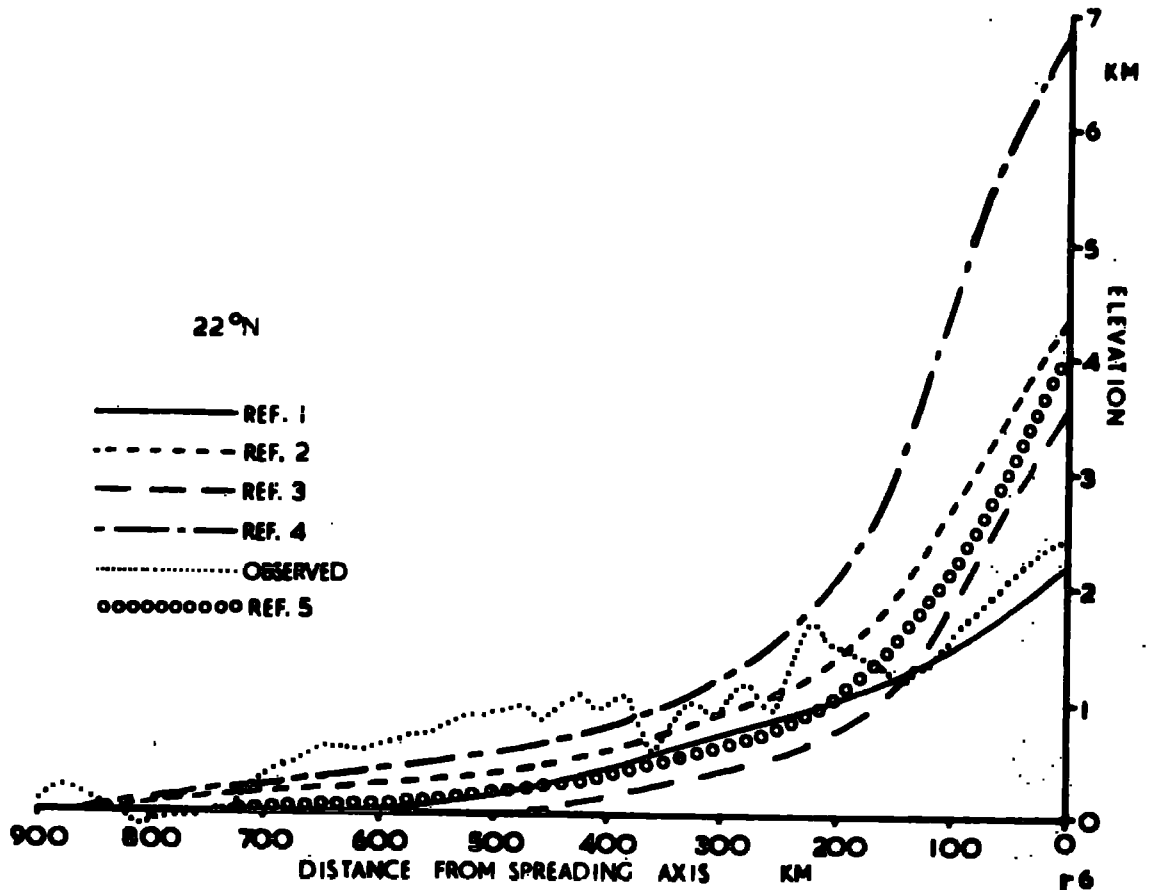


Figure 4.2.

(refer to phase diagram, fig 3.1). Consequently the cross-sectional area and bathymetric amplitude of an ocean ridge decrease with increasing mantle temperatures.

#### 4.5.2 Lithospheric composition

In the upper half of figure 4.2 five topographic profiles are compared with observed bathymetric data, and the major difficulty encountered in fitting the model to observed data is apparent: there is a strong tendency to produce excessive elevation at the ridge axis and insufficient elevation on the flanks.

The profiles 2 and 4 are from models similar in all respects except that the basalt fraction in the lithospheric material of profile 4 is double that of profile 2. As was predicted during consideration of possible phase changes in the lithosphere (see section 3.3.7), an increase in the basalt fraction produces an increase of ridge elevation.

Profile 1 corresponds to a model similar to that giving profile 2 except that the lithosphere of profile 1 is considered to contain trace amounts of water. The presence of water can be seen to reduce the topographic elevation of the ocean ridge and to produce a much flatter profile bearing closer resemblance to the observed data (see section 3.3.8).

Comparison of profiles 1, 2 & 4 with the observed bathymetry in figure 4.2 demonstrates that a lithosphere of a composition equivalent to a mixture of 1 part basalt to 3 parts dunite and including water is the only one of those tested which closely models observed topography. The shape of the profiles of the dry models 2 and 4 - involving a sharp peak at the ridge axis - makes it impossible to fit observed topography with these models simply by using a thinner lithosphere.

### 4.5.3 Thermal Conductivity Variation

This last conclusion also applies to models employing varying thermal conductivity. The model which produced profile 3 in figure 4.2 is similar in all respects to that which gave profile 2 except that the thermal conductivity increases linearly between 800°C and 1100°C from 0.006 to 0.016 cal/cm.s.°C, according to the suggestion of Clark and Ringwood (1964). This varying conductivity results in a more pronounced peaking of the elevation profile and makes it even more difficult to achieve a satisfactory fit to observed data. Recent work by Schatz and Simmons (1972) indicates that the thermal conductivity in the mantle may remain relatively constant below temperatures in the region of 1300°C. This figure is close to the maximum temperatures encountered in these models and consequently calculations involving varying thermal conductivity are not further considered. Similarly, the use of a higher value of thermal conductivity through<sup>-out</sup> the lithosphere (c.f profiles 2 and 5, figure 4.2) makes fitting of observed and calculated topography more difficult and is not pursued.

### 4.5.4 The preferred lithospheric model

The above sections may be summarized as follows:-

- 1) A composition equivalent to 1 part basalt to 3 parts dunite is preferable to a 1:1 mixture.
- 2) The lithosphere must contain trace amounts of water.
- 3) Thermal conductivity is sensibly constant throughout the lithosphere.
- 4) Raised temperatures in the asthenosphere produce an upward migration of phase boundaries, which results in a thinned lithosphere and consequent lessening of mid ocean ridge cross section and bathymetric amplitude.

These factors define the suite of models which give the best fits to observed topographic profiles, and the only variable (excluding spreading rates) which remains to be adjusted to fit a particular observed profile is the thickness of the lithosphere.

#### 4.6 Discussion

The composition of the lithosphere has been the subject of debate for some time, the suggested compositions ranging between peridotite and eclogite. Serious difficulties exist for an eclogitic upper mantle on geochemical grounds (Harris and Rowell 1960), and also because of the need to achieve the conditions necessary for a low velocity zone without causing widespread melting of the upper mantle (Ringwood, 1962a). These considerations led to the development of the "pyrolite" model of Ringwood (1962a and b), Green and Ringwood (1967) and Ringwood (1969). Pyrolite is essentially a peridotite with a composition equivalent to 1 part basalt to 3 parts dunite. This ratio was derived from the relative proportions of MgO, CaO and  $Al_2O_3$  in basalts, dunites and chondrites, but some variation is acceptable. Evidence of the existence of anisotropy in seismic velocities in the upper mantle (Hess, 1964; Keen and Tramontini 1970; Morris, Raitt and Shor 1969) further supports a peridotitic composition, as do the limitations on Poisson's ratio imposed by seismology (Bullen, 1963)

The debate has been renewed within the last three years by the results of Monte-Carlo inversion of a wide range of geophysical data (mass and moment of inertia of the earth,  $P$  and  $S$  wave velocity distributions, phase velocities of Rayleigh and Love waves, spheroidal and toroidal oscillations of the earth) presented by Press (1969, 1970) and Wang (1970), with comment by Birch (1970). Press found evidence for high density (3.5 to 3.6 gm/cm<sup>3</sup>) at the base of the lithosphere which suggests the presence of eclogitic material at that depth. In contrast, Wang (using slightly different shear velocity distributions) predicted lower densities corresponding to peridotite at the same depth. This conflict has been discussed by Worthington, Cleary and Anderssen (1972), who were unable to judge between the opposing views. A further Monte-Carlo inversion using group velocities of Rayleigh and Love waves in addition to the previously mentioned data lends support to the existence of high densities at the base of the lithosphere and suggests that variation of chemical composition and iron/magnesium ratio with depth may occur (Mizutani & Abe, 1972;

Ito, 1973). In addition Hart and Press (1973) have studied  $S_n$  waves recorded at stations around the Atlantic from earthquakes on the mid Atlantic ridge. The high velocities which they found further suggest the presence of eclogite at the base of the lithosphere.

It should be realised that in terms of overall composition eclogite represents an end member of the basalt + dunite mixtures, corresponding to a ratio of 1:0, and that a continuous series of compositions could be postulated between eclogite and dunite. The argument is thus one of degree rather than the choice between two totally different materials, which is the impression to be gained from much of the literature. Consequently published densities of "dunites" and "eclogites" must be treated with care as regards their impingement on the present discussion.

Both the present model and the similar one by Forsyth & Press (1971) reject eclogite rich lithospheres because of the unsatisfactory topographic elevation profiles which such compositions produce (see section 4.5, above). As previously stated (section 3.3.7) the variations of overall density due to phase changes (and hence their contribution to topographic elevation) are the result of

- 1) the existence of plagioclase at low pressures and
- 2) the existence of garnet at high pressures.

In a spreading oceanic lithosphere the reduction in depth of the plagioclase region as the slab cools has a far greater effect on the topographic profile than does the simultaneous appearance of garnet, which is always confined to a thin strip at the base of the lithosphere and may even be absent (see section 4.9, below). As a result of this, the conclusion of the present model that a 1:3 basalt:dunite composition is required and that a 1:1 mixture is unsatisfactory applies only to the top 30 km of the lithosphere (the maximum extent of the plagioclase region) and the composition below this depth is of little consequence as regards topographic profiles.

It is for this reason that Forsyth & Press (1971) found a "wet mixed model" to be the most satisfactory of those which they tested. In the model, pockets of eclogite were included in the base of a peridotitic lithosphere in order to achieve the necessary seismic velocities and densities, but the clumsiness of the physical arrangement involved was recognised by these authors as a possible source of criticism. However, since it is the larger quantities of garnet and the higher iron:magnesium ratios present in eclogite rich mixtures which are responsible for the higher densities (and since the effect on the densities is irrespective of the physical distribution of the minerals in the rock), a more elegant solution is simply to postulate a region containing a greater basalt fraction to be present at the base of the lithosphere.

Whatever the outcome of the present debate on these high densities at depth, the important fact relevant to the present work is that all the evidence points strongly to a peridotitic composition, including water, for that part of the lithosphere in which phase changes important in determining the topographic elevation of the ocean ridges take place. Accordingly, the detailed studies of ocean ridges in the following chapters are made using the preferred model detailed in section 4.5.4.

#### 4.7 The effect of spreading rates

It has been shown (Sclater, Anderson & Bell, 1971) that data from the Pacific, Atlantic and Indian oceans generally indicate the existence of a relationship between the age of the sea floor and its elevation from the ocean basin. The relative magnitudes of the vertical and horizontal temperature gradients within a spreading lithospheric slab (figure 2.1) suggest that vertical heat flow will dominate in cooling the slab and consequently the agreement of the present model with this relationship is to be expected. Figure 4.3 shows the elevations calculated



by the model for a fixed lithospheric thickness and spreading rates of 0.5, 1 and 3 cm/y, plotted against the age of the lithosphere, and the coincidence of the data for the different spreading rates confirms the agreement.

The only effect of the spreading rate on the calculated topographic profiles is thus that an increase in spreading rate stretches them horizontally and vice versa. Virtually no variation of vertical dimensions is produced by spreading rate differences, a conclusion which is in accordance with that of Forsyth & Press (1971).

#### 4.8 Calculation of topographic profiles from age-elevation data

As stated previously (section 2.2) it is possible to calculate topographic profiles for any combination of spreading rates by suitably fixing the width of the lithospheric blocks and varying the time between successive additions of new columns. However, since the ridge elevation for a given thickness and composition of lithosphere is a function only of age, irrespective of spreading rates within the range of interest to this work (see previous section), it is unnecessary to calculate every topographic profile from first principles. Once the age-elevation relationship for a given lithospheric thickness and composition has been calculated, it may be used to derive subsequent profiles for any spreading rates directly. Figure 4.4 shows some of the age-elevation curves calculated by twelve separate runs of the whole model for a range of lithospheric thicknesses between 50 and 100 km and a composition equivalent to 1 part basalt : 3 parts dunite + water (the preferred model of section 4.5). These curves are used as data for program SYN (appendix 8) which has been written to produce topographic profiles for any specified spreading rates and lithospheric thicknesses from such age-elevation relationships. The data shown in figure 4.4 are listed in appendix 4 in numeric form.

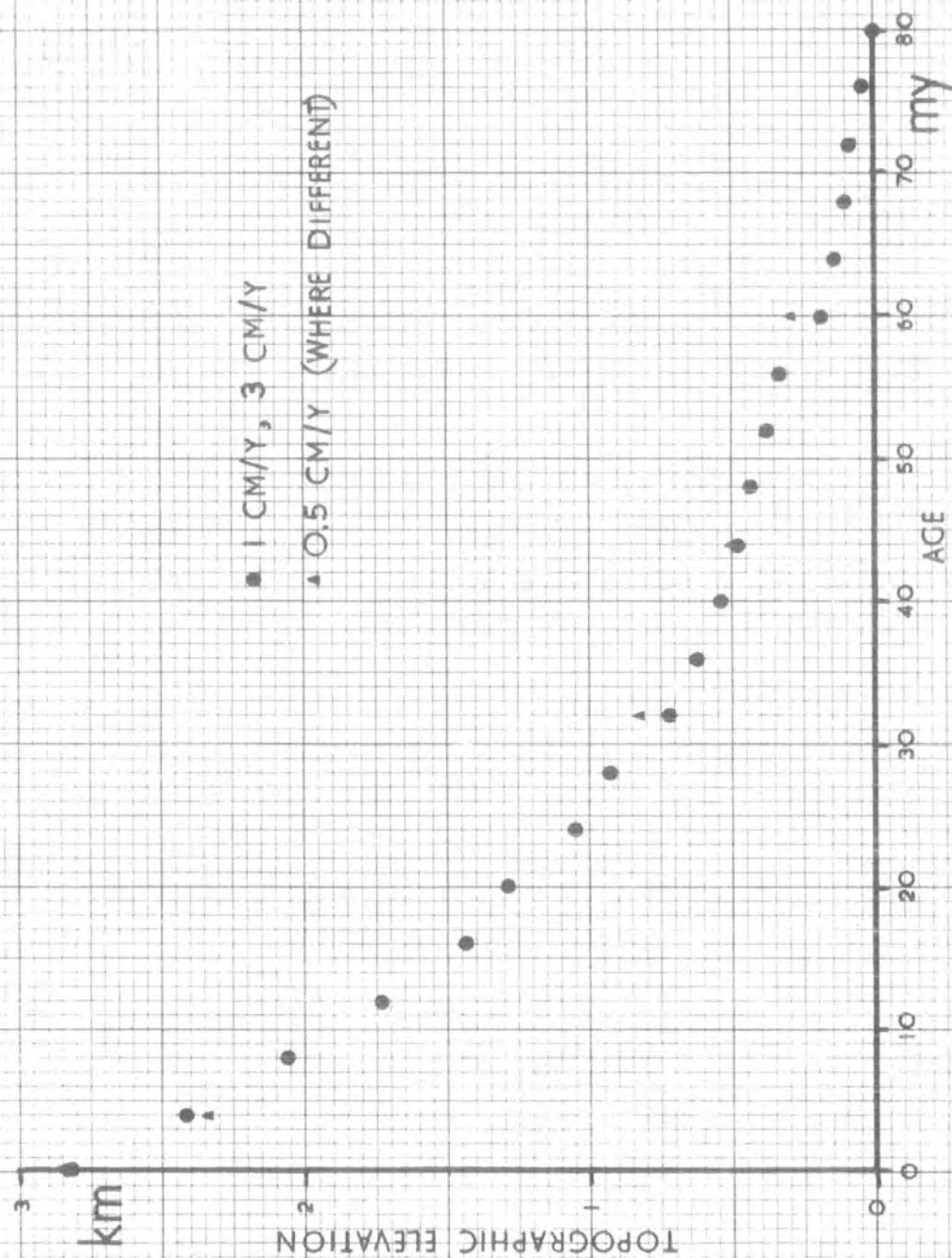
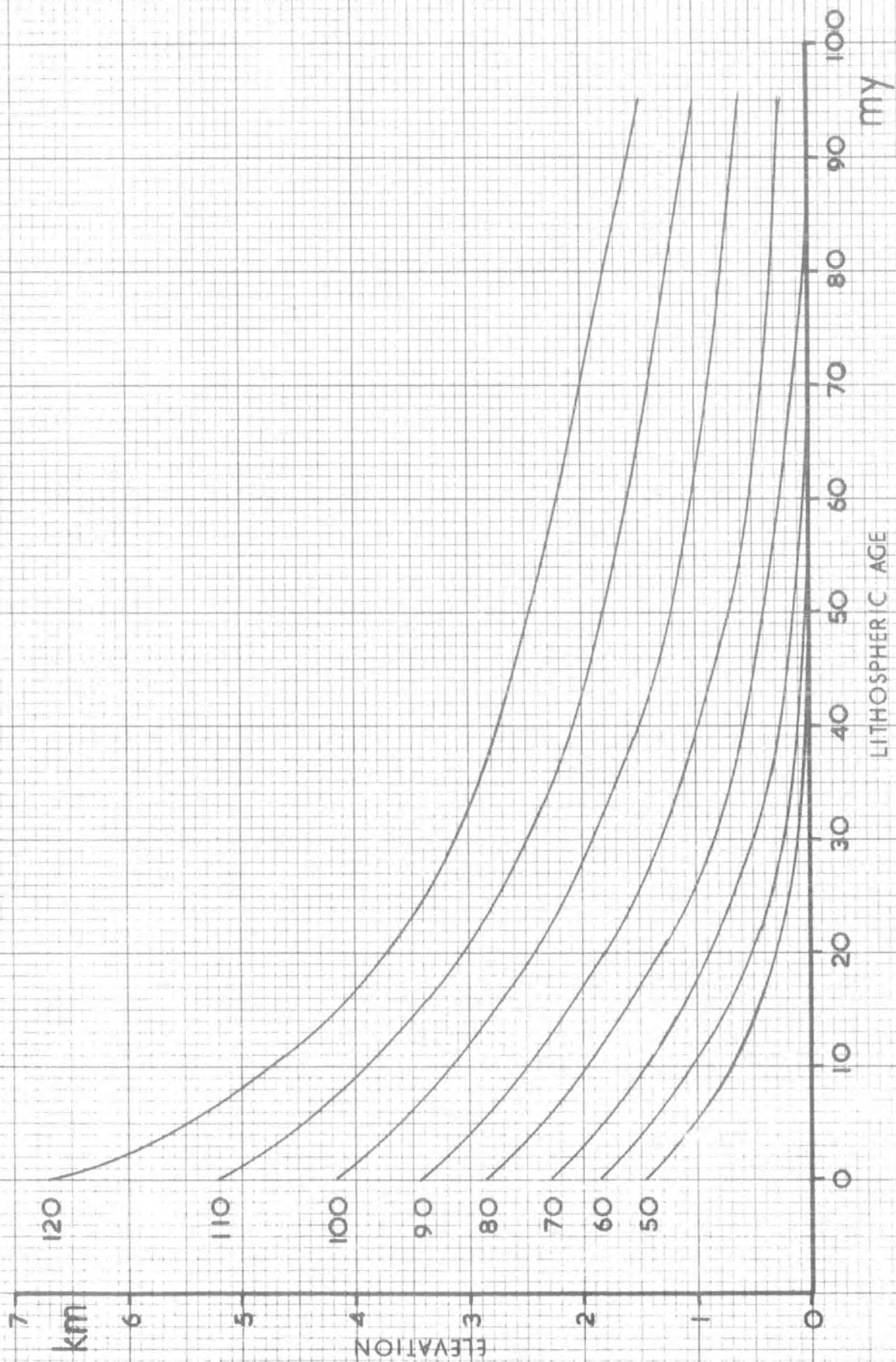


Figure 4.3. Age-elevation curves for various spreading rates- 0.5, 1.0, 3.0 cm/y. Lithospheric thickness 80km. Comp 1 basalt : 3 dunite, base temp wet solidus. A lack of dependance of elevation on spreading rate is indicated.

Figure 4.4. Age-elevation curves for lithospheres of various thicknesses (indicated in km), all with comp-  
 1 basalt : 3 dunite, base temperature wet solidus.  
 S See also Appendix 4.



#### 4.9 Density and Mineral phase distributions

Figure 4.5 shows typical density and mineral phase distributions in a modelled lithospheric slab. The particular distributions shown are those which give the best fit to topography in the North Atlantic at  $46^{\circ}\text{N}$  and the spreading rates used are appropriate to that latitude. The data in figure 4.5 are derived from the calculated temperature distribution by the program TEMDEN as steps in the production of the topographic profile (see section 4.3 and appendix 6). The same distributions are presented in figure 4.6 after smoothing the boundaries between the different zones to remove the steps which result from the digitised nature of the calculations. It is emphasized that the sharp density divisions do not indicate actual discontinuities in the mantle but are only shown for ease of presentation, densities in the model actually changing gradually with temperature and pressure.

Far from the spreading centre and above about 20 km, the density decreases with depth owing to the effect of increasing temperature outweighing that of increasing pressure. At about 20 km depth the breakdown of plagioclase causes an increase in density. With further increasing depth the density again falls, and when the garnet region is entered at about 60 km (see figure 3.1) the temperatures present are too high for garnet to exist in quantities sufficient to greatly affect the density, though nearer the spreading centre a slight increase can be detected in figure 4.6. In thinner lithospheres, where the temperature gradients are steeper (owing to the shallow slope of the solidus - section 4.5.1), the garnet region may be absent.

As the spreading centre is approached, the lithosphere becomes hotter causing the plagioclase region to grow and the garnet region to shrink (figure 4.6, lower).

Near the spreading centre a wedge shaped low density zone exists between 5 and 35 km depth (figure 4.6, upper). This zone shows marked similarity to that proposed

Figure 4.5. Temperature, density and mineral phase distributions in a lithosphere of the composition indicated. Spreading rates correspond to the North Atlantic at 46°N. The codes for the mineral phases correspond with the codes in the phase diagram of figure 4.1. The hot edge of the lithosphere is at the bottom of the diagrams, the sea bed at the right of same.

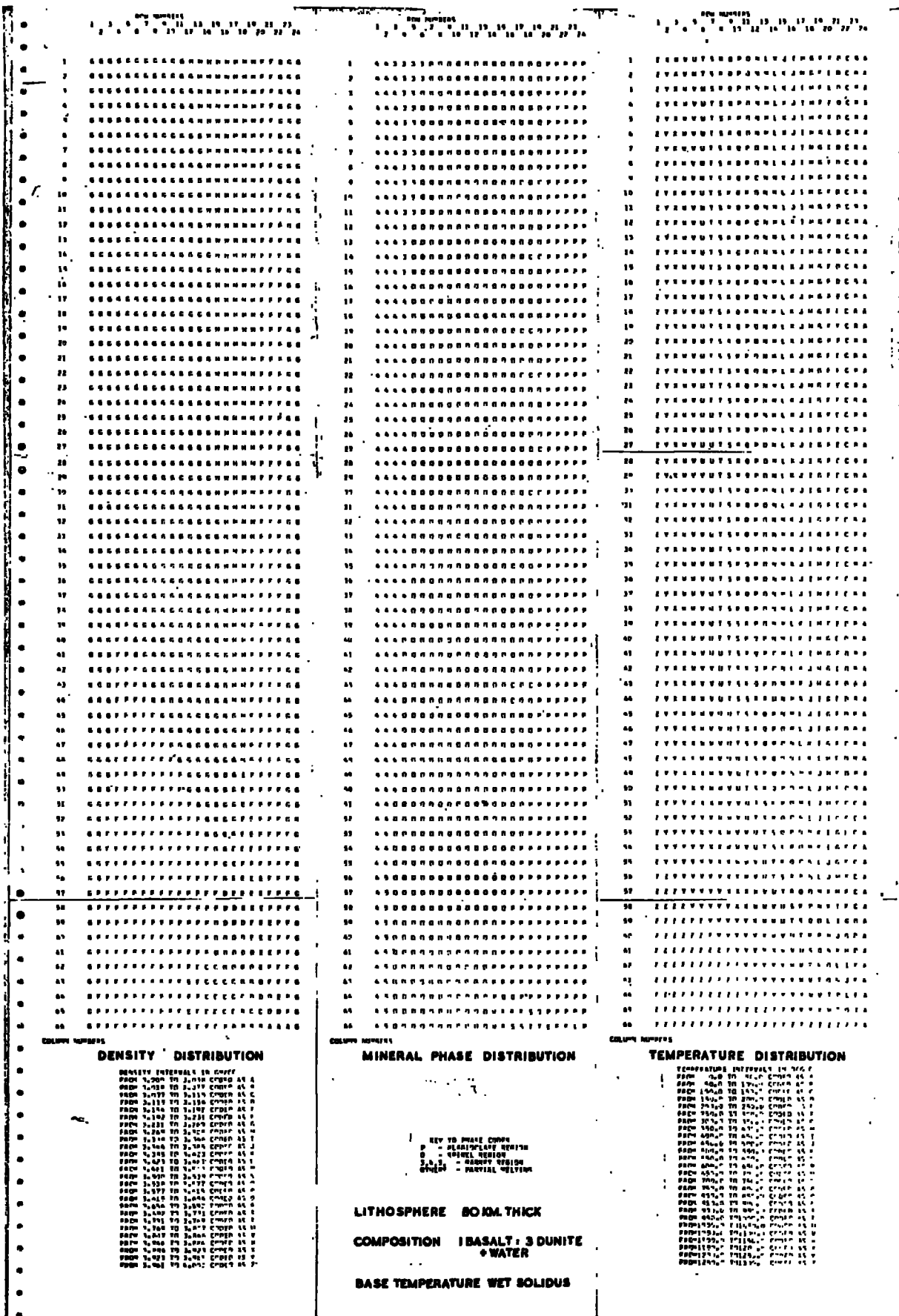
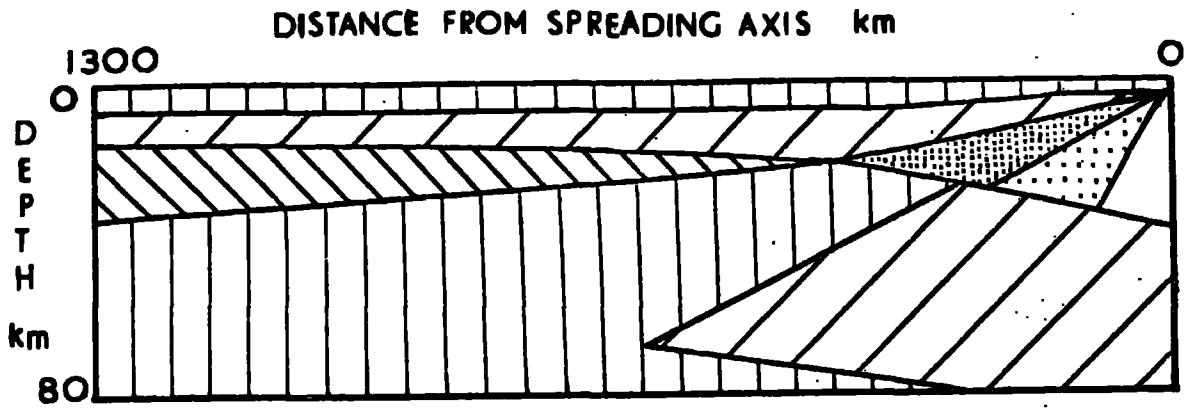


Figure 4.6. The density and mineral phase distributions of figure 4.5 redrawn to smooth the steps in the boundaries which result from the digitised nature of the calculations. The lithosphere is 80km thick, comp. 1 basalt : 3 dunite, base temp- wet solidus (1250°C). Spreading rates correspond to the North Atlantic at 46°N. The garnet region may be absent in hotter, thinner lithospheres. The sharp density boundaries have no significance, being only shown for ease of presentation.




KEY TO DENSITIES — g/cc


 3.31-3.27

 3.19-3.15

 3.27-3.23

 3.15-3.12

 3.23-3.19

 3.12-3.08

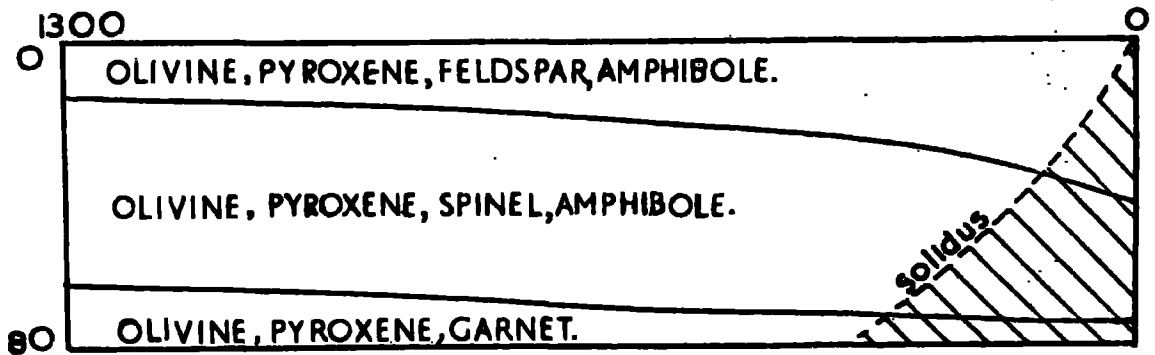


Figure 4.6.



by Talwani, Le Pichon and Ewing (1965) to satisfy seismic and gravity data, the differences of horizontal scale being attributable to differences in spreading rates between the latitudes  $30^{\circ}\text{N}$  of Talwani et al and  $46^{\circ}\text{N}$  of figure 4.6. The top surface of the wedge simply reflects the gradual cooling of the slab and the bottom surface is caused by the plagioclase to pyroxene and spinel phase change. Since these changes are gradual, no seismically detectable discontinuities are to be expected.

#### 4.10 Gravity anomalies over ocean ridges

Free air gravity data (see chapter 1) indicate that the ocean ridges are broadly in isostatic equilibrium. Typical Bouguer anomalies calculated by adding the effect of water depth variations to the free air anomalies show lows of 100 to 200 mgals centred over the spreading axes. Seismic evidence indicates that the oceanic crust is uniform in thickness except near the ocean ridge where it may be slightly thinned (Talwani, Le Pichon and Ewing, 1965). Low density material providing isostatic compensation for the ocean ridge must therefore exist in the upper mantle.

Since the ridges are in isostatic equilibrium, any model assuming isostasy and producing a satisfactory fit to the observed topographic profiles will necessarily give a good fit to the corresponding Bouguer anomalies, the only source of divergence being the non-zero free air anomaly associated with a deeply compensated body. (The theoretical free air gravity anomaly for a typical ocean ridge compensated at 60 km depth has a 50 mgal high over the ridge axis and 10 mgal lows over the flanks - figure 4.7).

However, in order to provide a further check on the model, a program LIGRAV (appendix 9) was written to calculate the free air and Bouguer anomalies produced by the density distributions determined for the modelled lithospheric slabs. In

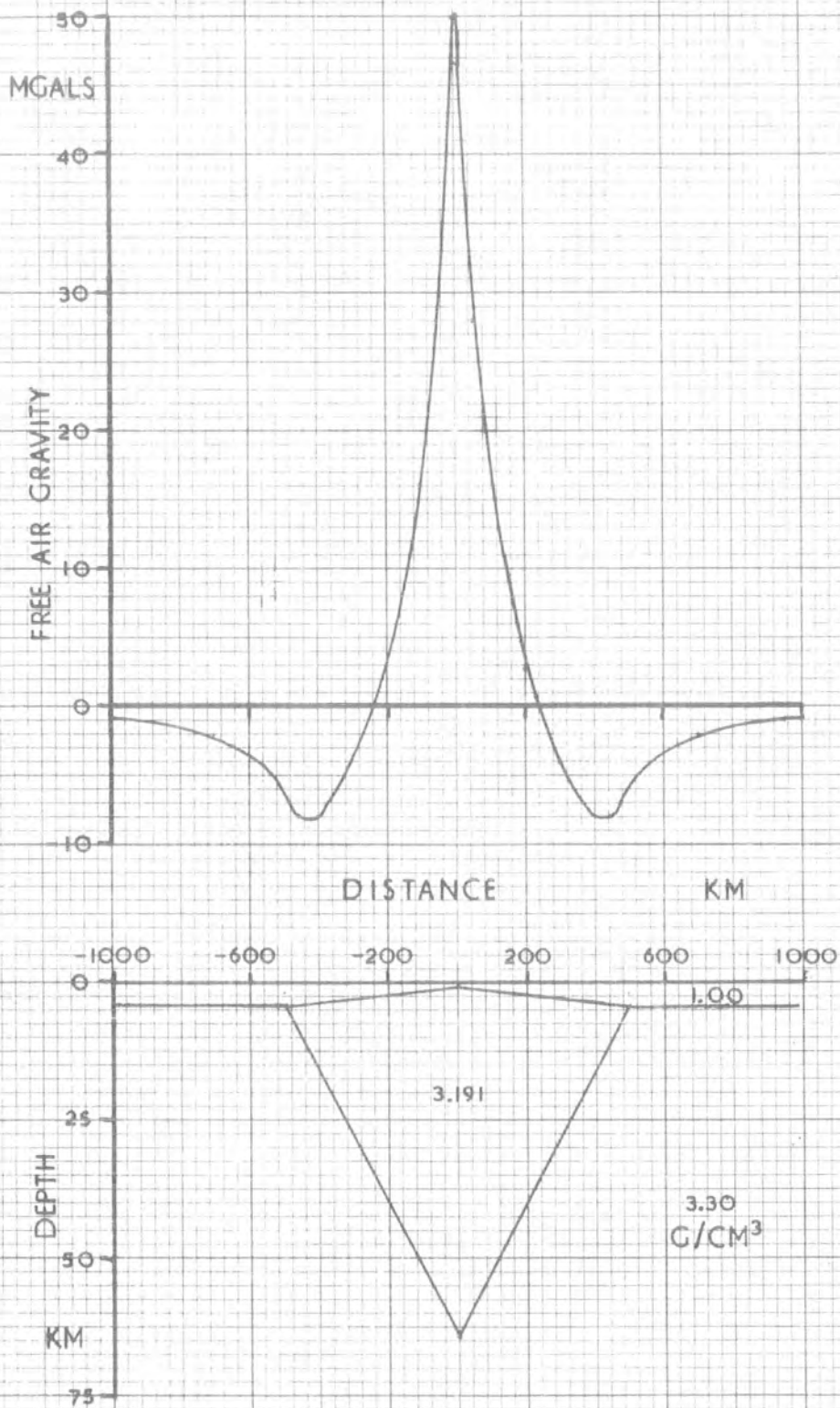


Figure 4.7 The free air gravity anomaly over the "ocean ridge" structure shown. The structure is isostatically compensated, but the depth at which the compensation takes place is such as to result in a non-zero free air anomaly.

this program the gravity anomalies are calculated by summing the effects of the individual blocks into which the lithosphere is divided in the model. Figure 4.8 shows typical results of the gravity calculations, the particular example shown being taken from the Reykjanes ridge at 61°N. Apart from the short wavelengths present in the observed free air anomaly which are produced by local ocean floor topography, both the free air and Bouguer anomalies are fitted satisfactorily by the model.

#### 4.11 Heat flow data

Since the modelled temperature distributions define the thermal gradients in the lithosphere, the heat flow at the sea floor above a cooling lithospheric slab is easily calculated. Figure 4.9 shows typical heat flow anomalies produced by the model, together with observed heat flow data. The values of heat flow at the ridge axis are heavily dependent on the mechanism of intrusion of the new lithosphere (McKenzie, 1967), but, in accordance with the results of McKenzie and also Forsyth and Press (1971), the shape of the anomaly is well modelled. Figure 4.10 shows the theoretical values of heat flow calculated from the temperature gradients existing in lithospheric slabs of the same composition but different thicknesses 80 My after their formation. The heat flow from a 70 km slab can be seen to differ by only few percent from the corresponding heat flow associated with an 100 km slab, indicating that, unless the lithosphere is substantially older than the 80 My which applies to figure 4.10, surface heat flow is insensitive as a boundary condition for a lithospheric modelling procedure (c.f. Sclater & Francheteau, 1970; Forsyth and Press, 1971). Furthermore, Langseth, Le Pichon & Ewing (1966) estimate that observed heat flow data are subject to such large inaccuracies that variations of 20 to 30% are the smallest which can be reliably detected. Consequently, although the model gives good general agreement with heat flow data expressed in terms of profiles across the ocean ridge, it is difficult to derive either support for or disagreement with the model from the variations of heat flow which may or may not

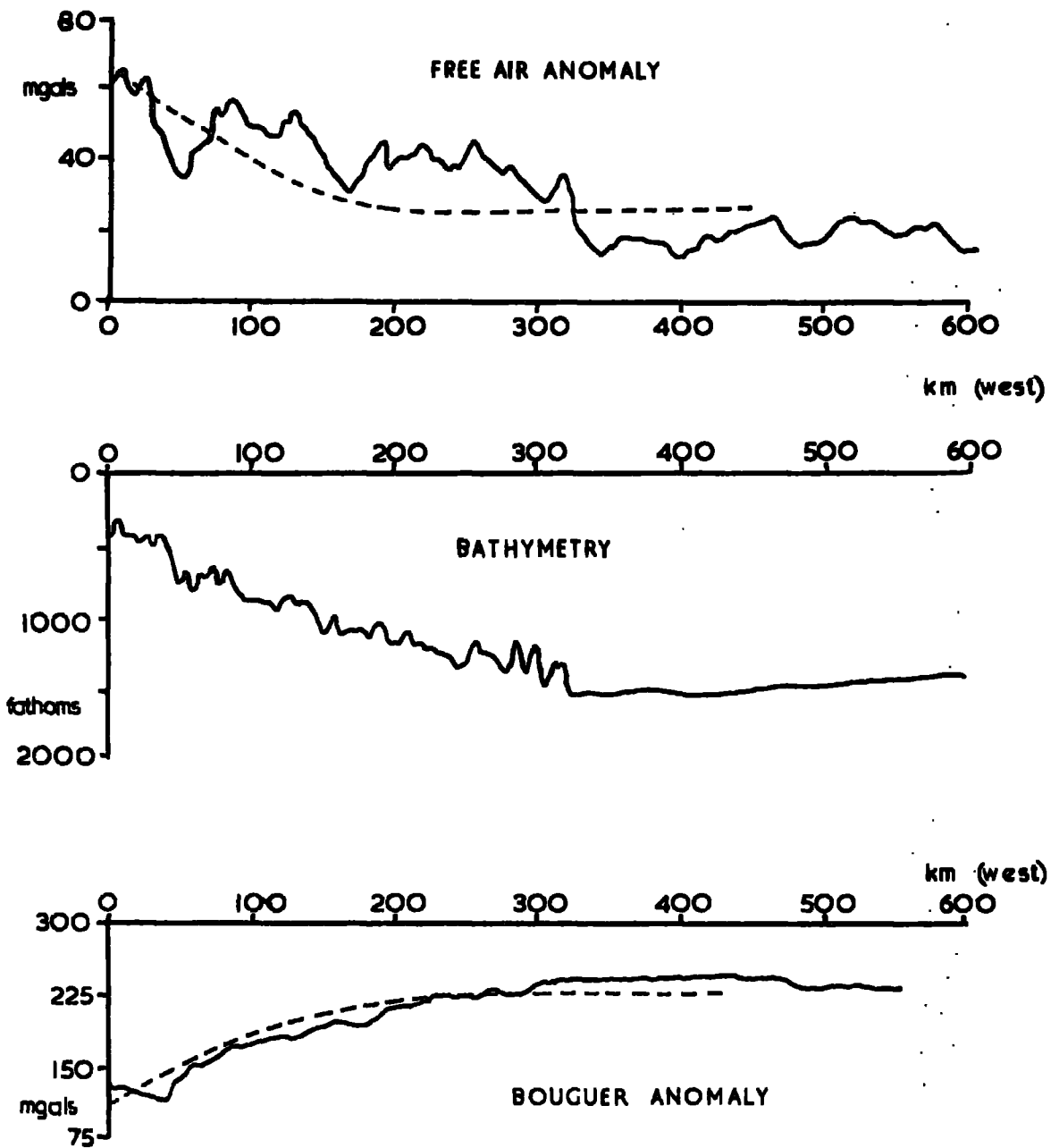


Figure 4.8 Observed and calculated gravity anomalies across the Reykjanes ridge at 61°N. Lithosphere 64km thick, comp. 1 basalt: 3 dunite, base temp-wet solidus. The observed data are uncorrected for sediments

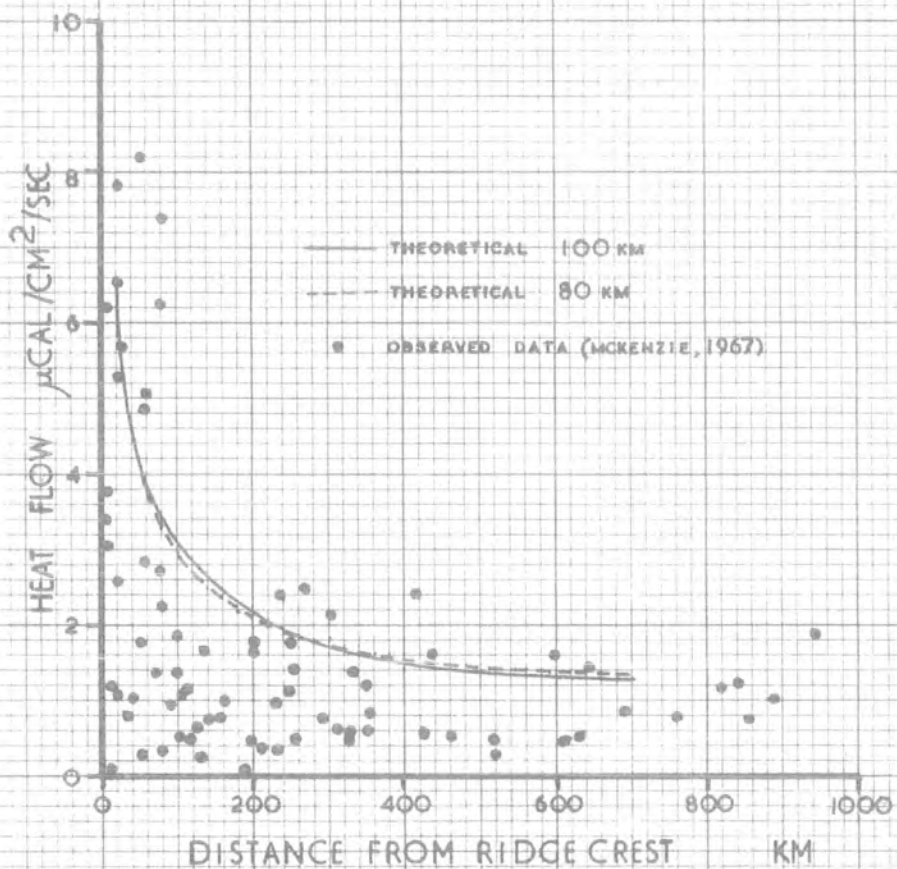


Figure 4.9. Heat flow anomalies calculated for the two lithospheric thicknesses indicated compared with observed heat flow data. Lithospheric composition 1 basalt : 3 dunite, base temp- wet solidus.

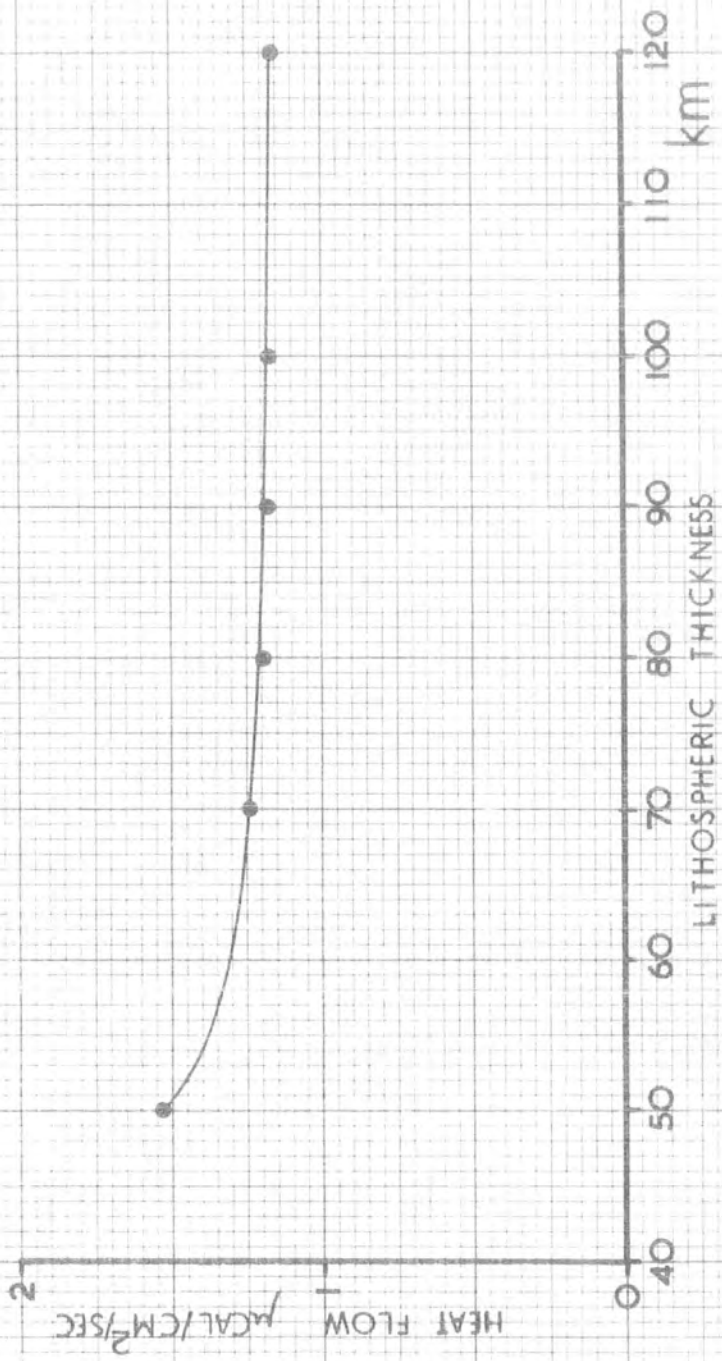


Figure 4.10.  
 Calculated heat flow from lithospheric slabs of various thicknesses 80My after their formation. Composition as for figure 4.9. Note the levelling of the curve towards higher thicknesses.

occur parallel to the ridge axis. The model is unable to explain the slightly lower than average values of heat flow reported to exist on the flanks of some of the ocean ridges (Lee & Uyeda, 1965). However, since this anomaly may be the result of circulation of sea water caused by local heating at the ridge axis (Elder, 1965), the inability may not be a serious defect.

#### 4.12 Seismic velocity in the modelled lithospheres

Figure 4.11 shows calculated velocity-depth profiles for  $P$ -waves in a typical modelled lithospheric slab, in this case 80 km thick. The velocities are calculated from the temperature and density distributions using the following relationships:-

$$v = -1.87 + 3.05\rho$$

where  $v = P$ -wave velocity at room conditions in material of density  $\rho$  gm/cm<sup>3</sup> (Birch 1961).

Also

$$v_{TP} = v(1 - 0.58T + 1.20P)$$

where  $v_{TP} = P$ -wave velocity at temperature  $T$  ( $^{\circ}\text{C} \times 10^{-4}$ ) and Pressure  $P$  (kbars  $\times 10^{-3}$ ) (Birch 1969, Forsyth and Press 1971, Anderson, Sammis and Jordan 1971).

Two profiles are shown, one corresponding to the equilibrium conditions far from the spreading centre and the other to the ridge itself, about 20 km or 2 My from the axis. Since the relevant phase changes are gradual rather than sudden in nature, smoothed profiles estimated from this data are also included in the figure.

The velocity profiles shown are in agreement with those of Green & Ringwood (1967), and indicate that seismic delays of 0.3 seconds relative to the basins would be expected at the ridge axis. Comment has already been made (section 4.6) on the failure of this model to produce the high densities and velocities at the base of the lithosphere which are evidenced by surface wave data. As previously stated,

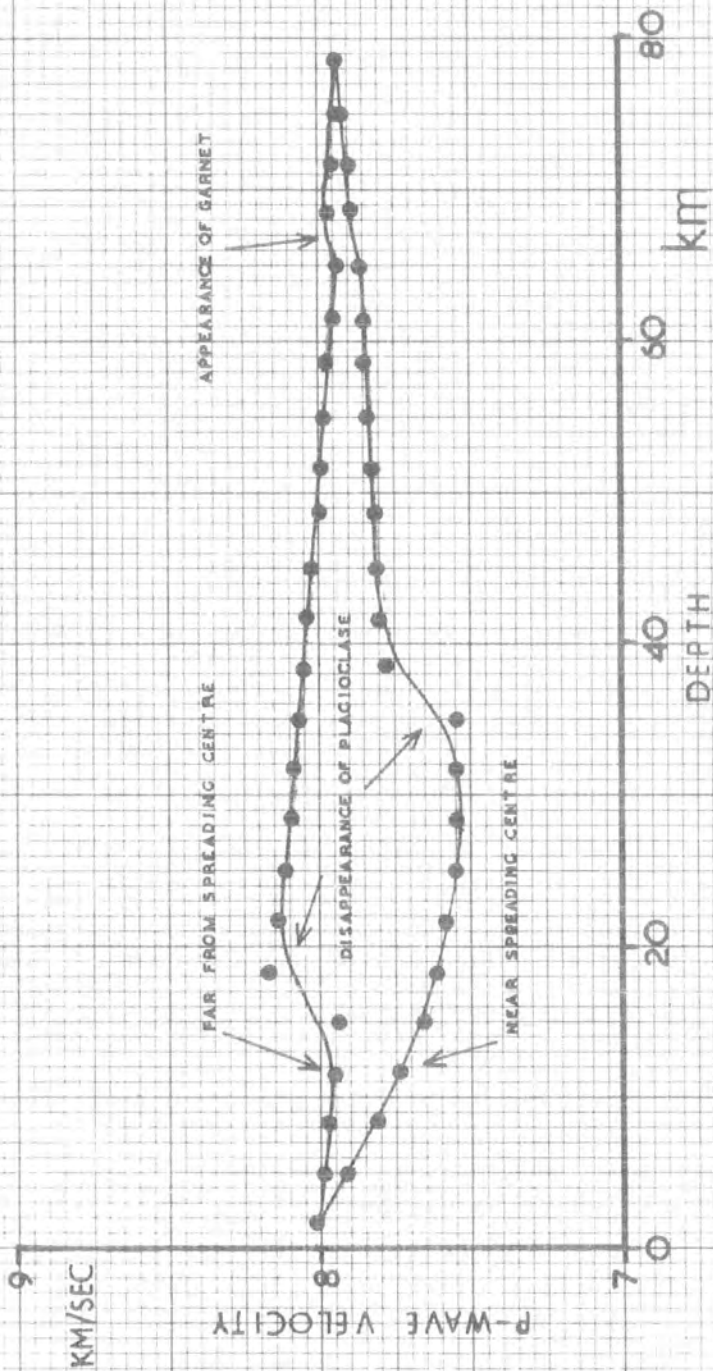


Figure 4.11. Velocity-depth profiles calculated for a lithosphere 80km. thick, with comp. 1 basalt : 3 dunite, base temp- wet solidus. Two profiles are shown, one from close to the spreading axis and the other from far out in the ocean basin, corresponding to a lithospheric age of 80My. The mineral phase transitions responsible for the kinks in the curves are marked.



this failure could be remedied by postulating an increase in the basalt fraction of the mantle in this region.

Although it is well known that seismic velocities are strongly affected by the existence of partially molten material (e.g. Kanamori and Press, 1970), no attempt to continue the modelled velocity-depth profiles into the asthenosphere was made, since Anderson and Spetzler (1970) have shown that the effect of molten material is critically dependant on the shape of the molten zones, rendering such estimations indeterminate.

## CHAPTER 5

Application of the model to observed dataIntroduction

In this chapter the thermal model of sea-floor spreading described earlier is applied to the observed data detailed in chapter 1. The application is made in three sections, the reasons for which are mainly historical:

Section 5.1. Preliminary study of the northern North Atlantic using data uncorrected for sediments.

Section 5.2. Study of the whole North Atlantic using sediment corrected data.

Section 5.3. Extension of the study to other oceans.

The work described in section 5.1 was carried out before the publication of the sediment isopach map of Ewing, Carpenter, Windisch and Ewing (1973) made sedimentary corrections possible, and formed the basis of Haigh (1973). Reworking the calculations of basin uplift using slightly different data to produce the same indication of compatibility of results (see section 5.1.5) would serve little purpose, and consequently the arrangement outlined above was adopted. In addition, this arrangement allows the magnitude of the effect of the sedimentary layers on the calculations to be easily determined by comparing the results of sections 5.1 and 5.2.

## 5.1 A preliminary study of the northern North Atlantic

### 5.1.1 The purpose of the study

Variations of structure exist beneath the northern North Atlantic and are evidenced by two distinct topographic trends (sections 1.2.5 and 1.2.6) :

- 1) a diminution of ocean ridge cross section and amplitude of elevation northwards from the Azores (figure 1.9 (b and c)).
- 2) an accompanying gradual uplift of the whole ridge-basin system relative to sea level towards the north (figure 1.9 (a)).

According to the thermal model of sea floor spreading described previously, a diminution of ridge dimensions may be associated with a thinning of the lithosphere, which in turn is caused by raised upper mantle temperatures (section 4.5.1). Furthermore, uplift of the whole ocean floor relative to sea level, if not caused by a thickened crust, requires anomalously low density material to be present in the upper mantle and this is also most simply explained by raised temperatures. The purpose of this initial study is to determine whether the estimates of the magnitudes of the suggested variations of mantle temperatures calculated from these two distinct bathymetric trends are compatible.

### 5.1.2 The data

The study is confined to the western ocean basins of the North Atlantic between the Azores and Iceland. The following bathymetric profiles were used: NL, NM, NN, NP, & NR. (figure 1.2). These cover the area between  $43^{\circ}\text{N}$  and  $61^{\circ}\text{N}$  and are shown in figures 1.5 and 1.6. Two other profiles in the area were not used: NQ because a gap in the record prevents identification of the ridge crest and thus renders the analysis indeterminate, and NO because the characteristic ocean ridge topography is absent, presumably as a result of its proximity to the Gibbs fracture zone.

### 5.1.3 Analysis of the northward diminution of ridge dimensions

Each of the observed bathymetric profiles was compared with several profiles calculated for a range of lithospheric thicknesses by the model described in chapters 2, 3 and 4. The comparisons were made by means of a simple least squares fitting procedure and the variance  $Q$  between each pair of bathymetric profiles was calculated according to

$$Q = \sum_{i=1}^{i=n} (EO_i - EC_i)^2 / n$$

where  $EO$  and  $EC$  are the observed and calculated bathymetry, and  $n$  is the number of points used in the calculation. For each of the observed profiles considered, the variances are plotted in figure 5.1 against the thicknesses of lithosphere used to derive the calculated profiles. The minimum variance for each observed profile occurs at the thickness of lithosphere which gives the best fit between observed and calculated topography. This thickness can be seen from figure 5.1 to vary with latitude. Some of the profiles used, together with the fits obtained, are shown in figure 5.2.

Subject to the adequacy of the model, the positions of the minima displayed by the curves in figure 5.1 indicate that the lithosphere thins from 85 km at 43°N to 64 km at 61°N. Consequently, since a thinned lithosphere is associated with raised temperatures (see section 4.5.1, above), it is inferred that the spreading of the ocean floor in the North Atlantic occurs above an asthenosphere whose temperature at a given depth increases gradually northwards. The calculated temperature profiles in the modelled lithospheric slabs suggest that at 65 km depth under the ocean basins, the temperature may rise by 150 C° between the Azores and Iceland. These figures are dependent on the values of the physical parameters used in the model and are therefore only quoted as estimates of the magnitudes of the suggested variations. Furthermore, no account of variations of

Figure 5.1. The variances of bathymetric fits between observed and calculated data plotted against the lithospheric thicknesses used to derive the calculated bathymetric profiles (see section 5.1.3). The profiles concerned are indicated, and come from the northern North Atlantic. The data are uncorrected for sediments. The origins for some of the variance curves are not at the origin of the axis, and are indicated as appropriate.

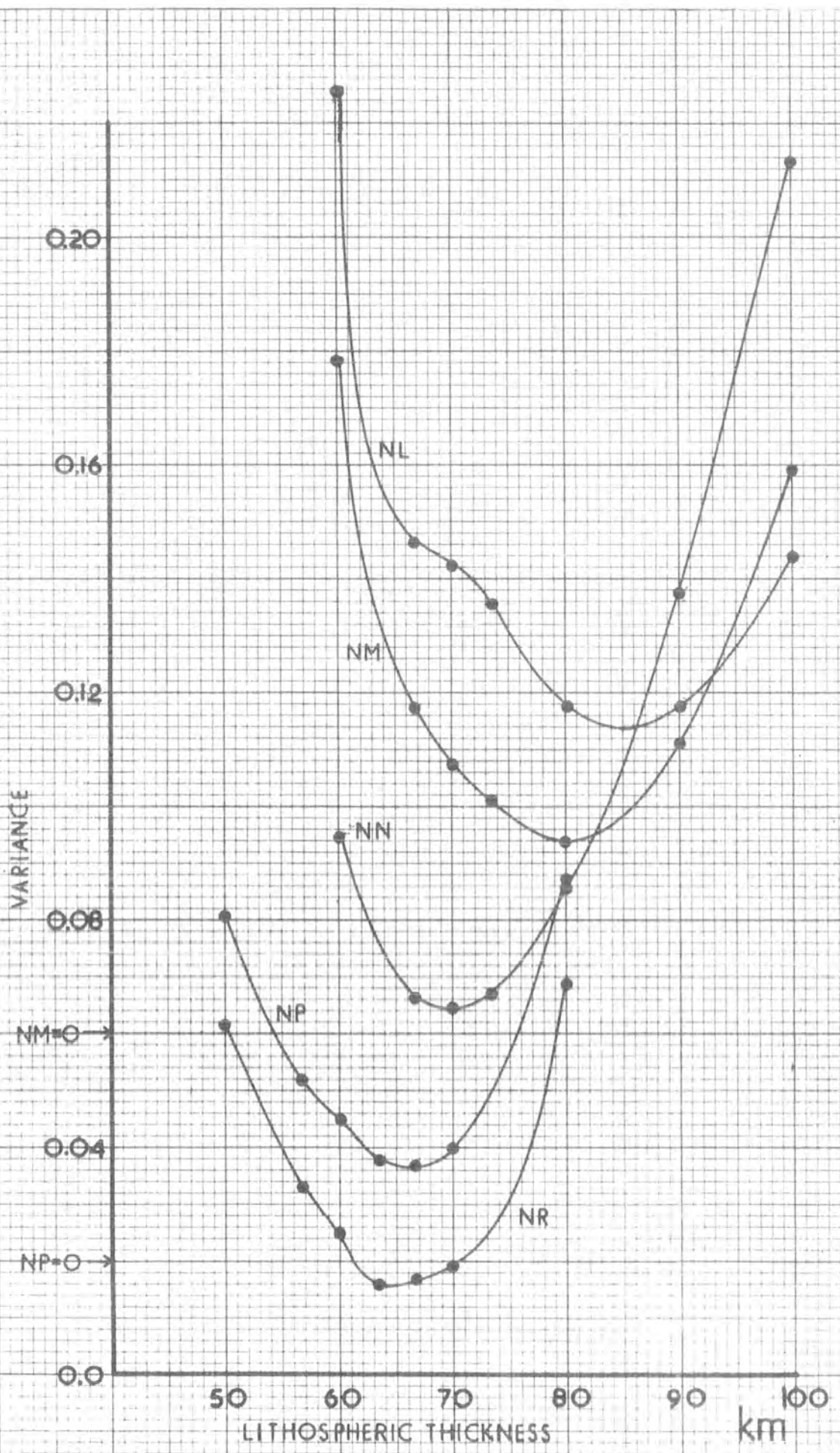


Figure 5.1.

Figure 5.2. Observed and calculated bathymetric profiles, uncorrected for sediments, at three latitudes in the northern North Atlantic. The thicknesses of lithosphere used in the models are indicated in km. Comp. 1 basalt : 3 dunite, base temp wet solidus.

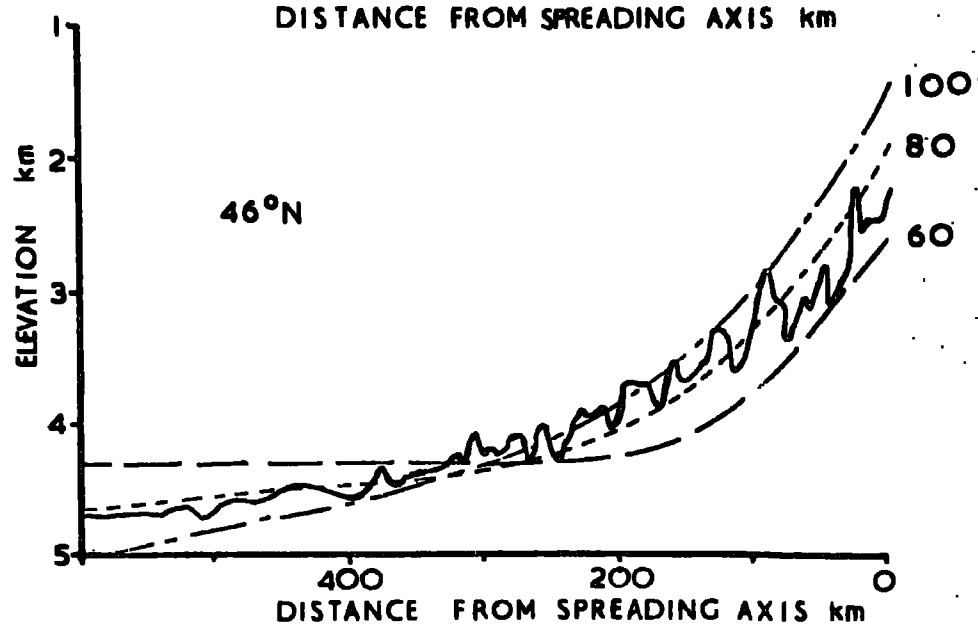
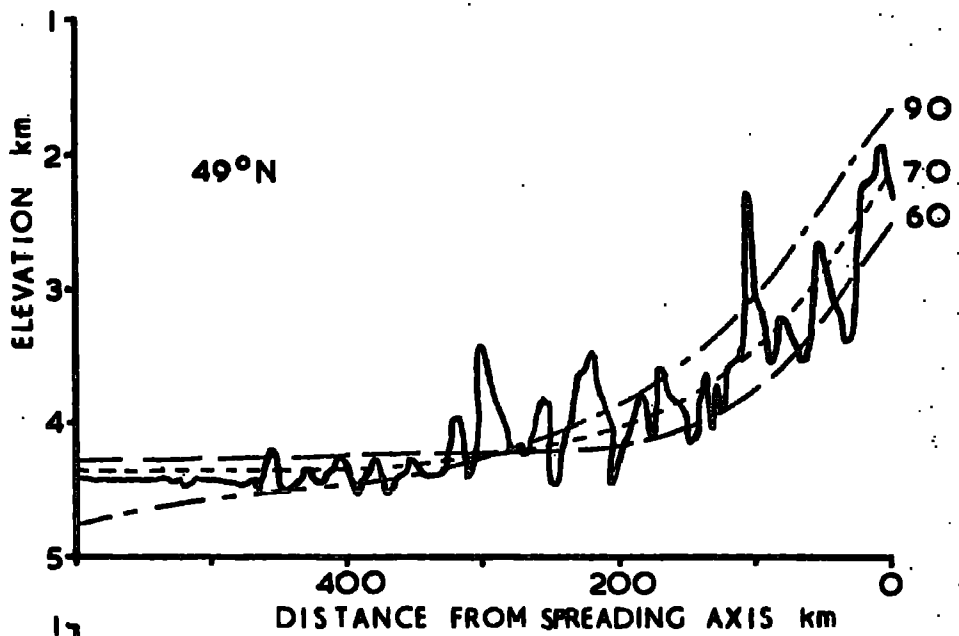
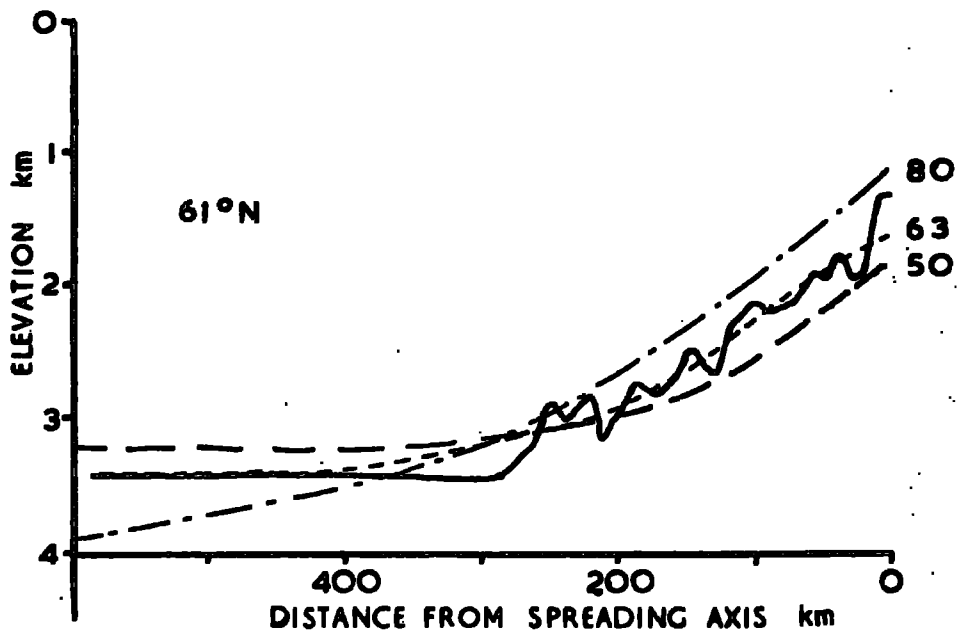


Figure 5.2.



sedimentary cover has been taken at this stage. However, the trends which the figures express are clear in the changes of ridge cross-sectional area (fig 1.9 (b)) upon which this analysis is based.

#### 5.1.4 Analysis of the general northwards decrease of sea depths

Whereas the dimensions of an ocean ridge <sup>are</sup> determined by temperatures in the lithosphere alone, the uplift of the whole ridge and basin system relative to sea level, if considered to be the result of regional variations of mantle temperatures, will be dependent on the distribution of density and temperature in both the lithosphere and asthenosphere. The temperature distributions, and thus the density distributions in the lithosphere are obtained as by-products of the analysis of ocean ridge dimensions given in section 5.1.3, above, but the extension of the data into the asthenosphere is subject to several uncertainties:-

- 1) the geotherm at depths below the lithosphere, where radiative heat transfer and mass motions may exist.
- 2) the degree of partial melting of the mantle material at depth.
- 3) the depth to which lateral variations of temperature persist.

These factors limit the accuracy of the following analysis of the uplift of the sea floor.

Relevant geotherms were produced by smoothly joining the calculated temperature profiles in the lithosphere to the oceanic geotherm of Ringwood et al (1964). The lithospheric profiles used were those calculated to exist far from the spreading centre in slabs of the thicknesses which gave the best fits to the observed bathymetry in section 5.1.3, above. Shallow temperature gradients below about 200 km lessen the uncertainty in this considerably since the calculations which follow are concerned with lateral variations of density at a given depth, and decreased temperature gradients result in decreased separation of the geotherms, as is evident in figure 5.3. On the basis of the convergence of these geotherms,

Figure 5.3. Geotherms produced by joining the calculated temperature gradients for 70, 80, 90 and 100 km thick lithospheres (with base temp at wet solidus) to the geotherm of Ringwood et al (1964). Also shown are the limits on the temperature at 370 km depth suggested by Fujisawa (1968) (see section 5.1.4).

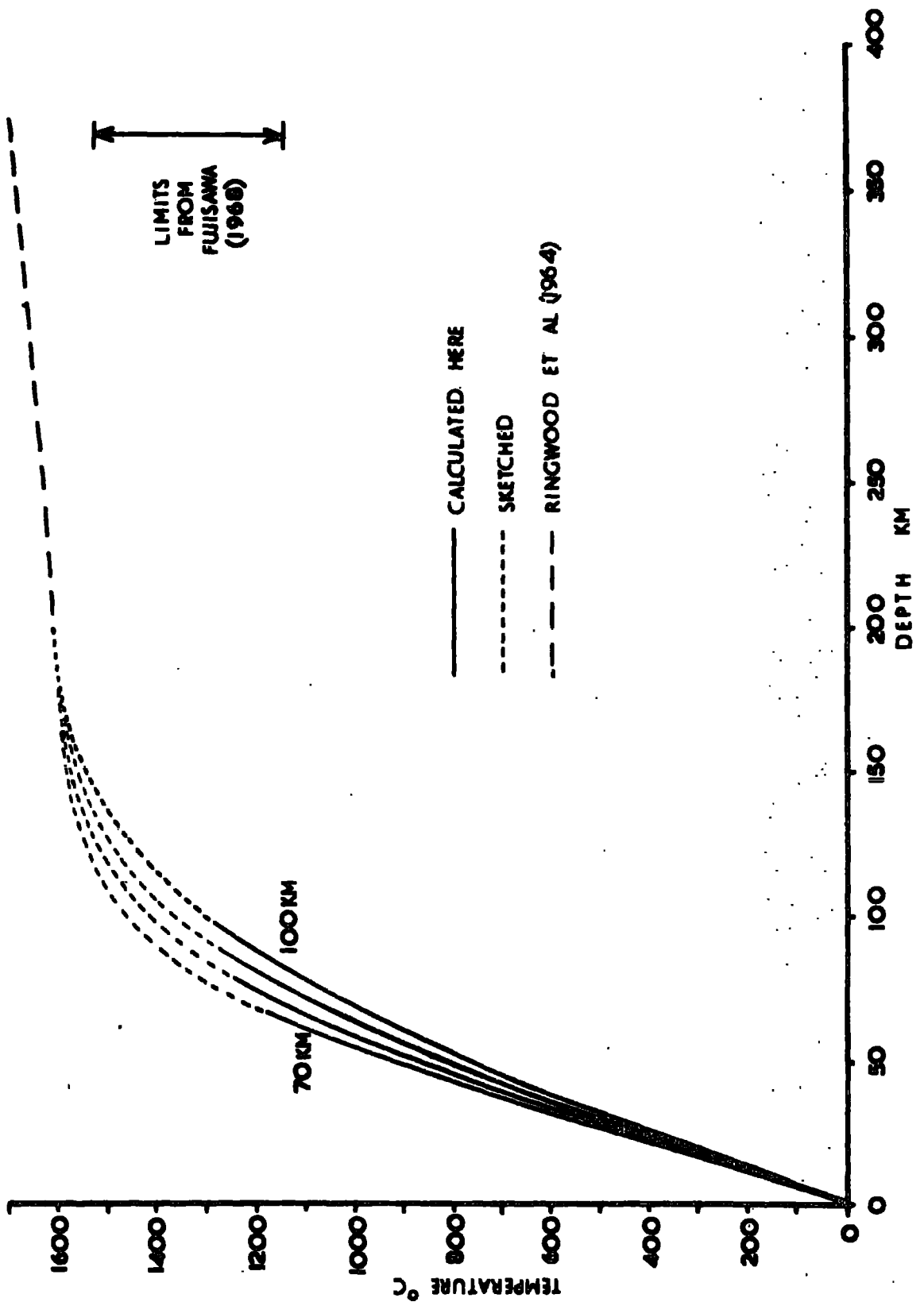


Figure 5.3.

it is suggested that the lateral temperature variations beneath the part of the Atlantic concerned may have effectively died out by about 200 km depth. Fujisawa (1968) suggested limits on the temperature present at 370 km depth based on the requirements of the olivine-spinel phase change to which the existence of the mantle transition zone is generally attributed. His limits are considerably lower than the corresponding temperature indicated by the geotherm of Ringwood et al (figure 5.3). Verhoogen (1973) has presented geotherms derived by smoothly joining lithospheric temperature profiles to asthenospheric profiles calculated by Turcotte & Oxburgh (1969) in accordance with these limits. Such geotherms require substantial increases in effective thermal conductivity at the base of the lithosphere which are in disagreement with the results of Schatz & Simmons (1972). However, the choice of asthenospheric temperature profiles is not critical, and in this work the geotherms shown in figure 5.3, based on that of Ringwood et al (1964) were adopted and applied to the diagram illustrating partial melting of wet pyrolyte given by Green (1970) (figure 5.3a) to estimate the density distributions in the asthenosphere (appendix 2). These were coupled to the calculated density distributions in the lithosphere to produce a density-depth profile from the sea floor down to 200 km for each of the geotherms studied. The profiles are listed in appendix 2. The masses of material in vertical columns subject to the differing geotherms above this 200 km base level were then determined and the discrepancies between them balanced by differences in mass due to water depth variations.

Figure 5.4 illustrates the method used. If  $M_a$  and  $M_b$  are the masses of mantle material present in 200 km high columns subject to geotherms A and B respectively, and if  $h$  is the uplift of the ocean floor at B relative to that at A, then for isostasy

$$\rho_w \cdot h + M_a = \rho_{200} \cdot h + M_b$$

where  $\rho_w$  = density of water and  $\rho_{200}$  = density of the mantle rocks at 200 km depth.

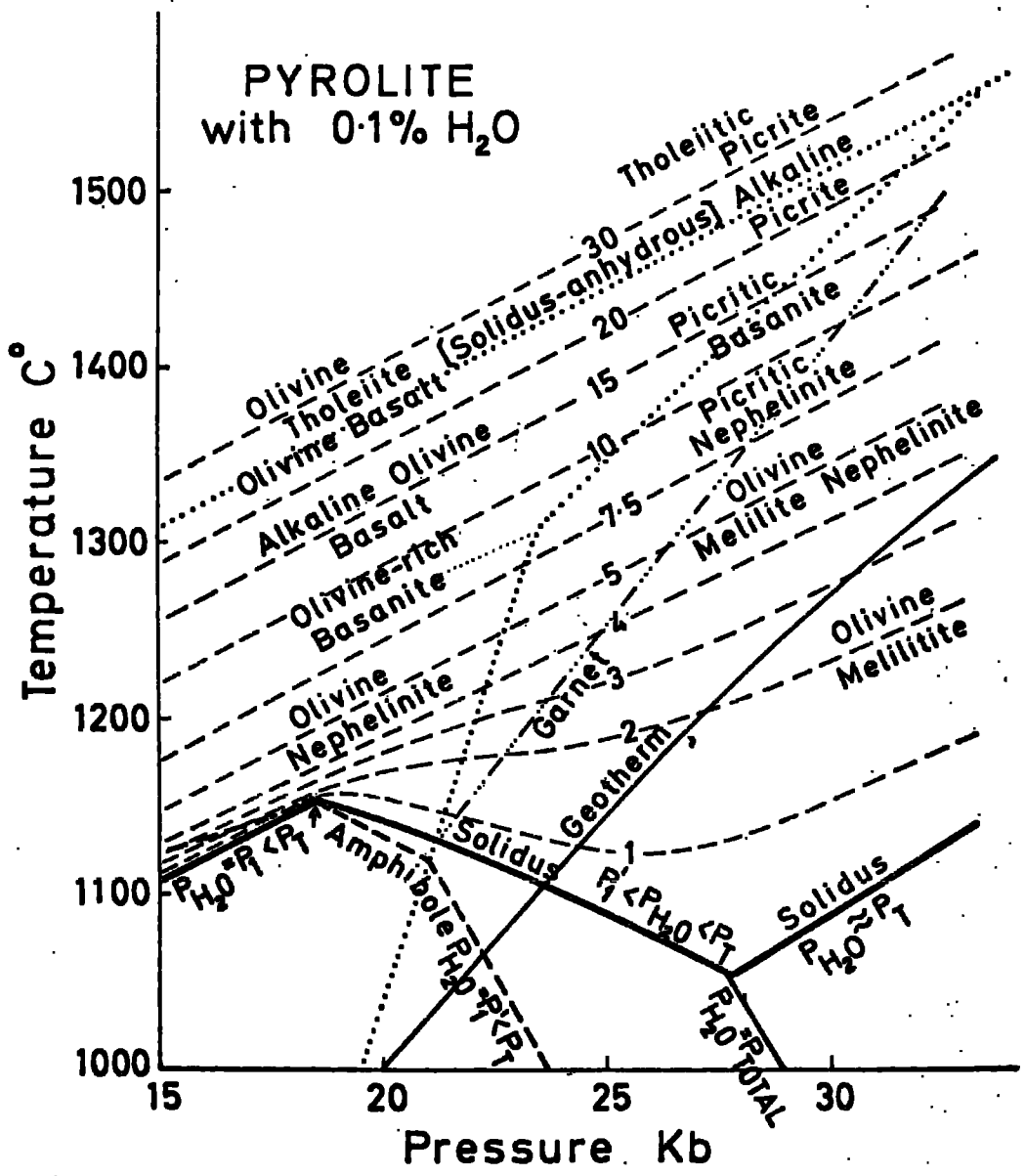


Figure 5.3a. Phase diagram for the partial melting of basalt. Reproduced from Green (1970).

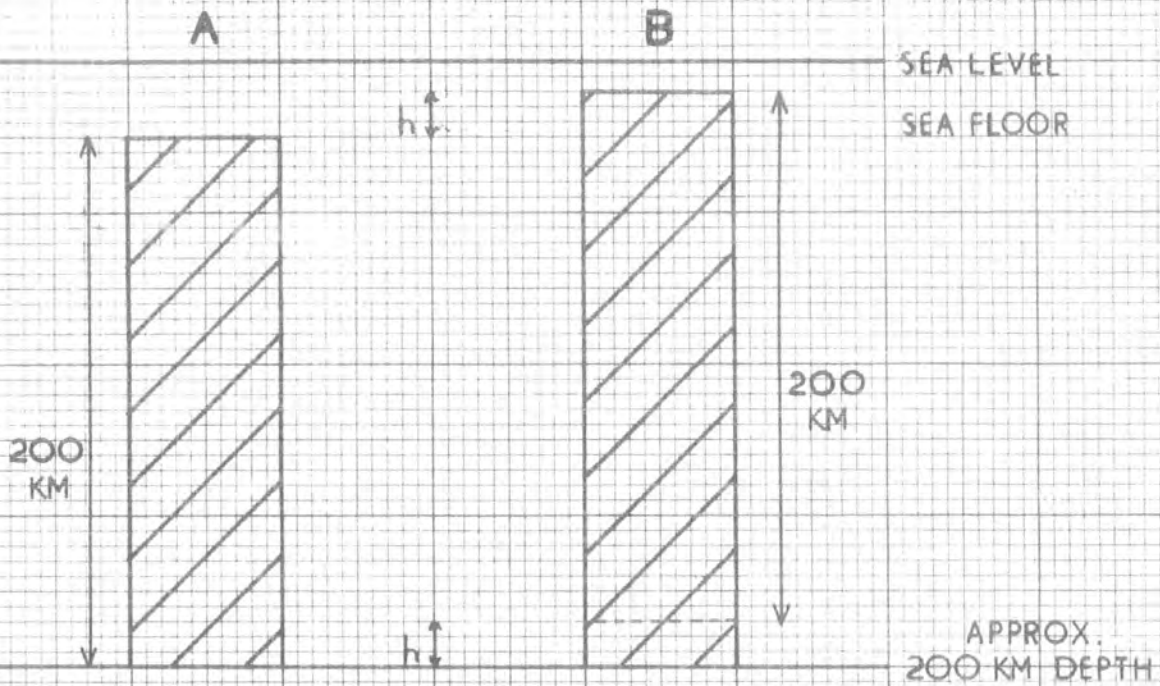
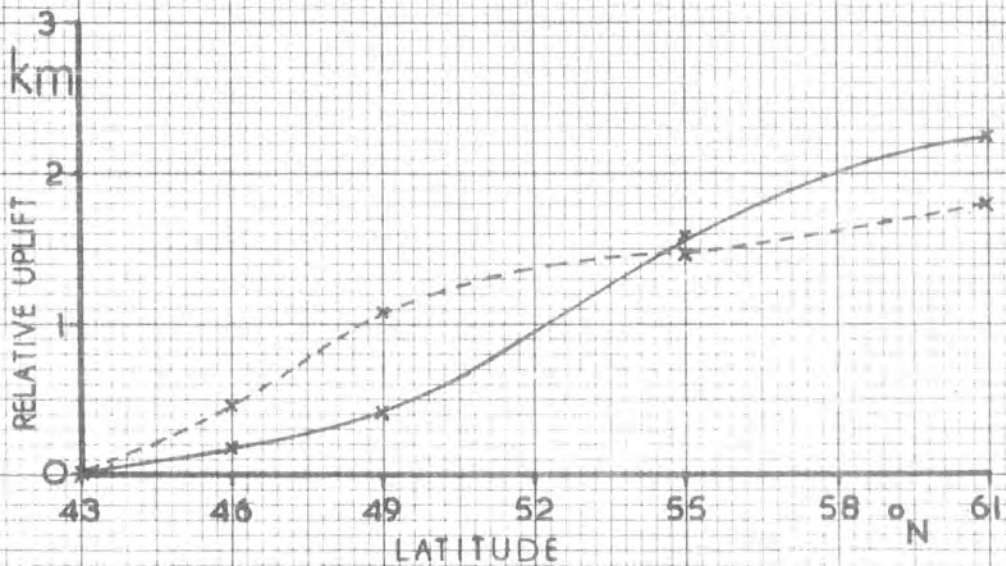


Diagram to illustrate the procedure employed to estimate the relative uplift of different parts of the ocean basins with respect to sea level. (see section 5.1.4.)



Relative uplift of different parts of the North Atlantic ocean basin. Observed as in figure 1.9(a), calculated obtained as described in section 5.1.4. The observed data are shown as a continuous line. The data are uncorrected for sediments.

Figure 5.4.

The relative uplift of different parts of the North Atlantic basins calculated by this method is shown, together with the observed uplift, in figure 5.4. About 60% of the uplift is caused by variations of density above 80 km depth, the remainder being from the less well defined variations in the asthenosphere. While not matching the observed uplift exactly, the results agree to within an order of two, and the differences between the observed and calculated data could be easily reduced by slightly adjusting the assumed asthenospheric geotherms.

#### 5.1.5 Results of the preliminary study

The calculations described in sections 5.1.3 and 5.1.4 show that the estimates of raised upper mantle temperatures based on (a) ocean ridge dimensions and (b) relative basin uplift are compatible, indicating that the topographic variations in the North Atlantic may be complementary results of sea floor spreading occurring above a thermally non-uniform asthenosphere (a suggestion which is considered in greater detail in sections 6.1 and 6.5). Conversely, variations of ridge dimensions can only be explained by this model if they are accompanied by appropriate variations of basin depths.

## 5.2 Detailed study of the North Atlantic between 15 and 61°N

### 5.2.1 Introduction

In this section bathymetric data for the whole North Atlantic are studied and an empirical relationship is derived between ocean ridge dimensions and the depths of the adjacent basins. The existence of such a relationship is to be expected from the results of the initial study described previously in section 5.1.

### 5.2.2 The data

#### 5.2.2.1 Bathymetric Profiles

The western halves of the following bathymetric profiles were used in this study:- NC, ND, NE, NF, NG, NH, NI, NL, NM, NN, NP and NR. The locations of these profiles are shown in figure 1.2, and the profiles themselves in figures 1.3 to 1.6. They cover the North Atlantic from the region of the equatorial fracture zones to Iceland. Four other available profiles from this area were not used:- NJ, NK, NO and NQ. The reasons for rejecting NO and NQ have already been given (section 5.1.2) and similarly NJ and NK were omitted because of the disturbance of the centres and eastern flanks of the profiles in the region of the Azores. As noted previously (section 1.2.6), the lack of disturbance of the oceanic topography to the west of the Azores suggests that the uplift of the islands themselves may be a result of the intersection of the Azores-Gibraltar fracture and the Mid Atlantic ridge, a situation which is outside the scope of the present work and thus justifies the exclusion of the profiles NJ and NK. The eastern halves of the profiles were not studied because of a number of complicating factors:-

- 1) the existence of the Hatton and Rockall Banks.



- 2) the extremely thick sediments known to exist to the west of the Hatton bank (figure 1.7).
- 3) the disturbance of the topography between  $30^{\circ}$  and  $45^{\circ}$ N, presumably by the Azores-Gibraltar fracture and the independent motions of the Iberian peninsular.

However, the bathymetric profiles are generally symmetric where such complicating factors are absent (figures 1.3 - 1.6).

#### 5.2.2.2 Sedimentary cover

Estimations of the approximate thicknesses of sediment present along the lines of the bathymetric profiles were made by examining the isopach map of Ewing, Carpenter, Windisch & Ewing (1973). The sedimentary cover was effectively removed by adding half the appropriate thicknesses to the water depths present at each point along the profiles, thus allowing for isostatic readjustment as noted in section 1.2.5. The thickness of sediment removed in this way varies from zero in the region of  $30^{\circ}$ N to more than one kilometre in higher latitudes. Since thicknesses generally increase with distance from the spreading centre, the removal of the sediment increases both the elevation of the ocean ridge above the basins and also the depths of the basins themselves.

The greater thicknesses of sediment present at higher latitudes result in larger adjustments of observed bathymetry being necessary to the north of the Azores than are required to the south. Nevertheless, the results of the model presented in the next section (5.2.3) and the data shown in figure 5.5 (the depths of the western basins before and after sediment removal plotted against latitude) demonstrate that the previously noted bathymetric trends in the North Atlantic remain.

Figure 5.5. Depths in the western North Atlantic ocean basin before and after removal of sediments. Water depths as in figure 1.9(a). Sedimentary thicknesses from Ewing, Carpenter, Windisch and Ewing (1973).

LATITUDE

°N

15 25 35 45 55 65

BASIN DEPTH

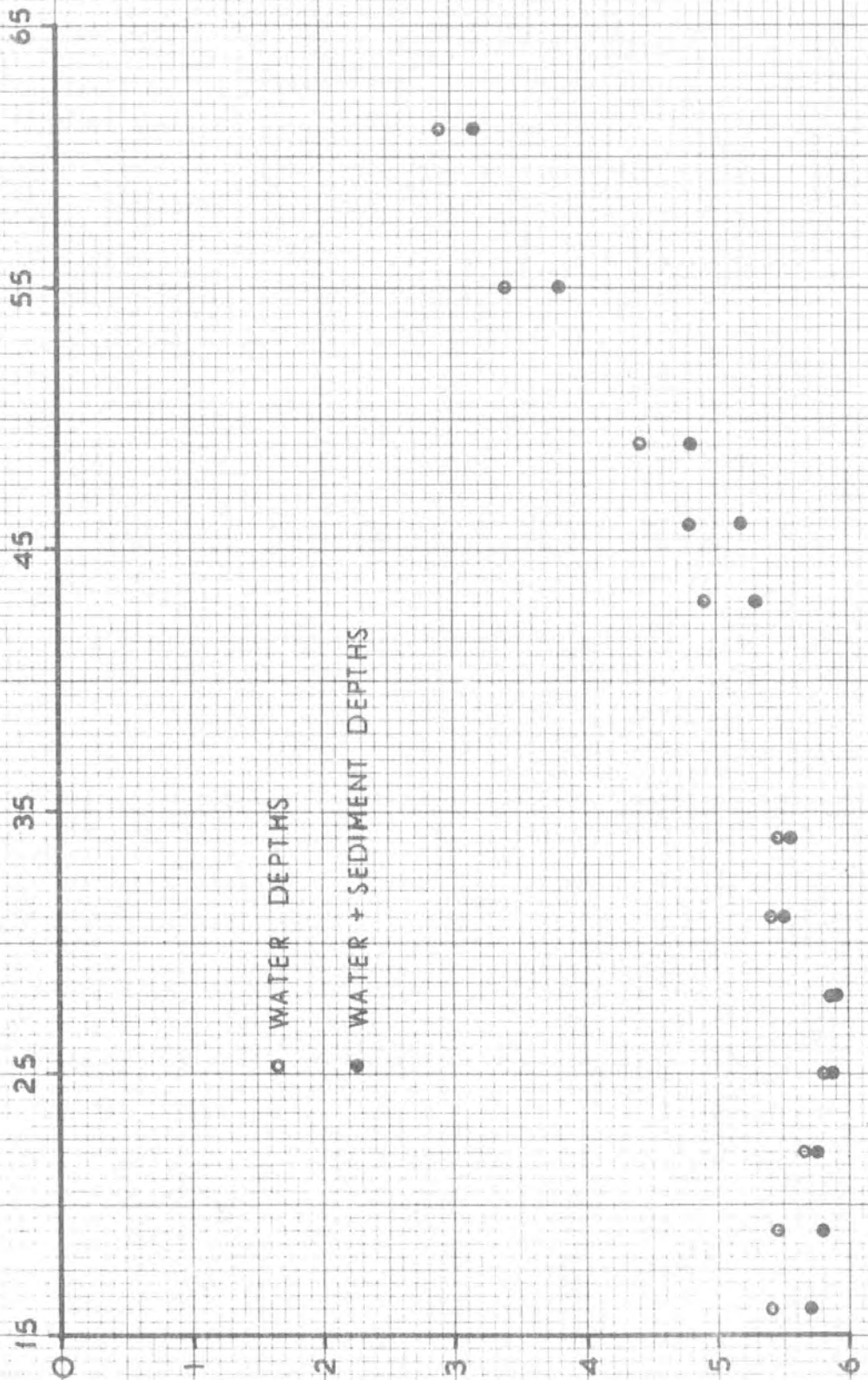
km

○ WATER DEPTHS

● WATER + SEDIMENT DEPTHS

0 1 2 3 4 5 6

Figure 5.5.



### 5.2.3 The analysis

Theoretical bathymetric profiles were generated by the program SYN (Appendix 8 and section 4.8) from age-elevation data (shown in figure 4.4 and appendix 4) which had been previously derived for an appropriate range of lithospheric thicknesses. The sediment corrected profiles obtained from the observed data by the method described in section 5.2.2.2 were then compared with these theoretical profiles, the comparison being done within the program SYN as follows. For each profile, the bathymetry was averaged over the extent of the abyssal plain to provide a datum level above which the ocean ridge might be considered to rise. The theoretical profile was then shifted vertically until the observed and calculated data for the abyssal plain coincided at this datum level. The variances of the resulting bathymetric fits (some of which are shown in figures 5.6 and 5.7) were then calculated according to the expression given in section 5.1.3, and for each of the profiles considered are plotted against lithospheric thickness in figures 5.8 and 5.9. The positions of the minima of these curves indicate the lithospheric thicknesses resulting in the best fits to the observed topography at the various latitudes and are plotted in figure 5.10. The error bars shown were determined from the shape of the variance curves for each profile and indicate the range of lithospheric thickness over which the variance is within 0.01 of the minimum value obtained for the profile concerned. More usual criteria for determining error bars (for example, the range over which the variance is less than or equal to twice the minimum value) were rejected because of the biasing effect of short wavelength topography, which is not modelled and which occurs to differing extents on each profile. Such biasing effectively applies different "D.C. shifts" to each of the variance curves. These shifts, however, have no relevance to the comparison of the accuracy of fitting the long wavelength topography of the various profiles with the model. The chosen criterion for the error bars ignores the biasing effect and thus provides a valid measure of the relative accuracy with which the minima of the variance curves are defined.

Figure 5.6. Observed and calculated bathymetric profiles at two latitudes in the North Atlantic. The thicknesses of lithosphere used in the calculations are marked (km). Comp. 1 basalt : 3 dunite, base temp-wet solidus. The data have been corrected for sediments.

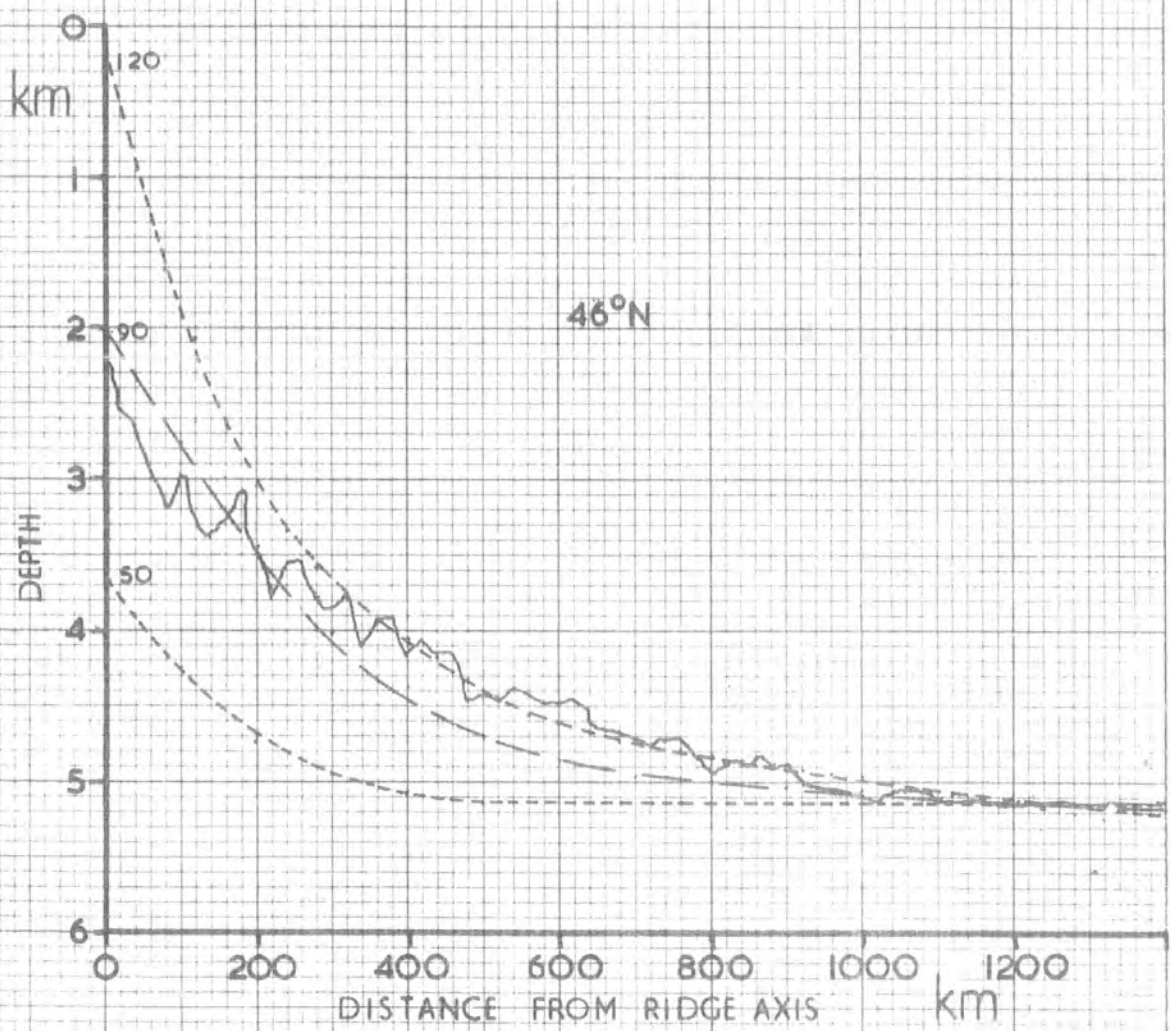
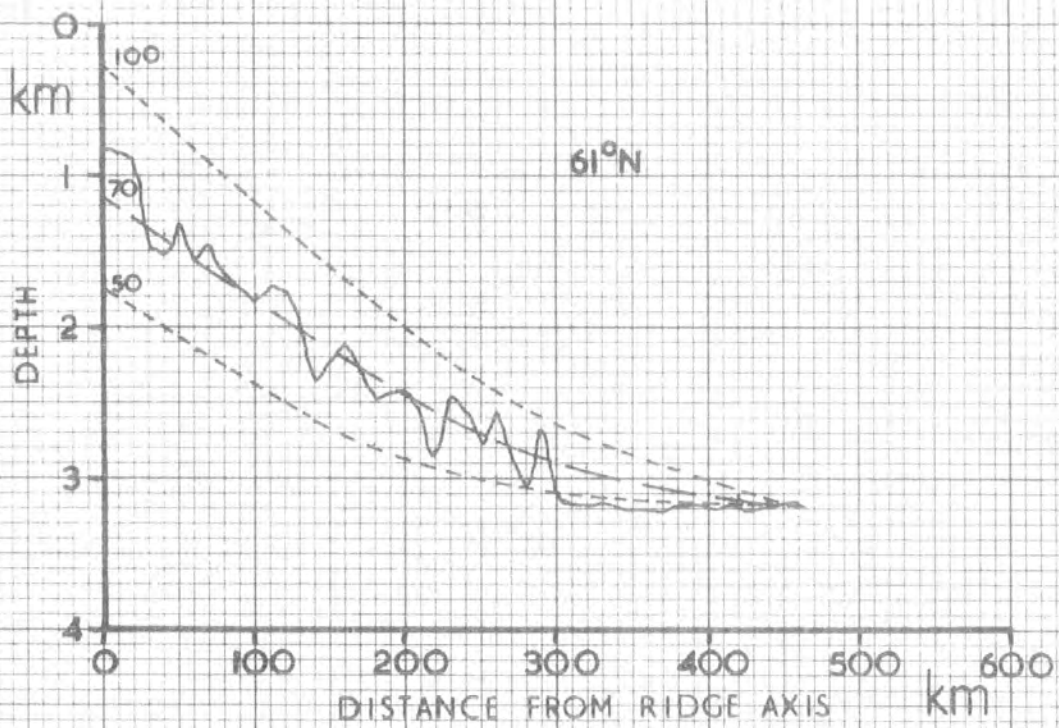


Figure 5.6.

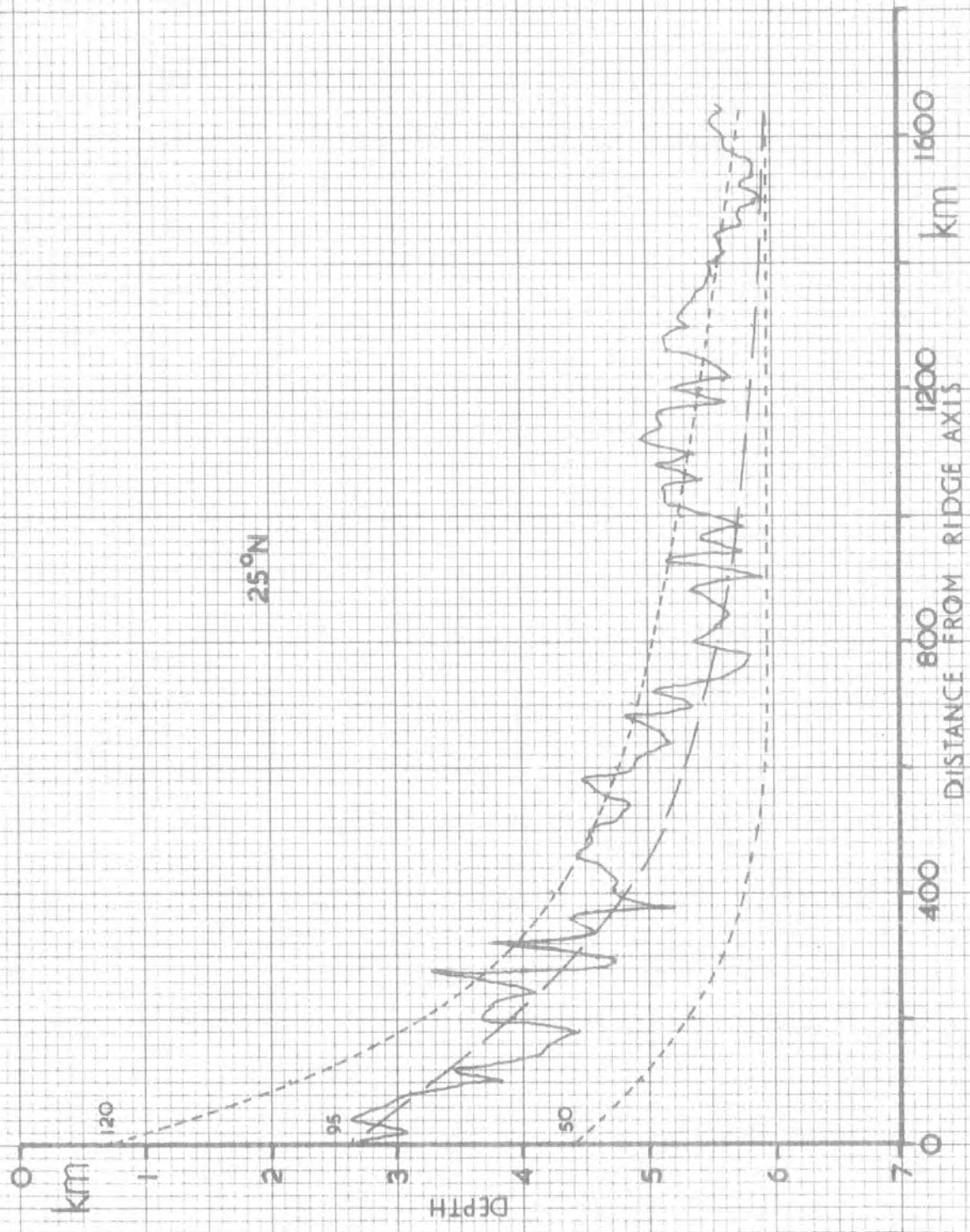


Figure 5.7. As figure 5.6, but one latitude only.

Figure 5.8. The variances of the bathymetric fits between observed and calculated data from the North Atlantic plotted against the lithospheric thicknesses used to derive the calculated profiles (see section 5.2.3). The data are corrected for sediments and the profiles concerned are indicated. The origins of some of the variance curves are not at the origin of the axis, and these are indicated as appropriate.



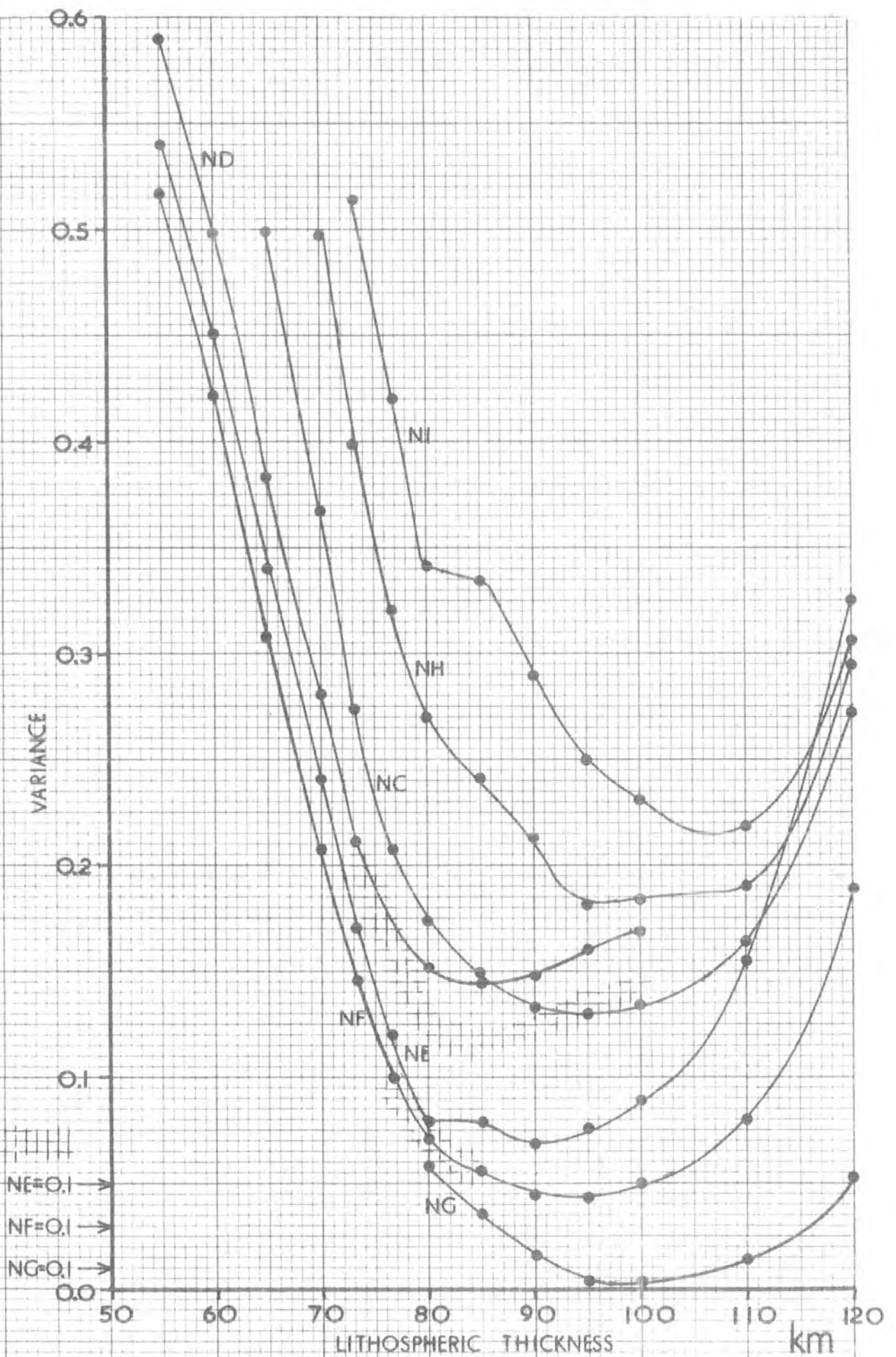


Figure 5.8.

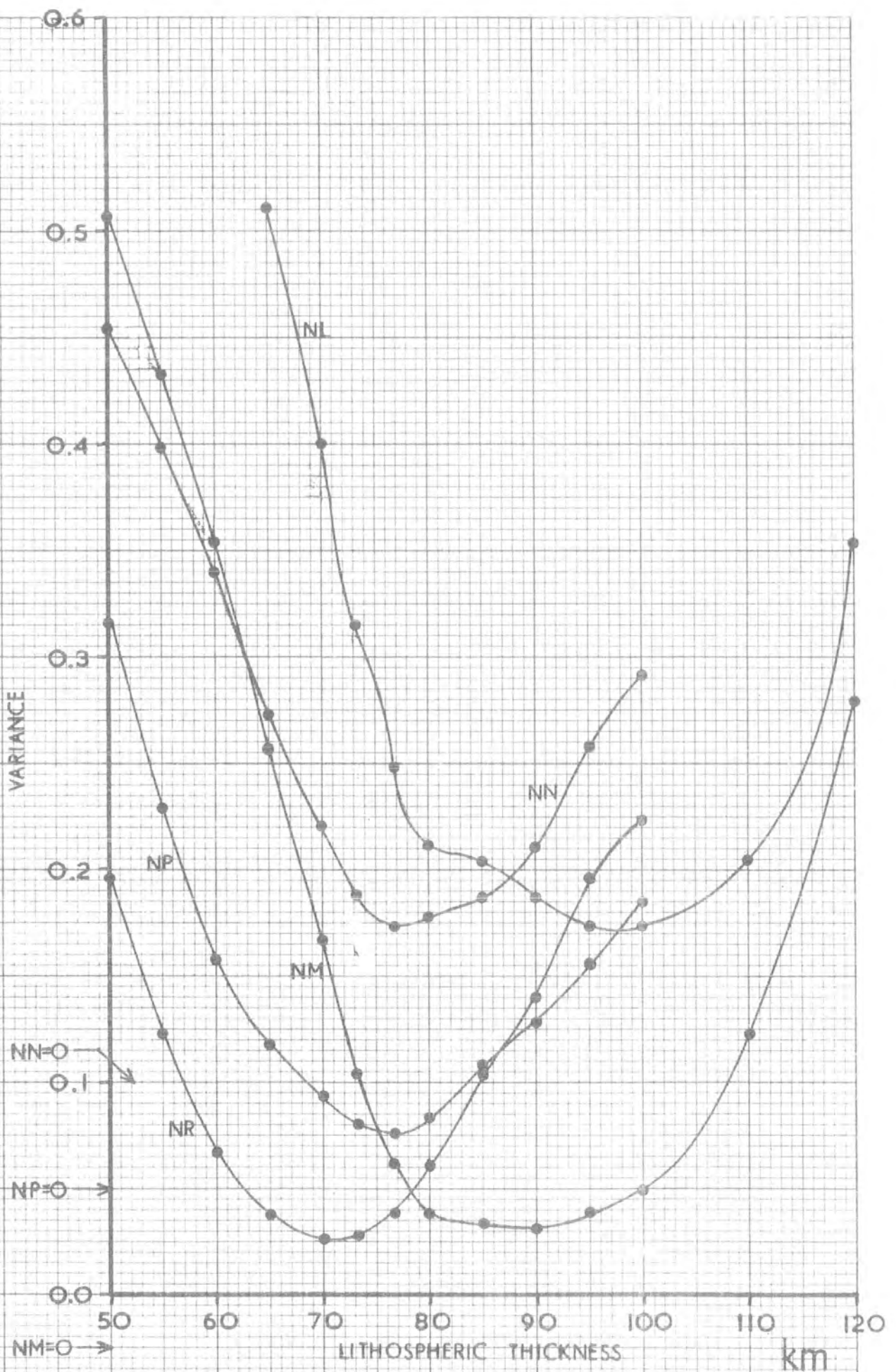


Figure 5.9. As figure 5.8.

Figure 5.10. The thicknesses of lithosphere which give the best fits to observed topography in the North Atlantic plotted against latitude. The thicknesses are indicated by the positions of the minima of the data shown in figures 5.8 and 5.9, and the error bars are calculated as described in section 5.2.3.

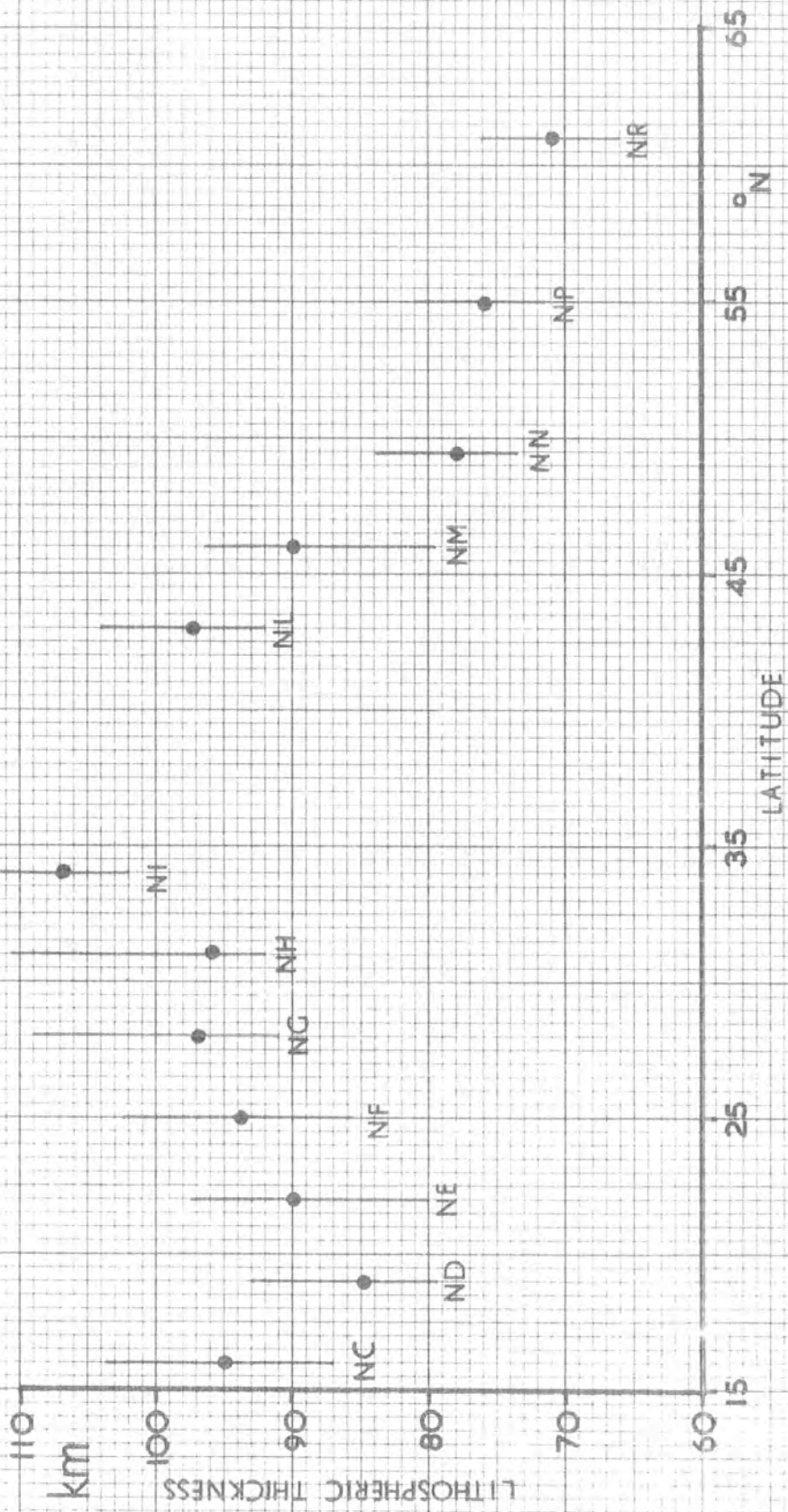


Figure 5.10.

North of the Azores a trend of decreasing lithospheric thickness with increasing latitude is shown, similar to that obtained using data uncorrected for sediment variations in section 5.1.3. However, the removal of the sediment layer results in different values being indicated for the thicknesses of the lithosphere. South of the Azores, the interpretation is less certain. Taken at face value, the data suggest a decrease of lithospheric thickness towards the equator, with a sudden reversal of the trend at about  $19^{\circ}\text{N}$ . This suggestion relies on the validity of the results for two profiles - ND and NI - which are both subject to some suspicion. NI is close enough to the Azores for its eastern half to be disturbed in a manner similar to that which caused NJ and NK to be excluded from this analysis (section 5.2.2.1) while ND is approaching the zone of major ridge offsets in the equatorial Atlantic, and gives a result in disagreement with NC. Taken without these two profiles, the data indicate little change of lithospheric thickness with latitude. As noted in section 5.1.5, the present model can only explain variations of ridge dimensions, and thus lithospheric thickness, if they are accompanied by appropriate variations in the depths of the neighbouring abyssal plains. Consequently, although a uniform lithospheric thickness in this region is to be expected from the constancy of the basin depths plotted in figure 5.5 and figure 1.9 (a), such an interpretation is in disagreement with the possible southward decrease of ridge cross-sectional area shown in figure 1.9 (b). The explanation for this apparent conflict may lie partially in the fact that the data shown in figure 1.9 (b) do not include any allowance for sediment variations, partially in the considerations discussed in section 5.2.4, below, and partially in the fact that, while the data plotted in figure 1.9 (b) express the area of the ridge cross-section alone, the lithospheric thicknesses are derived by modelling the cross-section and shape of the mid ocean ridge. Thus an isolated seamount, while being included in the cross-sectional area, is effectively excluded by the model from consideration during the derivation of the lithospheric thicknesses. In addition, the data of figure 1.9 show the measured ridge cross-section to be more

subject to disturbance by fracture zones than are the basin depths. This is to be expected from the relative ease with which representative basin depths may be determined, compared with the difficulties involved in sampling the depths above an irregular feature such as an ocean ridge. Taken together these factors suggest that the interpretation of the southern half of the North Atlantic as an area of relatively constant lithospheric thickness is more likely to be correct.

#### 5.2.4 Implications of the results

The calculations presented in section 5.1 imply that a decrease in ocean ridge dimensions should always be accompanied by a shallowing of the neighbouring basins, if underlying thermal inhomogeneities are considered to be the cause of the variations. Figure 5.11 shows the relationship between modelled lithospheric thicknesses and basin depths derived from the above data for the North Atlantic. There is, as expected, a general increase of lithospheric thickness with basin depth, but the graph, while steep for thicknesses between 70 and 85 km, becomes gradually flatter towards higher values. The cause of this lies in fact that the maximum age of the data analysed in the present work is about 80 My (see section 1.2.4) and at this age, lithospheres thicker than about 80 km have not yet cooled to equilibrium. Calculations made using the program HEAT (appendix 5 and chapter 2) show that an additional 150 My is required for the cooling of a lithosphere 100 km thick to be completed. However, the gradients of the age-elevation graphs beyond 80 My (figure 4.4) are so small that bathymetric profiles calculated from them display increases of basin depths with further distance from the ridge crests which are negligible compared with the increasing confusion of observed bathymetric data by seamount chains and thick and non-uniform sediment piles. Figure 5.12 shows the temperature profiles calculated to exist in lithospheric slabs of various thicknesses 80 My after their formation, and it can be seen that the separation of the profiles decreases as the lithospheric thickness increases. Accordingly, since the depths in the ocean basins may be related to the mantle temperatures (section 5.1.4), it is to be expected that the differences between the depths reached in basins above lithospheric slabs of various thicknesses after 80 My will also decrease with increasing lithospheric thickness, and the flattening of the curve shown in figure 5.11 is an expression of this.

One of the most important parameters of ridge shape which makes it possible to distinguish the bathymetric profiles produced by the cooling of lithospheres of

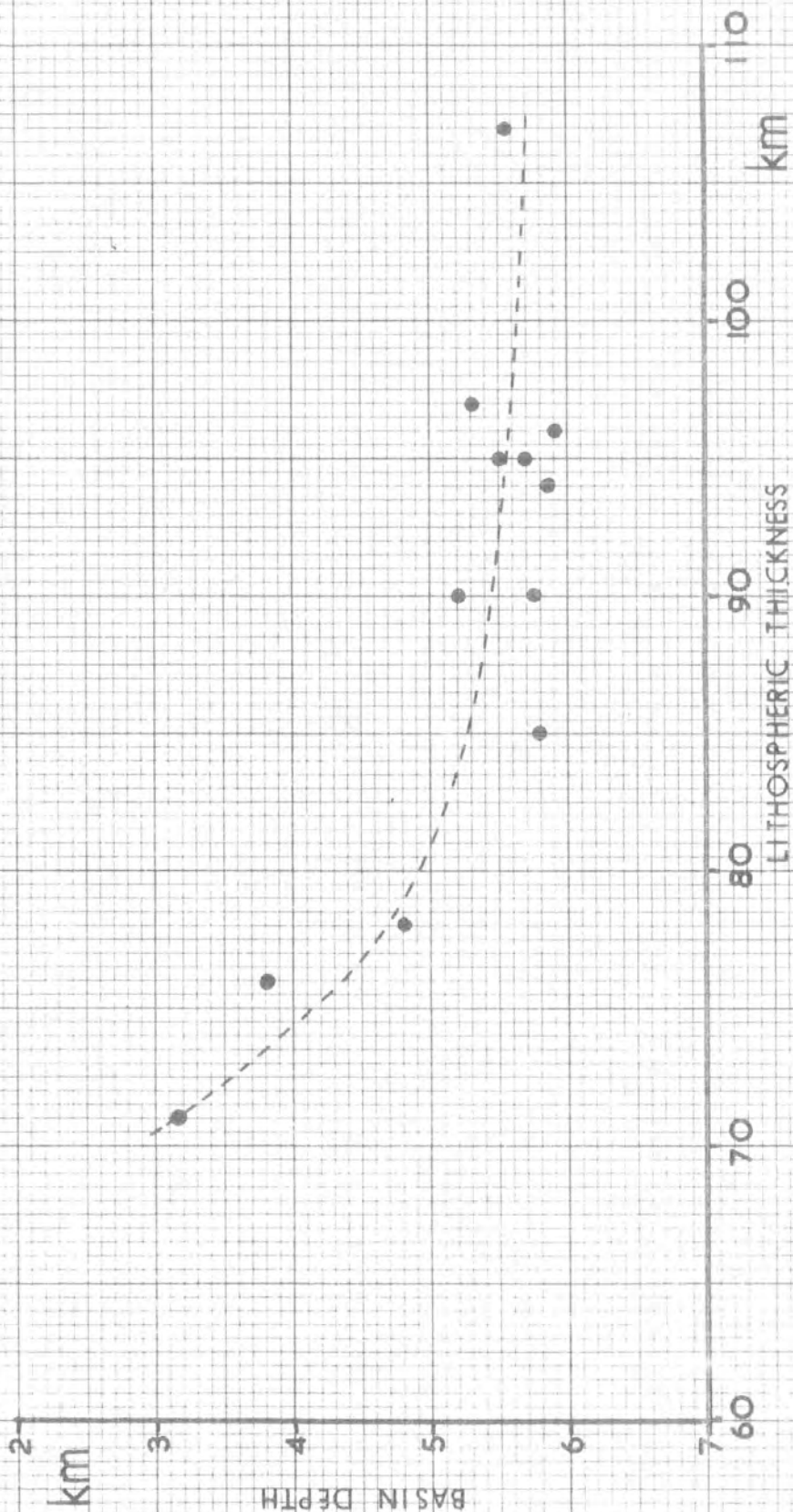


Figure 5.11. A relationship between lithospheric thickness and basin depth as indicated by the data from the North Atlantic.



Figure 5.12. Temperature profiles in lithospheric slabs of various thicknesses 80My after their formation. (comp. 1 basalt : 3 dunite +water). The relevant thicknesses are shown in km. Note the decrease in separation of the profiles as the lithospheric thickness increases.

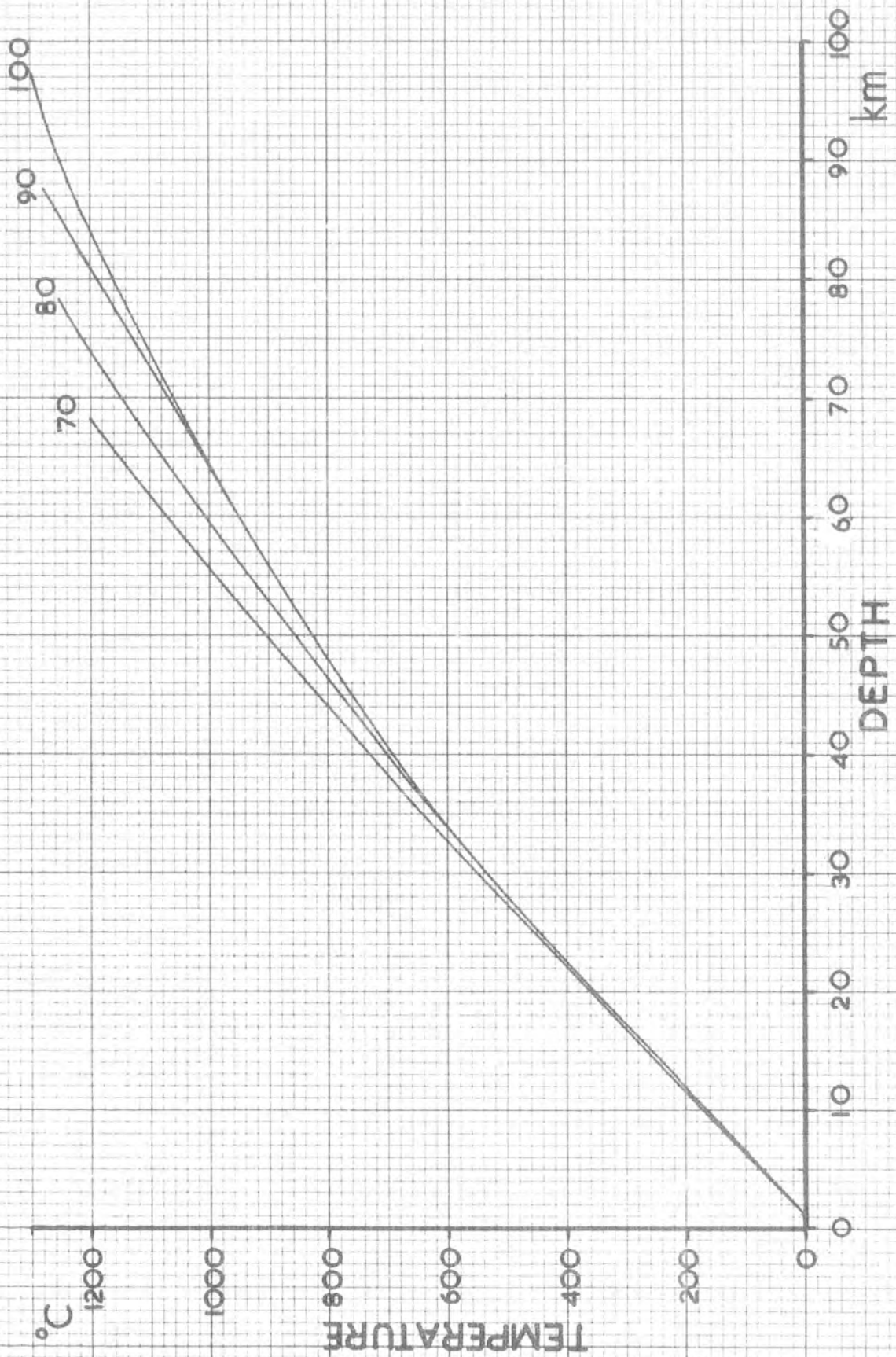


Figure 5.12.

different thicknesses from one another is thus the datum level above which the ocean ridges rise. Its importance is clearly shown by the age-elevation graphs of figure 4.4. Over parts of their lengths, adjacent graphs are effectively parallel and thus almost indistinguishable from one another; for example compare the curves for 95 & 100 km from 0 to 70 My, 90 & 80 km from 0 to 30 My, and 50 & 60 km from 0 to 15 My. The only major difference between these pairs of curves in the regions stated is the height of each above the datum level, and the ability of the model to distinguish topographic profiles produced by the cooling of lithospheres of different thicknesses from one another is thus subject to sufficient data being available, as is outlined below.

#### 5.2.5 Limitations of the model

In order to obtain a clear indication of lithospheric thickness by application of the model to ocean ridge topography, bathymetric data extending from the ridge crest to a distance sufficient to allow for cooling of the lithosphere to equilibrium must be available. The required distance increases with increasing lithospheric thickness for a given spreading rate, and is best expressed in terms of equivalent lithospheric ages as follows:-

Thickness of lithosphere	Required age
50 km	40 My
60	50
70	70
80	90
90	150
100	250

Failure to obtain data corresponding to sufficient age results in the lithospheric thickness being poorly defined (figure 5.8, profiles NG and NH, figure 5.14, profile PV16) or possibly indeterminate (figure 5.15). In some parts of the world's oceans sea floor spreading has been occurring for an insufficient length of time to allow an effective analysis of the ridge topography to be made (for example, the present episode of spreading north of Iceland). In others, while the duration of spreading may be sufficient, subsequent alteration of the topography, for

example by the formation of seamount chains (figures 1.3, 1.4, profiles NF, NH, NI), may render the data unreliable and the likelihood of this having occurred is obviously greater where the sea floor is older.

### 5.3 Study of data from oceans other than the North Atlantic

#### 5.3.1 Introduction

In this section the data presented in chapter 1 for the South Atlantic, Pacific and Indian Oceans and the Norwegian-Greenland Sea are analysed in a manner identical to that described for the North Atlantic in section 5.2. The results show general agreement with the relationship between basin depth and lithospheric thickness derived in section 5.2.4, but there is no evidence in the data studied for the existence of another area in which variations of structure comparable to those of the North Atlantic occur.

#### 5.3.2 The data

All the bathymetric profiles presented in sections 1.3, 1.4, 1.5, 1.6 and 1.7, were used in the following analysis. Where possible (see relevant sections of chapter 1) corrections for sedimentary layers were made as described in section 5.2.2.2. For most of the profiles it was necessary to confine the study to one flank of the ocean ridge. The parts of the profiles used and the reasons for choosing them are set out below.

Area	Profile	Part Used	Reasons for choosing, see also appropriate sections in chapter 1).
S. Atlantic	AV18	East flank	Avoidance of thick sediments off the River Plate.
"	AV20		
"	SAZ2		
"	AV22	West flank	Lack of sufficient length of profile to the east.
Indian Ocean	IOAB	S.W. flank	Avoidance of Indus Cone sediments.
"	IOCD	East flank	Disturbance of west flank by the triple junction of ridges
"	IOFE	N.E. flank	Avoidance of ill-determined but not insignificant thicknesses of sediment on S.W. flank.

cont....

Area	Profile	Part Used	Reasons for choosing
Australia- Antarctic Sea	EL39 EL41 EL45	North flank	As IOFE, extrapolating isopach map (see section 1.6.2).
Pacific	PV16	N.W. flank	Lack of sufficient spreading rate data to the S.E.
"	EL28	West flank	Avoidance of region of complicated spreading history between the East Pacific Rise and South America (see Herron, 1972).
"	EL29		
Norwegian- Greenland Sea	IJMS IJMN	East flank	Proximity of Greenland continental shelf.
"	MRAB	East flank	No reason other than uniformity with the preceding pair of profiles.
"	MRCO		

### 5.3.3 Analysis and Results

The analysis was carried out exactly as described for the North Atlantic in section 5.2.3. Figures 5.13, 5.14 and 5.15 show the variances of the resulting bathymetric fits plotted against lithospheric thickness. The thicknesses giving the best fits to observed topography (as shown by the minima of the curves) are plotted against either latitude (South Atlantic) or an approximate distance scale (Indian, Southern, Pacific) in figures 5.16 and 5.17, with error bars derived as in section 5.2.3. Figure 5.18 shows these thicknesses plotted against the depths of the adjacent ocean basins together with the data presented previously for the North Atlantic. Most of the results lie along the trend suggested by the North Atlantic data, and although a few lie far from it, there are no points which plot between these two extremes. With one exception (profile EL45), the points which do not lie on the North Atlantic trend are derived from topographic profiles subject to obvious local bathymetric anomalies as described below:-

Profiles IJMN, IJMS, MRAB, MRCO. Norwegian-Greenland Sea

The complexity of tectonics in this area has already been noted (section 1.4.4). Spreading about the present axes may only be about 40 My old (Vogt, Ostenso &

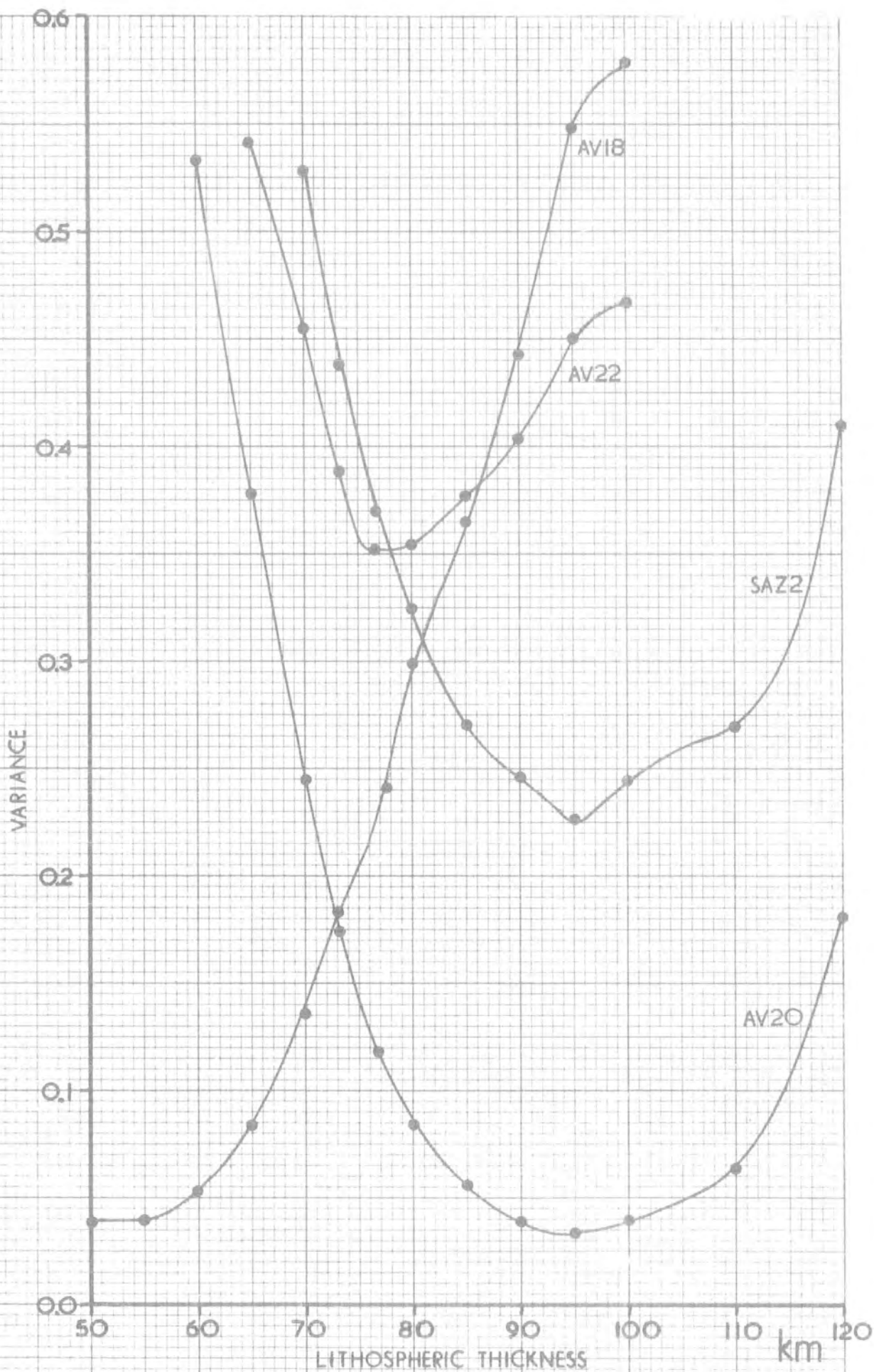


Figure 5.13. As figure 5.8, but for the South Atlantic.

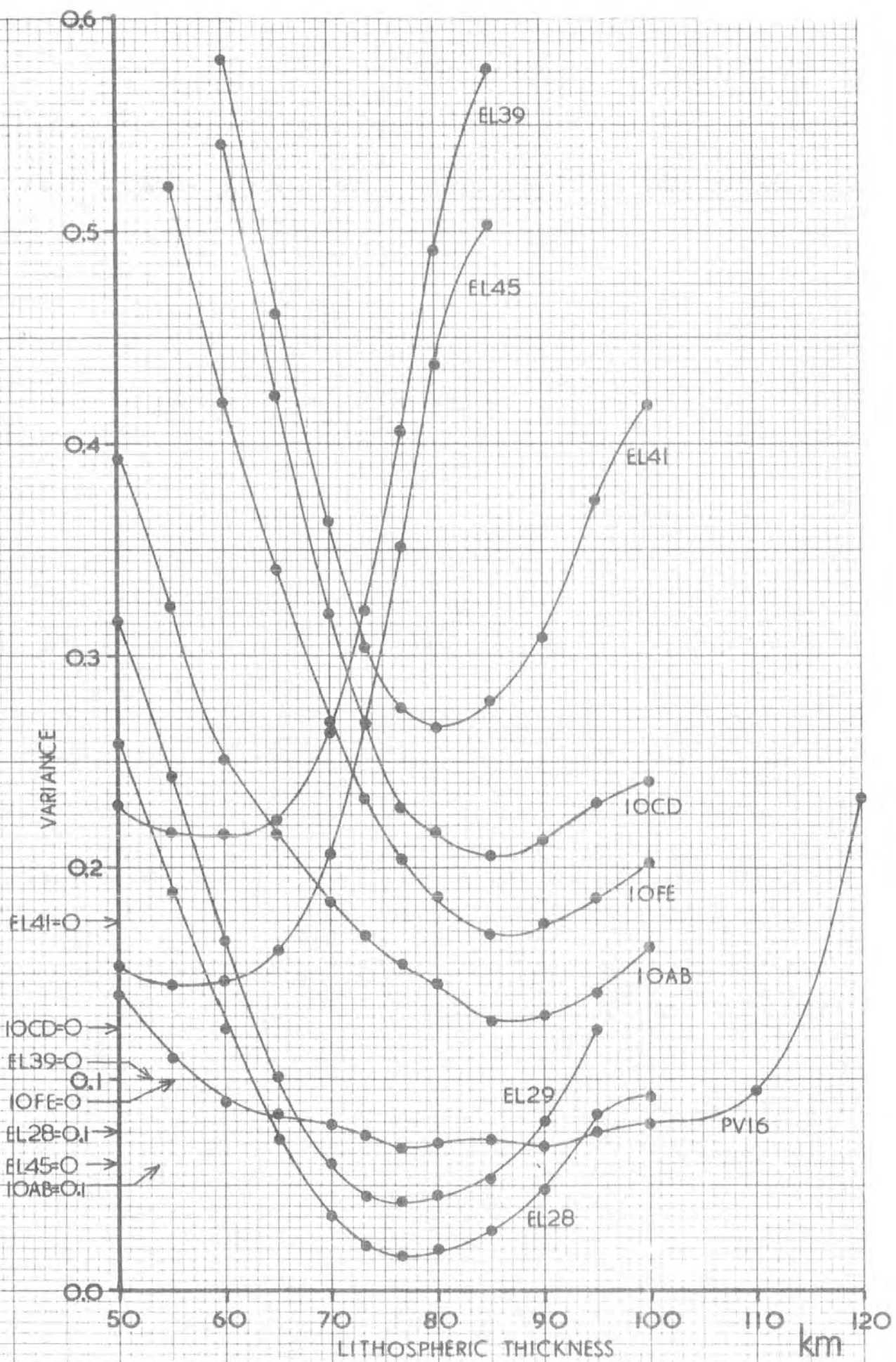


Figure 5.14. As figure 5.8, but for the Indian, Southern and Pacific oceans.



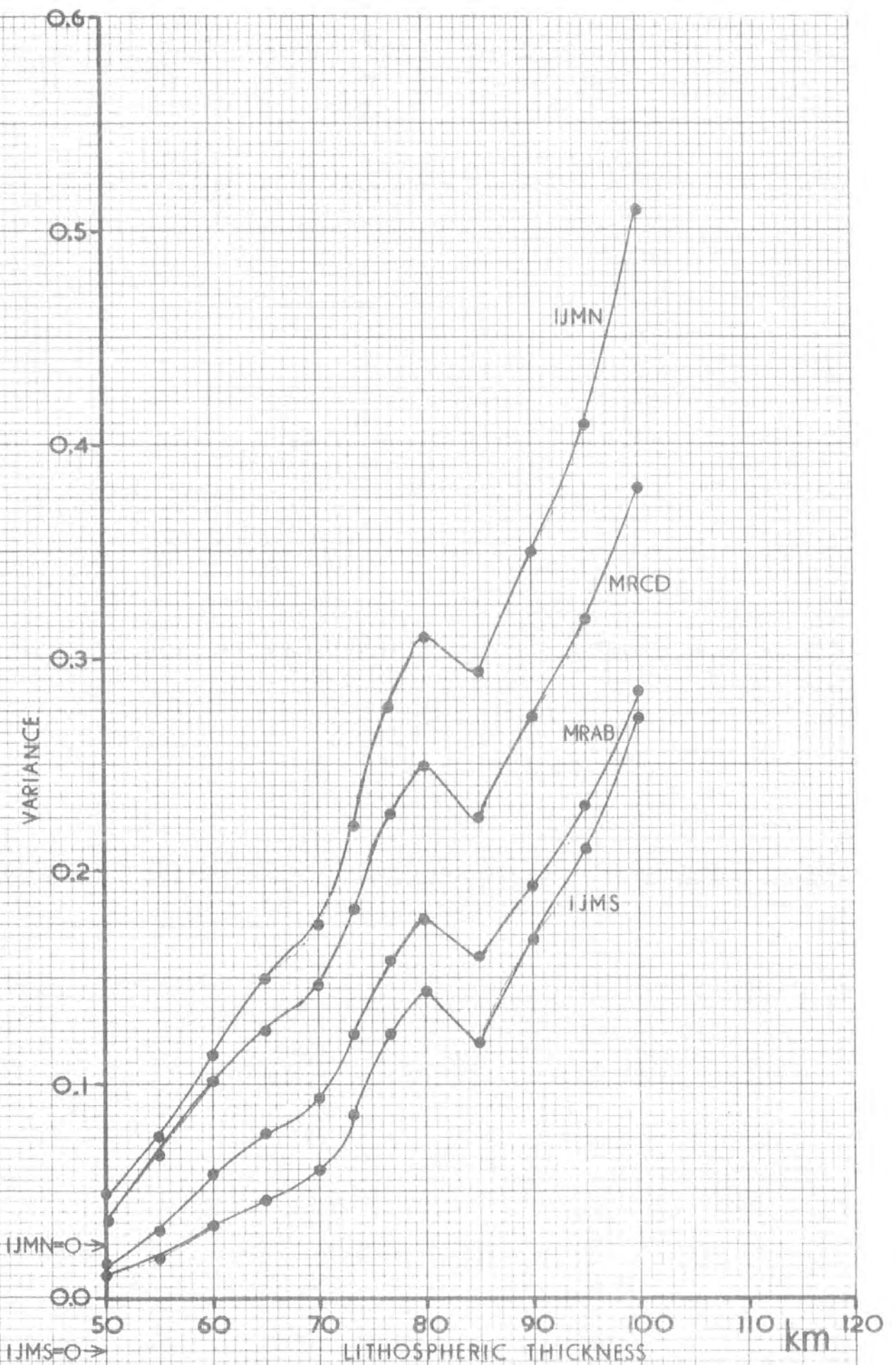


Figure 5.15. As figure 5.8, but for the Norwegian-Greenland sea. Note the absence of minima.

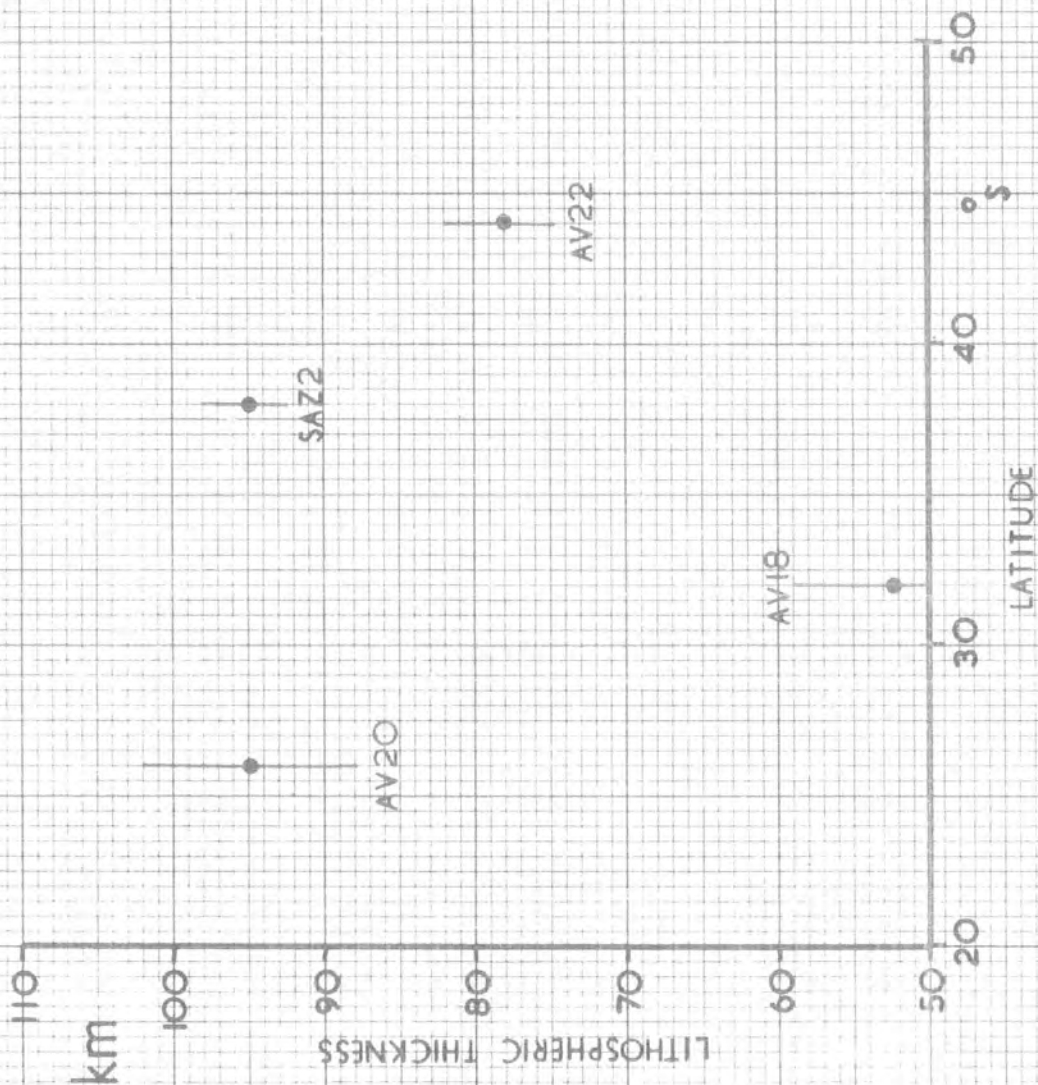


Figure 5.16. The thicknesses of lithosphere giving the best fits to observed topography in the South Atlantic plotted against latitude. Thicknesses from figure 5.13, error bars as described in section 5.2.3.

Figure 5.17. The thicknesses of lithosphere giving the best fits to observed topography in the Indian, Southern and Pacific oceans plotted against an approximate distance scale. Thicknesses from figure 5.14, error bars as described in section 5.2.3.

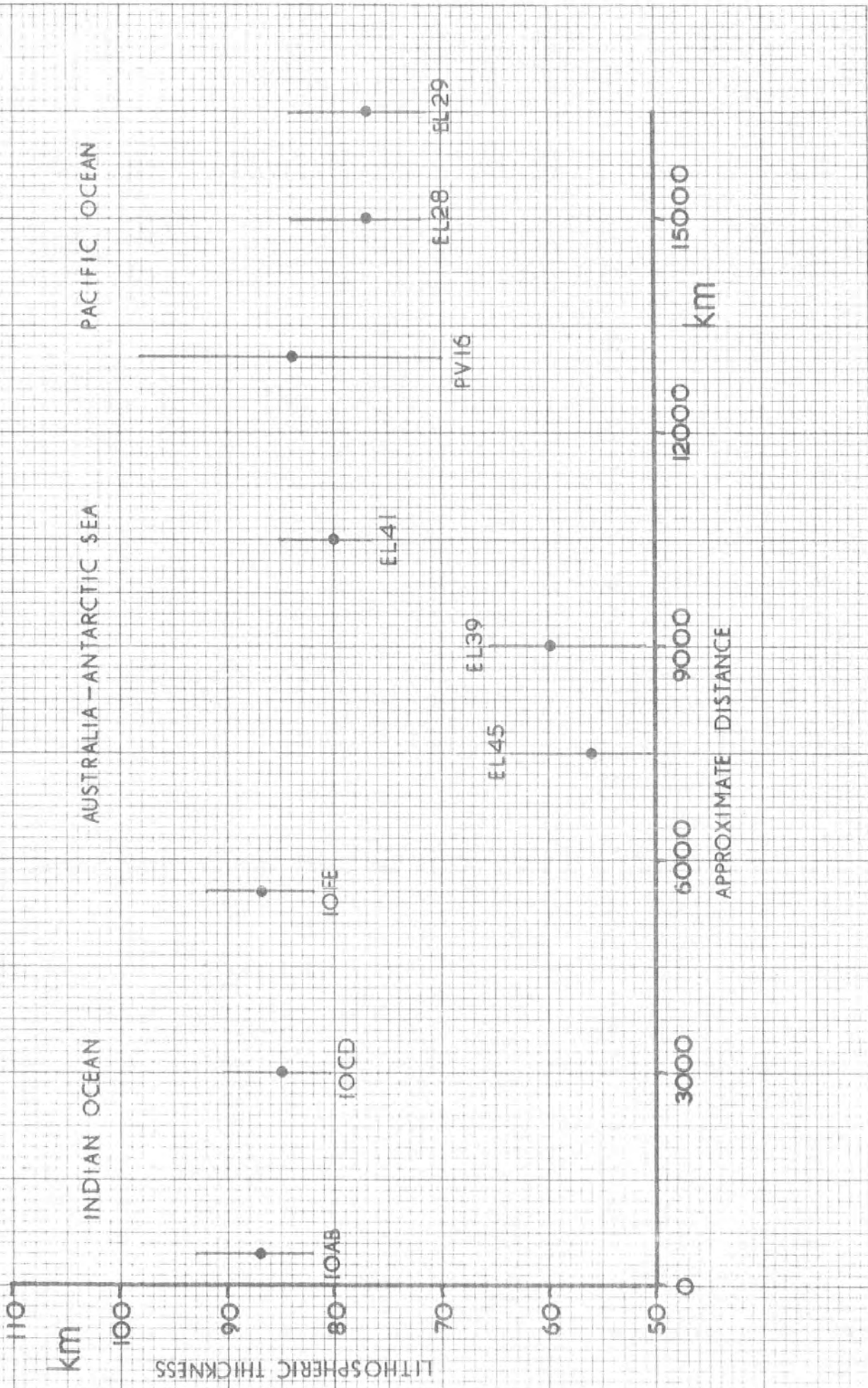


Figure 5.17.

Figure 5.18. The data of the North Atlantic from figure 5.11 (dark circles) and the relationship which they give between basin depth and lithospheric thickness (dashed line) plotted with corresponding data from other oceans. Note that the data from the other oceans is either close to or far from the North Atlantic relationship, but not between these two extremes.

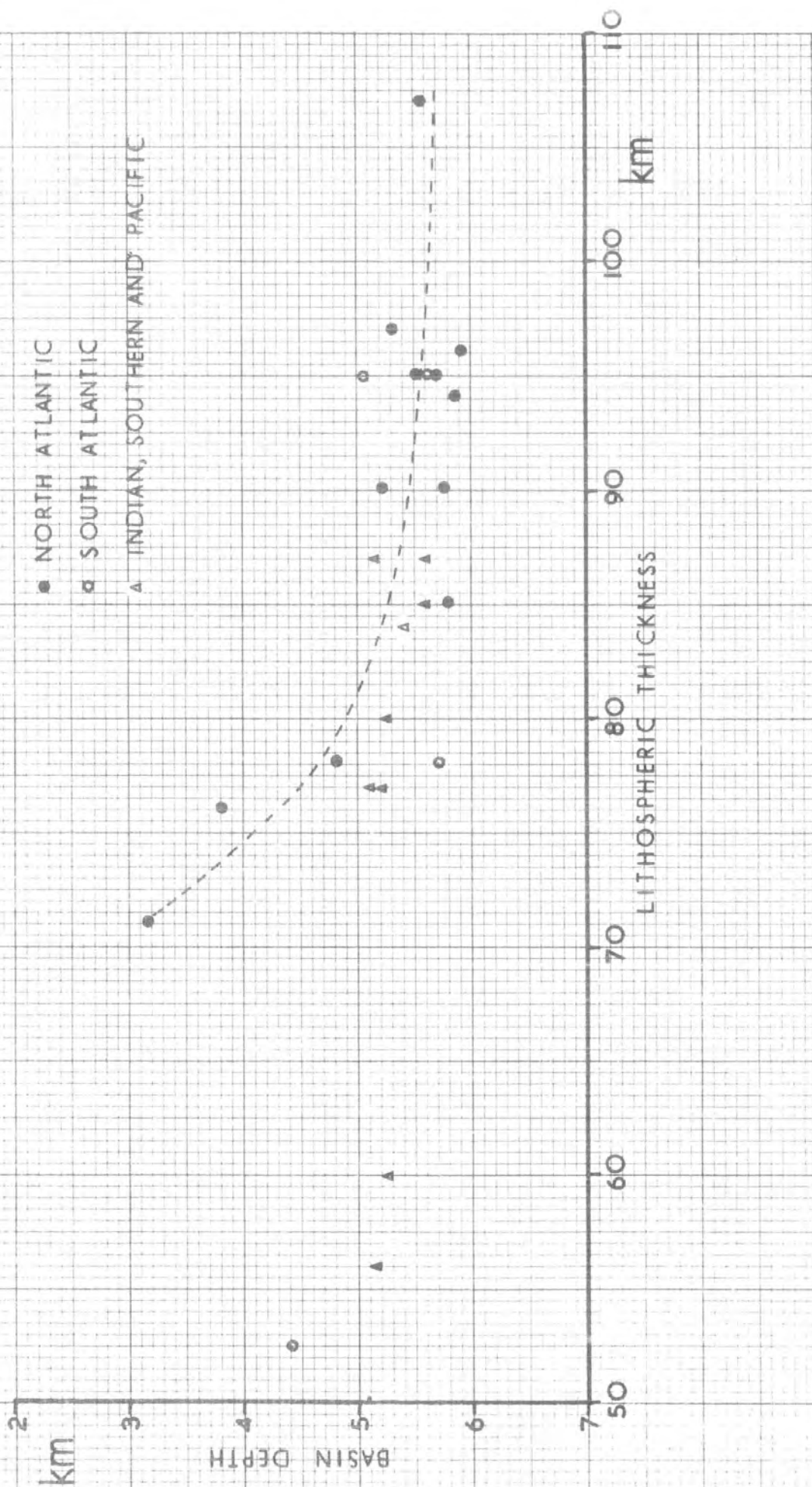


Figure 5.18.

Johnson, 1970) and clear bathymetric profiles exist only over distances equivalent to approximately 30 My of spreading. Since the lithosphere requires at least twice this time to cool to equilibrium (figure 4.4), it is not possible to estimate the datum level above which the ocean ridge rises from the data available. As noted in sections 5.2.4 and 5.2.5, this datum is of great importance in distinguishing between the topographic profiles produced by the cooling of lithospheric slabs of different thicknesses. The variance graphs plotted in figure 5.15 display no minima, indicating that the absence of sufficient data in this area is such as to render the lithospheric thickness indeterminate.

#### Profile AV18 - South Atlantic ocean

Whereas the depths of water above the ridge crests on profiles AV18 and AV20 are similar, the depths in the eastern ocean basin on AV18 are anomalously shallow for the South Atlantic. Since AV18 is the only profile on which the Walvis Ridge is crossed sufficiently close to the mid ocean ridge crest for its effects to register on the parts of the profile used in the model (figure 1.10), the shallower basin, and thus the indication of a very thin lithosphere, may be attributable to this factor.

#### Profile PV16 - Pacific ocean

The greatest lithospheric age represented by the data available is 40 My. Since this is much less than the time required for the lithosphere to cool, its thickness is poorly defined, values from 77 to 90 km fitting the observed bathymetry almost equally well (figure 5.14). The reasons for this have been discussed previously in sections 5.2.4 and 5.2.5, and also above in the case of the area north of Iceland.

## Profile EL39 - Australia-Antarctic Sea

This profile is taken from a part of the ocean in which major fracture zones exist (section 1.6.4), and the oceanic topography is disturbed to such an extent that even the position of the ridge crest is not immediately apparent (Wiessel and Hayes, 1971). Consequently meaningful results cannot be expected from this data.

## Profile EL45 - Australia-Antarctic Sea

Of all the profiles whose results plot away from the trend defined by most of the data in figure 5.18, this is the only one for which an immediate explanation is not available. The bathymetry differs from that of nearby profiles on either side (EL41 and IOFE) in two ways:-

- a) the ridge crest of EL45 is at a greater depth.
- b) the depths to the basin of EL45 are less.

As a result the dimensions of the ocean ridge are diminished relative to those of EL41 and IOFE, and a thinner lithosphere is thus indicated. A possible cause of (b) is the presence of the Diamantina fracture zone at the end of the profile (figure 1.19), but this is unlikely to explain the anomalous results completely.

Apart from the above mentioned profiles, the results from the other oceans are in agreement with the relationship between ridge dimensions and basin depths suggested by the North Atlantic data. There is some indication that the lithosphere beneath the Indian and Pacific oceans may be thinner than that existing beneath the North Atlantic to the south of the Azores (figure 5.10). In addition, three points derived from South Atlantic data indicate that the lithosphere may thin towards the south, but lack of a more convincing number of data points prevents this from being more than a suggestion (figure 5.16). There is, however, no indication in the data that another area exists in which variations of structure comparable to those found in the North Atlantic occur.



## CHAPTER 6

Interpretation of results and conclusions6.1 The North Atlantic

Analysis of observed bathymetric data has indicated that the thickness of the lithosphere beneath the North Atlantic may vary with latitude (sections 5.1 and 5.2), and the thicknesses estimated are plotted against latitude in figure 5.10. Subject to the adequacy of the model, the data suggest that the lithosphere may be of relatively constant thickness between  $15^{\circ}\text{N}$  and the Azores, but that it may thin from 95 km at  $43^{\circ}\text{N}$  to 70 km at  $61^{\circ}\text{N}$ . Consequently, since a thinned lithosphere is associated with raised temperatures (section 4.5.1) it is inferred that the temperature at a given depth beneath the North Atlantic may increase gradually northwards. The temperature profiles calculated to exist beneath the basins of the modelled lithospheric slabs suggest that at 70 km depth the temperature may rise from  $1000^{\circ}\text{C}$  to  $1200^{\circ}\text{C}$  between the Azores and Iceland. These figures are dependent on the values of the physical parameters used in the model, but the trends which they express are clear in the data on which the analysis is based. Furthermore, the estimates of the amount of uplift of the whole ridge-basin system relative to sea level expected from these lateral temperature variations are compatible with observed data, as was noted in section 5.1.5. The figures quoted here supersede those given by the results of the preliminary study (section 5.1) in which no account of sedimentary variations was taken. However, the indication that the North Atlantic overlies a thermally non-uniform region of the upper mantle remains unchanged.

## 6.2 Iceland, the flanking aseismic ridges and the Norwegian-Greenland Sea

### 6.2.1 Iceland

An immediate question arises as to how Iceland and its associated aseismic ridges can be related to the above interpretation. Seismic evidence summarised by Palmason (1970) shows that some of Iceland's elevation may be attributed to a thickened crust, but gravity calculations (Bott 1965, Einarsson 1954, Bott, Browitt & Stacey 1971) indicate that a substantial low density region must also exist in the upper mantle. This fact, coupled with Tryggvason's work on p-wave delays in Reykjavik (1964) and magnetotelluric measurements made by Hermance and Grillo (1970), has led to the suggestion of raised mantle temperatures beneath Iceland, which have been variously interpreted as a mantle plume (Morgan 1971, Vogt 1971, Schilling 1973, Vogt & Johnson 1973) or a convective overturn (Bott, 1973). These underlying raised temperatures allow Iceland itself to be easily fitted into the present work as the culmination of the temperature variations predicted under the Atlantic.

### 6.2.2 The Iceland-Faeroes Rise

Evidence presented by Bott et al. (1971) shows that the elevation of the Iceland-Faeroes Rise from the basins north and south may be explained by a thickened crust, seismic and gravity calculations yielding good agreement on the thickness required. There is no indication in this evidence of low density regions underlying the crust. The thickening is interpreted (Bott, 1973) as being the product of unusually active differentiation of basalt from the mantle material. However, the formation of a thickened low density region at the top of the lithosphere will only cause uplift of the ocean floor if the consequent depletion in basalt of the underlying mantle does not result in a corresponding increase of density at depth.

It is therefore of interest to examine the possible effect of upward concentration of basalt on mantle densities.

Concentration of alumina by basalt differentiation into low pressure regions allows the formation of large quantities of plagioclase, resulting in lowered densities. In intermediate pressure regions (below about 30 km) the minerals present will be mainly pyroxenes and olivine, whose densities at the high magnesium end of the solid solutions are similar (see chapter 3). Relative reduction of the pyroxene phases by this differentiation therefore results in only a small increase in density, which is offset by the effect of the reduction in the iron-magnesium ratio associated with the removal of basalt. At greater pressures (below about 80 km) depletion in aluminium restricts the development of the higher density garnet phase. However, at the temperatures present at this depth, garnet would in any case only be present in small quantities so that the effect on the overall densities would be negligible.

It is therefore to be concluded that, on a qualitative basis at least, the explanation of the Iceland-Faeroes Rise as the product of more than usually active basalt differentiation is feasible, that chemical inhomogeneities other than basalt differentiation are not necessary, and that underlying raised temperatures are not required to maintain its elevation.

### 6.2.3 The Norwegian-Greenland Sea

The analysis of topographic data from the Norwegian-Greenland sea failed to produce estimates of lithospheric thicknesses, mainly because of the relatively recent onset of the present episode of sea floor spreading and the complexity of tectonics in this area (section 5.3). However, the depths of the basins indicated by the bathymetric profiles (figure 1.14) are approximately 3.8 km beside the

Iceland-Jan Mayen Ridge and 3.0 km beside the Mohns Ridge further to the north. These figures are taken from parts of the profiles which correspond to lithospheric ages of only 30 My and include no allowance for sediments. Reference to the age-elevation data shown in figure 4.4 indicates that a further deepening of the basins by at least 0.5 km is to be expected before the cooling of the lithosphere is complete (assuming a minimum thickness of 70 km, as calculated for profile NR).

Consequently, while no detailed study of this region is possible, it can be seen that the trend of shallowing ocean basins with increasing latitude noted in section 6.1 is discontinued in the region of Iceland, the basins to the north showing greater depths than those to the immediate south. This lends support to the interpretation of Iceland as the focus of the lateral temperature variations beneath the North Atlantic which was suggested in section 6.2.1, above, although the fact that the basins immediately to the north of Iceland are deeper than those further north still shows that there are other factors to be accounted for in the Arctic area.

### 6.3 The South Atlantic

Because of the confusion of profile AV18 by the Walvis Ridge (section 5.3.3), only three reliable profiles are available in the South Atlantic. The lithospheric thicknesses indicated by modelling these profiles are plotted against latitude in figure 5.16. A possible trend of southwards decreasing ridge dimensions is suggested but, since all the thicknesses of lithosphere involved fall on the flattened portion of the curve relating basin depth to lithospheric thickness (figure 5.18), it is to be expected that the basin depths will be sensibly constant, and this can be seen from the figure to be the case. Consequently, confirmation or denial of the trend indicated by the ridge dimensions cannot be obtained from the basin depths, and this illustrates forcefully the limitations imposed on the

model by the time required for thicker lithospheres to cool to equilibrium (sections 5.2.4 and 5.2.5).

#### 6.4 The Indian, Southern and Pacific Oceans

The lithospheric thicknesses derived by the analyses of data from these oceans given in section 5.3 are plotted in figure 5.17. No convincing indications of bathymetric trends similar to those noted in the North Atlantic are apparent, but the data do suggest that the thickness of lithosphere beneath these oceans may be generally less than that indicated for the southern half of the North Atlantic. As in the case of the South Atlantic (above), study of basin depths can neither support nor disagree with this suggestion owing to the relatively high values of lithospheric thickness concerned.

#### 6.5 Lateral variations in the mantle

##### 6.5.1 Introduction

The results discussed in the previous sections imply the existence of large scale lateral variations of temperature within the upper mantle. They indicate that, relative to the temperatures beneath the southern half of the North Atlantic, raised temperatures may underly the following areas:-

1. Iceland and the northern North Atlantic.
2. The southern extremity of the South Atlantic.
3. The whole of the Indian and South Pacific oceans.

Several explanations of these lateral variations may be given, based on the different forms of mantle convection which have suggested to account for sea floor spreading (section 6.5.3). It is, however, of interest to examine the results for a possible correlation between spreading rates and the predicted mantle temperatures, and this is done in the next section.

### 6.5.2 Mantle temperatures and spreading rates

Langseth, Le Pichon and Ewing (1966) have shown that the quantity of heat which reaches the Earth's surface during the formation of new lithosphere at the ocean ridges is an order of magnitude greater than that which arrives by conduction through the lithosphere from the mantle immediately below. It might therefore be expected that the flow of heat from the Earth's interior would be aided by fast spreading ridges to such an extent that lowered temperatures would exist in the mantle nearby, and a relationship between mantle temperatures and spreading rates would result. Such a hypothesis involves assuming a relatively uniformly distributed pattern of heat flow, which would not be expected from a mantle in which convective movements took place, and the present results do not support it. In fact they show a lack of evidence for the existence of such a relationship since although bathymetric trends indicate raised temperatures beneath the extremities of the Atlantic ocean where spreading rates are low, the thinner lithospheres calculated to underly the Indian and South Pacific oceans also suggest raised temperatures in areas where spreading rates are high. In addition, the failure of the bathymetric trends in the North Atlantic to continue further north past Iceland, and the lack of any such trends associated with the differing spreading rates which occur in the Indian and South Pacific oceans represent other sources of disagreement. Furthermore, Lachenbruch (1973) has recently shown that the magnitude of horizontal transport of heat by cooling lithospheric slabs is such as to render obsolete any assumptions of a basically uniform heat flow distribution at depth which might be made as a result of surface observations.

### 6.5.3 Mantle convection

As originally suggested by Dietz (1961) and Hess (1962), the ideas on convection in the mantle were based on the existence of circulatory cells in the asthenosphere, the top surface of which extended to the ocean floor itself. Bott (1967) modified

this arrangement by postulating that the convective cells were confined to the asthenosphere and dragged the overlying lithospheric plates apart to form ocean ridges above the upwelling limbs. An alternative suggestion was made by Orowan (1965) and Elsasser (1969) in which the spreading lithosphere was itself the top surface of the convective cell, with the return flow occurring throughout the asthenosphere. In both of these hypotheses it is normally assumed that the convection causes the ocean ridges, and that the upwelling limbs of the convective movements are located geographically beneath the ridge crests. It is worth noting, in passing, that as far as the present model is concerned, the only difference between these two theories would be the temperatures at the base of the lithospheric slab, which might be expected to vary laterally by different amounts. Recent calculations by Andrews (1972) show that the amount by which these temperatures might vary is small (section 2.1) and consequently it is unlikely that the model would be able to distinguish between them.

There are, however, several strong objections which may be made to any hypotheses which require convective cells to be geographically positioned beneath the ocean ridges. These objections have been employed by authors who criticise the whole idea of sea-floor spreading. Einarsson (1968) pointed out that sudden offsets of convective cells by hundreds of kilometres at transform faults would be required, and that the pattern of heat sources within the earth which would be needed to give rise to such offsets would be extremely unlikely to occur. Furthermore, Belousov (1970) observed that because the ocean ridges remain, in almost all cases, in the centre of an expanding ocean, it is geometrically necessary for ocean ridges to migrate away from some continental blocks (for example, the ridges surrounding the southern half of Africa). Presumably, therefore, some mechanism would have to exist to couple the heat sources within the mantle to the migrating ridges in order that they should migrate as well, and the nature of such a mechanism is extremely difficult to envisage. Another objection lies in the fact that these hypotheses rely on the return flow being either accompanied by, or

formed of, descending lithospheric slabs at ocean trenches. A brief examination of a global map of lithospheric plates is sufficient to reveal that many plates have no descending boundaries, that ridges spread opposite ridges, and that almost every combination of different types of plate boundaries may be found on opposite sides of a lithospheric plate somewhere on the Earth's surface. Consequently, while the creation and destruction of lithospheric plates may be in balance on a global scale, the existence of a complete circulatory system beneath every moving plate cannot be accepted.

It is now generally accepted that hot mantle material does rise beneath the ocean ridges, and it is therefore fortunate that the above objections to sea-floor spreading theories can be simply removed by postulating that this upwelling is a secondary effect produced by the separating plates, rather than being a cause of the separation. In this situation, the amount of heat brought to the surface at the ridge crests will vary with the spreading rate and thus with the ability of the ridge to dissipate it. Consequently lateral variations of mantle temperatures would not be expected except locally at ridge crests, and the lack of correlation between spreading rates and the predicted variations, noted in section 6.5.2, is of no consequence. In order to explain such variations, a larger scale primary convective system must be postulated, and this need have no particular geographical relationship to the ocean ridges. Such primary convective movements might be related to mantle plumes and hotspots, as has been suggested by some authors (section 6.5.4) though this is not essential. In any event, whatever the form of the primary mantle convection, lateral temperature variations are to be expected as a result of it. The need for some primary convective movements is further evidenced by the difficulty which would be otherwise encountered in initiating ocean floor spreading. The balance of forces produced by an ocean ridge and a downgoing slab is such that, once started, a particular ridge may well be able to continue to spread under its own impetus in the Orowan-Elsasser mode (see above) but external forces must be required to set the process in motion.



McKenzie, Roberts and Weiss (1973) have recently made some calculations relating to the upwelling of hot mantle material beneath the ocean ridges and these apply whether the upwelling is primary or secondary. They showed that a positive free air anomaly should be associated with the rising limb of a convective cell. In addition, Anderson, McKenzie and Sclater (1973) have found a correlation between the depths to the crests of the ocean ridges and the values of free air gravity which exist above them. The sign of this correlation suggests that the variation in depth to the ridge crests may be explained by the existence of underlying areas of locally raised temperatures above ascending flows. The results of the present work are in agreement with these conclusions for, although the maximum elevation of an ocean ridge above the adjacent basin has been shown to diminish with increasing mantle temperatures (section 4.5.1 and 6.6), the uplift of the whole ridge-basin system relative to sea level correspondingly increases, and the results of the calculations presented in section 5.1 show that the latter effect predominates, causing a net uplift of the ridge crest to occur in areas of raised mantle temperatures.

#### 6.5.4 Mantle hotspots

Associated with the convective hypothesis described above is the evidence presented by several authors for the existence of unusually hot regions of the upper mantle. These have been termed "hotspots" and are most frequently considered to be the surface expression of rising mantle plumes (for example, see Morgan 1971). Evidence for interpreting the uplift of Iceland as being due to such a hotspot was given in section 6.2.1, where it was suggested that the bathymetric trends in the North Atlantic might thereby be simply explained. It must be noted, however, that several other of the hotspots suggested by Morgan (1971) lie on or near parts of the ocean ridge studied in this work - in particular note the Azores. None of these other suggested hotspots is surrounded by the wholesale shallowing of the sea which characterizes the Icelandic region. Consequently, without discussing the validity

or otherwise of Morgan's interpretation of these smaller topographic features as being due to mantle plumes, it is clear that the Icelandic hotspot must be in a different category from the others at least as far as magnitude is concerned.

#### 6.5.5 Stability of lateral inhomogeneities in the upper mantle

Examination of a bathymetric chart of the North Atlantic shows that the dimensions of the Iceland - Faeroes rise remain relatively constant throughout its length and may even increase towards Iceland. If the existence of the rise is attributed to unusually active differentiation of basalt from the mantle throughout the opening of the northern North Atlantic (see section 6.2), then it follows that the thermal conditions giving rise to this differentiation must have persisted for about 60 My without showing any signs of diminishing .

However, such lateral inhomogeneities of temperature and density are mechanically unstable, and order of magnitude calculations made to investigate the time scale involved in the natural decay of the variations of structure beneath the North Atlantic (appendix 3) yielded a half life of a maximum of 16 My. The calculations are obviously subject to a large number of assumptions and simplifications, but if this figure is at all accurate then it may be inferred that active replenishing of the thermal anomaly beneath the Atlantic must be occurring, and that an explanation of the structural variations based on a discreet thermal event and subsequent cooling is not feasible. The relatively rapid uplift of the Fennoscandian shield following glacial unloading (Haskell, 1935) suggests that the figure of 16 My quoted above may be an overestimation of the time scale, in which case such replenishment would be even more essential.

## 6.6 Summary of results

- 1) The size of an ocean ridge, measured in terms of its cross-sectional area and amplitude of bathymetric elevation, is directly related to the thickness of the lithosphere present beneath it, a thick lithosphere giving rise to a strongly developed ridge and vice versa.
- 2) The thickness of the lithosphere is related to the temperatures in the mantle, raised temperatures causing an upward migration of phase boundaries and therefore a thinned lithosphere.
- 3) The depths of water which exist in the ocean basins are related to the temperatures in the mantle. Raised mantle temperatures produce shallow ocean basins.
- 4) Calculations (section 5.1) show that the magnitudes of the effects noted in 1 and 3 above are compatible with those of observed data from the North Atlantic.
- 5) Consequently it is suggested that a direct relationship may exist between ocean ridge dimensions and the depths found in the oceans basins once the lithosphere has cooled to equilibrium.
- 6) However, the time required for lithospheres thicker than about 90 km to cool to equilibrium following their formation at the ridge crests is greater than the age of most oceans and, furthermore, the slope of topography for ages exceeding about 80 My is so small that further increases of depth with age cannot usually be detected in observed bathymetric profiles. Basin depths taken from profiles in areas where the lithosphere reaches these thicknesses will therefore not be true equilibrium values.
- 7) As a result the relationship of (5), derived by modelling observed data, does not show the approximate linearity which would be expected from theoretical calculations, but is modified to the shape indicated by the data plotted in figure 5.18.
- 8) Observed bathymetric profiles show that the depths of the ocean basins are

less subject to disturbance by transform faults and fracture zones than are the dimensions of the ocean ridges.

- 9) However, because of the shallow gradients of the relationships shown in figure 4.4, it is not possible to use the more reliable basin depths to predict lithospheric thicknesses (and thus estimate the thermal structure of the upper mantle) except in regions where the thickness is less than about 85 km. One result of this is to limit the area within which estimates of lithospheric thicknesses derived from basin depths may be usefully corroborated with those calculated from ocean ridge dimensions.
- 10) Consequently the model can only be successfully applied in areas where disturbance of the oceanic topography by fracture zones etc. does not occur. Transform faults usually result in a diminution of ridge dimension (see profiles EL39 and NO). Other types of fracture (e.g. the Azores area) may result in increased ridge dimensions which lack the classical shape attributable to a simple cooling of the lithosphere.
- 11) Analysis of observed oceanic topography indicates that:-
  - 1) There is a marked increase of mantle temperatures beneath the Atlantic northwards from about 40°N to Iceland.
  - 2) Some evidence exists for a gradual increase of temperatures with latitude in the South Atlantic.
  - 3) No comparable well-defined trends exist in the Indian and South Pacific oceans, but temperatures throughout the area may be slightly raised relative to those existing beneath the southern North Atlantic.
- 12) The suggested lateral variations of temperature could be produced by convection within the mantle and there are indications that continual replenishment of the thermal anomalies may be required to sustain them over geologically significant periods of time.

## 6.7 Conclusion

The work described in this thesis has analysed bathymetric data from the world's oceans in an attempt to explain regional variations of basin depths and ocean ridge topography in terms of underlying lateral inhomogeneities of temperature in the upper mantle. In regions where the lithosphere is thin, estimates of mantle temperatures based on ridge topography agree closely with those based on basin depths and thus support the explanation outlined above. Unfortunately, the time required for thicker lithospheres to cool limits the area within which such corroborative evidence may be obtained, although the results of analysing observed data do, in general, fall along a distinguishable trend. Since the number of data points is limited to the number of bathymetric profiles available, it is clear that the greatest possible number of profiles should be used. The results of further studies using additional data would therefore be of great interest.

## THE APPENDICES

General notes on the computer programs.

The programs which are described in some of the following appendices are written in either PL1 or FORTRAN and are designed for use on the IBM360/67 computer operated by the Universities of Durham and Newcastle upon Tyne. They were run under the MTS system, in which the standard method of passing information from one program to another is to use one or more magnetic disk "files". Owing to the pressure on such file space, much of the data, e.g., gravity and bathymetric profiles, temperature and density distributions, were also copied onto magnetic tape for long term storage. The exact formats of input and output are not given in the following descriptions since these can be readily ascertained from the accompanying program listings. In order to avoid confusion of data sets during the calculations, the programs are written to incorporate unique names for each data set, and these are recorded and checked at appropriate points throughout the computations.

### Erratum

Several of the programs make use of the subroutine GRAPH (appendix 10) to plot data on the line printer. For historical reasons only this routine writes "ANOMALY IN MGALS OR GAMMAS" at the top of each graph. This should be ignored where not applicable.

## Appendix 1.

## Theoretical geotherms in lithospheres containing heat productive materials.

Consider a column of lithosphere of cross section  $A$  and height  $h$ , with a flow of heat  $Q_0$  per unit area crossing the bottom surface. Let the temperature at the top of the slab ( $x = h$ ) be  $T_h$ , and the temperature at the bottom of the slab ( $x = 0$ ) be  $T_0$ . Then, for an element of the column

$Q = -KAdT/dx$ , where  $Q$  = heat flow and  $K$  is the thermal conductivity. But  $Q = Q_0 A + xA\rho\phi$  where  $\rho$  = density and  $\phi$  = rate of production of heat per unit mass. Thus

$$Q_0 + x\rho\phi = -KdT/dx, \text{ whence}$$

$$(x^2/2)\rho\phi + Q_0 x = K(T_0 - T).$$

Substituting  $K = 0.006 \text{ cal/cm.s.}^\circ\text{C}$

$$h = 73.33\text{km} (= 80\text{km} - 2 \times \text{block height}/2)$$

$$\rho = 3.4 \text{ gm/cm}^3, T_0 = 1100^\circ\text{C}, T_h = 0^\circ\text{C}$$

$$\phi = 60 \text{ cal} \cdot 10^{-8}/\text{g.y}$$

in order to correspond with the model whose results are plotted in figure 2.3 gives

$$T = T_0 - 0.0538x^2 + 11.03x, \text{ where } x \text{ is in km.}$$

The figures given by this equation are plotted in figure 2.3, and correspond with the modelled data.

## Appendix 2.

## Calculation of basin uplift.

## 1. Estimation of density distribution in the asthenosphere

A	65km lithosphere					70km lithosphere				
	B	C	D	E	F	B	C	D	E	F
168.3	1596	3.33	4.0	3.318	3.257	1595	3.33	4.0	3.318	3.257
165.0	1595	"	"	"	3.254	1595	"	"	"	3.254
161.7	1593	"	"	"	3.252	1590	"	"	"	3.252
158.3	1591	"	"	"	3.249	1590	"	"	"	3.249
155.0	1588	"	5.0	3.315	3.243	1588	"	5.0	3.315	3.243
151.7	1585	"	"	"	3.240	1586	"	"	"	3.240
148.3	1582	"	"	"	3.238	1582	"	"	"	3.238
145.0	1578	"	"	"	3.235	1578	"	"	"	3.235
141.7	1572	"	7.5	3.307	3.225	1572	"	7.5	3.307	3.225
138.3	1568	"	"	"	3.223	1568	"	"	"	3.223
135.0	1565	"	"	"	3.220	1560	"	"	"	3.221
131.7	1560	"	10.0	3.300	3.211	1555	"	10.0	3.300	3.212
128.3	1555	"	"	"	3.209	1550	"	"	"	3.210
125.0	1550	"	"	"	3.207	1543	"	"	"	3.208
121.7	1544	"	"	"	3.204	1534	"	"	"	3.206
118.3	1538	"	15.0	3.285	3.188	1530	"	"	"	3.203
115.0	1530	"	"	"	3.186	1519	"	15.0	3.285	3.187
111.7	1518	"	"	"	3.184	1509	"	"	"	3.186
108.3	1508	"	"	"	3.183	1500	"	"	"	3.184
105.0	1495	"	"	"	3.182	1484	"	"	"	3.183
101.7	1482	"	"	"	3.180	1469	"	"	"	3.182
98.3	1470	"	"	"	3.179	1456	"	"	"	3.181
95.0	1452	"	"	"	3.178	1433	"	"	"	3.181
91.7	1433	"	"	"	3.178	1410	"	10.0	3.300	3.195
88.3	1410	"	"	"	3.178	1387	"	"	"	3.195
85.0	1386	"	"	"	3.173	1355	"	"	"	3.197
81.7	1356	"	10.0	3.300	3.194	1330	"	7.5	3.307	3.204
78.3	1333	"	"	"	3.194	1300	"	"	"	3.205
75.0	1300	"	7.5	3.307	3.202	1270	"	5.0	3.315	3.214
71.7	1260	"	"	"	3.204	1232	"	"	"	3.216
68.3	1220	3.32	5.0	3.315	3.214					
65.0	1185	"	"	"	3.216					

## Key to columns

- A - depth in km.
- B - temperature in °C
- C - density of relevant mineral assemblage at R.T.P., assuming no partial melt.
- D - Percentage partial melt.
- E - density including partial melt.
- F - final density, accounting for compression and thermal expansion.

densities in  $\text{g/cm}^3$   
for sources see section 5.1.4.



1, continued.

A	80km lithosphere					85km lithosphere				
	B	C	D	E	F	B	C	D	E	F
168.3	1595	3.33	4.0	3.318	3.257	1595	3.33	4.0	3.318	3.257
165.0	1593	"	"	"	3.254	1590	"	"	"	3.255
161.7	1588	"	"	"	3.252	1588	"	"	"	3.252
158.3	1584	"	"	"	3.249	1584	"	"	"	3.249
155.0	1580	"	5.0	3.315	3.244	1578	"	"	"	3.247
151.7	1575	"	"	"	3.242	1573	"	5.0	3.315	3.242
148.3	1570	"	"	"	3.239	1565	"	"	"	3.240
145.0	1565	"	"	"	3.237	1560	"	"	"	3.238
141.7	1560	"	"	"	3.235	1553	"	"	"	3.236
138.3	1554	"	7.5	3.307	3.225	1548	"	"	"	3.233
135.0	1546	"	"	"	3.223	1538	"	7.5	3.307	3.224
131.7	1537	"	"	"	3.221	1530	"	"	"	3.222
128.3	1528	"	"	"	3.219	1517	"	"	"	3.221
125.0	1519	"	"	"	3.217	1507	"	"	"	3.219
121.7	1510	"	10.0	3.300	3.209	1495	"	"	"	3.218
118.3	1503	"	"	"	3.207	1485	"	"	"	3.216
115.0	1491	"	"	"	3.205	1470	"	"	"	3.215
111.7	1480	"	"	"	3.204	1455	"	"	"	3.214
108.3	1464	"	"	"	3.203	1440	"	"	"	3.213
105.0	1450	"	"	"	3.202	1425	"	"	"	3.212
101.7	1433	"	"	"	3.201	1403	"	"	"	3.212
98.3	1413	"	"	"	3.201	1385	"	"	"	3.211
95.0	1388	"	7.5	3.307	3.208	1362	"	"	"	3.212
91.7	1364	"	"	"	3.208	1334	"	5.0	3.315	3.220
88.3	1338	"	"	"	3.209	1310	"	"	"	3.220
85.0	1310	"	5.0	3.315	3.217	1280	"	4.0	3.318	3.224
81.7	1275	"	"	"	3.219					

## Key to columns

- A - depth in km.
- B - temperature in °C.
- C - density of relevant mineral assemblage at R.T.P., assuming no partial melt.
- D - percentage partial melt.
- E - density including partial melt.
- F - final density, accounting for compression and thermal expansion.

densities in g/cm<sup>3</sup>

for sources see section 5.1.4.

## 2. Density depth profiles.

depth km	lithospheric thickness, km.				
	65	70	80	85	
1.7	3.241	3.241	3.241	3.241	
5.0	235	235	236	236	
8.3	228	230	230	231	
11.7	222	224	224	225	
15.0	216	218	219	221	
18.3	289	292	293	295	
21.7	284	286	287	289	
25.0	278	281	282	285	
28.3	272	275	277	280	
31.7	267	270	272	276	
35.0	260	265	268	272	
38.3	255	260	263	268	
41.7	250	255	259	264	
45.0	245	251	255	260	
48.3	239	246	251	256	
51.7	236	242	248	253	
55.0	231	238	244	249	Asthenosphere
58.3	226	234	241	251	from data
61.7	223	230	238	258	presented
65.0	216	226	235	249	previously
68.3	214	222	241	252	in this
71.7	204	216	239	250	appendix.
75.0	202	214	236	247	
78.3	194	205	234	245	
81.7	194	204	219	244	Lithosphere
85.0	173	197	217	224	from models.
88.3	178	195	209	220	
91.7	178	195	208	220	
95.0	178	181	208	212	Densities
98.3	179	181	201	211	in g/cm <sup>3</sup> .
101.7	180	182	201	212	
105.0	182	183	202	212	
108.3	183	184	203	213	
111.7	184	186	204	214	
115.0	186	187	205	215	
118.3	188	203	207	216	
121.7	204	206	209	218	
125.0	207	208	217	219	
128.3	209	210	219	221	
131.7	211	212	221	222	
135.0	220	221	223	224	
138.3	223	223	225	233	
141.7	225	225	235	236	
145.0	235	235	237	238	
148.3	238	238	239	240	
151.7	240	240	242	242	
155.0	243	243	244	247	
158.3	248	249	249	249	
161.7	251	252	252	252	
165.0	254	254	254	255	
168.3	257	257	257	257	

### Appendix 3.

#### Stability of lateral variations in the mantle.

In this appendix, rough calculations are performed to investigate the period of time which would be required for lateral variations of density within the asthenosphere to be dissipated by viscous flow. It was shown in section 5.1 that the uplift of some parts of the ocean basins with respect to sea level could be explained in terms of the lowered densities associated with raised mantle temperatures, and it was also suggested that the lateral variations might die out by 200km depth. Figure A2 shows two columns of the mantle subject to differing geotherms above 200km. The hydrostatic pressure in column A will be equal to that in column B until the depth corresponding to the sea bed at A is reached, whence it will increase relative to B until the depth corresponding to the sea bed at B is reached. At this level, the excess pressure at A will be equal to  $2.0 \times Z = P_{\max}$ , (the density difference between the crust and water multiplied by the difference in water depths). Thereafter the excess pressure will decrease to zero at 200km. It is assumed for simplicity that this decrease is linear - see figure A2. The average value of the excess pressure which exists within the asthenosphere from the base level (200km) to the mean depth of the base of the lithosphere is then easily calculated  $= P_0$ . The asthenosphere is assumed to flow with the velocity profile shown in figure A2, and the velocity gradient is therefore  $V/h$ . However, the viscosity  $\eta$  is defined as  $\eta = \tau/dv/dx$ , where  $\tau$  is the shear stress and  $dv/dx$  is the velocity gradient perpendicular to the direction of flow. Consequently, in this case,

$$\eta = \tau/V/h \text{ or } \tau = \eta V/h.$$

If it is assumed that the flow is analogous to the motion of a viscous damper whose cross section is a rectangle of unit width and  $2h$  high (see figure A2), and whose length is  $D$  (figure A2), then the force on the damper is  $2D\tau = 2D\eta V/h$ . Thus  $2D\eta/h = \lambda$ , the equivalent dashpot constant.

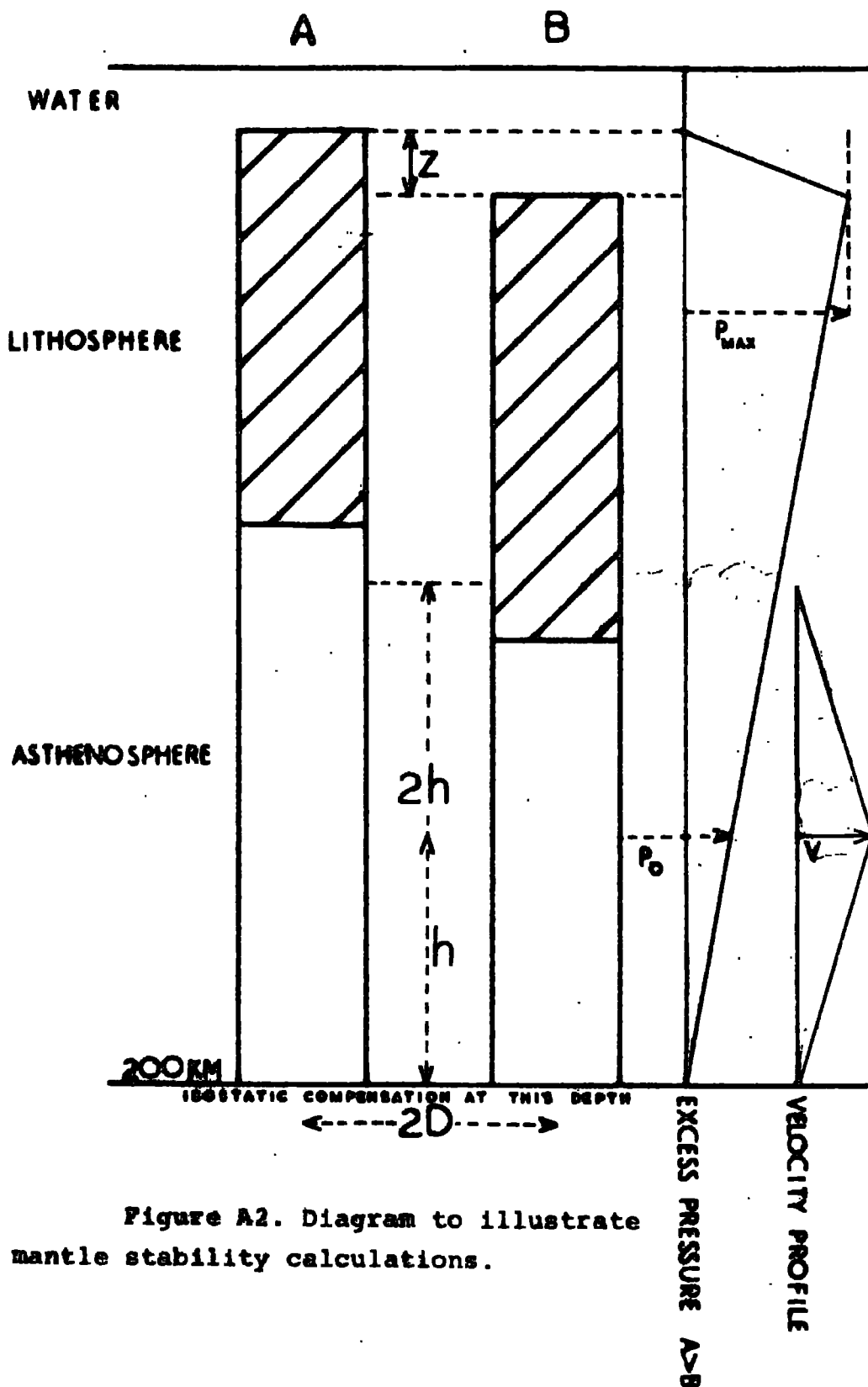


Figure A2. Diagram to illustrate mantle stability calculations.

Assuming a linear decrease of force with distance moved, (in order to model the linear decrease of excess pressure beneath the lithosphere as the bathymetric elevation of the sea floor decreases), then  $F = F_0(1-x/D)$  where  $x$  is the distance moved by the equivalent dashpot. Substituting in the dashpot equation

$$\begin{aligned} F &= \lambda dx/dt \text{ gives} \\ F_0(D-x)/D &= \lambda dx/dt \text{ whence} \\ t &= D\lambda/F_0 \cdot \log D/(D-x). \end{aligned}$$

But  $F_0 = P_0 \cdot \text{area/unit width of dashpot} = 2P_0h$ . Thus

$$t = D\lambda/2P_0h \cdot \log D/(D-x)$$

$= D^2\eta/P_0h^2 \cdot \log D/(D-x)$ , and the half life of the relaxation is given by

$$D^2\eta/P_0h^2 \cdot \log 2.$$

For the case of the uplift of the floor of the North Atlantic between profiles NR and NL (61 and 43°N), the following figures are applicable:-

Distance between profiles = 2000km :  $D = 1000\text{km}$ .

$\eta = 10^{21}$  poise.

Basin depth at NL = 5.3km, at NR = 3.1 km.

therefore  $Z = 2.2\text{km}$ .

Average thickness of the lithosphere = 84 km.

therefore  $h = 58\text{km}$ .

$P_0 = P_{\text{max}} \cdot 58/200$ , assuming the linear decrease of excess pressure mentioned above.

Substituting these figures gives a value of 50My for the half life of the relaxation of the asthenosphere in this region, which must be divided by  $\pi$  since the flow of material may occur radially in all directions. This yields a final figure of 16My, which is a maximum since no account of heat loss from the thermal anomaly has been taken.

APPENDIX 4. LISTING OF THE AGE-ELEVATION-THICKNESS TABLE USED THROUGHOUT THIS WORK  
SEE SECTION 4.8 FOR DETAILS, ELEVATIONS IN KM.

AGE(MY)	50	55	60	65	70	73	77	80	85	90	95	100	110	120
	LITHOSPHERIC THICKNESS KM													
0	-1.44	-1.62	-1.82	-2.00	-2.22	-2.44	-2.66	-2.84	-3.12	-3.43	-3.80	-4.21	-5.25	-6.70
5	-1.04	-1.23	-1.42	-1.62	-1.84	-2.00	-2.21	-2.41	-2.54	-2.90	-3.30	-3.61	-4.40	-5.47
10	-0.70	-0.84	-1.02	-1.23	-1.43	-1.65	-1.82	-2.00	-2.25	-2.47	-2.82	-3.17	-3.90	-4.67
15	-0.46	-0.58	-0.73	-0.93	-1.13	-1.29	-1.44	-1.61	-1.88	-2.10	-2.42	-2.73	-3.32	-4.03
20	-0.30	-0.38	-0.50	-0.68	-0.85	-1.00	-1.13	-1.30	-1.56	-1.79	-2.10	-2.40	-2.98	-3.62
25	-0.20	-0.25	-0.33	-0.48	-0.65	-0.77	-0.89	-1.04	-1.30	-1.52	-1.83	-2.10	-2.66	-3.31
30	-0.11	-0.15	-0.22	-0.34	-0.50	-0.61	-0.71	-0.85	-1.10	-1.30	-1.59	-1.82	-2.43	-3.08
35	-0.05	-0.09	-0.14	-0.25	-0.39	-0.49	-0.59	-0.70	-0.91	-1.11	-1.38	-1.64	-2.28	-2.90
40	-0.02	-0.05	-0.07	-0.17	-0.28	-0.39	-0.48	-0.59	-0.76	-0.94	-1.20	-1.48	-2.12	-2.74
45	-0.00	-0.01	-0.04	-0.12	-0.21	-0.30	-0.40	-0.49	-0.62	-0.81	-1.08	-1.35	-2.00	-2.60
50	-0.00	-0.00	-0.02	-0.09	-0.16	-0.24	-0.30	-0.39	-0.52	-0.70	-0.94	-1.21	-1.87	-2.47
55	-0.00	-0.00	-0.01	-0.05	-0.10	-0.18	-0.24	-0.31	-0.43	-0.60	-0.83	-1.11	-1.72	-2.32
60	-0.00	-0.00	-0.00	-0.02	-0.05	-0.11	-0.17	-0.25	-0.38	-0.51	-0.74	-1.01	-1.64	-2.21
65	-0.00	-0.00	-0.00	-0.00	-0.01	-0.07	-0.14	-0.20	-0.31	-0.44	-0.64	-0.94	-1.54	-2.11
70	-0.00	-0.00	-0.00	-0.00	-0.00	-0.05	-0.07	-0.13	-0.25	-0.40	-0.59	-0.88	-1.42	-1.99
75	-0.00	-0.00	-0.00	-0.00	-0.00	-0.00	-0.01	-0.09	-0.21	-0.36	-0.54	-0.81	-1.35	-1.90
80	-0.00	-0.00	-0.00	-0.00	-0.00	-0.00	-0.00	-0.05	-0.19	-0.31	-0.50	-0.75	-1.25	-1.80
85	-0.00	-0.00	-0.00	-0.00	-0.00	-0.00	-0.00	-0.01	-0.18	-0.29	-0.46	-0.69	-1.18	-1.70
90	-0.00	-0.00	-0.00	-0.00	-0.00	-0.00	-0.00	-0.00	-0.16	-0.27	-0.41	-0.62	-1.10	-1.60
95	-0.00	-0.00	-0.00	-0.00	-0.00	-0.00	-0.00	-0.00	-0.13	-0.24	-0.39	-0.58	-1.00	-1.50

END OF FILE

LIST OF MYST

## Appendix 5.

### The program HEAT.

#### Description

The purpose of this program is to calculate the theoretical temperature distribution in a spreading lithospheric slab. The method has been described fully in chapter 2 and only a brief resume is given here.

It is assumed that the temperature distribution is uniform along the strike of the ocean ridge and that the calculations are consequently only dealing with a 2-D situation. A 2-D cross-section of the slab is subdivided vertically and horizontally into rectangular blocks of uniform size. Appropriate physical parameters and the initial temperatures are specified for each of the blocks, and the subsequent changes of the block temperatures with time are calculated according to the equations (5) given in section 2.3, the temperatures of the outer ring of blocks remaining constant in order to provide the boundary conditions. Sea floor spreading is modelled by the addition of new columns of blocks to one end of the slab at intervals designed to reproduce the desired spreading rates. The process is illustrated in figure 2.1

A facility is provided to allow the initial temperature distribution to be calculated by the program itself. This makes it possible to enter a linear temperature-depth profile at the start, and use the program to calculate the necessary bowing of this profile due to radioactive heat production before starting to model the sea-floor spreading. The program is written in Fortran and makes use of the subroutine RKGS which forms part of the IBM Scientific Subroutine Package.

## Input

The input may be divided into three parts:-

- 1) the initialising input required to set up the model.
- 2) the input necessary to model sea-floor spreading.
- 3) the instructions for output of results.

### 1) The initialising input.

The initialising input may be specified in either of two formats:-

- 1) The parameters for each block are specified separately.
- 2) The parameters are specified by row.

The second form of input is adequate for most purposes and allows a considerable reduction in the number of data cards to be made.

Initialising input type 1 is read on device number 4 and consists of the following cards:-

CARD TYPE 1a NR,NC,NBL,BH,BW,A,B

NR is the number of rows of blocks in the model.

NC is the initial number of columns of blocks, before the start of sea-floor spreading.

NBL is the number of columns of blocks to be added during the simulation of sea-floor spreading.

BH is the height of the blocks (km).

BW is the width of the blocks (km).

A and B together form an 8 character name for the model, to enable unique identification of data sets to be made.

CARD TYPE 2a RHO(I,J),HP(I,J),CP(I,J),CON(I,J,1),CON(I,J,2),TH(I,J)

I counts the rows, numbering from 1 at the base of the lithosphere to NR at the ocean floor.

J counts the columns, numbering from 1 at the end of the slab remote from the spreading centre to NC at the future spreading centre itself.





For each block I,J:-

RHO is the density -  $\text{g/cm}^3$   
 HP is the heat production -  $\text{cals.}10^{-8}/\text{g.y}$   
 CP is the specific heat -  $\text{cals/g}^{\circ}\text{C}$   
 CON is the thermal conductivity in the horizontal  
 direction and in the vertical direction (1 and 2  
 respectively) -  $\text{cals/cm.s.}^{\circ}\text{C}$   
 TH is the initial temperature- $^{\circ}\text{C}$

There are NR x NC cards of this type.

CARD TYPE 3a PRMTR(I) I from 1 to 4

This data is concerned with the initialising solutions of the heat flow equations which allow the specified initial temperatures to settle to equilibrium values.

PRMTR(1) and PRMTR(2) define the time interval for which the model is to be left to settle. PRMTR(1) is set to zero, PRMTR(2) is set to the desired length of time in millions of years.

PRMTR(3). The Runge-Kutta method of solving simultaneous differential equations operates by increasing the value of the independent variable, in this case time, incrementally between successive solutions of the equations until the required total range (=PRMTR(2)) has been covered. In this work, PRMTR(3) is specified in millions of years and is the time increment to be used, which must be chosen according to the stability criterion discussed in section 2.4.

PRMTR(4) defines the round-off error permitted at each stage of the calculations. In this work it was set to 15 ( $^{\circ}\text{C}$ ).

Initialising input type 2 is read on device number 6 and consists of the following cards:-

CARD TYPE 1b As card type 1a, above.

CARD TYPE 2b RHOT,HPT,CPT,CON1T,CON2T,THAT,THLT

One card is supplied for each row of the model, NR cards in all, the first relating to the bottom of the lithosphere

and the others progressing upwards. For each row:-  
 RHOT is the density  
 HPT is the heat production  
 CPT is the specific heat  
 CON1T is the horizontal thermal conductivity  
 CON2T is the vertical thermal conductivity  
 THAT is the temperature of all the blocks in the row  
 except that at the future spreading centre.  
 THLT is the temperature of the block at the future  
 spreading centre.

The units are as for cards type 2a, above.

CARD TYPE 3b. As card type 3a, above.

An empty file assigned to either device number 4 or 6 causes the input to be read from the other, thus providing a simple switching mechanism for the alternative forms of input.

## 2) The sea-floor spreading input

This data is unaltered by the form of the initialising input selected previously. However, the program automatically reads it from whichever device (4 or 6) was used for the first section of the input. The data is as follows:-

EITHER CARD TYPE 4a RHO(I,K),HP(I,K),CP(I,K),CON(I,K,1),  
 CON(I,K,2),TH(I,K)

I counts the rows, numbering from the base upwards  
 K is set to the current number of columns plus one. The parameters are as for card type 2a. There are NR cards of this type.

OR CARD TYPE 4b 100.

This causes the parameters of card type 4a to be set to the corresponding values of the previous column, saving input for most models. Cards type 4a or 4b are followed by

CARD TYPE 5 PRMTR(I) I from 1 to 4

Similar to card type 3a.

PRMTR(1) = 0

PRMTR(2) = the time from the addition of this column of blocks to the addition of the next.

PRMTR(3) As card type 3a

PRMTR(4) As card type 3a

Cards type 4(a or b) and 5 are repeated NBL times to model the complete spreading history.

3) The instructions for output of results.

The calculated temperature distribution, together with other relevant information (see below), may be output at any stage in the calculations. However, in order to achieve a reasonable volume of output, the program is written to produce only the data applicable to specific, requested, modelled times. It should be noted that these times refer to the totals accumulated at any stage since the start of the program, and thus include any time spent in the initialising of the model (as specified on card type 3). The required times are read from device number 7 as follows:-

CARD TYPE 6 OTIME

OTIME is a modelled time (in My) for which output is required. Since the calculations proceed in discreet time steps as defined by card types 3 and 5, care must be taken to set OTIME to values which will be encountered. As many cards type 6 as desired may be supplied, with OTIME in order of ascending magnitude.

The complete input may thus be represented, in terms of card types, as follows:-

```

DEVICE 4  { either 1a - 2a - 3a  { 4a  } 5
           { or end-of-file      { 4b  }
DEVICE 6  { either end-of-file
           { or 1b - 2b - 3b  { 4a  } 5
                               { 4b  }
DEVICE 7 - 6

```

## Output

This is divided into four sections as follows:-

1) Listing of input data.

This section is self-explanatory and is output on device number 2.

2) Record of the progress of the calculations in terms of time increments, spreading history, etc. Also further similar details for each temperature distribution output. Self-explanatory, device number 5.

3) The temperature distributions requested, together with associated information as follows:-

A,B The model name.

NDIM The number of simultaneous equations solved to obtain this particular temperature distribution.

IHLF The number of times the time increment specified as PRMTR(3) on cards type 3 and 5 was halved in order to achieve the accuracy specified as PRMTR(4).

T The time interval since the preceding addition of a column of blocks.

NR Number of rows of blocks

NC Number of columns of blocks (this is equal to NC as specified on card type 1 plus the number of columns added since.

NO The number of this data set. A,B and NO together define a given data set uniquely.

TTT The total time accumulated since the start of this run.

PRMTR(I) I from 1 to 5. PRMTR(1 - 4) are as input on cards type 3 or 5. PRMTR(5) is not used in this program.

BH block height

BW block width

TH(I,J) block temperatures. I counts the rows upwards, J counts the columns towards the spreading centre.

This data is output on device number 3.

4) A list of sets of data actually output, containing name, number and modelled time for each set. Self-explanatory, written on device number 8. As stated previously, a particular data set is uniquely referenced by its name and number. This part of the output thus serves as an index to the data and is useful if the modelled times but not the corresponding numbers are known. Simple administrative programs may be written to use this index to link the program HEAT to the programs TEMDEN and HOTMAP automatically, thus saving the need for intermediate storing of the temperature distributions for manual inspection.

A listing of the program follows.

T=10 P=20 COPIES=10  
N WAS: 09:43.12 07-25-73  
SIGNLD ON AT 09:43.31 ON 07-25-73  
EAT -C

```
DIMENSION RHO(30,100),HP(30,100),CP(30,100),TH(30,100)
DIMENSION CON(30,100,2),PRMTR(5),TTH(3000),DEPT(3000),AUX(8,3000)
COMMON /A/ TH,A,B,TT,NDIM,NIC,NC,NR,NC,NTIME
COMMON /B/ BH,BW,PHO,CP,HP,CON
EXTERNAL FCT,OUTP
INPUT INITIAL DATA
OTIME=-1.
NO=0
TT=0
READ(4,1,END=801) NR,NC,NBL,BH,BW,A,B
DO 802 I=1,NR
802 READ(4,4)(RHO(I,J),HP(I,J),CP(I,J),CON(I,J,1),CON(I,J,2),TH(I,J),J
I=1,NC)
READ(4,4)(PRMTR(I),I=1,4)
ND=4
801 READ(6,1,END=803) NR,NC,NBL,BH,BW,A,B
DO 804 I=1,NR
READ(6,805) RHOT,HPT,CPT,CON1T,CON2T,THAT,THLT
805 FORMAT(7F10.3)
DO 806 J=1,NC
RHO(I,J)=RHOT
HP(I,J)=HPT
CP(I,J)=CPT
CON(I,J,1)=CON1T
CON(I,J,2)=CON2T
806 TH(I,J)=THAT
804 TH(I,NC)=THLT
READ(6,4)(PRMTR(I),I=1,4)
ND=6
1 FORMAT(3I10,2F10.3,2X,2A4)
803 WRITE(5,2)A,B
2 FORMAT('1HEAT FLOW CALCULATIONS FOR RUN ',2A4)
WRITE(5,3)NC,NR,BH,BW,NBL
3 FORMAT('0INITIAL NUMBER OF COLUMNS=',I4,/' NUMBER OF LAYERS(ROWS)=
1',I4,/' HEIGHT OF BLOCKS IN KILOMETRES=',F10.3,/' WIDTH OF BLOCK I
2N KILOMETRES=',F10.3,/' NUMBER OF BLOCKS TO BE ADDED=',I8)
DO 100 I=1,NR
4 FORMAT(6F10.3)
WRITE(2,5) I
5 FORMAT('1NUMERIC INPUT DATA FOR ROW',I4,/' CCLUMN DENSITY HEAT
1PRODUCTION SPECIFIC HEAT CONDUCTIVITY(H) CONDUCTIVITY(V) TEMPE
2RATURE',/' UNITS GM/CC CALS*10**-8/GM.YR CALS/GM.*C CALS/C
3M.SEC.*C CALS/CM.SEC.*C DEG C',/)
WRITE(2,6)(J,RHO(I,J),HP(I,J),CP(I,J),CON(I,J,1),CON(I,J,2),TH(I,J
1),J=1,NC)
6 FORMAT(I5,F11.3,F14.3,F17.3,F15.4,F16.4,F14.3)
100 CONTINUE
DATA READ IN AND WRITTEN OUT NOW CALCULATE STEADY STATE INITIAL CONDITIONS
THAT MEANS TEMPERATURES, READ IN RKGS PARAMETERS
WRITE(5,7)(PRMTR(I),I=1,4)
7 FORMAT('1INITIAL CALL TO RUNGE KUTTA ROUTINE PARAMETER VALUES',/'0
1INTEGRATION LIMITS(MY), MIN,MAX=',2F10.3,/' FIRST TIME INCREMENT(M
2Y)=',F10.3,/' TOP ERROR LIMIT(DEG.C)=',F10.3)
NIR=NR-2
NIC=NC-2
```

```

NDIM=NIR*NIC
DO 101 I=1,NIR
DO 101 J=1,NIC
N=(I-1)*NIC+J
101 TTH(N)=TH(I+1,J+1)
DO 102 N=1,NDIM
102 DERT(N)=1./NDIM
CALL RKGS(PRMTR,TTH,DERT,NDIM,IHLF,FCT,OUTP,AUX)
TT=TT+PRMTR(2)
TH NOW CONTAINS VALUES OF TEMPERATURES AT TIME T

NCT=1
IF (NCT.GT.NBL) GO TO 62
20 K=NC+1
WRITE(2,10) K
10 FORMAT('10DATA FOR NEW COLUMN',I4,/' LAYER DENSITY HEAT PRODUCT
11ON SPECIFIC HEAT CONDUCTIVITY(H) CONDUCTIVITY(V) TEMPERATURE'
2,/' UNITS GM/CC CALS*10**-8/GM.YR CALS/GM.*C CALS/CM.SEC.*
3C CALS/CM.SEC.*C DEG C',/)
READ(ND,4)RHO(1,K),HP(1,K),CP(1,K),CON(1,K,1),CON(1,K,2),TH(1,K)
IF(RHO(1,K).LT.99) GO TO 120
DO 121 I=1,NR
L=K-1
RHO(I,K)=RHO(I,L)
HP(I,K)=HP(I,L)
CP(I,K)=CP(I,L)
CON(I,K,1)=CON(I,L,1)
CON(I,K,2)=CON(I,L,2)
121 TH(I,K)=TH(I,L)
WRITE(2,122)
122 FORMAT(' DATA AS FOR PREVIOUS COLUMN')
GO TO 106
120 DO 106 I=1,NR
IF (I.EQ.1) GO TO 123
READ(ND,4)RHO(I,K),HP(I,K),CP(I,K),CON(I,K,1),CON(I,K,2),TH(I,K)
123 WRITE(2,6)I,RHO(I,K),HP(I,K),CP(I,K),CON(I,K,1),CON(I,K,2),TH(I,K)
106 CONTINUE
READ(ND,4)(PRMTR(I),I=1,4)
WRITE(5,11) NCT,(PRMTR(I),I=1,4)
11 FORMAT('0CALL NUMBER',I4,' TO RUNGE KUTTA ROUTINE. PARAMETER VALUE
1S',/'0INTEGRATION LIMITS(MY) MIN,MAX=',2F10.3,/' FIRST TIME INCRE
2MENT(MY)='F10.3,/' TOP ERROR LIMIT(DEG.C)='F10.3)
NC=NC+1
NIC=NIC+1
NDIM=NIR*NIC
DO 111 I=1,NIR
DO 111 J=1,NIC
N=(I-1)*NIC+J
TTH(N)=TH(I+1,J+1)
111 DEPT(N)=1./NDIM
CALL RKGS(PRMTR,TTH,DERT,NDIM,IHLF,FCT,OUTP,AUX)
TT=TT+PRMTR(2)
NCT=NCT+1
IF (NCT.LE.NBL) GO TO 20
62 WRITE(3,61)
61 FORMAT(' ')
WRITE(5,60)
60 FORMAT('ONORMAL ENDING')
CALL EXIT

```

END

```
SUBROUTINE FCT(X,Y,DERY)
DIMENSION Y(1),DERY(1),TH(30,100)
DIMENSION RHO(30,100),CP(30,100),HP(30,100),CON(30,100,2)
COMMON /A/ TH,A,B,TT,NDIM,NIC,NC,NR,NC
COMMON /B/ BH,BW,RHO,CP,HP,CON
PUT Y VALUES INTO THE ARRAY
DO 103 N=1,NDIM
I=2+(N-1)/NIC
J=N-(NIC*(I-2))+1
103 TH(I,J)=Y(N)
WORK OUT EQNS
FAC=3600.*24.*365.25/1.0E+4
DO 104 N=1,NDIM
I=2+(N-1)/NIC
J=N-(NIC*(I-2))+1
AA=CON(I,J-1,1)*(TH(I,J-1)-TH(I,J))/BW**2
BB=CON(I-1,J,2)*(TH(I-1,J)-TH(I,J))/BH**2
CC=CON(I,J,1)*(TH(I,J+1)-TH(I,J))/BW**2
DD=CON(I,J,2)*(TH(I+1,J)-TH(I,J))/BH**2
104 DERY(N)=(FAC*(AA+BB+CC+DD))/(RHO(I,J)*CP(I,J))+HP(I,J)*1.0E-2/CP(I
I,J)
RETURN
END
```

```
SUBROUTINE OUTP(T,TTH,DETR,IHLF,NDIM,PRMTR)
DIMENSION TTH(1),DETR(1),PRMTR(1),TH(30,100)
COMMON /A/ TH,A,B,TT,NDUM,NIC,NC,NR,NC,OTIME
COMMON /B/ BH,BW
NO=NO+1
PUT TTH VALUES INTO THE ARRAY TH
DO 105 N=1,NDIM
I=2+(N-1)/NIC
J=N-(NIC*(I-2))+1
105 TH(I,J)=TTH(N)
TH NOW CONTAINS TEMPERATURE FIELD AT TIME T
TTT=TT+T
DIS=TTT-OTIME
IF (DIS.LT.0.001) GO TO 303
READ(7,301) OTIME
301 FORMAT(F10.1)
303 DISCR=ABS(TTT-OTIME)
IF (DISCR.GT.0.001) GO TO 701
WRITE(3,51) A,B,NDIM,IHLF,T,NR,NC,NO,TTT
51 FORMAT(2H ',2A4,1H',I9,I10,F10.4,3I10,F10.4)
WRITE(3,52)(PRMTR(I),I=1,5),BH,BW
52 FORMAT(8F10.3)
DO 200 I=1,NR
200 WRITE(3,52)(TH(I,J),J=1,NC)
```



```
WRITE(5,53) A,B,NO,NR,NC,NDIM,IHLF,T,TTT
53 FORMAT('MODEL ',2A4,' CALL TO OUTPUT NUMBER',I4,' NUMBER OF ROWS
1=',I5,' NUMBER OF COLUMNS=',I5,' NUMBER OF DIFFERENTIAL EQUATION
2S SOLVED=',I6,' NUMBER OF TIMES INTEGRATION INTERVAL WAS HALVED=',
3,I4,' TIME INTERVAL OF INTEGRATION=',F10.4,' MYEARS',,' TOTAL TIM
4E ACCUMULATED IN THIS RUN=',F10.4,' MYEARS')
WRITE(5,54)
54 FORMAT(' RESULTS WRITTEN TO DEVICE NUMBER 3')
IF(TTT.EQ.0.0) TTT=0.00001
WRITE(8,302) A,B,NO,TTT
302 FORMAT(' MODEL ',2A4,' NO.',I4,' TIME',F10.3)
701 CONTINUE
RETURN
END
```

## Appendix 6.

### The program TEMDEN.

#### Description

TEMDEN is written in PL1 to process the data produced by the program HEAT described in appendix 5. From the temperature distribution in a modelled lithospheric slab and a mineralogical phase diagram, TEMDEN derives the following sets of data:-

- 1) The density distribution in the lithosphere in both numeric and diagrammatic form.
- 2) A diagram showing the mineral phase distribution in the lithosphere.
- 3) Graphs of the density profile either along a given row of blocks or up a given column.
- 4) The topographic elevation of the mid ocean ridge in both numeric and graphical form.

The method of calculation is described in chapter 4.

#### Input

The input may be divided into three sections:-

- 1) Temperature distributions and associated information.  
Read from file IN exactly as output on device number 3 by the program HEAT
- 2) The phase diagram and associated information. This is read in digitised form from file PH and consists of the following data:-
  - NP Number of divisions of the pressure range
  - NT Number of divisions of the temperature range
  - NKEY Number of differently identified zones within the phase diagram (see figure 4.1 and table 4.1)
  - KEY(I),DEN(I) I from 1 to NKEY. KEY(I) is the number or letter code for a given zone in the phase diagram. DEN(I) is the density at room temperature and pressure of the mineral assemblage represented by KEY(I).

TP Maximum value of pressure range

BP Minimum value of pressure range

TT Maximum value of temperature range

BT Minimum value of temperature range

P(I,J) I counts temperature steps from 1 to NT

J counts pressure steps from 1 to NP

Each element of P(I,J) is the number or letter code which corresponds to the mineral assemblage present at the particular pressure and temperature defined by I and J. The assembly of all the elements of P(I,J) forms the phase diagram as shown in figure 4.1.

3) Data selection and output instructions. These are read from file SCARDS and are as follows:-

1) Output options. Read by a GET DATA statement and selected by putting any option required = 'YES'. The available options are

PRINT - Prints out phase diagram.

GRAV - Writes density distribution in numeric form to file GR.

MAP - produces diagram of the density distribution.

PHASE - produces diagram of the mineral phase distribution.

PLOT - plots horizontal and/or vertical density profiles.

ELEV - calculates topographic elevation of the ocean ridge produced by the modelled slab and plots the result in digitised form on the line printer.

STORE - Writes the elevation profile calculated under ELEV to the file OUT in numeric form.

2) Data selection and output format instructions.

NAM - name of the temperature distribution

NOR - number of the temperature distribution (these two together specify the particular set of data to be processed).

- NCAT - Number of categories into which densities are to be divided (according to magnitude) for diagrammatic representation.
- NSP - Number of blank lines to be left between each column of densities in the diagram (allows adjustment of the horizontal scale of the diagram).
- NADE - Only if GRAV='YES'. Eight character name for the density distribution to be output.
- TYPE - Only if PLOT='YES'. Specifies whether the density profile to be plotted is to be taken horizontally or vertically (TYPE = 'ROW' or 'COLUMN'), or whether to continue to the next section of the program (TYPE = 'END').
- NN - Only if PLOT = 'YES'. Specifies the number of the row or column for which the density profile is desired.
- MO - Only if STORE = 'YES'. Eight character name for topographic profile on output.

The data (2) (NAM,NOR,NCAT,NSP + the optional items which follow above) may be repeated as often as desired if more than one temperature distribution is to be processed. All the temperature distributions output by a particular run of the program HEAT will follow each other sequentially in file IN. NAM and NOR must therefore be specified so that the order of the data sets on the cards is the same as in file IN. Intervening sets on file IN, which are not requested above are ignored. The program is terminated by requesting a non-existent set of data, the input line being completed with dummy data for NCAT and NSP.

### The Output

- 1) If PRINT = 'YES' the phase diagram is listed, together with the room temperature and pressure density data, as input. Self explanatory.
- 2) If GRAV = 'YES' the calculated density distribution is output as follows:-
 

NADE, NR, NC, BH, BW - data name, number of rows of blocks, number of columns of blocks, block height, block width.

Q(I,J) I counts rows from base upwards, 1 to NR, J counts columns towards the spreading centre, 1 to NC. Each element of Q(I,J) is the calculated density of one block of the lithospheric model.
- 3) If MAP = 'YES' the density range encompassed by Q(I,J) is divided into NCAT divisions (maximum 26). Each division is allotted a code letter and a map of the density distribution is produced by plotting the letter codes applicable to each block in the form of a rectangular grid. (see figure 4.5). The map is necessarily quantized by the use of the letter code representation. NSP blank lines are left between each column.
- 4) If PHASE = 'YES' the mineral phase distribution is plotted in a similar manner, using the letter codes of the input phase diagram and spacing the columns by NSP lines. (see figure 4.5).
- 5) If PLOT = 'YES' density profiles within the lithosphere are plotted on the line printer using the subroutine GRAPH (appendix 10). Self explanatory.
- 6) If ELEV = 'YES' the topographic elevation profile is calculated and plotted (in km) on the line printer. Both the profile caused by thermal contraction and phase changes, and the modified profile which results from this contraction being isostatic and submarine are plotted. Self explanatory.

- 7) If STORE = 'YES' then the second topographic profile mentioned above (contraction+isostasy) is written to file OUT as follows:-

MO, NC - Data name, number of points (= no. of columns).

ANOM(I), FPT(I) I from 1 to NC

ANOM is the elevation (km) relative to column 1.

FPT is the distance (km) from column 1.

### Important notes on the interpretation of the output of TEMDEN

- 1) The effects of the boundary conditions at the ends of the lithospheric slab.

1.1) The end remote from the spreading centre.

As described in appendix 5, a facility is included in the program HEAT to allow it to generate the equilibrium conditions existing far from the spreading centre in lithospheres which contain heat productive materials. This makes it possible to input a simple straight-line temperature profile as the initial boundary condition and allow the program to bend the profile to the required equilibrium values. However, the original profile is preserved in the end column of the model throughout the calculations, and usually affects the temperature profiles in the neighbouring columns of blocks. Consequently, when interpreting the topographic elevation profiles, these columns should be ignored since they do not represent any real part of the lithosphere. The base level for measurement of elevation must thus be adjusted as shown in figure A1.

1.2) The end at the spreading centre.

Similarly, the last column of blocks is also present only as a means of applying the boundary conditions, and is not intended to represent a molten zone in the lithosphere, twice the block width in extent at the surface. Consequently the elevation of this column is also to be ignored.

The effects of the above considerations are present not only in the topographic profiles but also in the other output data and diagrams, since all are derived from the same source.

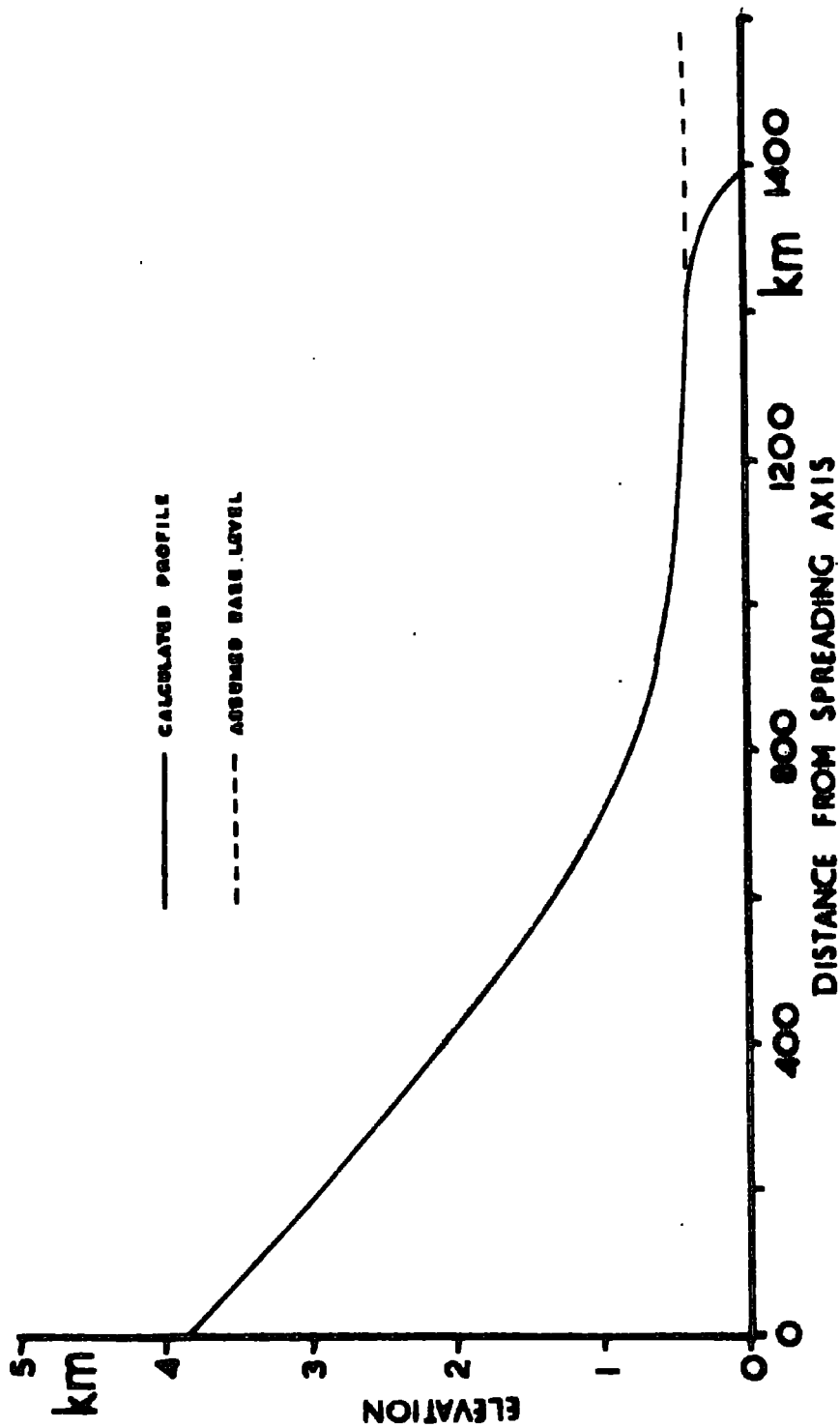


Figure A1. A typical topographic profile as output by the program TEMDEN. The effect on the topography of the boundary condition at the cool edge of the slab is easily seen, and the base level above which the topographic elevation should be measured is shown.

2) The effects of digitisation.

Since several stages of the calculations carried out by the programs HEAT and TEMDEN are concerned with digital representation of continuous data, discontinuities in the output profiles are to be expected. The major sources of such discontinuities are:-

- 1) the block representation of the lithosphere
- 2) the digitisation of the phase diagram
- 3) the methods of graph plotting and distribution mapping available on the line printer.

Consequently sharp boundaries in density or phase distributions and steps in the elevation profiles are to be interpreted with care, bearing in mind the above considerations. The data may normally be smoothed by interpolation if desired.

A listing of the program TEMDEN follows.



MDEN -F

```
TEM DEN: PROC OPTIONS(MAIN);
DCL(NAM,NAME) CHAR(8);
DCL P(100,50) CHAR(1);
  DCL FIX CHAR(3) VARYING INITIAL('NO');
DCL TYPE CHAR(8) VARYING;
L (ANOM,FPT)(200);
DCL PLOT CHAR(3) VARYING INITIAL('NO');
DCL ELEV CHAR(3) VAR INITIAL('NO');
DCL STORF CHAR(3) VAF INITIAL('NO');
  DCL MD CHAR(8);
DCL KEY(50) CHAR(1);
DCL PHASE CHAR(3) VAF INITIAL('NO');
DCL PS(30,100) CHAR(1);
  DCL S(26) CHAR(1);
  DCL GRAV CHAR(3) VAR INITIAL('NO');
DCL MADE CHAR(8);
DCL DEN(50);
  DCL R(30,100) CHAR(1);
DCL MAP CHAR(3) VARYING INITIAL('NO');
DCL PRINT CHAR(3) VARYING INITIAL('NO');
  DCL T(30,100); DCL Q(30,100);
  ON ENDFILE(IN) GO TO ERR;
GET DATA;
GET FILE(PH) LIST(NP,NT,NKEY,(KEY(I),DEN(I) DO I=1 TO NKEY));
GET FILE(PH) LIST(TP,BP,TT,BT);
T FILE(PH) EDIT(((P(I,J) DO J=1 TO NP) DO I=1 TO NT)){SKIP,(NP) A(1)};
  IF PRINT='YES' THEN DO;
PUT SKIP DATA(NP,NT,NKEY);
PUT SKIP LIST('TABLE OF PHASES AND DENSITIES');
PUT SKIP LIST('PHASE DENSITY');
DO I=1 TO NKEY;
PUT SKIP EDIT(KEY(I),DEN(I))(A(5),F(10,3));
END;
PUT PAGE LIST('PHASE EQUILIBRIUM DIAGRAM');
NS=NP-15;
PUT EDIT('T=',TT,'T=',TT)(R(DI));
PUT EDIT('P=',BP,'P=',TP)(R(DI));
DI: FORMAT(SKIP,A,F(10,3),X(NS),A,F(10,3));
PUT EDIT(((P(I,J) DO J=1 TO NP) DO I=1 TO NT)){SKIP,(NP) A(1)};
PUT EDIT('T=',BT,'T=',BT)(R(DI));
PUT EDIT('P=',BP,'P=',TP)(R(DI));
END;
HER: GET LIST(NAM,NOR,NCAT,NSP);
IND: GET FILE(IN) LIST(NAME,D,D,D,NR,NC,NO,TTT);
  GET FILE(IN) LIST(D,D,D,D,D,BH,BW);
GET FILE(IN) LIST(((T(I,J) DO J=1 TO NC) DO I=1 TO NR));
IF NAM~=NAME | NOR~=NO THEN GO TO IND;
ELSE GO TO ST;
ERR: PUT SKIP LIST('DATA REQUIRED NOT FOUND');
PUT SKIP EDIT('LOOKING FOR ',NAM,' CALL NUMBER',NOR)(A,A,A,F(4,0));
PUT SKIP EDIT('LAST DATA SET WAS ',NAME,' CALL NO.',NO)(A,A,A,F(4,0));
  PUT SKIP LIST('STOPPING'); STOP;
/* NOW DERIVE DENSITIES */
ST: DO I=1 TO NR;
  DO J=1 TO NC;
PR=BH*(NP+0.5-I)*47/150;
PINT=(TP-BP)/NP;
```

```

TINT=(TT-BT)/NT;
K=PR/PINT+1;
IF T(I,J)=0. THEN L=NT; ELSE L=NT-T(I,J)/TINT+1;
DO M=1 TO NKEY;
IF P(L,K)=KEY(M) THEN DO; Q(I,J)=DEN(M); PS(I,J)=P(L,K); END;
END;
Q(I,J)=Q(I,J)*(1-0.04*T(I,J)/1000+0.02*PR/23.25);
END; END;
IF GRAV='YES' THEN DO;
GET LIST(NADE);
PUT FILE(GR) EDIT(NADE,NR,NC,BH,BW)
(X(2),A(8),(2) F(10,0),(2) F(10,3));
DO I=1 TO NR;
PUT FILE(GR) SKIP EDIT((Q(I,J) DC J=1 TO NC))(8) F(10,3));
PUT FILE(GR) SKIP EDIT(' ')(A);
END; PUT SKIP LIST('DENSITY OUT PUT'); END;
/* THE NEXT 40 OR SO STATEMENTS ARE COPIED FROM HOTMAP */
* ONLY THE MIN CHANGING HAS BEEN DONE SO DON'T READ */
/* MUCH INTO VARIABLE NAMES */
IF MAP='YES' THEN DO;
PUT PAGE EDIT('MAP OF DENSITY FIELD FOR MODEL ',NAM,' CALL TO OUT
T NUMBER',NOR)(A,A,A,F(4,0));
/* WORK OUT CATEGORT LIMITS */
TMAX=0;
TMIN=10;
DO I=1 TO NR;
DO J=1 TO NC;
TMAX=MAX(TMAX,Q(I,J));
TMIN=MIN(TMIN,Q(I,J));
END;
END;
ITMAX=TMAX+1;
ITMIN=TMIN;
CATW=(ITMAX-ITMIN)/NCAT;
S(1)='A'; S(2)='B'; S(3)='C'; S(4)='D'; S(5)='E'; S(6)='F';
S(7)='G'; S(8)='H'; S(9)='I'; S(10)='J'; S(11)='K'; S(12)='L';
S(13)='M'; S(14)='N'; S(15)='O'; S(16)='P'; S(17)='Q'; S(18)='R';
S(19)='S'; S(20)='T'; S(21)='U'; S(22)='V'; S(23)='W'; S(24)='X';
S(25)='Y'; S(26)='Z';
PUT SKIP LIST('DENSITY INTERVALS IN GM/CC');
TB=ITMIN; TA=CATW+ITMIN;
DO K=1 TO NCAT;
PUT SKIP EDIT('FROM',TB,' TO',TA,' CODED AS ',S(K))
(A,F(6,3),A,F(6,3),A,A);
TB=TA;
TA=TA+CATW;
END;
DO I=1 TO NR;
DO J=1 TO NC;
N=(Q(I,J)-ITMIN)/CATW+1;
R(I,J)=S(N);
END; END;
/* NOW PLOT MAP */
PUT PAGE LIST(' ROW NUMBERS');
PUT SKIP EDIT((J DO J=1 BY 2 TC NR))(X(7),(20) F(4,0));
PUT SKIP EDIT((J DO J=2 BY 2 TO NR))(X(9),(20) F(4,0));
PUT SKIP(2);
DO J=1 TO NC;
IF NSP=0 THEN PUT SKIP(NSP);
PUT SKIP EDIT(J,(R(I,J) DO I=1 TO NR))(X(2),F(3,0),X(5),(30) A(2));

```

```

END;
PUT SKIP(2) LIST('COLUMN NUMBERS');
END;
IF PHASE='YES' THEN DO;
PUT PAGE LIST('MAP OF PHASES PRESENT');
PUT SKIP LIST('          ROW NUMBERS');
PUT SKIP EDIT((J DO J=1 BY 2 TO NR))(X(7),(20) F(4,C));
PUT SKIP EDIT((J DO J=2 BY 2 TO NR))(X(9),(20) F(4,0));
PUT SKIP(2); DO J=1 TO NC;
IF NSP $\neq$ 0 THEN PUT SKIP(NSP);
PUT SKIP EDIT(J,(PS(I,J) DO I=1 TO NR))(X(2),F(3,0),X(5),(30) A(2));
END; PUT SKIP(2) LIST('COLUMN NUMBERS'); END;
IF PLOT='YES' THEN DO;
PT: GET LIST(TYPE,NN);
IF TYPE='END' THEN GO TO ELE;
IF TYPE='ROW' THEN DO;
LM=NC;
DIS=BW;
END;
IF TYPE='COLUMN' THEN DO;
LM=NR;
DIS=BH;
END;
DO I=1 TO LM;
IF TYPE='ROW' THEN ANOM(I)=Q(NN,I);
IF TYPE='COLUMN' THEN ANOM(I)=Q(I,NN);
FPT(I)=DIS*(LM-I+0.5);
END;
CALL GRAPH(FPT,ANOM,LM,LM,100,FIX);
PUT SKIP EDIT('DENSITY PLOT FOR ',TYPE,NN,' FOR MODEL ',NAM,' CALL TO
TPUT NO.',NOR)(A,A,F(5,0),A,A,A,F(5,0));
GO TO PT;
END;
ELE: IF ELEV='YES' THEN DO;
ANOM=0.;
DO I=1 TO NC;
FPT(I)=BW*(NC-I+0.5);
END;
DO I=1 TO NR;
DO J=1 TO NC;
ANOM(J)=ANOM(J)+BH*(Q(I,J)-Q(I,1))/Q(I,1);
END; END;
DO J=1 TO NC;
ANOM(NC+J)=ANOM(J)*(1+1/(Q(1,J)-1));
FPT(NC+J)=FPT(J);
END;
NQ=NC+NC;
CALL GRAPH(FPT,ANOM,NC,NQ,100,FIX);
PUT SKIP EDIT('ELEVATION OF MODEL ',NAM,' OUTPUT NO.',NOR)
(A,A,A,F(4,0));
PUT SKIP LIST('*=CONTRACTION ONLY, +=CONTRACTION+ISOSTASY');
IF STORE='YES' THEN DO;
GET LIST(MO);
PUT FILE(OUT) EDIT(MO,NC)(X(2),A(8),F(10,0));
NQQ=NC+1; NQ=NC+NC;
PUT FILE(OUT) EDIT((ANOM(I),FPT(I) DO I=NQQ TO NQ))((8) F(10,3));
PUT FILE(OUT) EDIT(' ')(A(2)); PUT FILE(OUT) SKIP;
PUT SKIP EDIT(MO,' WRITTEN TO FILE OUT')(A,A);
END;
END;

```

## Appendix 7.

## The program HOTMAP.

Description

HOTMAP is a small program written, in PL1, to plot the temperature distribution in a modelled lithospheric slab according to a procedure similar to that used for the density distribution in the program TEMDEN. An option exists to produce a graph of the values of surface heat flow which exist across the top of the slab. For efficiency, this program should be incorporated into TEMDEN and it is only separate for historical reasons.

Input

The input may be divided into two sections:-

- 1) The temperature distributions and associated information, exactly as output by the program HEAT. Read from file IN.
- 2) Output instructions etc. Read from file SCARDS. The required output is selected by putting any of the available options equal to 'YES' in a GET DATA statement. The available options are:-

MAP - produces diagram of the temperature distribution.

PLOT - plots heat flow anomaly across the slab.

The required data set and the output format for the temperature distribution are specified in a manner identical to that used to produce the density distribution in TEMDEN. The required parameters are:-

NAM - name of data set	)	As for the program TEMDEN, appendix 6.
NOR - number of data set	)	
NCAT - number of categories	)	
NSP - number of spaces	)	

The heat flow anomaly is calculated from the vertical temperature gradient between corresponding blocks in the top two layers of the lithospheric model. The

necessary thermal conductivities may be specified in either of two formats:-

(only if PLOT = 'YES')

EITHER CON(I) I from 1 to NC. NC = number of columns, conductivities specified individually.

OR CON 0 (zero). Conductivities all set to CON by the program.

The conductivities are specified in cal/cm.s.<sup>o</sup>C.

#### Output

- 1) If MAP = 'YES', the temperature distribution is plotted on the line printer (for details see the density distribution in TEMDEN).
- 2) If PLOT = 'YES', the heat flow anomaly is plotted on the line printer using the subroutine GRAPH (appendix 10). Self explanatory.

Several consecutive temperature distributions may be processed in one run of the program, as in TEMDEN.

Interpretation of the output.

The notes given at the end of appendix 6 apply also to the output of HOTMAP.

A listing of the program follows.

TMAP -E

```
HOTMAP: PROCEDURE OPTIONS(MAIN);
DCL(NAM,NAME) CHAR(8);
DCL P(30,100) CHAR(1);
DCL T(30,100);
DCL S(26) CHAR(1);
DCL(MAP,PLOT) CHAR(3) VARYING INITIAL('NO');
ON ENDFILE(IN) GO TO ERR;
GET DATA;
HER: GET LIST(NAM,NOR,NCAT,NSP);
IND: GET FILE(IN) LIST(NAME,D,D,D,NP,NC,NO,TTT);
GET FILE(IN) LIST(C,D,D,D,D,BH,RW);
DO I=1 TO NR;
GET FILE(IN) LIST((T(I,J) DO J=1 TO NC));
END;
IF NAM=NAME | NOR=NO THEN GO TO IND;
IF MAP='YES' THEN DO;
PUT SKIP EDIT('MAP OF TEMPERATURE FIELD FOR MODEL ',NAM,' CALL TO OUT
T NUMBER',NOR)(A,A,A,F(4,0));
/* WORK OUT CATEGORT LIMITS */
TMAX=0;
DO I=1 TO NR;
DO J=1 TO NC;
TMAX=MAX(TMAX,T(I,J));
END;
END;
ITMAX=TMAX/100+1;
CATW=ITMAX*100/NCAT;
S(1)='A'; S(2)='B'; S(3)='C'; S(4)='D'; S(5)='E'; S(6)='F';
S(7)='G'; S(8)='H'; S(9)='I'; S(10)='J'; S(11)='K'; S(12)='L';
S(13)='M'; S(14)='N'; S(15)='O'; S(16)='P'; S(17)='Q'; S(18)='R';
S(19)='S'; S(20)='T'; S(21)='U'; S(22)='V'; S(23)='W'; S(24)='X';
S(25)='Y'; S(26)='Z';
PUT SKIP LIST('TEMPERATURE INTERVALS IN DEG C');
TB=0; TT=CATW;
DO K=1 TO NCAT;
PUT SKIP EDIT('FROM',TB,' TO',TT,' CODED AS ',S(K))
(A,F(6,1),A,F(6,1),A,A);
TB=TT;
TT=TT+CATW;
END;
DO I=1 TO NR;
DO J=1 TO NC;
N=T(I,J)/CATW+1;
P(I,J)=S(N);
END; END;
/* NOW PLOT MAP */
PUT PAGE LIST(' ROW NUMBERS');
PUT SKIP EDIT((J DO J=1 BY 2 TO NR))(X(7),(20) F(4,0));
PUT SKIP EDIT((J DO J=2 BY 2 TO NR))(X(9),(20) F(4,0));
PUT SKIP(2);
DO J=1 TO NC;
IF NSP=0 THEN PUT SKIP(NSP);
PUT SKIP EDIT(J,(P(I,J) DO I=1 TO NR))(X(2),F(3,0),X(5),(30) A(2));
END;
PUT SKIP(2) LIST('COLUMN NUMBERS');
END; GO TO HF;
ERR: PUT SKIP LIST('DATA REQUIRED NOT FOUND');
```

```

PUT SKIP EDIT('LOOKING FOR ',NAM,' CALL NUMBER',NOR)(A,A,A,F(4,0));
PUT SKIP EDIT('LAST DATA SET WAS ',NAME,' CALL NO.',NO)(A,A,A,F(4,0));
PUT SKIP LIST('NO MAP OR GRAPH PRODUCED');
STOP;
HF:  IF PLOT='YES' THEN DO;
      PUT SKIP LIST('PLOTTING HEAT FLCW GRAPH');
DCL CON(100),FPT(100),QE(100);
DCL FIX CHAR(2) INITIAL('NC');
GET LIST(CON(1),CON(2));
IF CON(2)<0.00001 THEN DO;
DO I=2 TO NC;
CON(I)=CON(1);
END;  END;
ELSE GET LIST((CON(I) DO I=3 TO NC));
PUT SKIP EDIT('HEIGHT OF BLOCKS=',BH,' KILOMETRES')(A,F(8,3),A);
PUT SKIP EDIT('WIDTH OF BLOCKS IN KILOMETRES=',BW)(A,F(8,3));
PUT SKIP LIST('CONDUCTIVITIES IN CALS/CM.SEC.*C');
PUT SKIP EDIT((CON(I) DO I=1 TO NC))((8) F(10,4));
DO I=1 TO NC;
FPT(I)=(I-1)*BW;
QE(I)=10*CON(I)*(T((NR-1),I)-T(NR,I))/BH;
END;
CALL GRAPH(FPT,QE,NC,NC,100,FIX);
PUT SKIP LIST('HEAT FLOW GRAPHS IN MICROCALS/CM**2.SEC');
PUT SKIP EDIT('MODEL ',NAM,' CALL TO OUTPUT NUMBER',NOR)
(A,A,A,F(4,0));
END;
GO TO HER;
END HOTMAP;

```

## Appendix 8.

### The program SYN.

#### Description

This program is written in PL1 to synthesize the bathymetric profiles produced by sea-floor spreading occurring at a specified combination of spreading rates from previously derived relationships between lithospheric age and the elevation of the ocean ridge above the basin. Age-elevation data for several different lithospheric thicknesses may be considered during one run of the program, and the resulting bathymetric profiles are fitted by a least squares procedure to observed data. A graph of the variances of the bathymetric fits so produced is plotted, and provides an immediate indication of the thickness of lithosphere which results in the best fit to the observed bathymetry.

The specified spreading rates and the periods during which they operated are examined to form a relationship between the age of the lithosphere and its distance from the spreading centre. Information relating the bathymetric elevation of the top surface of a lithosphere of a given thickness to its age may be simply derived from the output of the programs HEAT and TEMDEN (appendices 5 and 6) if a constant spreading rate is used during the calculation of the lithospheric temperature distribution. Repetition of this process for several lithospheric thicknesses enables a three-dimensional age-elevation-thickness table to be compiled (appendix 4). Bathymetric profiles for the various thicknesses are then produced by applying the above-mentioned age-distance relationship for the relevant spreading rates to this table.

The variance of each fit between observed and calculated profiles is determined by shifting one vertically relative to the other until the deepest part of the calculated profile coincides with a datum level derived from the observed profile by averaging the depths in the ocean basin over a specified horizontal distance. Since features such as seamounts lead to an upward biasing of this datum, a facility is provided to effectively remove such short wavelength topography from the



abyssal plain. The variance of the fit is then calculated as

$\sum(\text{Observed elevation} - \text{calculated elevation})^2 / \text{No. of points}$ ,  
and is plotted against the thickness of lithosphere used to generate the calculated profile.

### Input

This may be divided into three sections:-

- 1) The observed bathymetry - read from file OBS as follows:
  - NAMO - name of observed data
  - NOP - number of points
  - EO(I), DO(I) I from 1 to NOP - observed elevation (fathoms), observed distance (km). Since the interval of distance between adjacent points must be uniform along the profile, it may be necessary to sample or spline the observed data before running this program.
- 2) The age-elevation data - read from file AE as follows:
  - NAEM - name of the data
  - NA - number of values of age
  - NE - number of values of elevation for a given age
  - DAT(I) I from 1 to 14 - Alphabetic and/or numeric references to each individual age-elevation relationship (for identification purposes only, usually lithospheric thicknesses as appropriate).
  - AG(I), E(I,J), J from 1 to NE, I from 1 to NA - Ages (My), elevation (km), NE elevations per age, one per lithospheric thickness.
- 3) Spreading rate data and other parameters- read from file SCARDS as follows:
  - NR - number of different phases of spreading
  - TS(I) - start of spreading episode (My B.P.)
  - TF(I) - finish of spreading episode (My B.P.)
  - SR(I) - spreading rate between TS(I) and TF(I) (cm/y)

There are NR sets of TS(I), TF(I), SR(I), starting with 0 My B.P. and progressing into the past.

DMIN } - These together specify the positions of the  
 DMAX ) ocean ridge crest in units of kilometres  
 according to the coordinates of the observed bathymetry. Calculations are performed assuming the ridge crest to be at each point between DMIN and DMAX consecutively, and DMIN and DMAX must themselves fall on, and not between, data points. DMIN must be less than or equal to DMAX.

DF - This parameter defines the point on the observed bathymetric profile beyond which all topography is to be removed by setting the bathymetry to the value present at DF, so as to calculate an unbiased datum level as described above. "beyond which" in this context refers to points further from the ocean ridge crest than the point at DF. DF is specified in km according to the coordinate system of the observed profile and must be used with care. If the observed data is such as to either not require or not permit the use of this procedure for any reason, DF must be set to a point further from the ocean ridge than the horizontal extent of the calculated profile, in which case it will have no effect.

DD - specifies the position of the start of the abyssal plain for the purposes of the datum level calculation mentioned above, in units of km according to the coordinate system of the observed profile. The bathymetry at all points further from the spreading axis than that defined by DD is taken into account when calculating the average depth of the observed abyssal plain.

DPL - must be equal to either DMAX or DMIN or the distance coordinate of any point between these two. A graph of variance against lithospheric thickness is produced for the case in which the ridge crest is taken as being at DPL.

IREV - defines which half of the observed bathymetric profile is to be used in the calculations. If IREV=1, the distance coordinates of the half of the observed profile selected increase from the ocean ridge towards the basin, if IREV=-1 they decrease.

### Output

The following sets of information are produced:-

- 1) A list of the spreading rates and the periods over which they apply.
- 2) A table of lithospheric age against distance, the units of the distance scale being km but its origin being unspecified (this is a simple writing of some arrays, originally for program checking purposes. Hence the arbitrary datum).
- 3) A listing of the age-elevation table as input on file AE.
- 4) A listing of the calculated elevation- distance profiles using the distance scale of 2, above.
- 5) The results of the fitting process. For each lithospheric thickness the following are produced:-
  - 1) The variances of the fits between observed and calculated data for each position of the ridge crest between DMAX and DMIN.
  - 2) A listing of the observed and calculated profiles used in computing the fits, with the relative vertical shift applied ( the shift is also recorded).
  - 3) A plot of the observed and calculated bathymetric profiles superimposed on one another.

(2 and 3 are only produced for the ridge crest position which gives the lowest variance for the lithospheric thickness in question).
- 6) A graph of variance against lithospheric thickness for the ridge crest position specified by DPL.

A listing of the program follows.

TPOT -D

```
SYN: PROC OPTIONS(MAIN);
DCL NAMO CHAR(8); DCL (EO,DO) (800);
CL AG(800),E(800,20),EL(800,20);
DCL DAT(14) CHAR(20) VAR;
CL (TS,TF,SR)(10);
CL (A,D)(800);
DCL (SE,TH) (20);
DCL FIX CHAR(0) VAR INITIAL('NO');
CL NAEM CHAR(8);
PEN FILE(SPRINT) LINESIZE(132);
GET FILE(OBS) EDIT(NAMO,NOP)(X(2),A(8),F(10,0));
GET FILE(OBS) LIST((EO(I),DO(I) DO I=1 TO NGP));
DIS=ABS(DO(2)-DO(1));
ET LIST(NR);
UT DATA(DIS,NR);
ET LIST((TS(I),TF(I),SR(I) DO I=1 TO NR));
UT SKIP LIST('SPREADING RATES: FROM(MY) TO(MY) RATE(CM/Y)');
DO I=1 TO NR;
PUT SKIP EDIT(TS(I),TF(I),SR(I))(X(15),(3) F(10,3));
END;
D(1)=DO(1);
A(1)=DIS/(20*SR(1));
=2; J=1;
L2: IF A(I-1)<TF(J) THEN SPR=SR(J);
ELSE DO; J=J+1; IF J>NR THEN GO TO L1; GO TO L2; END;
A(I)=A(I-1)+DIS/(10*SPR);
(I)=D(I-1)+DIS; I=I+1; GO TO L2;
L1: NAGE=I-1;
PUT SKIP(2) LIST('NUMBER OF PTS AGE(MY) DIST(KM)');
DO I=1 TO NAGE; PUT SKIP LIST(NAGE,A(I),D(I)); END;
ET FILE(AE) EDIT(NAEM,NA,NE)(X(2),A(8),(2) F(10,0));
GET FILE(AE) SKIP EDIT((DAT(I) DO I=1 TO 14))
((13) A(6),A(2));
UT SKIP(2) EDIT(NAEM,NA,NE)(X(2),A(8),(2) F(10,0));
PUT SKIP EDIT((DAT(I) DO I=1 TO 14))
(X(5),(2) A(6),(11) (X(4),A(6)),A(2));
DO I=1 TO NA;
ET FILE(AE) LIST(AG(I),(E(I,J) DO J=1 TO NE));
ND;
DO I=1 TO NA;
UT SKIP EDIT(AG(I),(E(I,J) DO J=1 TO NE))((13) F(10,3));
D;
AG=AG(2)-AG(1);
DO J=1 TO NE;
DO I=1 TO NAGE;
M=1+A(I)/DAG;
(<=E(NM,J));
L(I,J)=X+(E((NM+1),J)-E(NM,J))*(A(I)-AG(NM))/(AG(NM+1)-AG(NM));
ND; END;
PUT PAGE;
DO I=1 TO NAGE;
UT SKIP EDIT(D(I),(EL(I,J) DO J=1 TO NE))((13) F(10,3));
ND;
GET LIST(DMIN,DMAX,DF,DD,OPL,IREV);
PUT SKIP DATA(DF,DD,IREV);
DO I=1 TO NE;
.L LESQ(EO,DO,EL,D,NAMO,NOP,NAEM,NAGE,DMIN,DMAX,DF,DD,OPL,IREV,I,DAT,S
```

```

TH);
ND;
CALL GRAPH(TH,SE,NE,NE,20,FIX);
PUT SKIP EDIT('ERROR CURVE FOR DISTANCE ',DPL)(A,F(8,3));
PUT SKIP EDIT('FITTING ',NAMO,' WITH ',NAEM)(A,A,A,A);
PUT SKIP LIST('FINISHED');
ND SYN;
SQ: PROC (FO, DO, EC, DC, NAMO, NOP, NAMC, NCP, DMIN, DMAX, DF, DD, DPL, IREV, NNN, DA
SE, TH);
DCL (NAMO, NAMC) CHAR(8);
DCL DAT(14) CHAR(20) VAR;
DCL (EO, DO, DC, AMNO, SQ) (800);
DCL (SE, TH) (20);
DCL EC(800,20);
DCL (OD, DS) (1600);
DCL SSQ(800);
DCL FIX CHAR(0) VAR INITIAL('NO');
PUT PAGE LIST('LEAST SQUARES FIT OF BATHYMETRIC DATA');
PUT SKIP(2) EDIT('OBSERVED DATA ', NAMO, ' CALCULATED ', NAMC)(A,A,A,A);
MMM=NNN+1;
PUT SKIP EDIT(' CALL NUMBER ', NNN, ' THICKNESS(KM)=' , DAT(MMM))
(A,F(5,0),A,A(6));
IDS=DO(2)-DO(1)+0.5; IDT=DC(2)-DC(1)+0.5;
NDD=(DD-DO(1))/IDS+1.5;
NS=(DMIN-DO(1))/IDS+1.5;
NF=(DMAX-DO(1))/IDS+1.5;
K=(NS+NF)/2;
KC=ABS(NDD-K)+1;
TOT=0; DO I=KC TO NCP; TOT=TOT+EC(I,NNN); END; AMNC=TOT/(NCP-KC+1);
PUT SKIP DATA(AMNC);
IF NNN=1 THEN DO; DO I=1 TO NCP; EC(I)=EO(I)*0.0018288; END; END;
IF IDT=IDS THEN DO; PUT SKIP LIST('DISTANCE UNEQUAL'); STOP; END;
NRCP=IREV*(NCP-1);
NFIK=(DF-DO(1))/IDS+1.5;
IF IREV=1 THEN NNF=NF; ELSE NNF=NS;
DO I=NFIK BY IREV TO NNF+NRCP; EO(I)=EO(NFIK); END;
PUT SKIP EDIT(' FIXING FROM ', DF, ' AT VALUE ', EO(NFIK))
(A,F(10,3),A,F(10,3));
PUT SKIP DATA(NRCP,NS,NF,IDS,NFIK,NDD);
DO I=NS TO NF;
TOT=0;
DO J=NDD BY IREV TO I+NRCP;
TOT=TOT+EO(J);
END;
AMNO(I)=TOT/(ABS(K+NRCP-NDD)+1);
END;
PUT SKIP LIST((AMNC(I) DO I=NS TO NF));
DO I=NS TO NF;
TOT=0;
DO J=I BY IREV TO I+NRCP;
K=ABS(J-I)+1;
TOT=TOT+(EO(J)-(EC(K,NNN)+(AMNO(I)-AMNC)))*2;
END;
SQ(I)=TOT;
SQ(I)=SQ(I)/NCP;
END;
PUT SKIP LIST((SQ(I) DO I=NS TO NF));
SQM=SQ(NS);
DO I=NS TO NF;
SQM=MIN(SQM,SQ(I));

```

```

IF ABS(SQM-SQ(I))<0.0001 THEN KEY=I;
END;
PUT SKIP LIST('COEFFICIENT FOR VARIOUS DISTANCES');
PUT SKIP LIST('DISTANCE (KM)    COEFFICIENT STANDARD ERROR');
DO I=NS TO NF;
  DIS=DMIN+(I-NS)*IDS;
PUT SKIP EDIT(DIS,SQ(I),SSQ(I)){F(10,3),(2) F(15,3)};
IF ABS(DPL-DIS)<0.001 THEN DO;
  GET STRING(DAT(MMM))LIST(TH(NNN));
  SE(NNN)=SSQ(I);  END;
END;
DCS=AMNO(KEY)-AMNC;
PUT SKIP EDIT('DC SHIFT IS ',DCS){A,F(10,3)};
PUT SKIP LIST('DISTANCE OBSERVED CALCULATED');
DO I=1 TO NCP;
DS(I)=(I-1)*IDS;
OD(I)=EC(I,NNN)+DCS;
OD(NCP+I)=EO(KEY+(I-1)*IREV);
DS(I+NCP)=DS(I);
END;
DO I=1 TO NCP;  NCPI=NCP+I;
PUT EDIT(DS(I),OD(NCPI),OD(I))
(SKIP,(3) F(10,3)); END;
PUT SKIP EDIT('OBSERVED=',NAMO,' CALCULATED=',NAMC,' CALL NO ',NNN)
(A,A,A,A,A,F(5,0));
PUT EDIT(' THICKNESS(KM)=' ,DAT(MMM))(A,A(6));
NST=NCP+NCP;
CALL GRAPH(CS,OD,NCP,NST,1600,FIX);
PUT SKIP EDIT('BEST FIT TO ',NAMO,' WITH ',NAMC,' CALL NO ',NNN)
(A,A,A,A,A,F(5,0));
PUT EDIT(' THICKNESS(KM)=' ,DAT(MMM))(A,A(6));
PUT SKIP EDIT('*=',NAMC,' +=',NAMO)(A,A,A,A);
RETURN;
END LESQ;

```

TESTDATA	7		3	
TESTA	TESTB	TESTC		
0	-6	-3	-9	
5	-5	-2.5	-7.5	
0	-4	-2	-6	
5	-3	-1.5	-4.5	
0	-2	-1	-3	
5	-1	-0.5	-1.5	
90	0	0	0	

## Appendix 9.

## The program LIGRAV.

Description

This program is written in PL1 to calculate the free air and Bouguer gravity anomalies which are associated with the modelled lithospheric slabs. Part of the output of the program TEMDEN (appendix 6) provides the distribution of density within the slab, and the vertical dimensions of all the blocks in each column are factored to account for thermal contraction etc according to the elevation profile also produced by TEMDEN. The calculation is based on the repeated application of the formula for the gravity effect of a rectangular prism (Garland, 1965), the effect of the slab alone providing the Bouguer anomaly and the effect of the water being added to produce the free air anomaly. It is assumed for the purposes of the calculations that the sea-floor spreading has occurred symmetrically, so that the second half of the ocean may be considered as a mirror image of the first. As noted in appendix 6, the temperature boundary condition at the cool edge of the slab often causes distortion of the modelled results in that region. Facilities exist in LIGRAV to remove these effects from the density distribution and the elevation profile before carrying out the calculations. No allowance for the curvature of the Earth is made.

Input

This may be divided into three sections as follows:

- 1) The elevation profile, read from file EL as follows
  - ENAM - name of profile
  - NEP - number of points
  - E(I), D(I) I from 1 to NEP - elevation, distance (km).
 This data is as output on file OUT by TEMDEN.
- 2) The density distribution, read from file GR as follows:
  - GNAM - name of density distribution
  - NR - number of rows of blocks in model
  - NC - number of columns of blocks in model

BH - height of blocks in model (before contraction etc.)

BWW - width of blocks

Q(I,J), I from 1 to NR, J from 1 to NC - I numbers  
from the base upwards, J numbers towards the hot  
edge. As output by TEMDEN on file GR. Densities.

3) Other instructions.

ENS - expected name of elevation profile } .checked  
GNS - expected name of density distribution } against  
ENAM,GNAM.

IPD } - instructions for removing distortion  
IPF } of modelled data by cool edge of slab. The  
elevation and density distribution of columns  
1 to IPF are set to those of column IPD.

BADE - depth of water in ocean basin (km).

Output

- 1) listing of the elevation profile
- 2) listing of the density distribution
- 3) listing of the gravity anomalies
- 4) graph of the gravity anomalies (on the line printer)

The output is self-explanatory.

A listing of the program follows.



```

GRAV: PROC OPTIONS(MAIN);
CL(ENAM,GNAM,ENS,GNS) CHAR(8);
CL (E,D,AN,ANW,ANF)(250) FLOAT(15);
CL(AG1,AG2,AG3,AG4,BADE,BH,PHL,BW,BWW,DD) FLOAT(15);
CL(R1,R2,R3,R4,RA,RB,TTH1,TH2,X) FLOAT(15);
CL FIX CHAR(3) VAR INITIAL('NO');
DCL (Q,QQ)(30,200);
ET LIST(ENS,GNS,IPD,IPF,BADE);
GET FILE(FL) EDIT(ENAM,NEP)(X(2),A(8),F(10,0));
GET FILE(EL) LIST((E(I),D(I) DO I=1 TO NEP));
DO I=1 TO IPF;
E(I)=E(IPD);
END;
W=D(1)-D(2);
DAT=E(IPD);
DO I=2 TO NEP;
(I-1)=E(I)-EDAT;
D(I-1)=BW/2+(I-2)*BW;
ND;
RR=NEP-2;
DO I=1 TO NRR;
D(I+NEP-2)=D(I+NEP-3)+BW;
E(I+NEP-2)=E(NEP-I-1);
END;
NEP=NEP-2+NRR;
L=0; DO I=1 TO NEP; TEL=MIN(TEL,E(I)); END;
K=0; IF KK=1 THEN GO TO A;
UT EDIT('ELEVATION CURVE ',ENAM)(A,A);
PUT SKIP DATA(IPD,IPF);
PUT DATA(BADE);
UT SKIP EDIT('REGIONAL DATUM=',EDAT)(A,F(10,3));
UT SKIP EDIT((E(I),D(I) DO I=1 TO NEP))((8) F(10,3));
GET FILE(GR) EDIT(GNAM,NR,NC,BH,BWW)(X(2),A(8),14) F(10,0));
DO I=1 TO NR;
ET FILE(GR) LIST((Q(I,J) DO J=1 TO NC));
ND;
DO J=1 TO NC-2;
DO I=1 TO NR;
Q(I,J)=Q(I,J+1);
END; END;
DO J=1 TO IPF-1;
DO I=1 TO NR;
QQ(I,J)=QQ(I,IPD-1); END; END;
DO J=1 TO NRR; DO I=1 TO NR;
Q(I,NC-2+J)=QQ(I,NC-J-1);
END; END;
C=NC-2+NRR;
K=0; IF KK=1 THEN GO TO AA;
DO I=1 TO NR;
UT SKIP EDIT((QQ(I,J) DO J=1 TO NC))((8) F(10,3));
END;
DISCR=ABS(BWW-BW);
IF NC=NEP | DISCR>0.0001 THEN DO;
UT SKIP LIST('DATA UNEQUAL');
UT SKIP DATA(NC,NEP,BWW,BW); STOP; END;
IF ENS=ENAM | GNS=GNAM THEN DO;
UT SKIP LIST('DATA WRONG');
UT SKIP EDIT('LOOKING FOR ',ENS,' ',GNS)(A,A,A,A);

```

```

UT SKIP EDIT('HAVE FOUND ',ENAM,' ',GNAM)(A,A,A,A);
STOP; END;
AN=0; ANW=0; DAT=BADF+NR*BH;
DO J=1 TO NC;
BHL=BH*(NR*BH-E(J))/(NR*BH);
DO I=1 TO NR;
D=BADE+RH*NR-BHL*I;
KD=J; RHO=GQ(I,J); CALL TRAP(AN); END;
D=BADF+TEL; BHL=-TEL+E(J); RHO=1.05; CALL TRAP(ANW); END;
NPE=NEP+1;
T=BW; D(NPE)=D(NEP)+BW/2+5000; BW=10000; KXD=NPE;
L=BH*(NR*BH-E(NEP))/(NR*BH);
DO I=1 TO NR; DD=BADE+BH*NR-BHL*I;
D=QQ(I,NEP); CALL TRAP(AN); END;
D=BADE+TEL; BHL=-TEL+E(NEP); RHO=1.05; CALL TRAP(ANW);
D(NPE)=D(1)-BWT/2-5000;
L=BH*(NR*BH-E(1))/(NR*BH);
DO I=1 TO NR; DD=BADE+NR*BH-BHL*I;
D=QQ(I,1); CALL TRAP(AN); END;
D=BADE+TEL; BHL=-TEL+E(1); RHO=1.05; CALL TRAP(ANW);
NNN=NEP/2;
DAT=AN(NNN)+ANW(NNN);
DO J=1 TO NC; ANF(J)=AN(J)+ANW(J)-GDAT; END;
KK=0; IF KK=1 THEN GO TO B;
UT PAGE EDIT('GRAVITY EFFECT OF SLAB ',GNAM)(A,A);
SKIP LIST(' DISTANCE ROCK GRAVITY WATER LAYER FREE AIR');
PUT EDIT((D(I),AN(I),ANW(I),ANF(I) DO I=1 TO NEP)) (SKIP ,(4) F(15,3));
KK=0; IF KK=1 THEN GO TO C;
N2P=NEP/2; DO I=1 TO N2P; AN(I)=AN(I+N2P); D(I)=D(I+N2P)-D(N2P); END;
X='NO'; DO I=1 TO N2P; AN(I+N2P)=ANW(I+N2P); D(I+N2P)=D(I); END;
CALL GRAPH(D,AN,N2P,NEP,200,FIX);
UT SKIP EDIT('*=ROCK GRAVITY, += WATER LAYER MODEL ',GNAM)(A,A);
KK=0; IF KK=1 THEN GO TO F;
DO I=1 TO N2P; ANF(I)=ANF(I+N2P); END;
CALL GRAPH(D,ANF,N2P,N2P,200,FIX);
UT SKIP EDIT('FREE AIR ANOMALY FOR ',GNAM)(A,A);
PUT SKIP LIST('FINISHED');
RAP: PROCEDURE(FN);
DCL FN (250);
DO K=1 TO NEP;
X=D(KXD)-D(K)-BW/2;
R1=SQRT(X**2+DD**2);
R2=SQRT(X**2+(DD+BHL)**2);
R3=SQRT((X+BW)**2+DD**2);
R4=SQRT((X+BW)**2+(DD+BHL)**2);
IF X=0 THEN AG1=3.14159/2; ELSE AG1=ATAN(DD,X);
IF X=0 THEN AG2=3.14159/2; ELSE AG2=ATAN((DD+BHL),X);
IF X+BW=0 THEN AG3=3.14159/2; ELSE AG3=ATAN(DD,(X+BW));
IF X+BW=0 THEN AG4=3.14159/2; ELSE AG4=ATAN((DD+BHL),(X+BW));
TH1=ABS(AG1-AG3);
TH2=ABS(AG2-AG4);
RA=R1*R4/(R2*R3); RB=R4/R3;
ZZ=(DD+BHL)*TH2-DD*TH1+X*LOG(RA)+BW*LOG(RB);
FN(K)=FN(K)+RHO*ZZ*41.87/3.14159;
END; END TRAP; END LIGRAV;

```

## Appendix 10.

### The subroutine GRAPH.

#### Description

This PL1 subroutine was written in order to provide a means of plotting data on the line printer, thereby facilitating quick examination of results. It forms an integral part of several of the preceding programs. The calling parameters are:-

FPT - An array containing the coordinates to be plotted across the printer page.

ANOM - An array containing the coordinates to be plotted up the printer page.

NS - the number of points in graph 1.

NST - the number of points in both graph 1 and 2 together (= number of elements of FPT and ANOM).

NNS - Dimension of the arrays FPT, ANOM.

FIX - Key as to whether the scales are to be set automatically by the program or to be input.

Two graphs may be plotted on the same set of axes. ANOM (1 to NS) and FPT(1 to NS) make up graph 1, which is plotted with asterisks. ANOM(NS+1 to NST) and FPT(NS+1 to NST) make up graph 2, which is plotted with plus signs. Common points are plotted with minus signs. If NS = NST, one graph only is plotted.

If FIX = 'NO', the scale units and end points are calculated automatically by the subroutine. If FIX = 'YES', the values of the scale end points must be input (via SCARDS) in the following order: Max ANOM, Min ANOM, Max FPT, Min FPT, and the scale units are then calculated from these figures. If Max ANOM is entered as a number greater than 999999, and a dummy value for Min ANOM is supplied, then the ANOM scale is calculated automatically and only the FPT scale is fixed to the values input.

A listing of the subroutine and a sample of the output follow.

```

GRAPH: PROCEDURE (FPT,ANOM,NS,NST,NNS,FIX);
  /* TO PLOT RESULTS OF GRAVN AN D MAGN */
  DECLARE (FPT,ANOM) (NNS),AXAN(51),AXFP(101);
  DECLARE (MAXAN,MINAN,MAXFP,MINFP) FLOAT;
  DECLARE PLOT(51,101) CHARACTER(1);
  DECLARE FIX CHARACTER(3) VARYING;
  DECLARE KEY CHARACTER(1);
  PLOT=' ';
  KEY='*';
  SCALE: PROCEDURE(VL,KK);
    VAL1=VAL;
    VAL=ABS(VAL);
  IF VAL<0 THEN KKK=-1;
  ELSE KKK=1;
    IF VAL>=1 THEN DO;
      ID=0;
    SL1: VAL=VAL/10;
      ID=ID+1;
      IF VAL>=1 THEN GO TO SL1;
    IVAL=VAL*10+1*KK*KKK;
    AVAL=IVAL*10**(ID-1);
      IF VAL<0 THEN AVAL=-AVAL;
    RETURN (AVAL);
  END;
    ELSE DO;
  IF VAL=0 THEN DO;
    IM=0;
  SL2: VAL=VAL*10;
    IM=IM+1;
    IF VAL<1 THEN GO TO SL2;
  IVAL=VAL+1*KK*KKK;
  AVAL=IVAL/10**(IM);
    IF VAL<0 THEN AVAL=-AVAL;
  END;
  ELSE AVAL=0;
  RETURN (AVAL);
  END;
  END SCALE;
  /* FIRST FIND RANGE OF VALUES */
  PUT SKIP(3);

MAXAN=ANOM(1);
MINAN=ANOM(1);
MAXFP=FPT(1);
MINFP=FPT(1);
DO I=1 TO (NST-1);
MAXAN=MAX(MAXAN,ANOM(I+1));
MINAN=MIN(MINAN,ANOM(I+1));
MAXFP=MAX(MAXFP,FPT(I+1));
MINFP=MIN(MINFP,FPT(I+1));
END;
  PUT LIST('MAXIMUM CO-ORDINATES OF POINTS');
  PUT SKIP LIST(' MAXAN MINAN MAXFP MINFP');
  PUT SKIP EDIT(MAXAN,MINAN,MAXFP,MINFP)
  ((4)(F(8,2)));
  PUT SKIP LIST(' ');
  IF FIX='YES' THEN DO;
  GET LIST(SMAA,SMIA,SMAF,SMIF);

```

```

IF SMAA>999999 THEN DO;
KK=1;
SMAA=SCALE{MAXAN, KK};
KK=-1;
SMIA=SCALE{MINAN, KK};
END;
END;
ELSF DO;
KK=1;
SMAA=SCALE{MAXAN, KK};
KK=-1;
SMIA=SCALE{MINAN, KK};
KK=1;
SMAF=SCALE{MAXFP, KK};
KK=-1;
SMIF=SCALE{MINFP, KK};
END;
JNA=(SMAA-SMIA)/50;
JNF=(SMAF-SMIF)/100;
/* UNA AND UNF GIVE VALUES OF UNITS ALONG AXES */
/* NOW DEFINE VALUES OF POINTS */
PUT SKIP EDIT('ANOMALY UNIT=', UNA, 'DISTANCE UNIT=', UNF)
(A, F(10, 2), X(2), A, F(10, 2));
PUT SKIP LIST('SCALE END POINTS');
PUT SKIP LIST(' SMAA SMIA SMAF SMIF ');
PUT SKIP EDIT(SMAA, SMIA, SMAF, SMIF)
((4)(F(8, 2)));
DO I=1 TO 51;
AXAN(I)=SMAA-(I-1)*UNA;
END;
DO I=1 TO 101;
AXFP(I)=SMIF+(I-1)*UNF;
END;
/* LOCATE POSITIONS OF POINTS */
/* AND ALTER PLOT */

IS=1; IF=NS;
L5: DO J=IS TO IF;
DO I=1 TO 51;
DISCR=ABS(ANOM(J)-AXAN(I));
IF DISCR<=UNA/2 THEN GO TO L1;
END;
PUT SKIP EDIT('ANOM(', J, ') IS OUTSIDE THE RANGE OF THE SCALES')
(A, F(3, 0), A);
PUT SKIP EDIT('VALUE OF ANOMALY=', ANOM(J), 'KEY=', KEY)
(A, F(7, 2), X(1), A, A);
.1: IP=I;
DO K=1 TO 101;
DISCR=ABS(FPT(J)-AXFP(K));
IF DISCR<=UNF/2 THEN GO TO L2;
END;
PUT SKIP EDIT('FPT(', J, ') IS OUTSIDE THE RANGE OF THE SCALES')
(A, F(3, 0), A);
PUT SKIP EDIT('VALUE OF FPT=', FPT(J), 'KEY=', KEY)
(A, F(7, 2), A, A);
.2: KP=K;

PLOT{IP, KP}=' ' | PLOT{IP, KP}=KEY THEN PLOT{IP, KP}=KEY;
ELSE PLOT{IP, KP}='-';

```

```

END;
  IF NST>NS THEN DO;
KEY='+';
IS=NS+1;
  IF=NST;
  NST=1;
GO TO L5;
END;
  /* NOW READY TO WRITE */
  /* AXES */
DO I=1 TO 51;
  IF PLOT(I,1)=' ' THEN PLOT(I,1)='X';
END;
DO K=1 TO 101;
  IF PLOT(51,K)=' ' THEN PLOT(51,K)='X';
END;
PUT PAGE LIST('ANOMALY IN MGALS OR GAMMAS');
PUT SKIP;
DO I=1 TO 51;
IF I=1 | I=11 | I=21 | I=31 | I=41 | I=51 THEN DO;
PUT SKIP EDIT(AXAN(I),' X',(PLOT(I,K) DO K=1 TO 101))
(F(10,2),A,(101) A);
END;
ELSE DO;
PUT SKIP EDIT(AXAN(I),(PLOT(I,K) DO K=1 TO 101))
(X(1),F(10,2),X(1),(101) A);
END;
END;
PUT SKIP EDIT('X','X','X','X','X','X','X','X','X','X','X')
(X(12),A,(10)(X(9),A));
PUT SKIP EDIT((AXFP(I) DC I=1 BY 10 TO 101))
(X(3),(11)(F(10,2)));
END GRAPH;

```



## Appendix 11.

The subroutine DISAZ.

Description

This subroutine is a FORTRAN version of that written in PL1 by Hutton (1970). It calculates the azimuth and distance across the spheroid between two points on the Earth's surface specified by latitude and longitude. It is called with the following parameters:-

	{	ALON - longitude of point A in degrees and decimals of degrees.				
Input -	{	ALAT - latitude of point A	"	"	"	"
	{	BLON - longitude of point B	"	"	"	"
	{	BLAT - latitude of point B	"	"	"	"
Output -	{	AZ - azimuth of B from A	"	"	"	"
	{	TD - distance from B to A in kilometres				

A listing of the subroutine follows.



T=10 P=20 COPIES=10  
WAS: 15:09.01 07-24-73  
SIGNED ON AT 09:43.12 ON 07-25-73

```
SUBROUTINE DISAZ(ALON,ALAT,BLON,BLAT,AZ,TD)
C=3.141592/180.
ALCN=ALON*C
ALAT=ALAT*C
BLON=BLON*C
BLAT=BLAT*C
UA=ATAN(0.996633*TAN(ALAT))
UB=ATAN(0.996633*TAN(BLAT))
GB=((0.99327733*TAN(UB))/TAN(UA))+((0.00672267)*COS(UA))/COS(UB)
AZ=ATAN2((SIN(ALON-BLON)),(SIN(ALAT)*COS(ALCN-BLON)-(GB)))
SA=SIN(AZ)
CA=COS(AZ)
AZ=AZ/C
XA=(6378388)*COS(UA)*COS(ALON)
YA=(6378388)*COS(UA)*SIN(ALON)
ZA=(6356912)*SIN(UA)
XB=(6378388)*COS(UB)*COS(BLON)
YB=(6378388)*COS(UB)*SIN(BLON)
ZB=(6356912)*SIN(UB)
CHORD=SQRT((XA-XB)**2+(YA-YB)**2+(ZA-ZB)**2)
AB=SIN((ALAT+BLAT)/2)
ZZZ=1-(0.00672267)*(AB**2)
V=(6378388)/SQRT(ZZZ)
P=((V)*(1-0.00672267))/(1-(0.00672267)*(AB**2))
R=((P)*(V))/(P*(SA**2)+V*(CA**2))
DIS=((CHORD)**3)/(24*(R)**2))+ (3*(CHORD)**5)/(640*(R)**4))
DIS=DIS+CHORD
DIS=DIS/1000
TD=TD+DIS
RETURN
END
```

BIBLIOGRAPHY

- Admiralty Hydrographic Office, 1967. NAVADO I, II and IV. Bathymetric, gravimetric and magnetic data, H.M.S. Vidal, photocopies from Hydrographer of the Navy, MOD, Taunton, Somerset.
- Anderson, D.L., Sammis, C. and Jordan, T., 1971. Composition and evolution of the mantle and core, *Science*, 171, 1103-1112.
- Anderson, D.L. and Spetzler, H., 1970. Partial melting and the low velocity zone, *Phys. Earth Planet. Int.*, 4, 62-64.
- Anderson, R.N., McKenzie, D.P., and Sclater, J.G., 1973. Gravity, bathymetry and convection in the Earth, *Earth Planet. Sci. Lett.*, 18, 391-407.
- Andrews, D.J., 1972. Numerical simulation of sea-floor spreading, *J. geophys. Res.*, 77, 6470-6481.
- Belousov, V.V., 1970. Against the hypothesis of ocean floor spreading, *Tectonophysics*, 9, 489-511.
- Berry, L.G. and Mason, B., 1959. *Mineralogy: concepts, descriptions, determinations*, W.H. Freeman and Company, San Francisco and London, 630pp.
- Birch, F., 1961. The velocity of compressional waves in rocks to 10 kilobars, Part 2. *J. geophys. Res.*, 66, 2199-2224.
- Birch, F., 1969. Density and composition of the upper mantle: first approximation as an olivine layer, *Am. geophys. Un., Geophys. Mono.*, 13, 18-36.
- Birch, F., 1970. Interpretations of the low velocity zone, *Phys. Earth. Planet. Int.*, 3, 178-181.
- Bott, M.H.P., 1965. The upper mantle beneath Iceland, *Geophys. J. R. astr. Soc.*, 9, 275-277.
- Bott, M.H.P., 1967. Terrestrial heat flow and the mantle convection hypothesis, *Geophys. J. R. astr. Soc.*, 14, 413-428.
- Bott, M.H.P., 1973. The evolution of the Atlantic north of the Faeroe Islands, in "Implications of continental drift to the Earth Sciences, Volume 1", ed. Tarling, D.H. and Runcorn, S.K., pub Academic Press, London, 175-189.

- Bott, M.H.P., Browitt, C.W.A. and Stacey, A.P., 1971. The deep structure of the Iceland-Faeroe Ridge, *Marine Geophys. Res.*, 1, 328-351.
- Bullard, E.C., Everett, J.E. and Smith, A.G., 1965. The fit of the continents around the Atlantic, *Phil. Trans. R. Soc.*, 258A, 41-51.
- Bullen, K.E., 1963. Introduction to the theory of seismology, 3rd ed., Cambridge University Press, 231pp.
- Carlslaw, H.S. and Jaeger, J.C., 1959. Conduction of heat in solids, Oxford, Clarendon Press, 510pp.
- Clark, S.P. and Ringwood, A.E., 1964. Density distribution and constitution of the mantle, *Rev. Geophys.*, 2, 35-88.
- Dane, E.B., 1941. Densities of molten rocks and minerals, *Am. J. Sci.*, 239, 809-818.
- Deer, W.A., Howie, R.A. and Zussman, J., 1966. An introduction to the rock-forming minerals, Longmans, London, 528pp.
- Deutschen Hydrographischen Institute, 1972. Bathymetric charts for Admiralty Plotting Sheets nos 2 and 3, scale 1:1000000, Hamburg.
- Dickson, G.O., Pitman, W.C., III and Heirtzler, J.R., 1968. Magnetic anomalies in the South Atlantic and ocean floor spreading, *J. geophys. Res.*, 73, 2087-2100.
- Dietz, R.S., 1961. Continent and ocean basin evolution by spreading of the sea floor. *Nature*, 190, 854-857.
- Einarsson, T., 1954. A survey of gravity in Iceland, *Soc. Sci. Islandica*, 30, 1-22.
- Einarsson, T., 1968. Submarine ridges as an effect of stress fields, *J. geophys. Res.*, 73, 7561-7576.
- Elder, J.W., 1965. Physical processes in geothermal areas, *Am. geophys. Un., Geophys. Mono.*, 8, 211-239.
- Elkins, T.A., 1951. The second derivative method of gravity interpretation, *Geophysics*, 16, 29-50.

- Elsasser, W.M., 1969. Convection and stress propagation in the upper mantle. In "The application of modern physics to the Earth and planetary interiors", ed. Runcorn, S.K., Wiley-Interscience, London, New York, Sydney and Toronto, 223-246.
- Ewing, M., Carpenter, G., Windisch, C. and Ewing, J., 1973. Sediment distribution in the oceans: the Atlantic, Bull. geol. Soc. Am., 84, 71-88.
- Ewing, M., Eittreim, S.L., Truchan, M. and Ewing, J.I., 1969. Sediment distribution in the Indian Ocean, Deep-Sea Res., 16, 231-248.
- Ewing, J. and Ewing, M., 1959. Seismic refraction measurements in the Atlantic ocean basins, in the Mediterranean Sea, on the Mid-Atlantic Ridge and in the Norwegian Sea, Bull. geol. Soc. Am., 70, 291-318.
- Ewing, M., Ewing, J.I. and Talwani, M., 1964. Sediment distribution in the oceans: the Mid Atlantic Ridge, Bull. geol. Soc. Am., 75, 17-36.
- Ewing, M., Houtz, R. and Ewing, J., 1969. South pacific sediment distribution, J. geophys. Res., 74, 2477-2493.
- Ewing, M., Le Pichon, X. and Ewing, J., 1966. Crustal structure of the mid ocean ridges, 4: sediment distribution in the South Atlantic ocean and the cenozoic history of the Mid Atlantic Ridge, J. geophys. Res., 71, 1611-1636.
- Ewing, M., Sutton, G.H. and Officer, C.B., 1954. Seismic refraction measurements in the Atlantic ocean, part VI, typical deep stations, North American basin, Bull. seism. Soc. Am., 44, 21-38.
- Forsyth, D.W. and Press, F., 1971. Geophysical tests of petrological models of the spreading lithosphere, J. geophys. Res., 76, 7963-7979.
- Fujisawa, H., 1968. Temperature and discontinuities in the transition layer within the Earth's mantle: geophysical application of the olivine-spinel transition in the  $Mg_2SiO_4$ - $Fe_2SiO_4$  system, J. geophys. Res., 73, 3281-3294.
- Garland, G.D., 1965. The Earth's shape and gravity, Pergamon Press, 183pp.

- Gaskell, T.F., Hill, M.N. and Swallow, J.C., 1958. Seismic measurements made by H.M.S. Challenger in the Atlantic, Pacific and Indian oceans and in the Mediterranean Sea, 1950-53, Phil. Trans. R. Soc. 251A, 23-83.
- Green, D.H., 1970. The origin of basaltic and nephelinitic magmas, Trans Leicester lit. phil. Soc., 64, 54pp.
- Green, D.H. and Ringwood, A.E., 1967. The stability fields of aluminous pyroxene peridotite and garnet peridotite and their relevance in upper mantle structure, Earth Planet. Sci. Lett., 3, 151-160.
- Haigh, B.I.R., 1973. North Atlantic oceanic topography and lateral variations in the upper mantle, Geophys. J. R. astr. Soc., in press.
- Harris, P.G. and Rowell, J.A., 1960. Some geochemical aspects of the Mohorovicic discontinuity, J. geophys. Res., 65, 2443-2459.
- Hart, R.S. and Press, F., 1973. S velocities and the composition of the lithosphere in the regionalised Atlantic. J. geophys. Res., 78, 407-411.
- Haskell, N.A., 1935. Motion of a viscous fluid under a surface load, I., Physics, 6, 265-269.
- Heirtzler, J.R., Dickson, G.O., Herron, E.M., Pitman, W.C., III, and Le Pichon, X., 1968. Marine magnetic anomalies, geomagnetic field reversals and motions of the ocean floor and continents, J. geophys. Res., 73, 2119-2136.
- Hermance, J.F. and Grillo, L.R., 1970. Correlation of magnetotelluric, seismic and temperature data from southwest Iceland, J. geophys. Res., 75, 6582-6591.
- Herron, E.M., 1972. Sea floor spreading and the cenozoic history of the East-Central Pacific, Bull. geol. Soc. Am., 83, 1671-1692.
- Hess, H.H., 1962. History of ocean basins, in "Petrologic studies: a volume in honor of A.F. Buddington", Geol. Soc. Am., 599-620.
- Hess, H.H., 1964. Seismic anisotropy of the uppermost mantle under the oceans, Nature, 203, 629-631.

- Houtz, R.E. and Ewing, J.I., 1963. Detailed sedimentary velocities from seismic refraction profiles in the western North Atlantic. *J. geophys. Res.*, 68, 5233-5258.
- Hutton, M.A., 1970. Interpretation of oceanic magnetic anomalies using a linear inverse technique, Ph. D. thesis, University of Durham, 139pp.
- Ito, K., 1973. Analytical approach to estimating the source rock of basaltic magmas: major elements, *J. geophys. Res.*, 78, 412-431.
- Ito, K. and Kennedy, G.C., 1971. An experimental study of the basalt-garnet granulite-eclogite transition, *Am. geophys. Un., Geophys. Mono.*, 14, 303-314.
- Johnson, G.L. and Heezen, B.C., 1967. Morphology and evolution of the Norwegian-Greenland sea, *Deep-Sea Res.*, 14, 755-771.
- Jones, E.J.W., Ewing, J.I., Ewing, M. and Eittrheim, S.L., 1970. Influence of Norwegian sea overflow water on sedimentation in the northern North Atlantic and Labrador sea, *J. geophys. Res.*, 75, 1655-1680.
- Kanamori, H. and Press, F., 1970. How thick is the lithosphere?, *Nature*, 226, 330-331.
- Katz, S., and Ewing, M., 1956. Seismic refraction measurements in the Atlantic ocean, Part VII: Atlantic ocean basin, west of Bermuda, *Bull. geol. Soc. Am.*, 67, 475-510.
- Keen, C., and Tramontini, C., 1970. A seismic refraction survey on the Mid Atlantic Ridge, *Geophys. J. R. astr. Soc.*, 20, 473-491.
- Lachenbruch, A.H., 1973. Differentiation and the gravitational driving force for material rising at an oceanic ridge, *J. geophys. Res.*, 78, 825-831.
- Lamont-Doherty Geological Observatory, 1972. Preliminary report of Volume 22, U.S.N.S. Eltanin cruises 28-32, March 1967 - March 1968, Technical Report No. CU-1-72, 232pp.
- Langseth, M.G., Le Pichon, X. and Ewing, M., 1966. Crustal structure of the Mid Ocean ridges: 5, heat flow through the Atlantic ocean floor and convection currents, *J. geophys. Res.*, 71, 5321-5355.
- Lee, W.H.K. and Uyeda, S., 1965. Review of heat flow data, *Am. geophys. Un., Geophys. Mono.*, 8, 87-190.

- Le Pichon, X. and Heirtzler, J.R., 1968. Magnetic anomalies in the Indian ocean and sea-floor spreading, *J. geophys. Res.*, 73, 2101-2117.
- Le Pichon, X., Houtz, R.E., Drake, C.L. and Nafe, J.E., 1965. Crustal structure of the Mid Ocean ridges, 1: seismic refraction measurements, *J. geophys. Res.*, 70, 319-339.
- MacDonald, G.J.F., 1965. Geophysical deductions from observations of heat flow, *Am. geophys. Un., Geophys. Mono.*, 8, 191-210.
- McKenzie, D.P., 1967. Some remarks on heat flow and gravity anomalies, *J. geophys. Res.*, 72, 6261-6273.
- McKenzie, D.P., Roberts, J. and Weiss, N.O., 1973. Numerical models of convection in the Earth's mantle, *Tectonophysics*, in press.
- Mizutani, H. and Abe, K., 1972. An Earth model consistent with free oscillation and surface wave data, *Phys. Earth Planet. Int.*, 5, 345-356.
- Morgan, W.J., 1971. Convection plumes in the lower mantle, *Nature*, 230, 42-43.
- Morris, G.B., Raitt, R.W. and Shor, G.G., 1969. Velocity anisotropy and delay time maps of the mantle near Hawaii, *J. geophys. Res.*, 74, 4300-4316.
- Netherlands Hydrographer, 1967. NAVADO III, bathymetric, magnetic and gravity investigations, H.NETH.M.S. Snellius, parts 1-3, Hydrographic newsletter, special publication number 3.
- Orowan, E., 1965. Convection in a non-Newtonian mantle, continental drift and mountain building, in "A symposium on continental drift", *Phil. Trans. R. Soc.*, 258A, 284-313.
- Palmason, G., 1970. Crustal structure of Iceland from explosion seismology, Science Institute, University of Iceland, 239pp.
- Pitman, W.C., III, Herron, E.M. and Heirtzler, J.R., 1968. Magnetic anomalies in the Pacific and sea-floor spreading, *J. geophys. Res.*, 73, 2069-2085.
- Pitman, W.C. and Talwani, M., 1972. Sea-floor spreading in the North Atlantic, *Bull. geol. Soc. Am.*, 83, 619-646.
- Press, F., 1969. The suboceanic mantle, *Science*, 165, 174-176.

- Press, F., 1970. Earth models consistent with geophysical data, *Phys. Earth Planet. Int.*, 3, 3-22.
- Ringwood, A.E., 1962a. A model for the upper mantle, *J. geophys. Res.*, 67, 857-866.
- Ringwood, A.E., 1962b. A model for the upper mantle 2, *J. geophys. Res.*, 67, 4473-4477.
- Ringwood, A.E., 1969. Composition and evolution of the upper mantle, *Am. geophys. Un., Geophys. Mono.* 13, 1-17.
- Ringwood, A.E. and Green, D.H., 1966. An experimental investigation of the gabbro-eclogite transformation and some geophysical consequences, *Tectonophysics*, 3, 383-427.
- Ringwood, A.E., MacGregor, I.D. and Boyd, F.R., 1964. Petrological constitution of the upper mantle, *Carnegie Inst. Wash. Yearbook*, 63, 147.
- Schatz, J.F. and Simmons, G., 1972. Thermal conductivity of Earth materials at high temperatures, *J. geophys. Res.*, 77, 6966-6983.
- Schilling, J.G., 1973. Iceland mantle plume: geochemical study of Reykjanes ridge, *Nature*, 242, 565-571.
- Sclater, J.G., Anderson, R.N. and Bell, M.L., 1971. The elevation of ridges and the evolution of the central eastern Pacific, *J. geophys. Res.*, 76, 7888-7915.
- Sclater, J.G. and Francheteau, J., 1970. The implications of terrestrial heat flow observations on current tectonic and geochemical models of the crust and upper mantle of the Earth, *Geophys. J. R. astr. Soc.*, 20, 509-542.
- Sleep, N.H., 1969. Sensitivity of heat flow and gravity to the mechanism of sea-floor spreading, *J. geophys. Res.*, 74, 542-549.
- Talwani, M. and Le Pichon, X., 1969. Gravity field over the Atlantic ocean, *Am. geophys. Un., Geophys. Mono.*, 13, 341-351.
- Talwani, M., Le Pichon, X. and Ewing, M., 1965. Crustal structure of the Mid Ocean ridges: 2, computed model from gravity and seismic refraction data, *J. geophys. Res.*, 70, 341-352.
- Talwani, M., Windisch, C.C. and Langseth, M.G., Jr., 1971. Reykjanes ridge crest: A detailed geophysical study, *J. geophys. Res.*, 76, 473-517.



- Tolstoy, I., Edwards, R.S. and Ewing, M., 1953. Seismic refraction measurements in the Atlantic ocean (part 3). Bull. seism. Soc. Am., 43, 35-48.
- Tryggvason, E., 1964. Arrival times of P-waves and upper mantle structure, Bull. seism. Soc. Am., 54, 727-736.
- Turcotte, D.L. and Oxburgh, E.R., 1969. Convection in a mantle with variable physical properties, J. geophys. Res., 74, 1458-1474.
- Verhoogen, J., 1973. Possible temperatures in the oceanic upper mantle and the formation of magma. Bull. geol. Soc. Am., 84, 515-521.
- Vogt, P.R., 1971. Asthenosphere motion recorded by the sea floor south of Iceland, Earth Planet. Sci. Lett., 13, 153-160.
- Vogt, P.R. and Johnson, G.L., 1973. A longitudinal seismic reflection profile of the Reykjanes ridge: part II - implication for the mantle hot spot hypothesis, Earth Planet. Sci. Lett., 18, 49-58.
- Vogt, P.R., Ostenso, N.A. and Johnson, G.L., 1970. Magnetic and bathymetric data bearing on the sea-floor spreading north of Iceland, J. geophys. Res., 75, 903-920.
- Wang, C., 1970. Density and constitution of the mantle, J. geophys. Res., 75, 3264-3284.
- Weissel, J.K. and Hayes, D.E., 1971. Assymetric sea-floor spreading south of Australia, Nature, 231, 518-522.
- Worthington, M.H., Cleary, J.R. and Anderssen, R.S., 1972. Density modelling by Monte-Carlo inversion - II: comparison of recent Earth models, Geophys. J. R. astr. Soc., 29, 445-457.
- Wyllie, P.J., 1970. Ultramafic rocks and the upper mantle, Mineral Soc. Am., Spec. Pap. 3, 3-32.

